



**Scuola Universitaria Superiore IUSS Pavia**

**From Record Selection to Risk Targeted Spectra for Risk based  
Assessment and Design**

A Thesis Submitted in Partial Fulfilment of the Requirements  
for the Degree of Doctor of Philosophy in

**EARTHQUAKE ENGINEERING AND  
ENGINEERING SEISMOLOGY/  
RISK AND EMERGENCY MANAGMENT /  
WEATHER RELATED RISK**

Obtained in the framework of the Doctoral Programme in  
Understanding and Managing Extremes

by

**Andrea Spillatura**

Supervisor: Prof. Paolo Bazzurro

October, 2017



*Luke:* All right, I'll give it a try.  
*Yoda:* No! Try not. Do or do not. There is no try.



## ABSTRACT

Performance Based Earthquake Engineering (PBEE) is a well-known and established approach that allows the user to evaluate the building behavior under seismic loading from a probabilistic perspective. Even though it is available since the early 2000s, there is still ample room for improvements and enhancements. Record selection procedures, for example, is one of the most important tool that allows linking the hazard with the structural response. In order to assess properly the performance of a building, it is necessary to model carefully its structural characteristics but also to subject it to ground motion that it could realistically experience during its lifetime. For this reason, hazard-consistent record selection procedures (e.g. Baker [2011]) have become increasingly popular, at least at the assessment level. Conditional Spectrum methods stem from the idea that the spectral shape is the only (or the main) characteristic of the ground motion that can affect the structural response. However, several studies have demonstrated that this is not the case and other characteristics could matter (e.g. duration or pulses due to directivity effects). The idea, here, is to develop a record selection procedure that is hazard consistent both in terms of spectral shape and of causal parameters (i.e. Magnitude and Distance), using the latter as proxies for other ground motion characteristics not explicitly accounted for.

Another aspect that could be tackled making use of PBEE framework is the evaluation of risk associated to code conforming buildings. Current design philosophy relies on designing structures to withstand actions that have a reasonably low probability (typically 10% in 50 years) of being exceeded during the building lifetime. In addition to this, safety factors are adopted to increase the actions and decrease the material resistances in order to make those structures safer. The main issue, here, is that we know that those factors are working in the right direction of making the design structure safer but we do not know how “safe” they make the structure be. Indeed, the designer will not be able to associate a collapse risk quantity to the building he/she has designed. How much is the risk that the building will reach a given limit state (be it operational or ultimate) within the foreseeable lifetime of the building? Would the risk be constant among different structures/locations? Would the structures be safe enough everywhere? The main goal of the research conducted herein is to provide an answer to all these questions when the risk is gauged in terms of nominal annual rate of collapse/damage for several structural typologies located at different sites.

As expected, the risk is proven to be non-uniform across sites and across structures. A design strategy that could ensure a homogenous (or, at least, less variable) risk across sites and buildings would certainly be fairer and more ethical. This objective could be achieved by applying directly the concepts of performance based design, which would result in a new, explicitly risk-based way of designing structures. A proposal in that direction that could be implemented in a code format is the one developed by Luco et al. [2007] (and currently adopted in ASCE7-10) who recommended to modify the acceleration inputs (via risk-based adjustment factors, SAF), on which design spectra are based, in order to ensure an explicitly accepted level of risk. This method, which defines for this purpose, the Risk Targeted design Spectra (RT-Spectra), as it turns out, guarantees the achievement of a conveniently chosen target collapse risk only under the assumption that a newly designed building is properly described by a generic code-conforming fragility curve representation. This means that, in practice, that the target can only be approximately achieved and, therefore, that the risk of different buildings at different sites would still be non-uniform. The research work done here intends to shed light on the various aspects that could influence the success of RT-spectra approach, namely fragility functions characteristics, performance objectives, design spectrum shape/parameterization and spectral ordinates optimization, in harmonizing if not homogenizing the risk..

## ACKNOWLEDGEMENTS

It is the third time, by now, that I face with acknowledgements and I can assert with certainty that writing them has a kind of cathartic function: you go back to the time you struggled with the topics you were working on, and you start thinking. Thinking about people, not your work, not what you have written, just people. You think to all the people that you met, that have asked you something about your work or about how you were feeling, that have encouraged you in some way. You do this because your thesis is not just yours, rather something that you collected, you put together with the help of people that entered (in different ways) in your life: a smile, a laugh, a question, a beer, whatever. Each of them owns a piece of this work by right! Therefore, thank you to all of you even though I will not cite directly your name in the following lines.

First, I want to thank sincerely my supervisor, Prof. Bazzurro: I do not want to be prosaic but it was a real pleasure to work with him during these years. I had the chance of challenging topics about which I had never heard before I came here in Pavia. Life is made of choices and the decision of working with him belongs to a column called "GOOD JOB YOU DID IT RIGHT, ANDREA!" Thank you Paolo, to have guided me through this hard path called PhD, to have encouraged me and helped me to fill my gaps. I hope I have fulfilled at least some of your expectations. Second in charge is Prof. Dimitrios Vamvatsikos: one of the most brilliant and humble minds I have ever met. Working in Athens with him for about four months was a treasure trove of information, knowledge and a boost in confidence. Besides that, I want to thank him also for his hospitality: I really felt to be at home during the past summer period (and, yes, I miss souvlaki, too). To be honest, the capstone of my experience in Attica was certainly the access to the huge knowledge and wisdom of Prof. Ulysses R. Garbaggio (thanks Dimitrios to have introduced me to him); as far as I understood he is a shy person but I hope I will have the chance of meeting him in person.

I want to thank also Prof. Iervolino of University Federico II of Napoli. Lucky me, I had the chance of cooperating with him in a project that is also part of my thesis. He is made of a mixture of intellect, commitment and knowledge: certainly an example to follow. Being part of this project was an amazing experience: I was in the same room with the best Italian expert in several engineering fields; having the chance of simply listening them exchanging their ideas was more than good fortune. For being involved in this project, I should thank again Prof. Bazzurro who has put his trust in my capabilities.

I should gratefully acknowledge also Prof. Ting Lin and Dr. Reagan Chandramohan for sharing their spectrally equivalent long/short record database used to test the model dependency on duration. A special thanks also to Dr. Maria Lancieri for her precious suggestions about records correction and scaling.

I cannot forget my dear friend Dr. Mohsen Kohrangi: I want to thank him for his support in terms of ideas, time, patience and trust: it happened several times that he trusted in my abilities and in me more than I do. Thank you my friend, I thank God to have met you and I hope we could keep continue working together and be in touch, hopefully in person (if the Italian embassy in Iran will give us the pleasure).

Then I want to thank sincerely Prof. Roberto Nascimbene who has hosted me in his section and helped me several times with precious suggestions. Next, all the people working in structural analysis section with particular mention to the lunch-coffee gang: Dumitru Beilic (differently to John Snow he knows everything!!), Emuanuele Brunesi, Daniele Cicola, Stefano Barone and Hector Perez. Thank you also to Dr. Emilia Fiorini for our very fruitful chats and exchanges of ideas.

Thank you also to all my good friends I met during the Rose Master: Andrea, Federica, Giorgio, Yen Shin, Sreeram we should meet more often! Thank you also to Danilo and Valentina, now they are rich people in Switzerland but very hospitable, I will come to visit you soon again: the Bernina Express is waiting for us (and also a tougher “via ferrata”). I want to acknowledge also Kostantinos Bakalis who was my neighbour in NTUA offices, I met a good friend and I hope we can be in touch in the future, maybe working together too (P.S.: Daphny, I miss you so much!! ☺ --Ed.). Obviously I cannot forget my dear engineers from Perugia: Benedetta, Cri, Dotty, Fabiola, Gius, Leo, Lollo, Lorenzo, Lucia , Michy, TittyZ. We are a bit scattered at the moment but I am sure that the “Possente Pilaf” is looking after all of us.

Now it is the time of family: it keeps growing and this is a wonderful thing to realize. Thank you to my parents: they are my strength, they taught me to do always my best, for me and for the people who love me. If I am here and I am a good person (I hope so) it is mainly because of you and your privations; you are always in my thoughts even if I am not a “phone call-addicted” kind of person. Thank you to my grandparents Ada, Giovanna, Renato and Tranquillo (rigorously in alphabetic order! --Ed.). They remind me the importance of simple things and good feelings: a word, a simple look, I always felt your support. Thank you also to Nando, Pia, Dalida, Michela, Roberto and Alessandra we should find more time to stay together and everything will be fine, I am sure about that. Next, Ornella, Piero, Elisa and Federico (also someone else that is arriving soon, I already know that I will love you!) we are a bit far physically but you are always in my heart.

Family is not only about blood ties, it is something more and you, my friends, are definitely part of mine. I want to thank you for being part of my life; as I said at the very start, this work is also yours: Adele (aka Didi), Aurora, Chele, Chiara, Diego, Fabio, Giacomo, Giorgia, Matteo, Tommy; I love you guys! Other people officially belong to this “section” for about a year now. Apart from “official signatures”, I really feel to be part of the same crew and, therefore, thank you to Elena, Emma, Filo, Giammo, Luca, Maria Rita, Ileana. (Yes, I know. I am still on probation but there is no harm in trying...)

Last but not the least, Chicchi my WIFE (what the heck!). I am not that kind of romantic person but I want to spend few words for you. I really do not know who I would have been without you on my side, supporting me, giving me strength and self-confidence. Sometimes I found myself remembering when I was a teenager and I was thinking about the future, what I wanted to have, who I wanted to be with: I am quite sure that, right now, I have definitely more than I wished. Thank you to be exactly as you are, I am the luckiest man in the world. I love you.

Yes, I was a bit too long-winded but it was deserved. Thanks again to all of you! May the force be with you (and with me also...)!



## TABLE OF CONTENTS

ABSTRACT .....	v
ACKNOWLEDGEMENTS.....	vii
TABLE OF CONTENTS .....	xi
LIST OF FIGURES .....	xv
LIST OF FIGURES IN THE APPENDIX.....	xix
LIST OF TABLES.....	xxiii
LIST OF TABLES IN APPENDIX.....	xxiii
1. INTRODUCTION .....	1
2. CS-BASED RECORD SELECTION CONSISTENT WITH MAGNITUDE AND SOURCE-TO-SITE DISTANCE OF FUTURE EARTHQUAKE SCENARIOS .....	5
2.1 SUMMARY .....	5
2.2 INTRODUCTION.....	5
2.3 CONDITIONAL SPECTRA INCLUDING CAUSAL PARAMETERS—CS-MR.....	8
2.3.1 Conditional spectra based record selection.....	8
2.3.2 Proposed post processing algorithm to CS accounting for causal parameters (CS-MR) 9	9
2.4 QUALITIES AND CHALLENGES OF CS-MR RECORD SELECTION .....	10
2.4.1 Which ground motion characteristics are correlated to M and R?.....	10
2.4.2 Bin selection, criteria and assumptions .....	12
2.5 CASE STUDY: RC MODERN FRAME LOCATED IN SEATTLE.....	15
2.5.1 Selected site and test building .....	15
2.6 GROUND MOTION SELECTION.....	17
2.7 RESULTS AND DISCUSSION .....	25
2.7.1 Robustness test.....	27
2.8 CONCLUSIONS .....	29
3. RINTC: ASSESSING IMPLICIT RISK OF CURRENT ITALIAN CODE.....	31

---

3.1 INTRODUCTION.....	31
3.2 METHODOLOGY.....	33
3.2.1 Seismic Hazard Analysis.....	36
3.2.2 Ground Motion Selection.....	39
3.2.3 Structural Analysis approach and risk calculation.....	43
3.3 RESULTS.....	45
3.3.1 Fragility Curves.....	46
3.3.2 Risk Nominal Rates.....	49
3.4 VALIDATION OF THE RESULTS.....	53
3.4.1 Calculation of annual rate of collapse.....	53
3.4.2 Influence of different record selection techniques and IM types.....	56
3.4.2.1 Analysis scheme and case study.....	57
3.4.2.2 Results.....	60
3.5 CONCLUSIONS.....	64
4. HARMONIZING SEISMIC PERFORMANCE VIA RISK TARGETED SPECTRA: STATE OF THE ART, DEPENDENCIES AND IMPLEMENTATION PROPOSALS.....	67
4.1 SUMMARY.....	67
4.2 INTRODUCTION.....	67
4.3 ELEMENTS OF RISK-TARGETED SPECTRA.....	70
4.3.1 Fragility Functions.....	70
4.3.2 Performance objectives.....	72
4.3.3 Design spectrum shape and parameterization.....	72
4.3.4 Optimized spectral ordinates.....	73
4.4 CASE STUDY BUILDINGS AND SITES.....	73
4.4.1 Selected sites and hazard computation.....	74
4.4.2 Structural systems, design procedure and limit state definition.....	74
4.5 FRAGILITY CURVES AND PRELIMINARY ASSESSMENT.....	76
4.5.1 Building and site specific fragility curves.....	76
4.5.2 Generic fragility curves.....	81
4.6 RISK TARGETED SPECTRA: CALCULATION AND PRACTICAL IMPACT.....	82
4.6.1 Estimation of SAFs.....	82

4.6.2	Target MAF and harmonization strategy .....	83
4.6.3	Practical implementation of SAFs: dependency on design spectrum characteristics .....	84
4.7	RESULTS .....	85
4.7.1	Application of SAF based on building-specific fragility curves.....	86
4.7.2	Application of SAF based on generic fragility curves.....	91
4.8	CONCLUDING REMARKS .....	94
5	CONCLUSIONS.....	96
5.1	FUTURE DIRECTIONS.....	101
	REFERENCES.....	103
	Appendix A . Additional details on CS-MR method.....	113
	Appendix B . Hazard Analysis and Record Selection details for Implicit Risk Project .....	131
	Appendix C . Notes on structural Modelling about Implicit Risk Project.....	138
	Appendix D . Fragility Curves and Nominal annual Rates from Implicit Risk Project .....	143
	Appendix E . SDoFs compliance with RINTC MDoFs .....	180



## LIST OF FIGURES

Figure 2.1 (a) Illustration of the expected spectral shape of ground motion of different M-R scenarios (Legend: circle, M=4.5; diamond, M=6.0; square, M=7.0; cross, M=8.0; triangle, M=9.0) based on BA08; (b) median duration, $D_{5-75}$ of selected earthquake scenarios based on AS96. ....	13
Figure 2.2 Comparison of record selection based on CS-exact and CS-MR methods for a site in Seattle corresponding to conditioning period of $T=1.6s$ for 5% in 50 years event with $Sa(T=1.6s)=0.37g$ , (a) M and R disaggregation; (b) M and R distribution of the selected records based on the CS-exact method, (c) median of the target and selected records' spectra, (d) conditional dispersion of the target and selected records. ....	15
Figure 2.3 Hazard analysis results at Seattle for Soil Type D based on the USGS web tool: a) hazard curves for spectral accelerations at $T=1s$ and 2s; (b) M-R disaggregation results for 2% in 50 year spectral acceleration at $T=1s$ . ....	16
Figure 2.4 Verification of the building model's sensitivity to ground motion duration; comparison of: (a) IDA curves for MIDR; and (b) collapse fragility curves for two sets of 146 spectrally-equivalent short- and long-duration records. ....	17
Figure 2.5 (a) Scatter plot of magnitude versus distance; and (b) Scatter plot of magnitude versus duration, for the ground motion database used in this study. ....	20
Figure 2.6 Comparison of the bin-specific $D_s$ and $S_a$ conditional distributions for the records selected by the GCIM, CS only and CS-MR approaches for the three bins 2, 7 and 12 identified by the disaggregation of the 5% in 50 years IM level for a site in Seattle. Left panels: $D_{5-75}$ distributions of the selected records and the target distribution from the GCIM method. Right panels: 2.5/50/97.5 <sup>th</sup> percentiles of spectral accelerations of the selected records. Note: the numbers in the parentheses in the title above each panel show the number of selected records associated to each bin (e.g., 46 out of 100 for Bin 12). ....	23
Figure 2.7 Comparison of the $D_{5-75}$ and $S_a$ conditional distributions for all the 100 records selected by the GCIM, CS only and CS-MR approaches for the 5% in 50 years IM level for a site in Seattle. (a) $D_{5-75}$ distribution of the selected records and the target obtained from GCIM; (b) 2.5/50/97.5-th percentiles of the empirically-derived conditional distribution of spectral acceleration of the records selected by the three approaches; (c) Scatter plot of the magnitude and distance pairs of the records selected by the four approaches. ....	24
Figure 2.8 a) Fragility curves and b) Drift hazard curves, estimated from the multistriple analyses of the structure subjected to the record sets defined according to the four selection	

methods. The dotted/lighter lines (for each method) represent the range of variability of 100 different combination of response estimates.....	26
Figure 2.9 Comparison of the selected records distributions based on CS-only approach using full (NGA West2 + subduction) and limited (only NGA Wests) databases. (a) Duration distribution; (b) spectral acceleration 2.5/50/97.5-th percentiles for the selected site in Seattle corresponding to IM level 5 with $S_a(1.6s)=0.37g$ .....	28
Figure 2.10 Robustness test: Changes in the duration distribution obtained by removing selected subduction records from the database.....	28
Figure 3.1 Location of the five selected cities. Legend: AQ=L'Aquila; NA=Napoli; CL=Caltanissetta; MI=Milano and seismic source model at the basis of the official Italian hazard map used to determine design seismic actions (Stucchi et al. [2011])..	33
Figure 3.2 Graphic representation of PEER Integral modules and interface variables.....	36
Figure 3.3 (a) UHS for Roma, Soil Type A, Return Period values of 475 e 975 years computed according to INGV, Openquake and NTC08. (b) The OQ and the NTC08 hazard values are computed at the exact location (red dot) while the INGV hazard is computed at the grid point #28512 (capture from SpettriNTCver1.0.3(CSLP) [2008]).....	38
Figure 3.4 PGA hazard curve comparison for Roma, Soil Type A, $T=1s$ . PoE is the acronym for Probability of Exceeding.....	38
Figure 3.5 UHS, for Soil A, at L'Aquila according to Ambraseys (1996), red line, and Akkar and Bommer (2010), blue line. ....	39
Figure 3.6 Response spectra of both horizontal components of selected records for the case of L'Aquila, Soil Type C, and Intensity Level 3(a) and 6(b). ....	41
Figure 3.7 Original vs shortened versions of one of the records selected for the 10 <sup>th</sup> IM level for Roma, Soil C, $T_1=0.5s$ .....	42
Figure 3.8 Roof drift ratio, RDR, distribution for 10 IM levels, $S_a(T_1)$ . Each stripe shows the record to record variability for the specific IM level. The results are related to an Unreinforced Masonry building located in L'Aquila soil type C. The red cross in the last IM Level represent the only case of numerical/dynamic instability that was assumed to be collapse.....	44
Figure 3.9 Mean Fragility curves for SLC of RC structures on soil type C. The x axis is normalized by the elastic $S_a$ value extracted from the UHS corresponding to the 10% in 50 years hazard level .....	47
Figure 3.10 Mean Fragility curves for SLD of RC structures on soil type C. The x axis is normalized by the elastic $S_a$ value extracted from the UHS corresponding to the 63% in 50 years hazard level. ....	48
Figure 3.11 Mean Fragility curves for SLC of URM structures on soil type C. The x axis is normalized by the elastic $S_a$ value extracted from the UHS corresponding to the 10% in 50 years hazard level. ....	48

Figure 3.12 Mean Fragility curves for SLD of URM structures on soil type C. The x axis is normalized by the elastic  $S_a$  value extracted from the UHS corresponding to the 63% in 50 years hazard level.....49

Figure 3.13 Annual collapse rates for different structural typologies located at five sites on soil type C.....49

Figure 3.14. Annual collapse rates related to different structural typologies placed in five sites on soil typology A.....50

Figure 3.15 Annual rates of onset of damage for different structural typologies located at five sites on soil type C.....52

Figure 3.16 Annual rates of onset of damage for different structural typologies located at five sites on soil type A.....52

Figure 3.17 Proposed Hazard curve discretization approaches: (a) Method 1, IML assigned to the lower bound of the interval and (b) Method 2, IML assigned to the middle point of the interval. The dashed lines defines the 11 points in which the hazard curve is discretized; in the panel (a) the first one is the rate of all the earthquakes above minimum magnitude in the region around the site and the others coincide with the rates of the 10 IMLs.....54

Figure 3.18. Impact of convolution integral approximation for some configurations of masonry building located at five cities on soil type C.....55

Figure 3.19. Impact of convolution integral approximation for six-story RC frame buildings (in three configurations, namely bare, BF, infilled, IF, and pilotis, PF) located at five cities on soil type C.....56

Figure 3.20 Regression analyses on output data for each of the three structures carried out separately for each horizontal direction. The markers represent the RDR collapse threshold and the corresponding MIDR.....59

Figure 3.21 Fragility curve for a pilotis six-story frame designed for L’Aquila on soil type C.....61

Figure 3.22 Fragility curves for a pilotis six-story frame designed for L’Aquila on soil type C. The left column is related to Approach2 (site-specific, AvgSA-based) while the right one refers to Approach3 (multi-site, AvgSA-based). Each row represents a different EDP choice namely RDR (first), MIDR<sub>SD</sub> (second) and MIDR<sub>SF</sub> (third)....63

Figure 4.1 (a) Hazard curves for three sites having the same design PGA at 10% in 50 years but different slope\shape, and (b) three different fragility curves to be employed for risk harmonization, each representing a different weighting of the importance of the shape of the hazard curve.....69

Figure 4.2 (a) Map of cities chosen as representative of high (red) and medium (blue) hazard zones, and (b) the corresponding PGA hazard curves on rock.....74

Figure 4.3 Single degree of freedom backbone curves expressed in terms of the ductility and the strength ratio (base shear over yield base shear) and limit state definition according to building’s ductility class: DCH - high ductility (left) and DCM - medium ductility (right).....76

Figure 4.4. Records selected for Athens and SDOFs with $T_1=1s$ using $S_a(T_1)$ (left) and $AvgSA$ (right) as conditioning IM.....	77
Figure 4.5 Example of IM impact, $S_a(T_1)$ (left panels) versus $AvgSA$ (right panels) on Collapse fragility curves. These cases are related to a DCH structure with $T=1.0s$ designed for Athens. The vertical lines of the upper panels represent the (median) displacement threshold used to define LS1 (green), LS2 (yellow) and LS3 or collapse (red).....	78
Figure 4.6 Initial MAF distribution for LS1 (green), LS2 (yellow) and LS3 (red) for different system periods and IM types.....	79
Figure 4.7 Initial MAF distribution for LS1 (green), LS2 (yellow) and LS3 (red) differentiated by cities belonging to (a) high and (b) moderate hazard zones.....	80
Figure 4.8 Comparison of MAFs computed using three different IMs: PGA, $S_a(T_1)$ and $AvgSA$ .	81
Figure 4.9 Graphical representation of the hunting and bisection procedure through which the SAFs are computed. The figure refers to the case where we start with $MAF_{tgt} > MAF_1$ .....	83
Figure 4.10 Effect of the target MAF on the resulting MAF distribution for LS3. Narrow (left) or broad (right).....	84
Figure 4.11 Building-specific C fragilities with Flexible spectrum. COV (left) and SRSS (right) using $S_a$ as IM. Each row represents a different target LS, from 1 (top row) to 3 (bottom row). SAFs are estimated only for the DCH subset at each period. ....	89
Figure 4.12 Building-specific C fragilities with Flexible spectrum. COV(left) and SRSS (right) using $S_a$ as IM and targeting LS2. SAFs are estimated only for the DCH subset at each period.....	89
Figure 4.13 Building-specific C fragilities with Rigid/Semi-Flexible/Flexible spectra. Impact of the IM and CS record selection approach when targeting LS2 and employing only the DCH designs to achieve harmonization: There is little difference when using site-specific selection with (a) $S_a$ or (b) $AvgSA$ . Employing (c) $AvgSA$ with record sets compatible with multiple sites of similar seismicity does seem to improve harmonization but to a small degree and may be an artificial effect of lower fragility variability.....	91
Figure 4.14 Generic A fragilities with a Rigid spectrum shape. Box-plot (top), COV (middle) and SRSS (bottom) results when targeting LS2 and harmonizing with respect to (a) $S_a(0.5sec)$ , (b) $S_a(1.0sec)$ and (c) $S_a(2.0sec)$ .....	92
Figure 4.15 Generic B fragilities with a Rigid spectrum shape. Box-plot (top), COV (middle) and SRSS (bottom) results when targeting LS2 and harmonizing with respect to (a) $S_a(0.5sec)$ , (b) $S_a(1.0sec)$ and (c) $S_a(2.0sec)$ .....	93
Figure 4.16 Generic B fragilities with a Flexible spectrum shape: (a) Box-plots, (b) COV, and (c) SRSS results when targeting LS2 and harmonizing each system at its corresponding oscillator period. ....	94

## LIST OF FIGURES IN THE APPENDIX

Figure A.1 Pushover approximation for 0.5 (a), 1.6(b), 2.5(c) seconds structures .....	115
Figure A.2 Drift Hazard curves for SDoF characterized by T=0.5 s (a), T=1.6 s (c), T=2.5 s (e) for modelling approach 1 (EPH). .....	117
Figure A.3 Drift Hazard curves for SDoF characterized by T=0.5 s (a), T=1.0 s (b), T=1.6 s (c), T=2.0 s (d), T=2.5 s (e) for modelling approach 2 (Stiffness and Strength degradation with Pinching). .....	118
Figure A.4 Charts representing collapse rates varying periods and selection approach for the two SDoF model analyzed, namely Pinch (a), EPH (b).....	119
Figure A.5 Comparison of the $D_{35-75}$ and $S_a$ conditional distributions for all the 100 records selected by the GCIM, CS only. CS approx. and CS-MR approaches for the 56% in 50 years IM level for a site in Seattle. (a) $D_{35-75}$ distribution of the selected records and the target obtained from GCIM; (b) 2.5/50/97.5-th percentiles of the empirically-derived conditional distribution of spectral acceleration of the records selected by the four approaches; (c) Scatter plot of the magnitude and distance pairs of the records selected by the four approaches.....	121
Figure A.6 Comparison of the $D_{35-75}$ and $S_a$ conditional distributions for all the 100 records selected by the GCIM, CS only. CS approx. and CS-MR approaches for the 29% in 50 years IM level for a site in Seattle. (a) $D_{35-75}$ distribution of the selected records and the target obtained from GCIM; (b) 2.5/50/97.5-th percentiles of the empirically-derived conditional distribution of spectral acceleration of the records selected by the four approaches; (c) Scatter plot of the magnitude and distance pairs of the records selected by the four approaches.....	122
Figure A.7 Comparison of the $D_{35-75}$ and $S_a$ conditional distributions for all the 100 records selected by the GCIM, CS only. CS approx. and CS-MR approaches for the 17% in 50 years IM level for a site in Seattle. (a) $D_{35-75}$ distribution of the selected records and the target obtained from GCIM; (b) 2.5/50/97.5-th percentiles of the empirically-derived conditional distribution of spectral acceleration of the records selected by the four approaches; (c) Scatter plot of the magnitude and distance pairs of the records selected by the four approaches.....	123
Figure A.8 Comparison of the $D_{35-75}$ and $S_a$ conditional distributions for all the 100 records selected by the GCIM, CS only. CS approx. and CS-MR approaches for the 9% in 50 years IM level for a site in Seattle. (a) $D_{35-75}$ distribution of the selected records and the target obtained from GCIM; (b) 2.5/50/97.5-th percentiles of the empirically-derived conditional distribution of spectral acceleration of the records selected by the four approaches; (c) Scatter plot of the magnitude and distance pairs of the records selected by the four approaches.....	124
Figure A.9 Comparison of the $D_{35-75}$ and $S_a$ conditional distributions for all the 100 records selected by the GCIM, CS only. CS approx. and CS-MR approaches for the 5% in 50 years IM level for a site in Seattle. (a) $D_{35-75}$ distribution of the selected records	

- and the target obtained from GCIM; (b) 2.5/50/97.5-th percentiles of the empirically-derived conditional distribution of spectral acceleration of the records selected by the four approaches; (c) Scatter plot of the magnitude and distance pairs of the records selected by the four approaches. .... 125
- Figure A.10 Comparison of the  $D_{5-75}$  and  $S_a$  conditional distributions for all the 100 records selected by the GCIM, CS only. CS approx. and CS-MR approaches for the 2% in 50 years IM level for a site in Seattle. (a)  $D_{5-75}$  distribution of the selected records and the target obtained from GCIM; (b) 2.5/50/97.5-th percentiles of the empirically-derived conditional distribution of spectral acceleration of the records selected by the four approaches; (c) Scatter plot of the magnitude and distance pairs of the records selected by the four approaches. .... 126
- Figure A.11 Comparison of the  $D_{5-75}$  and  $S_a$  conditional distributions for all the 100 records selected by the GCIM, CS only. CS approx. and CS-MR approaches for the 1% in 50 years IM level for a site in Seattle. (a)  $D_{5-75}$  distribution of the selected records and the target obtained from GCIM; (b) 2.5/50/97.5-th percentiles of the empirically-derived conditional distribution of spectral acceleration of the records selected by the four approaches; (c) Scatter plot of the magnitude and distance pairs of the records selected by the four approaches. .... 127
- Figure A.12 Comparison of the  $D_{5-75}$  and  $S_a$  conditional distributions for all the 100 records selected by the GCIM, CS only. CS approx. and CS-MR approaches for the 0.8% in 50 years IM level for a site in Seattle. (a)  $D_{5-75}$  distribution of the selected records and the target obtained from GCIM; (b) 2.5/50/97.5-th percentiles of the empirically-derived conditional distribution of spectral acceleration of the records selected by the four approaches; (c) Scatter plot of the magnitude and distance pairs of the records selected by the four approaches. .... 128
- Figure A.13 Comparison of the  $D_{5-75}$  and  $S_a$  conditional distributions for all the 100 records selected by the GCIM, CS only. CS approx. and CS-MR approaches for the 0.6% in 50 years IM level for a site in Seattle. (a)  $D_{5-75}$  distribution of the selected records and the target obtained from GCIM; (b) 2.5/50/97.5-th percentiles of the empirically-derived conditional distribution of spectral acceleration of the records selected by the four approaches; (c) Scatter plot of the magnitude and distance pairs of the records selected by the four approaches. .... 129
- Figure A.14 Comparison of the  $D_{5-75}$  and  $S_a$  conditional distributions for all the 100 records selected by the GCIM, CS only. CS approx. and CS-MR approaches for the 0.4% in 50 years IM level for a site in Seattle. (a)  $D_{5-75}$  distribution of the selected records and the target obtained from GCIM; (b) 2.5/50/97.5-th percentiles of the empirically-derived conditional distribution of spectral acceleration of the records selected by the four approaches; (c) Scatter plot of the magnitude and distance pairs of the records selected by the four approaches. .... 130
- Figure B.1 Hazard curves for PGA, and  $S_a$ 's at  $T=0.5s$  and  $T=2$  computed for Soil Type A conditions for L'Aquila (a), Napoli (b), Roma (c), Caltanissetta (d) e Milano (e). .... 132
- Figure B.2. Spectra of selected records with percentiles curves for the case of L'Aquila, soil C, and conditioned on Spectral acceleration at 0.5s (a), 1.0s (b), 2.0 s (c). .... 133

Figure B.3	Spectra of selected records with percentiles curves for the case of Napoli, soil C, and conditioned on Spectral acceleration at 0.5s (a), 1.0s (b), 2.0 s (c).....	134
Figure B.4	Spectra of selected records with percentiles curves for the case of Roma, soil C, and conditioned on Spectral acceleration at 0.5s (a), 1.0s (b), 2.0 s (c).....	135
Figure B.5	Spectra of selected records with percentiles curves for the case of Caltanissetta, soil C, and conditioned on Spectral acceleration at 0.5s (a), 1.0s (b), 2.0 s (c).....	136
Figure B.6	Spectra of selected records with percentiles curves for the case of Milano, soil C, and conditioned on Spectral acceleration at 0.5s (a), 1.0s (b), 2.0 s (c).....	137
Figure D.1	Fragility curves and quantile-quantile plots for RC buildings designed for L'Aquila on soil C. The curves on the left column are related to Infilled Frame buildings while on the right refer to Pilotis (soft story) buildings. The rows distinguish the number of stories, in particular 3-, 6- and 9-story structures respectively.....	148
Figure D.2	Fragility curves and quantile-quantile plots for RC 6-story frame buildings designed for Caltanissetta on soil C. The curve on the left column is related to an Infilled Frame Building while on the right refers to a Pilotis (soft story) building. ....	148
Figure D.3	Fragility curves and quantile-quantile plots for RC 9-story frame buildings designed for Napoli on soil C. The curve on the left column is related to an Infilled Frame Building while on the right refers to a Pilotis (soft story) building.....	149
Figure D.4	Fragility curves and quantile-quantile plots for RC 6-story frame buildings designed for Roma on soil C. The curve on the left column is related to an Infilled Frame Building while on the right refers to a Pilotis (soft story) building.....	149
Figure D.5	Fragility curves and quantile-quantile plots for RC buildings designed for L'Aquila on soil C. The curves on the left column are related to Infilled Frame buildings while on the right refer to Pilotis (soft story) buildings. The rows distinguish the number of stories, in particular 3-, 6- and 9-story structures respectively.....	151
Figure D.6	Fragility curves and quantile-quantile plots for RC 6-story frame buildings designed for Caltanissetta on soil C. The curve on the left column is related to an Infilled Frame Building while on the right refers to a Pilotis (soft story) building. ....	151
Figure D.7.	Fragility curves and quantile-quantile plots for RC buildings designed for Milano on soil C. The curves on the left column are related to Infilled Frame buildings while on the right refer to Pilotis (soft story) buildings. The rows distinguish the number of stories, in particular 3-, 6- and 9-story structures respectively.....	153
Figure D.8	Fragility curves and quantile-quantile plots for RC buildings designed for Napoli on soil C. The curves on the left column are related to Infilled Frame buildings while on the right refer to Pilotis (soft story) buildings. The rows distinguish the number of stories, in particular 3-, 6- and 9-story structures respectively.....	154
Figure D.9	Fragility curves and quantile-quantile plots for RC 6-story frame buildings designed for Roma on soil C. The curve on the left column is related to an Infilled Frame Building while on the right refers to a Pilotis (soft story) building.....	155

- Figure D.10 Fragility curves and quantile-quantile plots for URM buildings designed for L'Aquila on soil C. The line-style helps to distinguish among different structural characteristics. Solid and dashed lines represent, respectively, 2- and 3- story structures while the use of circle markers depicts an irregular configuration. Each panel represents a different configuration whose code is given in the legend name.156
- Figure D.11 Fragility curves and quantile-quantile plots for URM buildings designed for Napoli on soil C. The line-style helps to distinguish among different structural characteristics. Solid and dashed lines represent, respectively, 2- and 3- story structures while the use of circle markers depicts an irregular configuration. Each panel represents a different configuration whose code is given in the legend name.158
- Figure D.12 Fragility curves and quantile-quantile plots for URM buildings designed for Roma on soil C. The line-style helps to distinguish among different structural characteristics. Solid and dashed lines represent, respectively, 2- and 3- story structures while the use of circle markers depicts an irregular configuration. Each panel represents a different configuration whose code is given in the legend name.159
- Figure D.13 Fragility curves and quantile-quantile plots for URM buildings designed for L'Aquila on soil C. The line-style helps to distinguish among different structural characteristics. Solid and dashed lines represent, respectively, 2- and 3- story structures while the use of circle markers depicts an irregular configuration. Each panel represents a different configuration whose code is given in the legend name.161
- Figure D.14 Fragility curves and quantile-quantile plots for URM buildings designed for Caltanissetta on soil C. The line-style helps to distinguish among different structural characteristics. Solid and dashed lines represent, respectively, 2- and 3- story structures while the use of circle markers depicts an irregular configuration. Each panel represents a different configuration whose code is given in the legend name.162
- Figure D.15 Fragility curves and quantile-quantile plots for URM buildings designed for Milano on soil C. The line-style helps to distinguish among different structural characteristics. Solid and dashed lines represent, respectively, 2- and 3- story structures while the use of circle markers depicts an irregular configuration. Each panel represents a different configuration whose code is given in the legend name.164
- Figure D.16 Fragility curves and quantile-quantile plots for URM buildings designed for Napoli on soil C. The line-style helps to distinguish among different structural characteristics. Solid and dashed lines represent, respectively, 2- and 3- story structures while the use of circle markers depicts an irregular configuration. Each panel represents a different configuration whose code is given in the legend name.166
- Figure D.17 Fragility curves and quantile-quantile plots for URM buildings designed for Roma on soil C. The line-style helps to distinguish among different structural characteristics. Solid and dashed lines represent, respectively, 2- and 3- story structures while the use of circle markers depicts an irregular configuration. Each panel represents a different configuration whose code is given in the legend name.167
- Figure E.1 Pushover bi-linearization according to NTC08 provisions..... 180
- Figure E.2 Pushover curves and their bi-linearization for L'Aquila (a), Napoli(b) and Roma(c) .. 181

## LIST OF TABLES

Table 2.1 Magnitude and Distance bounds considered as reference for CS-MR record selection procedure.....	13
Table 3.1 Location and design PGA levels (for soil types A and C) of the five selected cities .....	34
Table 3.2 Soil type A and C defined as a $V_{s,30}$ (Table 3.2II, NTC08).....	34
Table 3.3 Main Characteristics of the selected structural type .....	34
Table 3.4 Return periods for 10 Intensity Measure Levels .....	41
Table 3.5 Assumed EDP thresholds for Collapse and Damage limit states. ....	58
Table 3.6 Collapse threshold assumed for different EDPs of reference .....	60
Table 3.7 Parameters of the computed Fragility curves and corresponding collapse rate. ....	61
Table 3.8 Parameters of Fragility curves and corresponding collapse rates based on different EDPs and derived by means of Approach 2. ....	64
Table 3.9 Parameters of Fragility curves and corresponding collapse rates based on different EDPs and derived by means of Approach 3. ....	64
Table 4.1 Behavior factor and over-strength assumptions .....	75
Table 4.2 Limit state definitions .....	76
Table 4.3 Target MAF for each LS considered .....	84
Table 4.4 Different definitions of RT-Spectra determination approaches as adopted in the literature and as proposed herein for the case of EN1998. ....	86

## LIST OF TABLES IN APPENDIX

Table A.1 Ground motion recordings from subduction events added to the NGA-w2 crustal database.....	113
Table A.2 Details about MDoF systems taken as reference.....	115
Table A.3 Number of records selected according to the considered selection criteria.....	116
Table A.4 Collapse rates differentiated by Period, Structural type and Record Selection procedure.....	118

---

Table D.1 Damage- and Collapse- fragility curves parameters for Masonry structures on soil C.	143
Table D.2 Damage- and Collapse- fragility curves parameters for Masonry structures on soil C.	145
Table D.3 Collapse and Damage rates Masonry Structures in L'Aquila when local site condition is C according to Eurocode 8 classification .....	168
Table D.4 Collapse and Damage rates Masonry Structures in L'Aquila when local site condition is A according to Eurocode 8 classification .....	168
Table D.5 Collapse and Damage rates Masonry Structures in Napoli when local site condition is C according to Eurocode 8 classification .....	168
Table D.6 Collapse and Damage rates Masonry Structures in Napoli when local site condition is A according to Eurocode 8 classification .....	169
Table D.7 Collapse and Damage rates Masonry Structures in Roma when local site condition is C according to Eurocode 8 classification .....	169
Table D.8 Collapse and Damage rates Masonry Structures in Roma when local site condition is A according to Eurocode 8 classification .....	170
Table D.9 Collapse and Damage rates Masonry Structures in Caltanissetta when local site condition is C according to Eurocode 8 classification .....	170
Table D.10 Collapse and Damage rates Masonry Structures in Caltanissetta when local site condition is A according to Eurocode 8 classification .....	170
Table D.11 Collapse and Damage rates Masonry Structures in Milano when local site condition is C according to Eurocode 8 classification .....	171
Table D.12 Collapse and Damage rates Masonry Structures in Milano when local site condition is A according to Eurocode 8 classification .....	171
Table D.13 Collapse and Damage rates for Precast Structures in L'Aquila when local site condition is C according to Eurocode 8 classification .....	172
Table D.14 Collapse and Damage rates for Precast Structures in L'Aquila when local site condition is A according to Eurocode 8 classification .....	172
Table D.15 Collapse and Damage rates for Precast Structures in Napoli when local site condition is C according to Eurocode 8 classification .....	172
Table D.16 Collapse and Damage rates for Precast Structures in Napoli when local site condition is A according to Eurocode 8 classification .....	173
Table D.17 Collapse and Damage rates for Precast Structures in Milano when local site condition is C according to Eurocode 8 classification .....	173
Table D.18 Collapse and Damage rates for Precast Structures in Milano when local site condition is A according to Eurocode 8 classification .....	173
Table D.19 Collapse and Damage rates for Reinforced Concrete Structures in L'Aquila when local site condition is C according to Eurocode 8 classification .....	174

Table D.20	Collapse and Damage rates for Reinforced Concrete 9-storey frames in L'Aquila when local site condition is A according to Eurocode 8 classification .....	174
Table D.21	Collapse and Damage rates for Reinforced Concrete Structures in Napoli when local site condition is C according to Eurocode 8 classification .....	175
Table D.22	Collapse and Damage rates for Reinforced Concrete Structures in Roma when local site condition is C according to Eurocode 8 classification .....	175
Table D.23	Collapse and Damage rates for Reinforced Concrete Structures in Caltanissetta when local site condition is C according to Eurocode 8 classification .....	175
Table D.24	Collapse and Damage rates for Reinforced Concrete Structures in Milano when local site condition is C according to Eurocode 8 classification .....	176
Table D.25	Collapse and Damage rates for Steel Structures in L'Aquila when local site condition is C according to Eurocode 8 classification .....	176
Table D.26	Collapse and Damage rates for Steel Structures in L'Aquila when local site condition is A according to Eurocode 8 classification .....	177
Table D.27	Collapse and Damage rates for Steel Structures in Napoli when local site condition is C according to Eurocode 8 classification .....	177
Table D.28	Collapse and Damage rates for Steel Structures in Napoli when local site condition is A according to Eurocode 8 classification .....	177
Table D.29	Collapse and Damage rates for Steel Structures in Milano when local site condition is C according to Eurocode 8 classification .....	177
Table D.30	Collapse and Damage rates for Steel Structures in Milano when local site condition is A according to Eurocode 8 classification .....	178
Table D.31	Collapse and Damage rates for Steel Structures in L'Aquila when local site condition is C according to Eurocode 8 classification .....	178
Table E.1	Ultimate ductilities computed from bi-linearized pushover curves .....	181
Table E.2	Over-strength computed from bi-linearized pushover curves .....	182



## 1. INTRODUCTION

The notion of performance-based seismic assessment and design has been conceived and developed during the early 2000s by Cornell and Krawinkler [2000]. In line with what had been done before for other structures, such as reactors in nuclear plants and offshore platforms, they proposed the idea that the adequacy of existing buildings and of those to be designed should be evaluated using a probabilistic approach. This means that the actual objectives of the engineering assessment and analyses are not just achieving an acceptable level of physical characteristics (e.g. shear/displacement capacities, still obviously used in the evaluation process) but also of quantities such as the mean annual frequency (MAF) of the loss exceeding a given amount of dollars or the MAF of a properly defined limit state (LS), e.g. Collapse. Those MAFs are computed for critical decision variables (DV) that form the basis for judging the considered structure/design satisfactory or not. The evaluation of the distribution of a DV needs information coming from structural analysis as well as from other related fields like engineering seismology, i.e. the seismic hazard. In particular, the introduction of structural damage measures (DM), structural response measures (EDP) and ground motion intensity measures (IM) allows deconstructing the calculation of DV rates,  $\lambda_{DV}$ , in four main parts, namely i) hazard analysis, ii) demand analysis, iii) fragility analysis and iv) failure or loss estimation. The following expression shows the well-known risk integral that constitute the strong basis of performance-based earthquake engineering (PBEE):

$$\lambda_{DV} = \iiint G(DV | DM) \cdot dG(DM | EDP) \cdot dG(EDP | IM) \cdot d\lambda_{IM} \quad (1.1)$$

Where  $G(DV | DM)$  is the probability that DV (e.g. monetary loss) exceeds a specified value conditional on knowing that DM assumes a particular value (e.g. response threshold associated to Collapse or any other limit state). Moreover,  $G(DM | EDP)$  represents the probability that the DM exceeds this threshold given the structural response quantified in terms of EDP.  $G(EDP | IM)$  is the probability of observing a certain response (EDP) given that IM equals a particular ground motion intensity value. The connection between EDP and IM requires careful structural modelling and analyses, e.g. Incremental dynamic analysis (IDA) (Vamvatsikos and Cornell [2002]) or Multiple Stripe Analysis (MSA) (Baker [2007]; Jalayer and Cornell [2009]). Finally,  $\lambda_{IM}$  is the MAF of the intensity measure typically extracted from a hazard curve calculated by means of classical Probabilistic Seismic Hazard Analysis (PSHA). The integral (1.1) is written hypothesizing that the conditioning information does not propagate; this means, for example, that the

intensity measure (IM) should be chosen in order to avoid dependence of the structural response (or damage measure, DM) on any parameters of the causative earthquake (e.g. magnitude and distance) that have already been accounted for in PSHA calculations. Moreover, the proper choice of intermediate random variables should be done balancing two aspects apparently in contrast: simplicity and effectiveness. For example, describing the ground motion by means of Peak Ground Acceleration (PGA) as an IM is certainly appealing for its diffusion and simplicity but this choice will affect the definition of the distribution  $G(DM|IM)$  resulting in high variability for DM structures whose response is not much affected by short natural periods. However, this broad variability does not imply that the structural response cannot be assessed with sufficient confidence but simply that a large sample of carefully selected ground motion records are necessary to cover the poor choice of PGA as the only piece of information that characterize an entire ground motion time history. In general, one could argue that the perfect IM does not exist: even a complex scalar IM (Kohrangi et al. [2017a]), or a set of vector IMs (Kohrangi et al. [2015a], [2015b]) could possibly miss information with the result that some bias may occur in response estimation. In this context, a careful record selection plays an important role by implicitly fixing the deficiencies caused by a poor IM choice. The present work investigates different aspects of this PBEE framework with the final scope of loss assessment and, possibly, loss reduction and safety enhancement.

The thesis is organized in three main chapters that can be seen also as stand-alone works. *Chapter 2* regards the development of a record selection procedure that is hazard-consistent in terms of both spectral shape and parameters of the causative earthquake. The studies of Baker and his associates (Baker [2011]; Baker and Jayaram [2008]; Chandramohan et al. [2016a]; Jayaram et al. [2011]; Lin et al. [2013a]; Lin et al. [2013b]; Lin et al. [2013c]) developed a record selection procedure focused on the assumption that spectral shape is the only ground motion characteristic that influence structural response. In particular, the well-known Conditional Spectrum method allows selecting sets of records that, after scaling, are coherent with the distribution of all the spectral accelerations different than the chosen IM conditioned on observing at the site of interest the chosen IM, i.e. spectral acceleration at the natural period of the structure,  $Sa(T_1)$ . Recent studies have further refined this approach by extending the procedure to more sufficient<sup>a</sup> spectral IMs (e.g. AvgSA, Kohrangi et al. [2017a]) that are more suitable for response prediction than, for example,  $Sa(T_1)$  or PGA or to other quantities that have nothing to do with spectral shape (e.g., duration) (*GCIM*, Bradley [2010], [2012]), if these quantities are considered crucial for response prediction. Our proposal here is to work within the boundaries of the CS method framework but forcing the selection to be

---

<sup>a</sup> An IM is defined sufficient if the distribution of building response, EDP, conditioned on the IM is independent from other ground motion properties, such as magnitude, distance, etc.

consistent with both spectral shape, as traditionally done, but also with the parameters of earthquakes that contribute significantly to the site hazard. In this way, other quantities that could influence structural response (e.g. duration, PGV, PGD or any other quantity) are implicitly, albeit not perfectly, accounted for in a statistical manner. The proposed selection procedure will be tested against other approaches (*GCIM*-based and *CS*-based) in the literature in order to verify its effectiveness and define its pros and cons. The tests are performed subjecting a 2D prototype building to ground motion sets chosen according to selection procedures characterized by different working hypotheses.

The second part of this work (*Chapter 3*) takes advantage of the record selection procedure developed in *Chapter 2* to assess the implicit collapse risk of buildings designed according to the Italian seismic code provisions (NTC [2008b], NTC08). A code-conforming building is typically designed to withstand a ground motion intensity associated with a conveniently low probability of being exceeded (typically 10% in 50 years) at the site during the lifetime of the structure. The code imposes the adoption of safety factors that amplify the loads and decrease the resistance in order to achieve an acceptable but undefined level of safety. In some codes, the safety factors are selected on the basis of extensive Load and Resistance Factor Design (LRFD) studies. Unfortunately, this is not the case for the NTC08 code. Hence, the designer does not know, for example, the annual probability of buildings designed according to those load and resistance factors. The aim, herein, is to fill this gap defining the implicit risk of collapse (and of damage) associated to NTC08 code-compliant buildings. The calculation will follow the Performance Based Earthquake Engineering framework accounting solely for some sources of uncertainties (e.g. the record-to-record variability thanks to a careful record selection technique). Since not all the possible sources of uncertainties are modelled, the computed rates are labelled as nominal. The research conducted herein is part of an important (still ongoing) project (RINTC-Workgroup [2017]) funded by Italian Civil Protection and involves several research units from all over Italy, each of them with their own field of expertise. Beyond the importance of knowing the risk associated to code-conforming buildings, the outcomes and the framework of this project could serve as a strong basis for possible future developments of code provisions.

Since widely adopted code provisions (e.g. NTC08 and Eurocode) dictate design for fixed levels of hazard, they are likely to ‘produce’ structures characterized by a non-uniform risk of reaching collapse and other limit states that vary with the location of the building in Italy and with its structural typology. Luco et al. [2007] proposed a procedure that theoretically allows designing structures characterized by a constant collapse risk. In particular, for each site across the country, the distribution  $G(DM|IM)$  of equation (1.1) is iteratively changed until one is found that ensures a targeted acceptable level of risk. This process introduces the definition of ‘risk factors’ or ‘adjustment factors’ that should be applied at design accelerations in order to guarantee the wanted risk level. The final

products are the so-called Risk-Targeted ground motion (RTGM) maps, such as those currently adopted in US code provisions, ASCE [2010]. In particular, two maps are provided in that reference: one for each of the anchoring points of the US design spectrum, namely  $Sa(0.2s)$  and  $Sa(1.0s)$ . Clearly this procedure is theoretical and considerably affected by the assumptions done about the  $G(DM|IM)$  that describes the structural behavior under various level of seismic excitation. In other words, the iterative procedure alluded to before assumes that one knows the vulnerability of a building during the design procedure, which is clearly not the case. Designing a building according to RTGM maps ensures a final risk of, say, collapse that is close to the target one only if the assumed collapse fragility curve is indeed close to that of the building to be designed. In the last part of the thesis (*Chapter 4*), the idea of a risk-based design paradigm is investigated with particular emphasis on Europe. Simplified structures, conforming to Eurocode provisions and consistent with those designed in the RINTC project are adopted to define a Risk Targeted Spectra that can guarantee not a uniform risk, as claimed by the original proposers of this concept, but at last a more harmonized risk among different sites and different building types. More specifically, the use of simplified structures is practical since it allows a quick iterative design by updating the main parameters (i.e. ductility and strength factor) and, therefore, investigating the actual impact of the adoption of Risk Targeted-Spectra. Several strategies and targets are evaluated in order to investigate the strengths and weaknesses of the procedure and, possibly, provide insights on actual implementation in future building codes.

Finally, the *Conclusion* summarizes the entire thesis revisiting the objectives and the findings and offers some suggestions about future research that might help making this work more fruitful and increment the likelihood of its adoption in common practice.

## 2. CS-BASED RECORD SELECTION CONSISTENT WITH MAGNITUDE AND SOURCE-TO-SITE DISTANCE OF FUTURE EARTHQUAKE SCENARIOS

### 2.1 SUMMARY

Record selection comes at the interface of seismic hazard and structural analysis in order to repair any loss of essential seismological dependencies caused by an insufficient intensity measure. Site-specific selection is best exemplified by the prominent Conditional Spectrum (CS) approach that attempts to ensure a hazard consistent response prediction by involving site hazard disaggregation results. Specifically, CS utilizes a target spectrum (mean and dispersion of) that, in its most recent formulation, is generated by accounting for all the contributing scenarios (in terms of magnitude,  $M$ , and closest to rupture distance,  $R$ ) to the hazard of the site at a given intensity level. The records are selected to match this target spectrum, regardless of the underlying M-R characteristics. The main focus of this study is to explore whether the reintroduction of M-R criteria in the selection process preserves hidden dependencies that may otherwise be lost through a spectral-shape-only proxy. The proposed selection procedure method, termed *CS-MR*, offers a simple approach to maintain a higher order of hazard consistency that should be able to indirectly account for metrics that depend on M-R (e.g. duration, Arias Intensity, CAV). Herein the *CS-MR* response prediction is favorably compared to CS and the generalized conditional intensity measure (*GCIM*) methods that collect records accounting, respectively, for spectral shape only, and spectral shape plus duration.

### 2.2 INTRODUCTION

State-of-the-art performance based earthquake engineering (PBEE) Cornell and Krawinkler [2000] includes evaluation of the structural response, i.e. engineering demand parameters (EDPs), at multiple levels of ground motion intensity. In this framework, EDPs caused to a structure by a ground motion are predicted only through the knowledge of a single intensity measure (IM) that describes it, be it PGA or spectral acceleration at a given period of vibration. Given the significant advances in finite element software, nonlinear dynamic analysis (NDA) has become the most commonly used tool in research, and often in practice, for structural response analysis. NDA requires a suite of records to represent the expected seismic actions at the site and record selection is the tool that allows connecting the structural response to the seismic hazard. In a full probabilistic PBEE, probabilistic seismic hazard analysis (PSHA) Cornell [1968]; McGuire [1995] provides the rate of exceedance of the IM of choice; consequently, at any intensity level, the computed hazard can be disaggregated Bazzurro and Cornell [1999] to identify the contributing scenarios (e.g. magnitude, distance to rupture, tectonic regime) to that specific IM level. Disaggregation analysis has shown that the contribution of

different earthquake scenarios changes with the intensity level. On top of that, recent studies have also shown that, in general, the knowledge of a single IM is not sufficient to predict structural response of buildings because it is affected by other quantities, such as spectral shape and duration of the motion. In other words the vulnerability/fragility representation based on a single IM is also dependent on the types of ground motions that are caused by the peculiarity of the future seismic events that may affect the site (e.g. Kohrangi et al. [2017c]) beyond just the probabilistic knowledge of the chosen IM. A more accurate prediction of the response can be achieved by selecting sets of records that best represents the ground motions that can be experienced at the site.

Record selection does not always receive the attention it deserves by practitioners. In fact, NDA is often performed using predefined site independent record sets, such as those proposed in FEMA P695 (ATC-63 [2009]) and at times by means of an *ad-hoc* record selection schemes that in some way account for site-hazard characteristics. In the existing literature, different record selection schemes were proposed in order to guarantee the *consistency* of the selected records with the hazard. These schemes might be classified into two main categories: namely ‘scenario-based selection’ and ‘target-based selection’ Beyer and Bommer [2007]. In the former, the selected records fall in bins around central values of seismic parameters such as magnitude, source-to-site distance, site class and epsilon (Baker and Cornell [2005]; Bommer and Acevedo [2004]; Jayaram and Baker [2010]; Stewart et al. [2001]). If PSHA is available, the parameters of the scenario that contribute most to the hazard at the site are obtained from disaggregation analysis. In this class of methods, one assumes that all the seismic effects of the site that matter for structural response will be implicitly carried by selecting records on the basis of the parameters of the scenario earthquakes of interest. Therefore, the hazard consistency is somehow considered only in terms of the selection of the scenario(s) contributing the most to the hazard. In the ‘target based’ approach, instead, a set of records is selected to match a target spectrum or a target distribution of any ground motion intensity measure of interest (Baker [2011]; Beyer and Bommer [2007]; Bradley [2010]; Jayaram et al. [2011]; Kottke and Rathje [2008]; Naeim et al. [2004]; Shantz [2006]; Wang [2011]; Watson-Lamprey and Abrahamson [2006]; Youngs et al. [2007]). The conditional mean spectrum (CMS), the conditional spectrum (CS) and the generalized conditional intensity measure (GCI) approaches belong to this second group.

CMS (Baker [2011]; Baker and Cornell [2006a]) accounts for hazard consistency only in terms of the median of the target spectrum, while CS (Jayaram et al. [2011]) goes one step forward including, as its target, both the median and variance of the spectral ordinates. CS and CMS, in their most recent formulation, are able to implicitly account for the contributing scenarios to the seismic hazard only when generating the target spectra. For these methods spectral shape is the most important (or better, the only important) quantity that is presumed to affect the structural response. Therefore, according to this

assumption, there is no need or, better, no gain in enforcing record selection to be hazard consistent also in terms of any other earthquake causative parameter. Spectral shape is for sure of paramount importance in estimating building response but it is often not all that matters. Although some studies on this topic did not find any effect, for example, of duration on building response (Bommer et al. [2004]; Hancock and Bommer [2006]; Hancock and Bommer [2007]; Iervolino et al. [2006]), some other works argued that the building response could be significantly affected by parameters other than the spectral shape (e.g. record duration Raghunandan and Liel [2013]) if appropriate modeling assumptions are adopted. Among others, Chandramohan et al. [2016a]; Chandramohan et al. [2016b] showed this dependence by subjecting a building characterized by cyclic degradation behavior, to two spectrally equivalent record sets, representing ground motion records with short and long durations, respectively. This study demonstrated that the response of a properly modeled duration sensitive structure could be highly influenced by record duration.

*GCIM* (Bradley [2010]) extends the concept of CS to a generalized format by explicitly including any parameter that is supposed to impact the structural response (not only the spectral acceleration); thus it prescribes the consistency of those parameters with the site hazard. On the same lines, Chandramohan et al. [2016a] used *GCIM* method in order to test the impact of hazard-consistent ground motion duration on structural collapse risk assessment. This study concluded that, neglecting the impact of duration at sites with distinct duration importance, e.g. at sites whose hazard is affected by both nearby crustal faults and also by subduction zones farther away, may result in biased estimates of the collapse rate. Additionally, the cited work has analyzed a selection procedure employing causal parameters in tandem with the application of the CS method (namely *CS and causal parameters*). The authors concluded that, due to the limited number of records able to satisfy the typical constraints on the causal parameters, such approach will provide poor consistency with the hazard both in terms of spectral acceleration and ground motion duration. On the other hand, recent studies on this topic (Baker and Lee [2016]; Tarbali and Bradley [2016]), proposed to filter out the record database according to M-R bounds prior to the actual selection. They showed that the choice of a wide bound on causal parameters effectively removes ground motions with drastically different characteristics with respect to the target seismic hazard (e.g. CS and *GCIM*) and results in more efficient record selection.

In the present study, we provide an alternative record selection procedure for the *CS and causal parameters* approach of Chandramohan et al. [2016a]; Chandramohan et al. [2016b] forcing the selection to hold the consistency with both the spectral shape and the distribution of the parameters of the causative earthquakes, namely magnitude and distance (hereafter abbreviated by M and R). This approach performs well in matching the target spectrum (mean and variance) and implicitly provides acceptable hazard

consistency in terms of duration, as well. NDA results based on the proposed method are compared with those obtained using *GCIM* and the ‘classical’ CS approach (conjugated both in the most and the least accurate version) for a reference duration sensitive structure located in Seattle.

## 2.3 CONDITIONAL SPECTRA INCLUDING CAUSAL PARAMETERS—CS-MR

### 2.3.1 Conditional spectra based record selection

CS record selection approach (Jayaram et al. [2011]; Lin et al. [2013a]; Lin et al. [2013c]) consists of two main steps of: i) generation of target spectra including a conditional mean and dispersion of spectral accelerations at multiple vibration periods conditioned on the IM of choice and, ii) an efficient simulation algorithm integrated with an optimization technique which allows selecting and scaling a suite of records that collectively “match” the simulated target. The conditioning IM could be any spectral ordinate that is relevant to the response of the structure such as spectral acceleration at the first modal period of the structure,  $Sa(T_1)$ , or the spectral acceleration averaged in a period range,  $AvgSA$  (Kohrangi et al. [2017a]) for which PSHA and disaggregation analysis could be conducted. Target CS stands on the application of available ground motion prediction equations (GMPEs), with the input of (causal) parameters that represent the hazard, together with the correlations between the spectral accelerations at different periods (e.g. Baker and Jayaram [2008]). In generating the target spectrum, some studies made use of the mean value of causal parameters (e.g. mean of magnitude and distance); this approach is usually labeled as the ‘approximate’ method. Lin et al. [2013a], accounting for the variability in the target spectra due to multiple causal parameters (from disaggregation analysis) and GMPEs (adopted in hazard computations), proposed an ‘exact’ method, that modifies the target spectra by inflating the target conditional dispersion and adjusting the target conditional median values.

Once the target spectra are generated, using the multivariate lognormal distribution and based on the lognormality assumption of the spectral accelerations (Jayaram and Baker [2008]),  $N$  spectra (with  $N$  representing the number of required records in the set) are simulated. Then, the  $N$  records that ensure, one by one, the best match with the simulated spectra are selected from a reference strong ground motions database. CS benefits also from a ‘greedy’ optimization technique: the selected records’ spectra are substituted one at a time with the unselected ones in order to further improve the match with the target mean and dispersion. The CS procedure, even when utilizing the exact method, ideally reproduces the expected spectral shape at the site; however, the selected records will not necessarily reproduce the distribution of the causal parameters  $M$  and  $R$  obtained from disaggregation analysis. It could be argued that magnitude and distance of the recorded events could be considered as proxy measures (in addition to spectral shape) for other ground motion characteristics (e.g. duration,  $PGV$ ) that may be considered

important for predicting the behavior of the structure. *GCIM* (Bradley [2010]) can explicitly account for the distribution of such characteristics in record selection but its application is not straightforward for users that are not very well versed in probability and statistics. Therefore, in practice there is still a tendency on application of causal parameter bounds in selection of records (Torbali and Bradley [2016]). In the following section, we propose a supplementary algorithm that improves the existing CS record selection algorithm to explicitly account for magnitude and distance distributions.

### 2.3.2 Proposed post processing algorithm to CS accounting for causal parameters (CS-MR)

Herein, the method of CS record selection has been extended developing a post-processing algorithm, from now on called *CS-MR*, which accounts for the earthquake ground motion's causal parameters. Disaggregation analysis quantifies the contribution of the causal parameters at any specific hazard level (e.g. 10% in 50 years). Therefore, after the user has chosen multiple bins for magnitude and distance, the proposed algorithm provides a set of records that, in addition to the spectral shape of the CS, considers the contribution of each M-R bin identified by the disaggregation results. In particular, after the CS record selection is completed, the algorithm discards the records that do not belong to any of the desired M-R bins and those that exceed (in number) the contribution of each bin to the specific hazard level; then it adds other ground motions creating a set that is consistent with both disaggregation results and spectral acceleration distribution.

Let  $N$  be the total number of records in the set (say 20),  $N_i$  the number of records in the  $i^{th}$  bin and  $P_i$  the percentage of the  $i^{th}$  bin's contribution to the hazard (say 22%). The number  $N_i$  of desired records from the  $i^{th}$  bin in the final ensemble is the nearest integer of  $P_i \times N$  (here 4). Therefore, if in the first pass there are too few records from the  $i^{th}$  M-R bin (say 3) the missing number of records with this M-R characteristics (in this case 1) is added to the ensemble and the same number is removed from other bins that had too many records. Given the overall criterion of matching the CS, among all possible records in the database from the  $i^{th}$  M-R bin the algorithm adds the one that has the closest spectral shape to one that has been removed. The similarity between a ground-motion response spectrum and a discarded response spectrum is evaluated using the sum of squared errors (*SSE*) shown in Equation (2.1):

$$SSE = \sum_{n=1}^H \left( \ln Sa(T_n) - \ln Sa^{(s)}(T_n) \right)^2 \quad (2.1)$$

where  $\ln Sa(T_n)$  is the logarithmic spectral acceleration of the scaled ground motion at period  $T_n$ ,  $\ln Sa^{(s)}(T_n)$  is the target  $\ln Sa$  at period  $T_n$  from one of the discarded response spectra,  $H$  is the number of periods considered and *SSE* is the sum of squared errors, which is a measure of dissimilarity. This procedure is repeated for all the bins to

cover all of the missing records of the set. However, this procedure is not all performed once but  $K!$  times where  $K$  is the number of M-R bins considered in the disaggregation. The final selected ensemble is the one among the  $K!$  sets that provides the lowest discrepancy (namely the lowest  $SSE_s$  according to Equation (2.2)) from the original target spectrum. The error  $SSE_s$  is computed according to what suggested by Jayaram et al. [2011]:

$$SSE_s = \sum_{n=1}^H \left( \hat{m}_{\ln Sa(T_n)} - \mu_{\ln Sa(T_n)}^{(t)} \right)^2 + w \cdot \left( \hat{s}_{\ln Sa(T_n)} - \sigma_{\ln Sa(T_n)}^{(t)} \right)^2 \quad (2.2)$$

where  $SSE_s$  is the sum of squared errors of the set, which is the parameter to be minimized,  $\hat{m}_{\ln Sa(T_n)}$  is the set mean  $\ln Sa$  at period  $T_n$ ,  $\mu_{\ln Sa(T_n)}^{(t)}$  is the target mean  $\ln Sa$  at period  $T_n$ ,  $\hat{s}_{\ln Sa(T_n)}$  is the set standard deviation of  $\ln Sa$  at period  $T_n$ ,  $\sigma_{\ln Sa(T_n)}^{(t)}$  is the target standard deviation of at  $\ln Sa$  period  $T_n$  and  $w$  is a weighting factor indicating the relative importance of the errors in matching the standard deviation and the mean. In line with the procedure performed for the exact CS approach (Lin et al. [2013a]),  $w$  has been assumed equal to 2, giving a higher degree of importance in the matching the target standard deviation rather than the target mean.

## 2.4 QUALITIES AND CHALLENGES OF CS-MR RECORD SELECTION

### 2.4.1 Which ground motion characteristics are correlated to M and R?

At this stage, a question could be raised: ‘what is the advantage of selecting the records consistent with hazard disaggregation of M and R?’ Intuitively, this procedure, besides imposing the spectral shape via the CS framework, ‘naturally’ accounts for other ground motion characteristics that are correlated with M and R. Two supporting arguments to the usefulness of M-R based CS record selection and challenges in implementing it are provided in the following lines.

Firstly, since it makes use of the same target spectrum of the CS method, one may think that adopting the *CS-MR* approach may not bring any additional advantage in terms of improving the hazard consistency of the spectral shapes of the selected records. However, this is not completely true: the CS approach selects a set of records that collectively reproduce the target conditional distribution of spectral accelerations at site. However, the CS method does not check whether the single spectral shape of each selected record is “appropriate” for the site and intensity level of interest. The CS method could lead to selecting records that were not caused by earthquake scenarios with the same M and R that are expected to cause the exceedance of that ground motion level at the site. In other words, given the high dependency of the spectral acceleration on M and R, the selected records may only have collectively the desired spectral shape but not

singularly. For instance, considering a high IM level mainly controlled by large magnitude and short distance events, records associated with low magnitudes and large distances might be selected to fit the distribution of the set because of their large  $S_a$  values at short periods and low  $S_a$  values at longer periods. The *CS-MR*, however, provides an internal control on the selected records avoiding the choice of spectral shapes that may not be experienced at the site by using M and R as its proxy. Of course, the *CS-MR* method has also some challenges. Due to the limited available database of records, finding ground motions that simultaneously have both the expected M and R and the required spectral shape is not an easy task. Therefore, when using *CS-MR*, one has to accept a slightly less adherence with the target CS than what provided by the CS method. This is a compromise that needs to be in exchange for using ground motion records from earthquake scenarios that are likely to affect the site.

Secondly, since ground motion duration is a parameter that can significantly affect the structural response, a proper record selection procedure should account for its hazard consistency. Several metrics that consider duration exist in literature, e.g. significant duration ( $D_{S5-75}$  or  $D_{S5-95}$ ) (Trifunac and Brady [1975]), Arias Intensity ( $\mathcal{A}$ ) (Arias [1970]), cumulative absolute velocity ( $CAV$ ) (Electrical Power Research Institute [1988]; Reed and Kassawara [1990]), bracketed duration ( $D_{b,0.05}$ ) (Bolt [1973]). Chandramohan et al. [2016b] performed a comprehensive study and showed that  $D_s$  is superior to other duration metrics mainly because: i) it is not correlated to other common IMs (e.g.  $S_a(T, 5\%)$  and  $PGA$ ); ii) it is not dependent on record scaling; iii) it is not a hybrid metric of duration and intensity; iv) for a fixed spectral shape it is a more efficient predictor of the collapse capacity than other metrics. Herein, in line with the mentioned study,  $D_s$  is considered as the reference measure for validating *CS-MR* method in terms of duration's hazard consistency. Since  $D_s$  is strongly dependent on M and R and it is not function of scaling, the selected *CS-MR* record sets are expected (especially if the number of records is large) to naturally reproduce the duration distribution at the site. Because of the database limitation, *CS-MR* method needs the records to be scaled in order to fulfill the requirements in terms of spectral shape and causal parameters distribution. For this reason, unless the scaling factors are close to one, *CS-MR* approach may not be able to select records that match the distribution of intensity based metrics such as  $PGV$  and  $CAV$ . Indeed, even though they depend on causal parameters, they are not dimensionless and, therefore, sensitive to scaling.

Thirdly, the *CS-MR* method is less rigorous but intuitively simpler than the *GCIM* method where the user forces the selected records to match the distribution of pre-specified quantities (e.g., spectral ordinates and duration). Unlike the *GCIM* method, also the user of the *CS-MR* method does not need to decide a priori which ground motion characteristics are important for the response of the structure under consideration.

Besides spectral shape, the *CS-MR* method selects naturally records with the characteristics proper of the M and R bins that affect the hazard.

#### 2.4.2 Bin selection, criteria and assumptions

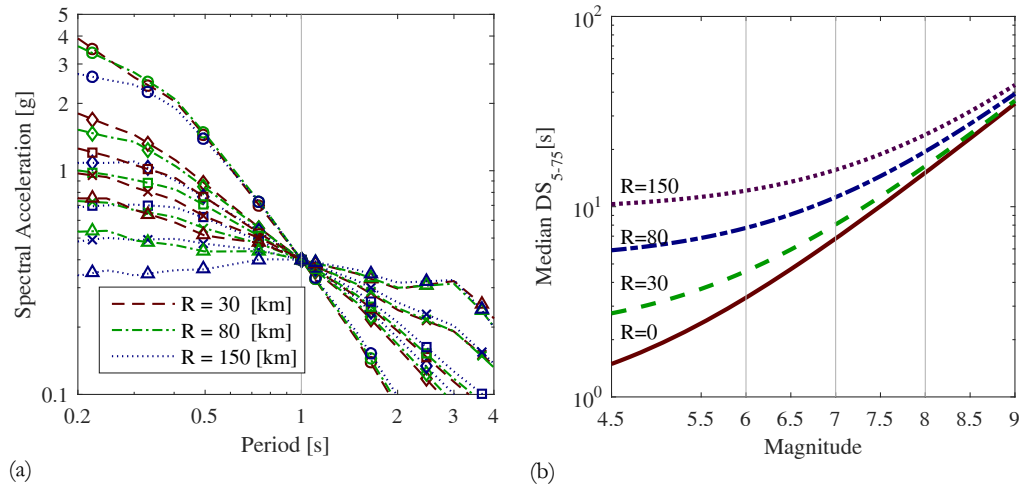
Prior to a target based record selection, typical and widespread approaches (e.g. Baker [2011]; Baker and Lee [2016]; Bommer and Acevedo [2004]) call for constraining the ground motion database on the basis of the causal parameters related to the scenarios that dominate the seismic hazard. These studies, however, either deal with a single scenario ground motion, with specific M and R values, or, if they are conducted for a PSHA-based record selection, they do not specifically introduce causal parameter bins to reproduce the distribution obtained from disaggregation. Tarbali and Bradley [2016], on the basis of a comprehensive test for thirty-six PSHA cases, investigated the impact of causal parameter bins prior to a *GCIM* based record selection. In order to be able to match the desired target, they suggested the application of wide bounds, especially on M and R, in accordance with the hazard disaggregation. That approach has the main advantages of i) reducing the computational effort because of the use of a trimmed database and, ii) avoiding the selection of records characteristics that are very different than those of the scenarios controlling the target seismic hazard. However, none of these approaches is capable to preserve the causal parameters' distribution provided by the hazard disaggregation.

*CS-MR*, on the other hand, aims to overcome the shortcomings of the aforementioned approaches maintaining a higher order of hazard consistency. In particular, as said, once appropriate bounds for M and R are defined, the procedure selects a set of ground motions consistently with the expected spectral shape and also with proper M-R characteristics. More specifically, an 'a-posteriori' M-R disaggregation of the record set will reflect exactly the same scenarios that contribute to the exceedance rate of the IM level for which the CS has been constructed. Table 2.1 shows the 12 M and R bins that were chosen in such a way that ground motions belonging to each bin, on average, have markedly different spectral shapes and  $D_{35-75}$  values. In addition, particular care was taken to account for diverse tectonic regimes that potentially could influence the hazard. It is known (e.g. Chandramohan et al. [2016a]) that the large interface subduction events are mainly characterized by magnitudes (typically  $>8$ ) higher than those of crustal and in-slab earthquakes. It should be pointed out that, for diverse locations, the bins could be modified according to the seismic sources that could potentially influence the seismic hazard. Finer and coarser bins were not considered since the former choice could make the record selection too computationally heavy (and sometimes impossible because of intrinsic limitation of the database), and the latter choice may not be sufficiently effective for the purpose of preserving the causal parameters distribution. Figure 2.1a shows the changes in the median spectral shape for the selected bins based on the GMPE of Boore

and Atkinson [2008] (BA08) for rock site conditions (i.e.  $V_{s30}=800\text{m/s}$ ). In this figure, all the spectra are normalized to  $Sa(T=1\text{s})=0.4\text{g}$  in order to make the differences in the expected spectral shape more obvious. Figure 2.1b shows the median  $D_{5-75}$  for the selected bins based on the GMPE of Abrahamson and Silva [1996] (AS96). Even though this GMPE is applicable to magnitudes up to M7.5, for illustration purposes only the median values have been extrapolated here to estimate durations until M9.0. Finally, it should be noted that the CS-MR algorithm can be applied for any user-defined set of bins that may be customized for the regional seismicity of interest. However, the bins proposed in this study represent a reasonable choice for most sites.

**Table 2.1** Magnitude and Distance bounds considered as reference for CS-MR record selection procedure

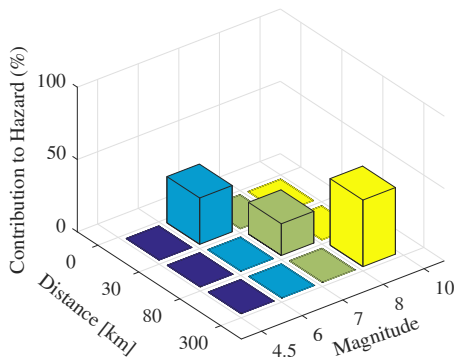
	<b>Bound 1</b>	<b>Bound 2</b>	<b>Bound 3</b>	<b>Bound 4</b>
<b>Magnitude (M)</b>	$4.5 \leq M < 6.0$	$6.0 \leq M < 7.0$	$7.0 \leq M < 8.0$	$M \geq 8.0$
<b>Distance (R) [km]</b>	$0 \leq R < 30$	$30 \leq R < 80$	$R \geq 80$	---



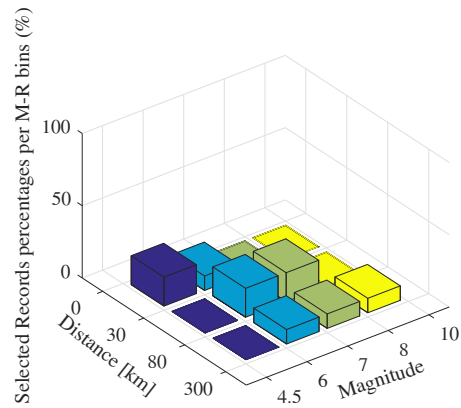
**Figure 2.1** (a) Illustration of the expected spectral shape of ground motion of different M-R scenarios (Legend: circle, M=4.5; diamond, M=6.0; square, M=7.0; cross, M=8.0; triangle, M=9.0) based on BA08; (b) median duration,  $D_{5-75}$  of selected earthquake scenarios based on AS96.

Figure 2.2 shows an illustrative example that compares the spectrum and M-R characteristics of a set of records before and after the application of the CS-MR procedure. In particular, Figure 2.2a shows the disaggregation results based on the coarse binning defined in Table 2.1 obtained from PSHA carried out for a site in Seattle for 5% in 50 year  $Sa(1.6\text{s}) = 0.37\text{g}$ . Initially, at the specified hazard level, a set of 100 records was assembled according to the CS-exact approach. Then the set was modified according to

the *CS-MR* procedure proposed here. The upper panels of Figure 2.2 compare the site disaggregation (Figure 2.2a) and the M-R records characteristics of the set selected according to the CS-exact method (Figure 2.2b), showing a clear discrepancy. In particular, while most of the hazard contributions at this hazard level come from bins with ‘M~6.0–7.0, R~0–30km’, ‘M~7.0–8.0, R~30–80km’ and ‘M~8–10, R~80–300km’, the records selected by the CS-exact method for this case are rather uniformly distributed among all the bins. Of course, the *CS-MR*’s selected record set by design exactly reproduces the disaggregation of MR distribution shown in Figure 2.2a. Figure 2.2c and 1.2d compare the two sets in terms of conditional median and dispersion, respectively. The price paid by keeping track of the M-R causative scenarios can be inferred comparing the red (CS-exact) and the blue lines (*CS-MR*) of Figure 2.2c and 2.2d, namely a slight inferior consistency with the target CS, particularly in terms of conditional dispersion. This discrepancy is only due to the limitation on the record database and it typically increases as the IM level grows. However, since these high levels of ground shaking are very rare, the observed differences do not influence significantly the loss estimation and only mildly the estimation of the collapse rate of most structures.



(a)



(b)

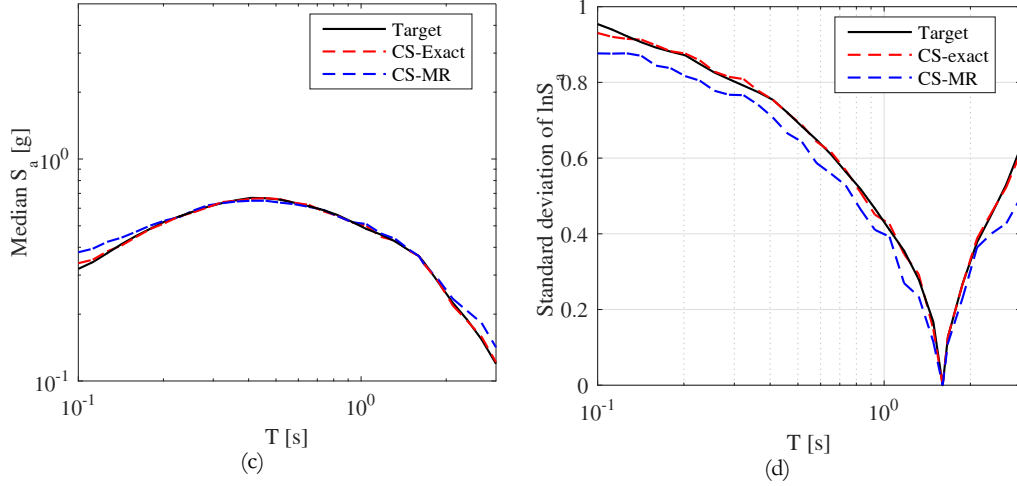


Figure 2.2 Comparison of record selection based on CS-exact and CS-MR methods for a site in Seattle corresponding to conditioning period of  $T=1.6$ s for 5% in 50 years event with  $S_a(T=1.6s)=0.37g$ . (a) M and R disaggregation; (b) M and R distribution of the selected records based on the CS-exact method, (c) median of the target and selected records' spectra, (d) conditional dispersion of the target and selected records.

## 2.5 CASE STUDY: RC MODERN FRAME LOCATED IN SEATTLE

### 2.5.1 Selected site and test building

The site of Seattle,  $122.3^\circ$  W longitude and  $47.6^\circ$  N latitude, was chosen as reference to illustrate the impact of different types of seismic sources on the evaluation of seismic hazard. Seattle is located in a tectonic region that is exposed to both crustal and subduction events due, respectively, to the faults located under the city and to the proximity of the Cascadia subduction zone. Figure 2.3b shows disaggregation results extracted from the USGS web tool (USGS [2012] and USGS [2008]) at 2% in 50 years exceedance probability for spectral acceleration at  $T=1$ s. The multimodal nature of the scenarios contributing to the hazard can easily be observed. In particular, the far and high magnitude earthquakes are caused by the Cascadia subduction zone while the closer events are due to the crustal faults beneath the city. Seven Ground Motion Prediction Equations (GMPEs) are included in the hazard model, namely Zhao et al. [2006], Youngs et al. [1997], Boore and Atkinson [2008], Campbell and Bozorgnia [2008], Chiou and Youngs [2008], Atkinson and Boore [2003].

The test building model is a 7 stories modern plan-symmetric reinforced-concrete moment-resisting frame designed according to post-1980 provisions for high seismicity regions (site class D) with the first modal period of vibration equal to  $T_1=1.6$ s. Because

the building is plan-symmetric, it has been modeled as 2D multi degree of freedom system; beam and columns are modeled as linear elements while the non-linearity is concentrated to the springs (represented as zero length elements) localized at the end of the elements. The chosen moment-curvature law that characterizes the springs follows the modified Ibarra-Medina-Krawinkler model (Ibarra et al. [2005]) which, on the basis of the cumulative hysteretic energy dissipated, is capable of capturing in-cycle deterioration, as well as cyclically deteriorating strength and stiffness. Moreover, the springs properties were estimated according to the proposal of Panagiotakos and Fardis [2001]. A pinned leaning column is included to model the destabilizing P-Delta effects of the gravity system. Additional details about modeling can be found in Kazantzi and Vamvatsikos [2015]. Maximum inter-story drift ratio (MIDR) larger than 10% and maximum residual drift ratios (RDR) larger than 4% are assumed to be the deterministic collapse thresholds in this study ATC-58 [2011].

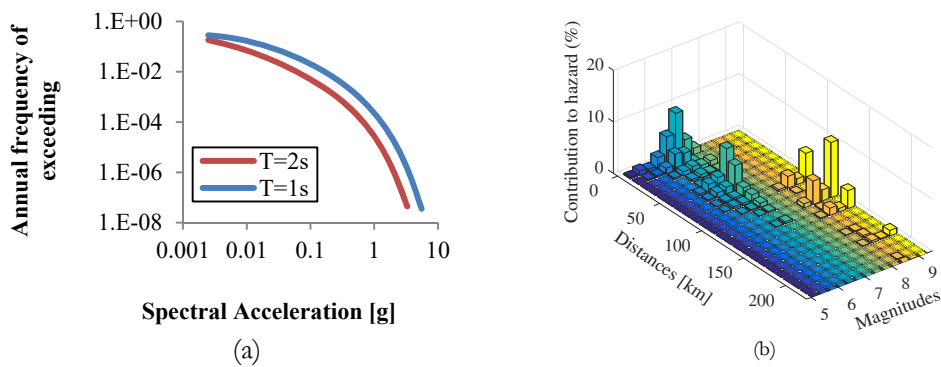


Figure 2.3 Hazard analysis results at Seattle for Soil Type D based on the USGS web tool: a) hazard curves for spectral accelerations at  $T=1s$  and  $2s$ ; b) M-R disaggregation results for 2% in 50 year spectral acceleration at  $T=1s$ .

Using the approach introduced by Chandramohan et al. [2016b], the sensitivity of the building model response to duration has been verified by performing a series of Incremental Dynamic Analyses (IDA) Vamvatsikos and Cornell [2002] based on two sets of 146 spectrally equivalent long- and short-duration records. More details about the selected records are available in Appendix A. Figure 2.4 **Errore. L'origine riferimento non è stata trovata.** shows IDA and the subsequent fragility collapse curves illustrating a clear building model's sensitivity to record duration. The building model's median collapse capacity, expressed in terms of  $Sa(T_1=1.6s)$  is equal to  $0.67g$  and  $0.46g$ , when using short- and long-duration sets respectively. This difference, given the equivalence in the spectral shape of the two sets, stems mainly from the cumulative damages due to the longer excitations of the long-duration record set. The impact of records duration observed here is probably emphasized with respect to a more realistic case analyzed using

a hazard consistent record set. Even though the record sets used herein are not meant to represent any particular site, this exercise serves the purpose of considering a building model whose response is indeed duration-sensitive and, consequently, suitable to test the differences caused by the proposed record selection method.

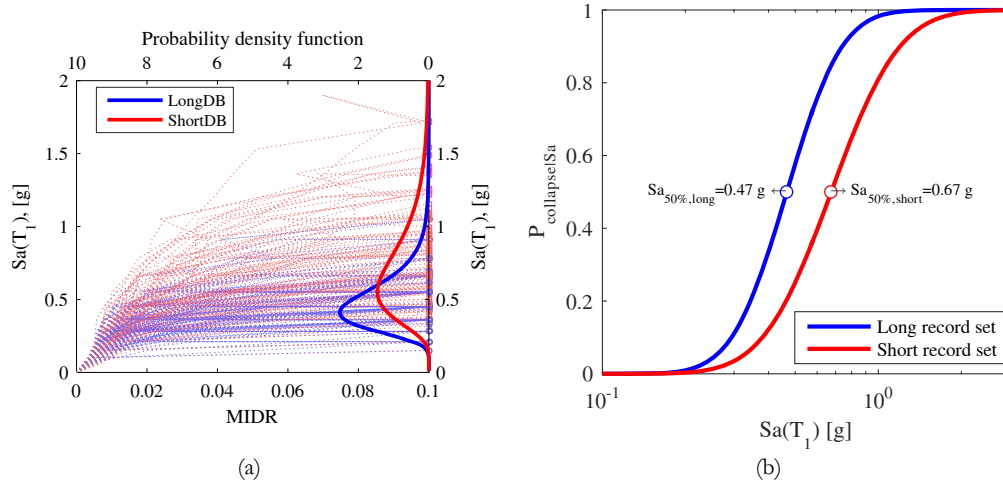


Figure 2.4 Verification of the building model's sensitivity to ground motion duration; comparison of: (a) IDA curves for MIDR; and (b) collapse fragility curves for two sets of 146 spectrally-equivalent short- and long-duration records.

## 2.6 GROUND MOTION SELECTION

The multiple stripe analysis technique (Jalayer [2003]), which allows the use of a different set of hazard consistent ground motions at each intensity level, was used to estimate the response of the structure until collapse. In order to evaluate the impact of including ground motion causal parameters in record selection, a risk-based assessment of the case study building has been carried out for three record sets selected according to different methods. Each of these approaches accounts for the causal parameters in a different manner. Given the demonstrated importance of spectral shape in predicting the building response, the scenario-based approaches are not examined since they do not explicitly account for it. Here the focus is on the target-based approaches, such as CS and *GCIM*. In particular, four different hazard consistent record sets conditioned on  $Sa(T_1)$  were considered. Each method includes 1,000 records equally split in ten sets, one per intensity level, corresponding to  $Sa(T_1=1.6s)$  equal to 0.06, 0.12, 0.17, 0.25, 0.37, 0.5, 0.63, 0.74, 0.83, 0.97g, which are associated to return periods between 30 and  $2 \cdot 10^4$  years at the site. Seismic hazard disaggregation results for  $Sa(T=1s)$  and  $Sa(T=2s)$  from USGS were interpolated to compute the targets conditioned on  $Sa(T_1=1.6s)$ .

The first set, called *CS-only* group, is selected on the basis of the exact approach of CS (Lin et al. [2013a]) that accounts for hazard consistency in terms of spectral shape only. In this record set, the M and R hazard contributions are only considered while defining the target CS spectra while the selected records, at each IM level, are not necessarily consistent with the M-R disaggregation and with the ground motion duration distribution. The computationally efficient algorithm developed by Jayaram et al. [2011]; Lin et al. [2013a]; Lin et al. [2013c] is the reference method used to assemble this set ground motion records. .

The second records set is selected by means of the proposed *CS-MR* method, which accounts for hazard compatibility in terms of both spectral shape and M-R distributions (defined in accordance with the binning proposed in Table 2.1). Even though this method does not explicitly account for ground motion duration, it is expected to define a record set that is able to naturally reproduce its distribution at the site. This assumption is supported by the  $D_s$  duration's dependency on M and R. Again, this method can be seen as a post processor of the original CS method. The associated computational algorithms and MATLAB scripts needed for the implementation of this method are available at the [web link](#).

The *GCIM* approach of Bradley [2010] is the reference method for the third ground motion set and it is structured in order to account explicitly for both spectral shape and duration, measured as  $D_{S5-75}$ , but does not care about records' native M-R characteristics. In particular, the algorithm of Lin et al. [2013a] has been modified by adding  $D_{S5-75}$  as an additional intensity measure to a vector of response spectral ordinates at different periods. *GCIM* has been tested also by using  $D_{S5-95}$  as duration metric but, since the results are fairly similar to those obtained with  $D_{S5-75}$ , they are presented only in terms of this latter duration measure. In line with what assumed in Chandramohan et al. [2016a], the quality of fit for the considered  $Sa$  and  $D_{S5-75}$  vector is assessed by means of the Kolmogorov-Smirnov test (K-S test) statistics. Similarly to the first approach, this third record set does not account for M and R distribution but includes explicitly the expected duration distribution at the site.

In addition to the aforementioned three record sets, a fourth set based on the original CS record selection has been adopted. In particular, this fourth set is based on the CS original method (Baker [2011]) (i.e. it considers the earthquake scenario that has the largest contribution to compute the target conditional spectrum), which does not contemplate a bin-specific record selection. This latter approach will be marked as '*CS approximate*' hereafter. The introduction of this fourth record is useful to compare the actual impact in risk estimates of adopting more advanced methods instead of the simplest CS-based approach (i.e. this *CS approximate*).

For sites where the hazard stems from multiple mixed scenarios or seismic source types (i.e., subduction in-slab, subduction interface and crustal), special attention should be given to selecting records such that they thoroughly represent each of the seismic source types. Chandramohan et al. [2016a] argued that computing only one target, using the method of Lin et al. [2013a], without discriminating between contributing earthquake scenarios coming from different seismic sources, would not reflect the related differences in ground motions characteristics. As such, in lines with the approach of Goda and Atkinson [2011], Chandramohan et al. [2016a] proposed the application of source-specific target by splitting the selection between possible contributing scenarios in terms of seismic sources. This approach also selects the number of records for each type of seismic source in proportion with its contribution to the hazard. Bradley [2012], on the other hand, suggested, without performing it, the selection of ground motions with causal parameters that are consistent with contributing earthquake scenarios from a probability mass function defined by the seismic hazard disaggregation weights. Practically, Tarbali and Bradley [2016] attempted to utilize the latter concept by allowing *GCIM* to select the records from a limited database. Nevertheless, since the ground motions are not allocated to different causal parameter bins in consistency with the related contributions, the selected record set does not necessarily reflect the hazard disaggregation's distribution.

Herein, to address the seismic source type impact on record selection, the *CS only* and *GCIM* sets are defined based on multiple bin-specific *CS* and duration target distributions. However, the actual record selection is performed regardless of the specific *M* and *R* of the causative earthquakes. The *CS-MR* method, on the other hand, does not generate multiple targets for each bin but it accounts for different seismic sources by selecting the records with hazard-consistent *M* and *R* characteristics. A first advantage of using the *CS-MR* method instead of the source-specific method of Chandramohan et al. [2016a] is that the former avoids multiple record selections runs by defining the whole set in one round.

The four methods were applied for selecting hazard-consistent records from the same user-defined database. In particular, the crustal events from the NGA West2 database were integrated with 4106 ground motions recorded in subduction zone earthquakes. The subduction ground motions were caused by earthquakes with magnitudes between 7.5 and 9.0, namely the 2003 Tokachi (Japan), 2007 Kuril Island (Russia), 2011 Tohoku (Japan), 2011 Iquique (Chile), 2013 Okhotsk Sea (Russia), 2015 Chi Chi Shima (Japan) and the 2015 Illapel (Chile) earthquakes CESMD [2012]. Figure 2.5a shows the scatter plot of *M* and *R* of the ground motion database along with the *M-R* bounds that limit the bins defined Table 2.1 and properly numbered herein. This additional effort was necessary mainly for the *CS-MR* method, which needs a reference database that includes records with *M-R* characteristics compatible with the scenarios that mainly contribute to the site hazard. As already pointed out earlier, Seattle's seismic hazard is known to be

influenced by both crustal and subduction regimes (Figure 2.3) that typically produces motion with different durations. In particular, the latter regime is usually connected with longer motions. Figure 2.5b shows the scatter plot of magnitude versus  $D_{5-75}$ , somehow highlighting the diverse ground motion durations that characterize the two databases.

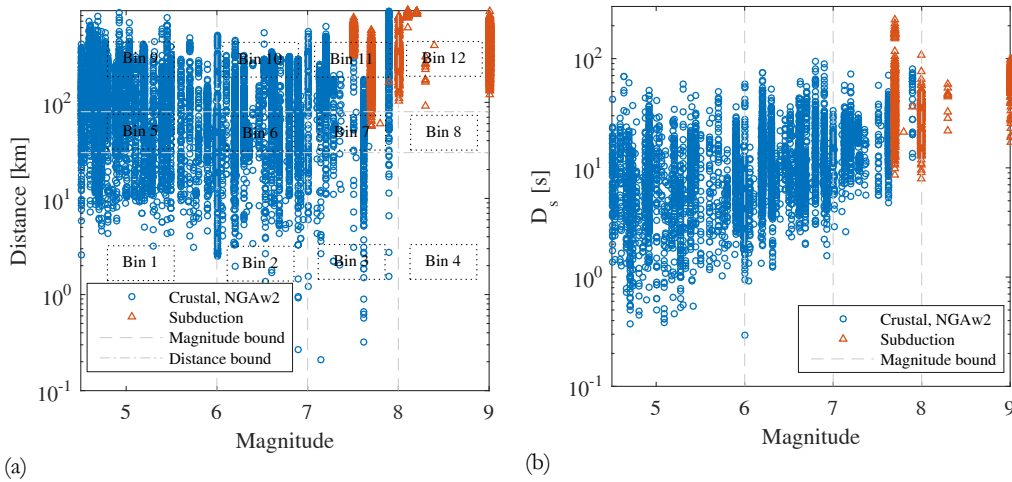


Figure 2.5 (a) Scatter plot of magnitude versus distance; and (b) Scatter plot of magnitude versus duration, for the ground motion database used in this study.

The main assumptions and working hypotheses related to the adopted record selection approaches are summarized below:

- The full set of seven GMPEs used in the PSHA calculations were included in the target spectra generation for the *CS-MR*, *GCIM* and *CS* methods (along with their corresponding weights defined in the logic tree). On the other hand, the *CS-approximate* method considered solely the attenuation law with the highest logic tree weight, which could be different among the ten hazard level for which the selection is carried out. The GMPE parameters were estimated on the basis of the suggestions in Kaklamanos et al. [2011].
- Since *GCIM* explicitly models duration, a prediction equation for duration was needed to define the proper target distribution. In line with what suggested by Chandramohan et al. [2016a], the AS96 Abrahamson and Silva [1996] was adopted.
- The target conditional distributions of  $Sa$  and  $D_{5-75}$  were defined using the correlation coefficient models of Baker and Jayaram [2008]; Bradley [2011], respectively.
- The records were selected on the basis of the geometric mean of the two horizontal components of the ground motion.

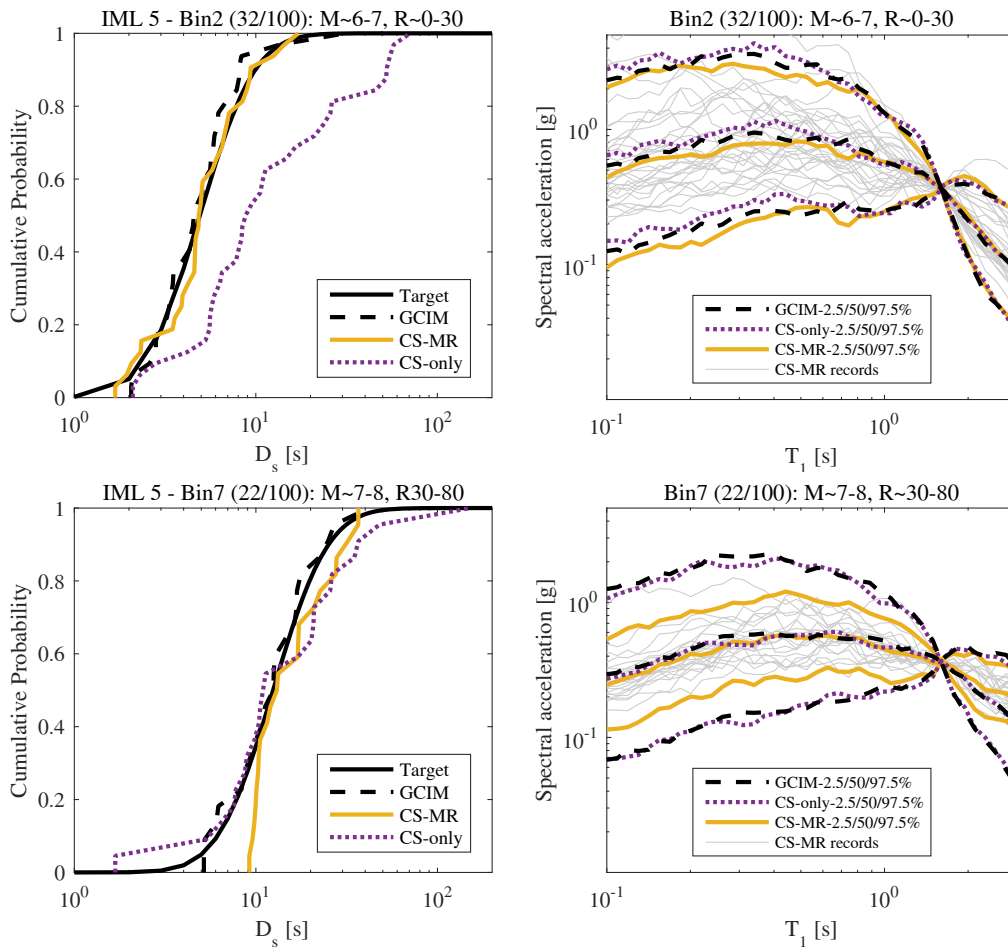
- Until the 8<sup>th</sup> IM level the scale factors (SF) were limited to 7, while for higher levels SFs up to 10 were allowed.
- The target spectral accelerations are defined for 40  $Sa$  values in the range between 0.1 and 3.0 s, considered as the most significant spectral ordinates for the selected structural response.
- The structure is assumed to be placed on a type D soil (NEHRP classification) that is usually associated with a  $V_{s,30}$  (the average shear wave velocity of the top 30m of the soil profile) of 270 m/s. Consequently, the selection was limited to accelerograms recorded at stations characterized by  $V_{s,30}$  between 100 and 400 m/s.

Figure 2.6 shows and compares the distributions of the selected records in terms of both  $D_{55-75}$  (left panels) and of spectral acceleration (right panels) for the 5% in 50 years IM level (called IML 5 in the figure). The results of the *CS approximate* method are not shown here because this method does not consider the M-R characteristics either at the simulation stage or at the record selection phase making such a comparison meaningless. This figure presents the results for bins 2, 7 and 12, which are characterized by 32%, 22% and 46% contributions to the hazard, respectively. The bins 2 and 7, representing scenarios with ‘M~6–7, R~0–30’ and ‘M~7–8, R~30–80’, are mainly related to crustal and subduction-in-slab events, while bin 12 considers scenarios with ‘M~8–10, R~80–300’ is related to subduction-interface earthquakes. The charts in the left panel of Figure 2.6 include the target  $D_{55-75}$  of each bin obtained from the *GCIM* method with median values of about 5, 12 and 43s for crustal, in-slab and interface events. This graph clearly shows the higher duration of ground motions generated by large subduction events compared to those from smaller crustal events.

By design, *GCIM* provides a very good match with the target in terms of  $D_{55-75}$ . However, it is interesting to notice that the *CS-MR* method, with only minor discrepancies, produces a satisfactory match with the  $D_{55-75}$  distribution although this match was not explicitly imposed by the method. The *CS-only* method, instead, fails in matching the  $D_{55-75}$  distribution because it does account for duration, neither explicitly, as the *GCIM* method does, nor implicitly, as the *CS-MR* method does. As expected, the discrepancies between the target and the selected  $D_{55-75}$  distribution, for *CS-MR* record set, are larger at higher magnitude bins, typically characterized by longer durations. These differences are likely due to the limitation of the adopted duration-GMPE that, strictly speaking, was not applicable to events with magnitudes larger than 7.5.

The right panels of Figure 2.6 show the 2.5/50/97.5<sup>th</sup> percentiles for spectral accelerations of the selected records for the already mentioned bins. Note that the *CS-only* and the *GCIM* methods make use of the same bin-specific target spectra, which are generated for the earthquake scenario of the each one of the three bins that

disaggregation identified for this IM level. On the other hand, the *CS-MR* method relies on a single target spectrum for the entire IM level and it guarantees, by means of the record selection scheme described in section 2, that the final a record set contains the proportions of records from each bin consistent with the hazard disaggregation. This consideration explains why the *Sa* distributions of the records selected by the *GCIM* and *CS-only* approaches are very similar to each other, while the *Sa* distributions based on *CS-MR* are, by design, quite different, especially for bins number 7 and 12. However, the duration and spectral distribution characteristics that really matters for the response are those of the record sets selected for the entire IM level. These aspects will be addressed in the following lines.



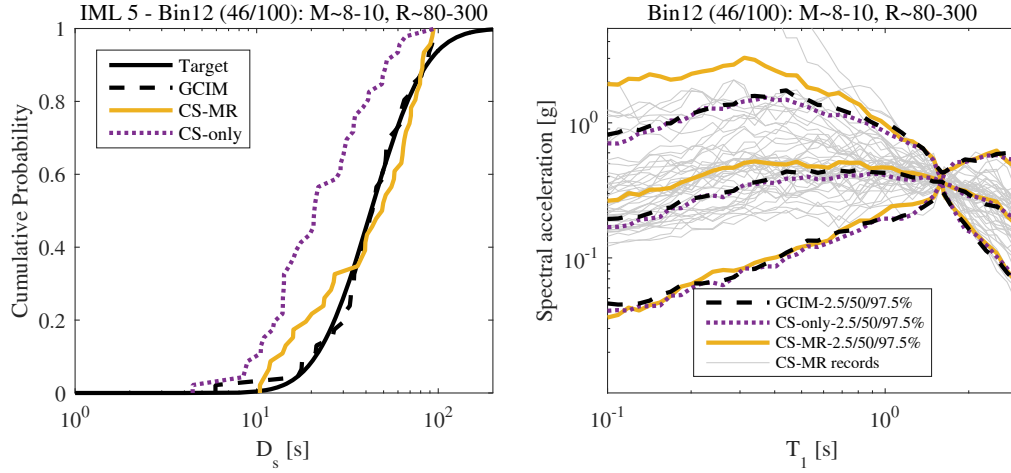
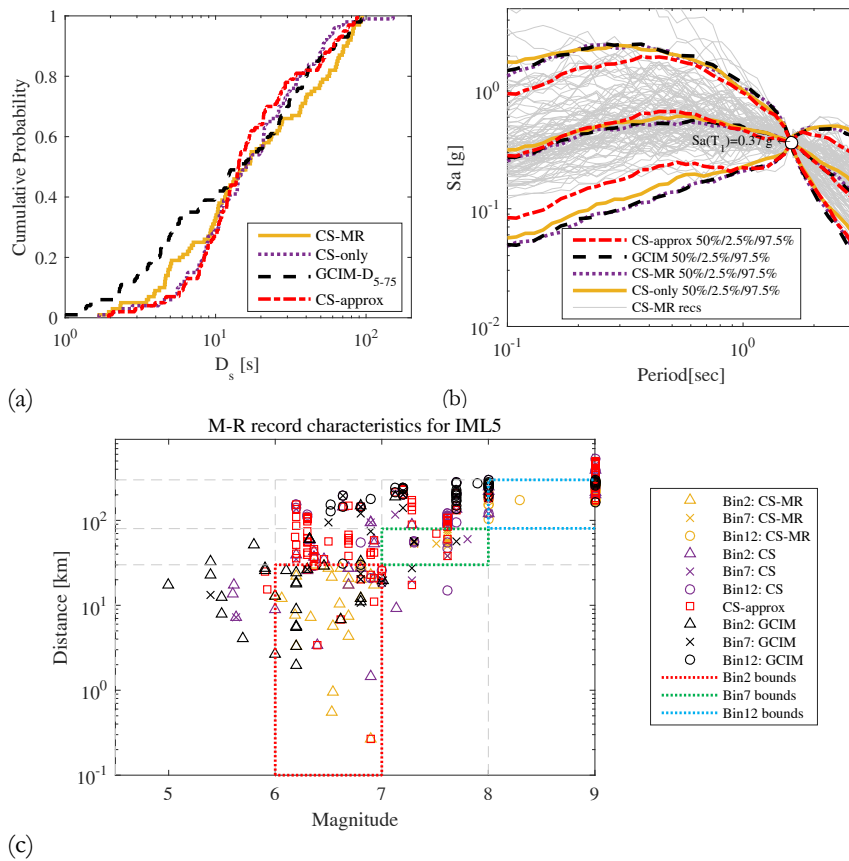


Figure 2.6 Comparison of the bin-specific  $D_s$  and  $S_a$  conditional distributions for the records selected by the GCIM, CS only and CS-MR approaches for the three bins 2, 7 and 12 identified by the disaggregation of the 5% in 50 years IM level for a site in Seattle. Left panels:  $D_{S_{5-75}}$  distributions of the selected records and the target distribution from the GCIM method. Right panels: 2.5/50/97.5<sup>th</sup> percentiles of spectral accelerations of the selected records. Note: the numbers in the parentheses in the title above each panel show the number of selected records associated to each bin (e.g., 46 out of 100 for Bin 12)

Figure 2.7 shows the distributions, for the entire IML 5, of  $D_{S_{5-75}}$  and  $S_a$  and M-R characteristics of the records selected according to all the four methods considered herein. At this stage of IM Level comparison, *CS-approx* too has been included in the charts in order to have a reference of a simpler but more approximate selection approach. A clear difference can be observed in the conditional dispersion of  $S_a$  that is considerably lower than those of the other sets; the median too presents a clear discrepancy between periods of 0.4s and 0.7s. The duration distribution too observes a lower dispersion (the distribution is more “vertical”) selecting lower duration records. About the other methods, despite the differences between *CS-MR*, *CS-only* and *GCIM* in terms of  $S_a$  and  $D_{S_{5-75}}$  distributions observed at the bin level (see Figure 2.6), the whole set of 100 records shows a higher degree of coherence. It seems that different bins somehow manage to collectively produce the desired distribution of  $S_a$  and  $D_{S_{5-75}}$  by compensating each other. For instance, at this IM level, even though *CS-only* at bins number 2 and 12, respectively, overestimated and underestimated the  $D_{S_{5-75}}$  distribution of GCIM, the combination of the records from these two bins with those coming from bin 7 results in a moderately good  $D_{S_{5-75}}$  global distribution (Figure 2.7a). For instance, as shown in the selected records of bin 12 in Figure 2.6, *CS-only* might select records with spectral shape characteristics of a subduction ground motion from a crustal event with short durations but irrelevant M and R characteristics (see also Figure 2.7c for bin 12 related to M and R of the selected records in *CS-only*). This provides evidence that *CS-only* would not reflect

the known differences in the characteristics of ground motion produced by different bins or different source types, even if the selection is performed bin- or source-specific. It is worth noticing the asymmetry of the *CS-MR* spectra (gray lines in Figure 2.7b) with respect to the quantile curves. The percentiles are computed according to the lognormal assumption showing a sufficiently accurate match in the dispersion. However, the skewness is probably not well captured but this is not of main concern since all the selection methods were built to be consistent with the first two moments only, namely mean and standard deviation. The same peculiarity can be observed in the *CS/GCIM* record sets too demonstrating that this asymmetry cannot be attributed to the proposed algorithm.



**Figure 2.7** Comparison of the  $D_{s-75}$  and  $S_a$  conditional distributions for all the 100 records selected by the GCIM, CS only and CS-MR approaches for the 5% in 50 years IM level for a site in Seattle. (a)  $D_{s-75}$  distribution of the selected records and the target obtained from GCIM; (b) 2.5/50/97.5-th percentiles of the empirically-derived conditional distribution of spectral acceleration of the records selected by the three approaches; (c) Scatter plot of the magnitude and distance pairs of the records selected by the four approaches.

## 2.7 RESULTS AND DISCUSSION

In this section, we discuss the impact of different record selection procedures on the prediction of both ultimate capacity and collapse rates. The focus here is on structural collapse since the duration of a ground motion, due to possible damage accumulation, has a higher impact on the ultimate behavior of a building rather than on the less severe parts of its response. In line with Shome and Cornell [1999], the rate of exceeding different values of an  $EDP$ ,  $\lambda(edp > EDP)$ , can be computed using the conditional complementary cumulative distribution function of  $EDP|IM$  for the no-collapse (NC) data,  $P(edp > EDP|NC, IM)$ , and the probability of collapse given IM,  $P_{col|IM}$ , along with the rate of occurrence of the IM of interest,  $\lambda_{IM}$ , formally:

$$\lambda(edp > EDP) = \int \left[ P(edp > EDP|NC, IM) \cdot (1 - P_{col|IM}) + P_{col|IM} \right] \cdot |d\lambda_{IM}| \quad (2.1)$$

Logistic regression (Kutner et al. [2004]) was used to compute the probability of collapse for each IM level while  $P(edp > EDP|NC, IM)$  is evaluated by means of the empirical CDF extracted from the multiple strip analysis results. Figure 2.8 shows the collapse fragility curve and MIDR response hazard curve computed using records selected by the four approaches. Since the record selection methods, in line with the PSHA, are based on the geometric mean of the two horizontal components and the analyzed structure is 2D, the choice of the proper component to use in the NDA is not trivial. Consequently, the NDA runs were performed using both components of the selected records (i.e., for each record set, a total of 200 NDA runs for each of the 10 stripes were carried out). Following the approach of Baker and Cornell [2006b] the response dispersion was inflated creating 100 different sets of 100 responses, picking them randomly in one direction or the other. Finally, by choosing for each pairs of horizontal components one at random, we obtained 100 different estimates of the structural response. All the generated outputs, both in terms of fragility and drift hazard curves, along with the mean curves are shown in Figure 2.8. The observed differences among the four selection methods, in terms spectral shape and duration, are clearly reflected in the collapse prediction. More specifically, the records selected according to  $CS-MR$  predict higher collapse probability with respect to the other approaches because of the longer duration ground motions. It can be argued that the  $CS-MR$  method explicitly and properly includes high-magnitude records, which are typically longer than the others. This aspect can be verified by comparing the duration distributions in Figure 2.7 where the  $CS-MR$  distribution is shifted to the right with respect to the  $GCIM$  sets. Consequently, since the structural response has been shown to be dependent on record durations, the longer the time history the higher the collapse rate. However,  $CS-MR$ ,  $GCIM$ ,  $CS-only$  and  $CS-approx$  sets provides fairly similar collapse rates, namely  $4.66 \times 10^{-4}$ ,  $4.13 \times 10^{-4}$ ,  $3.47 \times 10^{-4}$ ,  $3.06 \times 10^{-4}$ . Comparing to the  $GCIM$  rates, the collapse rates of the other three methods

have relative differences of about +13%, -16% and -26% for *CS-MR*, *CS-only* and *CS-approximate* record sets, respectively. The most approximate method is giving the less reliable results since it captures less precisely both the spectral shape (the target was defined solely according to the most contributing scenario and GMPE) and the duration (not accounted at all).

One could argue that on a theoretical basis the GCIM method could be considered as the reference one. In this case, however, we question, this assertion. This would indeed be true if the *GCIM* approach could count on a GMPE suitable for predicting hazard consistent duration (or any other relevant IM) distribution. As pointed out previously, this is not the case here since the Abrahamson and Silva [1996] GMPE that is tailored on crustal events was extrapolated by necessity out of its field of applicability to predict durations of high magnitude subduction events. In addition, the *GCIM* method, in addition to being more complex than the *CS-MR* method,, needs a certain level of arbitrariness in deciding the IMs that are likely to influence the structural response. Therefore, a selection method (like *CS-MR*) that is able to implicitly and naturally account for characteristics beyond the “classical” spectral shape, could be certainly an useful alternative. Nonetheless, the differences between the *CS-MR* and *GCIM* methods remain not very significant but it can be certainly argued that not including duration, either implicitly (*CS-MR*) or explicitly (*GCIM*), might lead to a non-negligible underestimation of collapse fragility and rate.

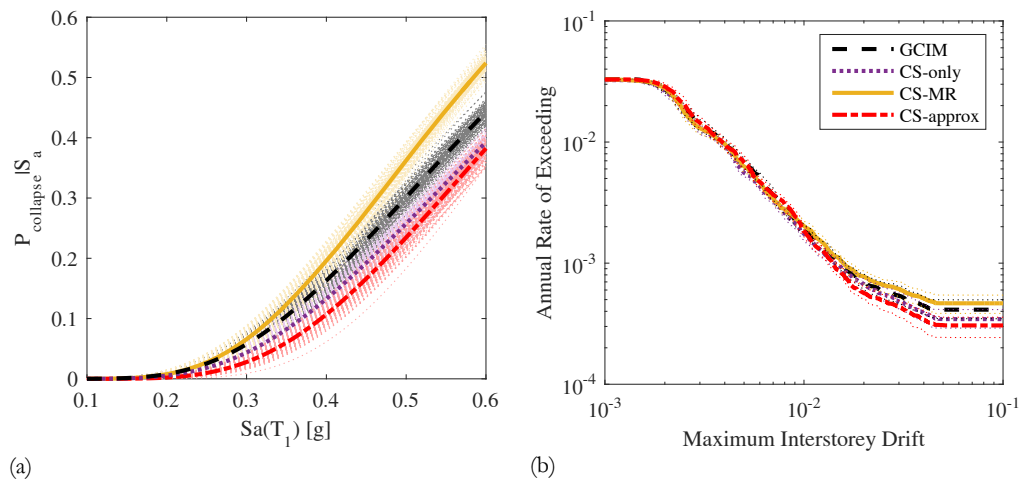


**Figure 2.8** a) Fragility curves and b) Drift hazard curves, estimated from the multistriple analyses of the structure subjected to the record sets defined according to the four selection methods. The dotted/lighter lines (for each method) represent the range of variability of 100 different combination of response estimates

### 2.7.1 Robustness test

Given the ease of implementation, the lower degree of arbitrariness and the lack of requirement for GMPEs and/or correlation coefficients for IMs beyond spectral quantities, the CS-MR method could in certain cases be preferred to the GCIM one. In general, it could be argued that the best way of tackling a problem is to find the simplest approach that can guarantee a satisfactory level of robustness and reliability of the outputs. In line with this, since the collapse rates coming from the CS-only and CS-MR methods are not far from each other, the simplest method, i.e. CS-only, could appear as the most appealing. Therefore, we developed a simple exercise aiming to prove the superiority, in terms of robustness, of the CS-MR method with respect to the CS-only method. Until now, in order to be fair and to avoid biased results, the compared algorithms were left free to select records from exactly the same database, i.e. the NGA West2 integrated with the subduction events (later labelled as *complete database*). Therefore, the CS-only algorithm might have selected by chance some subduction event long-duration records that provided a better spectral consistency than other crustal event ones. Hence, by chance rather than design, these subduction event records may have helped increasing the CS-only failure rates thank to their long duration. The idea, herein, is to investigate whether removing those subduction records from the database, the CS-only method is able to reproduce again, in a successive selection, a satisfactory duration distribution. Along these lines, the extreme case would be to remove all the subduction records and perform the selection solely picking records from the NGA West2 crustal database. Clearly, for a tectonic regime characterized by subduction events, the CS-MR method would fail if given a crustal-only record database since it would look for records with magnitudes identified by the PSHA-based disaggregation results that are not present in it. On the contrary, the CS-only method, simply focusing on spectral shape, would still be able to collect a set of records that satisfy its requirements. Obviously, despite a good spectral matching, the duration distribution (Figure 2.9) would be significantly different from the one obtained selecting records from the complete database (i.e. including the subduction events). The same result can be achieved, after some iterations, by removing from the *complete database* solely the subduction records that were chosen by the selection algorithm. Figure 2.10 shows the evolution of the duration distribution for *CS-only* and *CS-MR* approaches that result from this test for the 5<sup>th</sup> IM level ( $S_a(1.6s)=0.37g$  corresponding to 5% in 50 years probability of exceeding). The first attempt of database modification has led to the removal of 20 and 46 subduction records for the *CS-only* and *CS-MR* methods, respectively. The impact of record removal on the two approaches is quite different: the new *CS-only* set (light gray dash-dotted line) is significantly moving away from the distribution of the previous set (purple solid line). On the other hand, the *CS-MR* duration distribution remains almost unchanged. Moreover, removing about the same number of records from the database (i.e., about 50) the *CS-only* distribution become (after 5 step of removal procedure) basically coincident with the one obtained

selecting the records only from the NGA west2 crustal database (see the purple “CS-crystal curve and the CS-all-step5 one in Figure 2.10). The results of this exercise shows that the *CS-MR* method is indeed more stable than the *CS-only* algorithm in selecting records that properly represent the expected duration at the site.

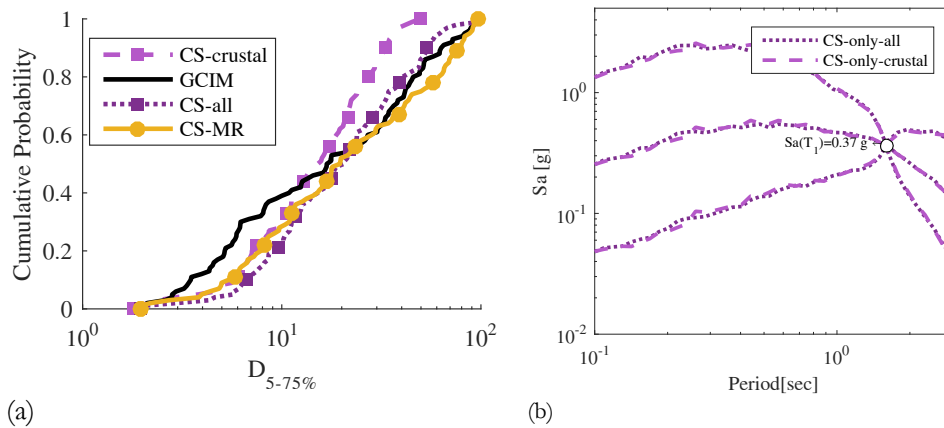


Figure 2.9 Comparison of the selected records distributions based on CS-only approach using full (NGA West2 + subduction) and limited (only NGA Wests) databases. (a) Duration distribution; (b) spectral acceleration 2.5/50/97.5-th percentiles for the selected site in Seattle corresponding to IM level 5 with  $Sa(1.6s)=0.37g$

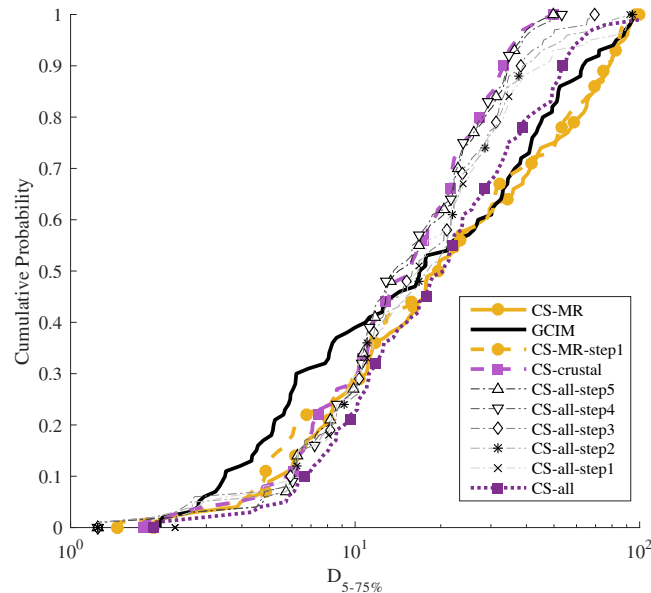


Figure 2.10 Robustness test: Changes in the duration distribution obtained by removing selected subduction records from the database

## 2.8 CONCLUSIONS

This work proposes a post-processing technique that guides the CS algorithm in selecting ground motion records with Magnitude (M) and Distance (R) characteristics that are consistent with the earthquake scenarios that contribute mostly to the site hazard for each IM level. M and R can be seen as proxies useful for considering ground motion parameters, other than the spectral shape, that could potentially matter in the structural response prediction.

An archetype RC 2D modern ductile frame has been tested with four record selection procedures, namely *CS-MR* (our proposal), *GCIM* (seen as the reference, although with the caveat that the duration distribution is not appropriate for large M subduction events), *CS-only* and *CS-approximate*. The effective duration has been chosen as the measure, beyond the spectral shape, that significantly influences the structural response. The building response has been, indeed, proved to be duration-sensitive according to a procedure proposed by Chandramohan et al. [2016b]. The building is located in Seattle, a site whose hazard is affected by both crustal and subduction events (typically associated with longer durations). Integrating the NGA-west2 database with records from subduction events and let the selection procedures being free to choose the records, the results, apart from the *CS-approximate* case, do not present a high degree of difference, even if the *CS-only* (exact) method, which does not account for duration, is adopted. In this case, molding the target spectrum on the basis of the M\_R scenarios identified by disaggregation, probably directs the CS-only procedure to select records with satisfactory duration characteristics. However, forcing the selection to pick records with proper M-R characteristics (*CS-MR* method) further improves the final response. In addition, the *CS-MR* method has been proven to be more robust than the *CS-only* one, maintaining a satisfactory duration distribution and spectral shape even if the ‘preferred’ subduction records were screened out from the database.

Moreover, the *CS-MR* method is intuitively appealing and less complicated than the *GCIM* method. Indeed, the *CS-MR* method relies on M and R to identify records that are appropriate for the site and have the “right” distribution of all IMs (e.g., duration) other than spectral accelerations. The consistency of the distribution of these other IMs, however, is not enforced explicitly as the *GCIM* method does. Because of this capability of explicitly accounting for any parameter that could possibly influence the structural response, the *GCIM* method is, in theory, more precise than *CS-MR* but:

1. It requires selecting a priori the IMs that matter for the prediction of the structural response. This introduces some arbitrariness. The GC-MR method does not.

2. It may happen that the IM selected, such as duration for the case study considered here, does not have a proper GMPE necessary for computing a hazard consistent distribution. This renders the practical application of *GCIM*, as originally intended, inaccurate. This problem is bypassed by the *CS-MR* method.
3. The *CS-only* and the *GCIM* methods enforce the overall distribution of the spectral shape of records conditioned on a single IM at a given level. It is possible that some of the records selected may come from M and R that do not matter for the site at hand. These records may not be like any ground motion records that the structure will ever experience in its lifetime. The *CS-MR* does not have this problem. The spectral shape of each records selected is relevant to the site hazard and not only relevant in the overall spectral shape distribution.
4. The *GCIM* method allows the consideration of different IMs in addition to the spectral accelerations. However, since the record database is limited, one could not simply match perfectly all the IM target distributions. The *CS-MR* does not have this issue.
5. The *GCIM* method assigns weights to the preferred IMs. This is philosophically equivalent to decide which IMs are the most important ones. In contrast, the *CS-MR* method, using Magnitude and Distance as proxies, is able to bring to bear additional information naturally.

Additionally, it should be underlined that the *CS-MR* method, being stricter in the record selection than the *CS-only* method may not always be able to have the same consistency with the target CS achieved by the records selected by CS only method. Nonetheless, what may be lost in the spectral shape hazard consistency is gained in the selection of records that, via M and R, have characteristics similar to those that may be experienced by the structure at the site. Finally, we foresee that this practical problem may gradually go away as the ground motion records database become more populated after new earthquakes.

## 3. RINTC: ASSESSING IMPLICIT RISK OF CURRENT ITALIAN CODE

### 3.1 INTRODUCTION

Current Italian seismic code provisions are based on settled and widespread concepts: new structures are designed in order to withstand, with a proper behaviour, earthquake ground motions that are rare enough to ensure them an “adequate” level of safety. With “proper behaviour” it is meant that the design admits that damage can occur but controlled and localized, in order to guarantee, for the given level of shaking, certain performances, e.g. Life safety. Therefore, the definition of the design ground motion intensities is crucial in performing a reliable structural design. In particular, the current code links the target performance (often called Limit State) with a return period of the design ground motion that depends on the seismic hazard of the site where the structure will be placed. This means that the design is performed for a constant ground motion hazard level but the structural performance that is achieved with those design provisions is not known. This design paradigm does not explicitly consider risk, a measure that integrates structural response and ground motion hazard data. Via structural analysis the engineer can assess structural response at a given ground motion level and through the hazard can define how often this ground motion is expected to occur, or exceeded, at the structure’s site. Risk is a measure able to summarize the knowledge about these two fields defining, for example, the occurrence frequency of a certain structural response or limit state. Unfortunately, the engineer that applies the current code does not really know what is the risk of damage or collapse of the building under design or, more explicitly, the chance that an occupant will be injured or killed during an earthquake inside the house. In other words, designing different buildings for a given, uniform ground motion hazard, which is what the current Italian code (and that of many other countries) prescribes to do, does not guarantee that the level of risk is the same but only that it is “adequate” but only in the sense that it is code compliant.

Therefore, theoretically speaking, designing different types of buildings at different sites for a constant, uniform risk rather than for uniform ground motion hazard would arguably be a superior, more fair and ethical design paradigm. This idea is not novel. Luco et al. [2007] proposed a systematic method to do exactly what’s stated above, namely providing a method for designing different structures at different sites not for uniform hazard ground motion levels but for different hazard levels computed in such a way that, subject to some reasonable but not un-debatable assumptions, the resulting risk of collapse could be uniform. In particular, he proposed a target collapse rate (i.e.,  $2e-4$  or 1% probability in 50 years) that is the average risk observed in US territory and obtained assuming a fixed, theoretical collapse fragility curve (and here lies the main assumptions behind the method) as a measure of structural performance. The application of this

method would provide a so-called “risk factor”, which is defined for each site as the ratio between the new design ground motion level that guarantees the desired level of risk and the design ground motion level prescribed by the code (e.g., that exceeded with 10% chances in 50 years). These factors could be applied to scale up and down the code design ground motion in order to obtain the wanted uniformity (or, at least, harmonization if not uniformity) of collapse risk. This topic will be treated in the next Chapter 4 that discusses a series of strategies to make the risk more uniform for different buildings at different sites throughout a territory.

The aim of the work presented in this chapter is to define a systematic methodology to assess the implicit risk of structures designed according to the current Italian code (Norme Tecniche per le Costruzioni, NTC [2008b]) and, therefore, to provide a sound basis for future improvements of these provisions. As previously stated, following code rules, a generic structure is designed to implicitly have safety margins with respect to collapse and other limit states that are assumed to be adequate if compared to those for other risks. However, these margins are not quantified but derive implicitly by the application of code requirements. Therefore the designer can argue that the structure is verified against a certain level of ground motion but he/she does not know the collapse risk. For example, a typical residential non-strategic building is designed to “guarantee” Life Safety for a ground motion level with a 10% probability of being exceeded in 50 years at the site but its collapse risk is not quantified.

The risk is quantified here as an annual rate of observing a given limit state, such as collapse or damage. This risk is understood to be a “nominal” risk since not all the possible sources of uncertainty (e.g., human errors in design or construction phases) are not accounted for. The onset of these limit states are defined as the exceedance of some deterministic values of response measured by a so-called Engineering Demand Parameter, EDP. The variability related to material characteristics and structural elements’ geometric dimensions is not modelled. Finally, the thresholds selected for the collapse limit state were chosen to represent incipient collapse since life safety is of critical importance. However, for monetary loss estimation the total loss can occur earlier. A structure can be considered as a total loss even if it still stands but the damage is so spread and severe that its restoration is uneconomical and, therefore, it can only be demolished.

The present work has been funded by the Italian Civil Protection (Dipartimento Protezione Civile, DPC) and developed in cooperation with other Italian research units working within the Laboratories University Network of seismic engineering (ReLUIS). Each research unit is responsible for modelling one or more buildings of a given typology (e.g., reinforced concrete) and to perform the engineering analyses for the response assessment. The content of this chapter outlines the risk assessment methodology and

provides the computation of the seismic risk by convolving the hazard and the vulnerability.

### 3.2 METHODOLOGY

Considering all the possible sites in Italy, all structural typologies/configurations commonly used and their combinations, the potential risk assessment work is massive. For this reason, a set of case-study buildings were selected covering the most common structural typologies belonging to the Italian building portfolio. Those structures were designed as if they were located at sites characterized by different seismic hazard levels. In particular, we considered five structural typologies (i.e., unreinforced masonry, reinforced concrete cast-in-place, unreinforced masonry, reinforced concrete pre-cast, steel and base isolated buildings) located at five sites, namely Milano, Caltanissetta, Roma, Napoli and L'Aquila (Figure 3.1, Table 3.1). For some site-structure combinations, the case study was designed considering soil classes A and C that are defined as a function of the  $V_{s,30}$  (average shear wave velocity in the top 30m of soil) in line with the NTC08 classification (Table 3.2). Table 3.3 summarizes all the combinations city-structure-soil that considered herein.

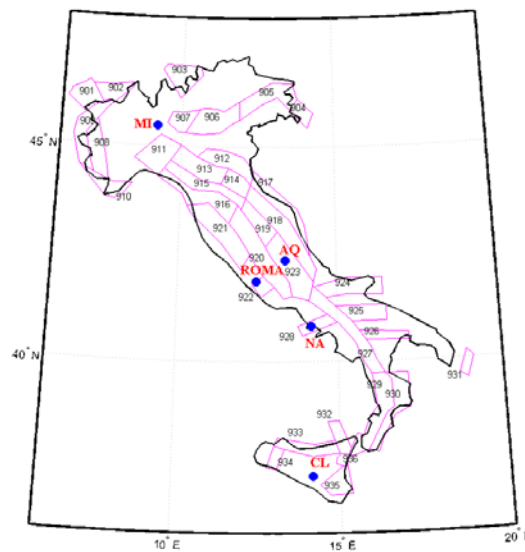


Figure 3.1 Location of the five selected cities. Legend: AQ=L'Aquila; NA=Napoli; CL=Caltanissetta; MI=Milano and seismic source model at the basis of the official Italian hazard map used to determine design seismic actions (Stucchi et al. [2011]).

Table 3.1 Location and design PGA levels (for soil types A and C) of the five selected cities

City	Longitude	Latitude	PGA (475 years) (Soil A) [g]	PGA (475 years) (Soil C) [g]
Milano	9.186	45.465	0.0495	0.0743
Caltanissetta	14.060	37.480	0.0762	0.11428
Roma	12.479	41.872	0.1204	0.1806
Napoli	14.268	40.854	0.1668	0.24338
L'Aquila	13.399	42.349	0.2607	0.3451

Table 3.2 Soil type A and C defined as a  $V_{s,30}$  (Table 3.2II, NTC08)

Soil Type	$V_{s,30}$ [m/s]
A	$> 800$
C	$180 < V_{s,30} < 360$

Table 3.3 Main Characteristics of the selected structural type

	Soil Type	Milano	Caltanissetta	Roma	Napoli	L'Aquila
RC, cast in place	A	---	---	---	---	9-story
	C	3/6/9-story	6-story	6-story	3/6/9-story	3/6/9-story
Masonry	A	2/3-story, regular	2/3-story, regular	2/3-story, regular	2/3-story, regular/irregular	2/3-story, regular
	C	2/3-story, regular	2/3-story, regular	2/3-story, regular	2/3-story, regular/irregular	2/3-story, regular/irregular
RC, Precast	A	1-story, geometry 1/2/3/4	---	---	1-story, geometry 1/2/3/4	1-story, geometry 1/2/3/4
	C	1-story, geometry 1/2/3/4	---	---	1-story, geometry 1/2/3/4	1-story, geometry 1/2/3/4

Steel	A	1-story geometry 1/2, height 6m/9m	---	---	1-story geometry 1/2, height 6m/9m	1-story geometry 1/2, height 6m/9m
	C	1-story geometry 1/2, height 6m/9m	---	---	1-story geometry 1/2, height 6m/9m	1-story geometry 1/2, height 6m/9m
Base Isolated	A	---	---	---	---	6-story, HDRB/HDRB +Slider/ DCFP
	C	---	---	---	---	---

The Risk assessment of the selected case studies has been conducted in line with the classical approach of Performance Based Earthquake Engineering (PBEE), developed by PEER (Pacific Earthquake Engineering Research Center) in the early 2000s (Cornell and Krawinkler [2000]). This method is expressed by the well-known risk integral:

$$\lambda(DV) = \iiint G(DV | DM) |dG(DM | EDP)| \cdot |dG(EDP | IM)| \cdot |d\lambda(IM)| \quad (3.1)$$

Where the  $\lambda$ s represent the Mean Annual Rate (MAR) of exceeding of the quantity in parentheses, G is the CCDF (Complementary Cumulative Distribution Function) while the other parameters are:

- a. DV: Decision Variable, e.g. Loss in USD.
- b. DM: Damage measure, e.g. the level of damage the user is interested in.
- c. EDP: Engineering Demand Parameter that is thought to describe reasonably well the structural response, e.g. Maximum Interstory Drift Ratio (MIDR), Roof drift Ratio (RDR), Peak Floor Acceleration (PFA).
- d. IM: Intensity Measure that should represent the severity of the seismic input, e.g. Spectral Acceleration at a given period, Average Spectral Acceleration (AvgSA) over a period range.

The integral ( 3.1 ) can be subdivided into four parts that contribute to the definition of Risk (quantified, in the most general case, as the Mean Annual Rate of Exceeding the

DV). First module from the right side of equation (3.1) describes the seismic hazard and quantifies the MAR of exceeding the chosen IM. Then, moving to the left, the Demand Module represents the probability of observing a certain response (EDP) of the structure once the IM is known. The third part can be labelled as Fragility Module: here the probability of observing a given Damage level is defined once the response of the structure is known; finally the Loss Analysis represents a link between the Damage and the Decision Variable (e.g. monetary loss). Figure 3.2 is useful to clearly comprehend the aforementioned modules.

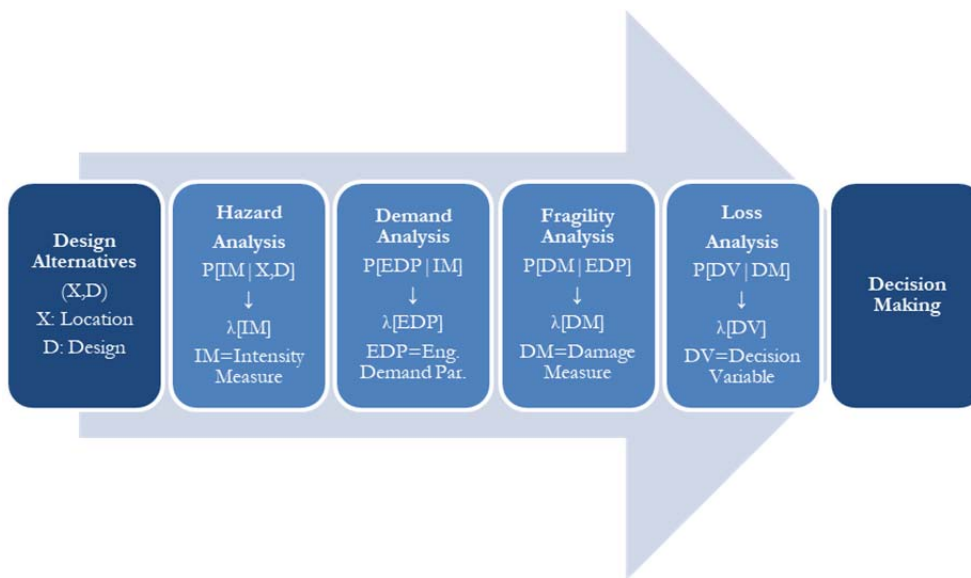


Figure 3.2 Graphic representation of PEER Integral modules and interface variables.

This work will focus mainly on the first stages, leaving aside the monetary loss and quantifying the risk as MAR of collapse or damage. Following the path shown in Figure 3.2, the next sections will deepen the details of the hazard, demand and fragility analyses and, finally, will show how all these information will be combined to obtain a reliable risk measure.

### 3.2.1 Seismic Hazard Analysis

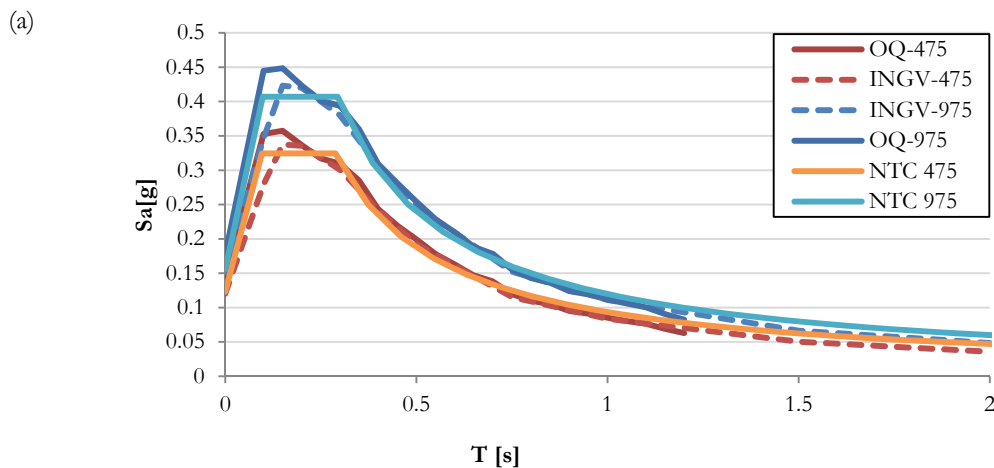
The reference seismic hazard model is the MPS04 (Meletti and Montaldo [2007]; Montaldo and Meletti [2007]; Stucchi et al. [2011]) which is the basis of the seismic input adopted by the NTC08. An on-line tool (INGV-DPC [2004 – 2006]; Spallarossa and Barani [2007]) developed by the Istituto Nazionale di Geofisica e Vulcanologia (INGV) is available but its data are limited to rock sites and the disaggregation of the seismic hazard is offered for PGA only. To support the record selection needed for response assessment

on both soil types A and C, this is not sufficient. Therefore, the GMPE of Ambraseys et al. [1996] together with the branch 921 of the logic tree belonging to the MPS04 hazard model have been implemented on the Openquake platform (Monelli et al. [2012]). This particular combination of source model and GMPE was selected because it provides hazard estimates that are very close to the mean hazard estimates (Meletti and Montaldo [2007]).

This additional effort has allowed us to compute  $S_a$  hazard curves and the contributing earthquakes in terms of  $M$  and  $R$  for any combination of:

- Oscillator Period,  $T$ ;
- Soil Type, as defined in terms of shear wave velocity in the top 30m of soil,  $V_{s30}$ , in the NTC08;

In order to assess the reliability of the tool, the Openquake hazard estimates were compared to the hazard for rock conditions (i.e., soil Type A) from INGV and from the NTC [2008b] code provisions. Figure 3.3 and Figure 3.4 show a satisfactory comparison of uniform hazard spectra (UHS) and hazard curves for  $T=1s$  for the city of Roma, respectively. Figure 3.3 (a) compares the 475yr and the 975yr UHS spectra obtained using Openquake. The spectrum obtained with the INGV online tool and the code spectrum. The small discrepancies are in part due to the exclusive use of branch 921 instead of the entire logic tree and in part to a slight mismatch in site coordinates: indeed, Openquake performs its computation at the exact Longitude and Latitude that the user specifies, while the INGV spectra are computed for the grid point that is closest to the location of interest (Figure 3.3 (b)).



(b)

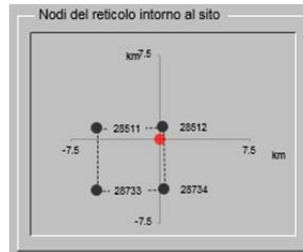


Figure 3.3 (a) UHS for Roma, Soil Type A, Return Period values of 475 e 975 years computed according to INGV, Openquake and NTC08. (b) The OQ and the NTC08 hazard values are computed at the exact location (red dot) while the INGV hazard is computed at the grid point #28512 (capture from SpettriNTCver1.0.3(CSLP) [2008])

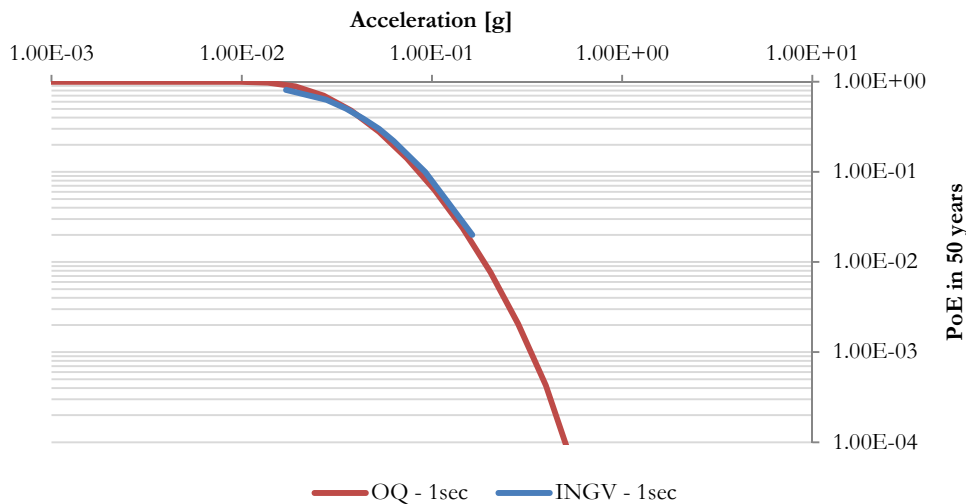


Figure 3.4 PGA hazard curve comparison for Roma, Soil Type A,  $T=1s$ . PoE is the acronym for Probability of Exceeding.

The hazard curves computed using OQ for the five selected sites (i.e., L'Aquila, Napoli, Roma, Caltanissetta and Milano), Soil Type A ( $V_{s30} > 800$  m/s) and Type C ( $180 < V_{s30} < 360$  m/s), and oscillator period of  $T=0s$  (i.e., PGA),  $T=0.5s$  and  $T=2s$  are given in the Appendix of this document.

However, some of the analysed structures, i.e. the base isolated buildings, are characterized by long oscillation periods for which the INGV hazard estimates are not available because the Ambraseys et al. [1996] GMPE is not defined. In order to overcome this issue, an *ad-hoc* seismic hazard calculation has been performed for those long period

spectral values. In particular, the same branch 921 has been combined with the GMPE developed by Akkar and Bommer [2010] that is applicable to Europe and predicts Spectral accelerations at periods up to 4 seconds. Figure 3.5 displays the UHS computed for L'Aquila soil A for the 475 years return period by means of Ambraseys et al. [1996] and Akkar and Bommer [2010]

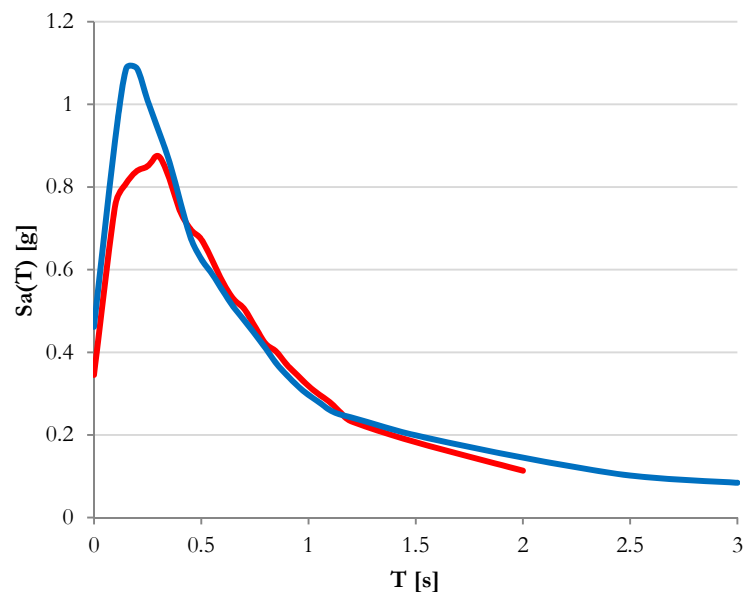


Figure 3.5 UHS, for Soil A, at L'Aquila according to Ambraseys (1996), red line, and Akkar and Bommer (2010), blue line.

The capability of computing hazard and disaggregation for all the possible cases included in this study is particularly useful for ground motion record selection. The ground motion selection algorithm adopted herein, in fact, allows defining sets of ground motions that are consistent with the hazard at the site at the IM of choice. For this reason, it was necessary to compute the hazard for long period spectral accelerations.

### 3.2.2 Ground Motion Selection

Ground motion selection represents the link between the seismic hazard and the structural analysis and the record-to-record variability of the EDP given the IM can significantly affect the structural response prediction. Several selection procedures exist in the literature, with different levels of complexity and, therefore, precision. The simplest ones, which can be labelled as *Site Independent* procedures, suggest the definition of generic ground motion sets selected, for example, simply accounting for causal parameters such as Magnitude, Distance or other parameters affecting the frequency content of the

ground motion at the site, such as  $V_{s,30}$ . In those cases, structures located at different sites are subjected to the same record sets facilitating vulnerability comparison. These approaches, however, were not consistent by design with site hazard and, therefore, with the kind of motions that any specific structure is likely to observe during its lifetime. On the other hand, more recent works (e.g. Baker [2011]; Lin et al. [2013b]; Lin et al. [2013c]) focused their attention on choosing ground motions that are *Site Specific*: for example the NTC suggests the use of a set of 7 records that match the code spectrum of the site over a certain range (§ 7.3.5 NTC [2008b]). In particular, the code spectrum was built in agreement with the Uniform Hazard Spectrum (UHS) coming from PHSA, which is an envelope of spectral accelerations characterized by the same exceedance rate. However, no ground motion is likely to have spectral ordinates so rich at all oscillator periods to be consistent with a UHS. Hence, sets of ground motion records identified according to this approach are site specific but not hazard consistent. Since the main goal of this work is to assess the collapse risk of particular structures designed for specific locations, the ground motion set used to assess their vulnerability must be, to the extent possible, representative of the site hazard. In line with these premises, the adopted selection approach is based on the Conditional Spectrum method (Jayaram et al. [2011]) in its “exact” formulation (Lin et al. [2013a]) with the post-processing procedure fully described in the first chapter. In this way, the structures will be subjected to sets of ground motions that are representative of the hazard of the site and, additionally, are characterized by the causal parameters that mostly influence the site seismic hazard.

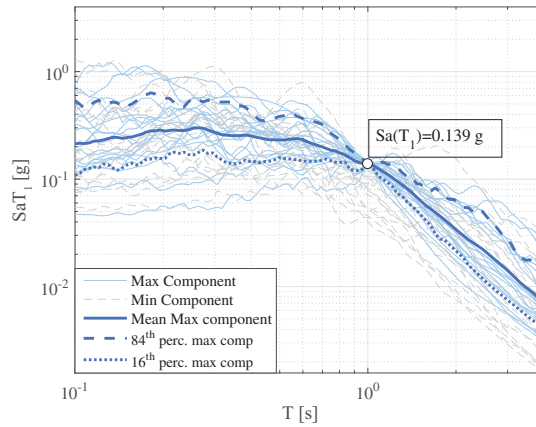
The selection procedure has been performed specifically for each city, soil type and conditioning Spectral Acceleration at several oscillator periods,  $T_1$ , namely 0.15-0.5-1.0-1.5-2.0-3.0 seconds. This effort was necessary because of the wide variety of structural typologies, whose dynamic characteristics are different especially for some cases (e.g., unreinforced masonry versus base isolated structures). In particular, in order to cover a significant range of the hazard curve, a step necessary to achieve accurate risk estimates, the procedure was designed to select a set of 20 records conditioned on the  $S_a(T_1)$  at 10 different hazard levels. In particular, the ground motions were scaled and selected in order that the maximum horizontal component is consistent with the CS distribution (in terms of mean and standard deviation) conditioned on  $T_1$  for all values of  $T_1$  with the exception of 3s. The GMPE of Ambraseys et al. [1996], that has been built to predict the maximum horizontal component of the ground motion dictated this choice for the first five oscillator periods. For  $T_1=3.0$  s, however, the record selection followed the spectral acceleration definition of Akkar and Bommer [2010], namely the geometric mean of the two horizontal components. It should be noted that for the highest IM levels, it was necessary to use scaling factor up to 10 in order to satisfy all the procedure’s requirements. In the end, each case study is subjected to 200 pairs of records of increasing IM levels spanning from values corresponding to 10 to  $10^5$  years return periods at each site and soil conditions (Table 3.4). Figure 3.6 shows, as an example, the spectra of 20 pairs of records

for the case of L'Aquila, soil type C and  $S_a(T_1=1s)=0.139g$ , and  $S_a(T_1=1s)=0.558g$  which are, respectively, the 3<sup>rd</sup> and the 6<sup>th</sup> Intensity Measure Levels (i.e., IML #3 and IML #6) for that building-site-soil case.

**Table 3.4 Return periods for 10 Intensity Measure Levels**

IML #	1	2	3	4	5	6	7	8	9	10
Return Period [years]	10	50	100	250	500	1000	2500	5000	10000	100000

(a)



(b)

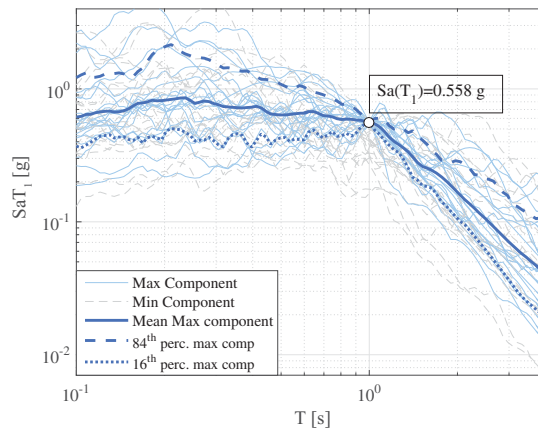


**Figure 3.6 Response spectra of both horizontal components of selected records for the case of L'Aquila, Soil Type C, and Intensity Level 3(a) and 6(b).**

In order to reduce the computational effort, the initial and final portions of the selected records that do not significantly influence the structural response were removed. In particular, only the central part of the record that is between the instants  $t_{0.05\%}$  and  $t_{99.95\%}$  is used for the structural analyses. The quantities  $t_{0.05\%}$  and  $t_{99.95\%}$  represent the times that bracket the Normalized Arias Intensity (Arias [1970]; Husid [1969]),  $I_{a,N}$ , between 0.05% and 99.95% of its total value. More precisely,  $I_{a,N}$  is defined as:

$$I_{a,N} = \frac{\int_0^t a^2(t) dt}{\int_0^T a^2(t) dt} \quad (3.2)$$

Where  $t$  is the instant at which the  $I_{a,N}$  is computed,  $a(t)$  the time history and  $T$  is the total duration of the record. It is emphasized that this procedure is independent from the scaling factor that is applied to meet the record selection requirements described above. Figure 3.7 compares the original (blue) and the cut (red) records for one accelerogram extracted from the set selected for Roma,  $T_1=0.5s$  and soil type C.

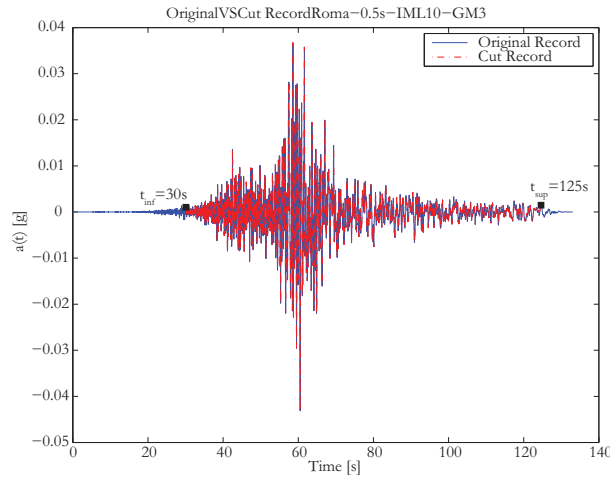


**Figure 3.7** Original vs shortened versions of one of the records selected for the 10<sup>th</sup> IM level for Roma, Soil C,  $T_1=0.5s$ .

### 3.2.3 Structural Analysis approach and risk calculation

The ground motions were scaled in order to match a target value of *conditioning* spectral acceleration. Therefore, the representation of the structural response versus the ground motion intensity will have the shape of 10 stripes where the record-to-record variability is evident only for fixed spectral acceleration values (see Figure 3.8 to come). This way of conducting structural response assessment is called the Multiple Stripe Analysis, in contrast with the Cloud Analysis where the ground motions are not scaled to the same IM and the responses are represented as a cloud of points.

Recalling the PBEE framework depicted in Figure 3.2, the *Demand Analysis* phase concerns the effective test of the structural models and the representation of the output versus the seismic intensity, IM. In this way, it is possible to quantify the response variability in terms of EDP distribution conditioned on observing a certain IM level. Once an EDP threshold value for a given limit state (e.g., Collapse) is properly defined, it is possible to quantify the probability of observing that Limit State or higher for each stripe. For each stripe, this value can be estimated either non-parametrically by counting the number of occurrences higher than the threshold, or parametrically by fitting distribution on the finite response values (i.e., from the analyses that did converge, see below). This latter approach is adopted herein and was proposed by Shome and Cornell [1999]:

$$P[LS | IM_i] = \left[ 1 - \Phi \left( \frac{\log(EDP_{LS,threshold}) - \mu_{\log(EDP|IM_i)}}{\sigma_{\log(EDP|IM_i)}} \right) \right] \cdot \left( 1 - \frac{N_{LS,i}}{N_{tot}} \right) + \frac{N_{LS,i}}{N_{tot}} \quad (3.3)$$

Where  $LS$  represents the Limit State of interest,  $\Phi$  the normal distribution,  $\mu_{\log(EDP|IM)}$  and  $\sigma_{\log(EDP|IM)}$ , respectively, the mean and the standard deviation of the response, EDP, at the  $i^{\text{th}}$  IM level,  $N_{tot}$  the total number of responses at each IM Level, and  $N_{LS,i}$  the number of cases in which  $LS$  is observed. This approach is designed to account for cases when the analyses may not converge because of either numerical or dynamic instability. The last addend of (3.3) quantifies the incidence of these occurrences that are combined with the prediction of responses exceeding the threshold based on “finite” data. For example, Figure 3.8 shows the 10 stripes, the record to record variability of the response, the collapse threshold, and the a single collapse case due to model instability for one of the unreinforced masonry buildings

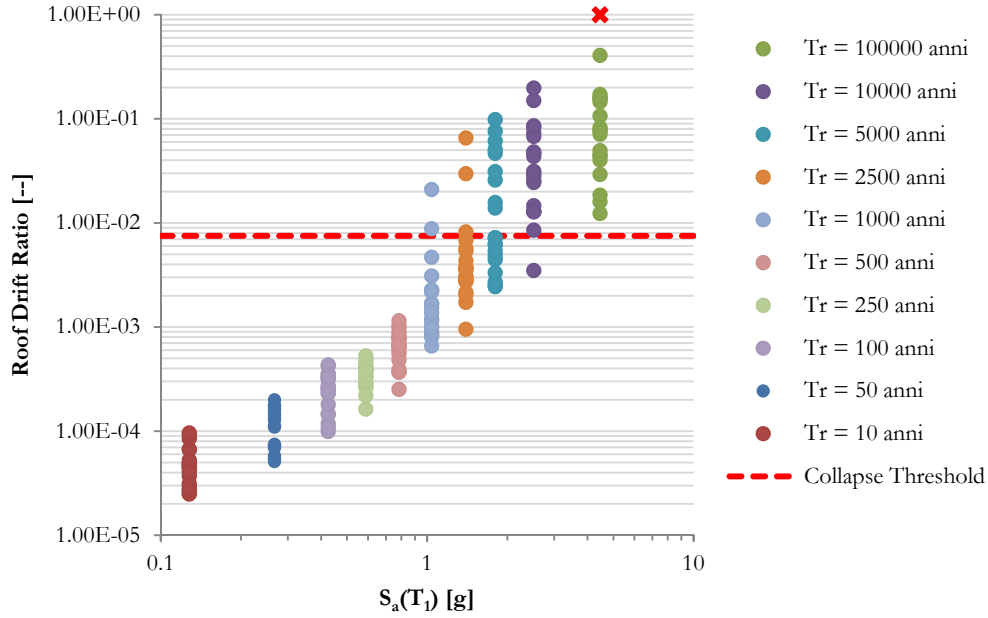


Figure 3.8 Roof drift ratio, RDR, distribution for 10 IM levels,  $S_a(T_1)$ . Each stripe shows the record to record variability for the specific IM level. The results are related to an Unreinforced Masonry building located in L'Aquila soil type C. The red cross in the last IM Level represent the only case of numerical/dynamic instability that was assumed to be collapse.

The computed probabilities for each IM level can be fitted by a probabilistic distribution (e.g. lognormal) defining what is usually called the *Fragility* curve. This function quantifies the probability that the considered structure will experience a fixed Limit State or worse for a set of continuous IM values. The fragility curve, however, does not account for the probability of occurrence of each IM level at the building site in any given period. This latter information is carried by the site hazard curve for the specific IM. The combination of building- and site-specific fragility curve and site hazard curve provides an estimate of how often the particular case study building is likely to observe the Limit State of interest, e.g., Collapse. This computed rate represents the result at the *Fragility Analysis* stage (see Figure 3.2); in particular, equation (3.1) can be approximated as:

$$\lambda_{LS} = \int_{all\ IM\ L} P[LS | IM = x] \cdot |dH_{IM}(x)| + \lambda_{IM \geq IM_{10}} \quad (3.4)$$

Where the first part represents the output coming from the convolution of conditional probability of exceeding the *LS* threshold at  $IM=x$ ,  $P[LS | IM=x]$ , with hazard,  $dH_{IM}(x)$ ,

while the second one,  $\lambda_{IM \geq IM10}$ , refers to the contribution to risk related to intensities with return period higher than  $10^5$  years (the last analyzed herein). The approximation of equation (3.4) assumes for simplicity that all the ground motions with an IM level rarer than  $10^5$  years return period will cause (i.e.  $P[LS | IM=x]=1$ ) collapse of the structure. This approximation is tenable in most cases and even when it is not (i.e., for reinforced concrete structures in low hazard areas such as Milano) this approximation is inconsequential for all practical purposes. In line with this, the term  $\lambda_{IM \geq IM10}$  is set to be equal to the constant value of  $10^{-5}$  which corresponds to the hazard of the  $10^{\text{th}}$  IM level:

$$\lambda_{IM \geq IM10} = \int_{IM \geq IML10} P[LS | IM = x] \cdot |dH_{IM}(x)| = \int_{IM \geq IML10} 1 \cdot |d\lambda_{IM}(x)| = H_{IM \geq IML10} = 10^{-5} \quad (3.5)$$

The computed rate is, therefore, an upper bound of the true value. An important aspect related to the structural response post-processing phase is certainly the definition of the Limit State threshold. Indeed, the assumptions on this field can affect significantly the final outcome and, therefore, it should be stated clearly and properly justified. Herein the thresholds, both for Collapse and Damage LS, were assumed to be deterministic and specific for the structural characteristics of each single building. In particular, the reference for both cases is the non-linear static analysis (aka pushover); this choice was driven by a need of defining a global criterion that allows cross-typology comparisons. Therefore, for all the structural types, but the base isolated cases, the collapse thresholds are assumed to be the roof drift values corresponding to the 50% drop in the base shear along the negative stiffness branch of the pushover curve. For the base-isolated structures, collapse was intended to be reached either when the previous roof drift ratio thresholds were exceeded or when the maximum displacement of the base isolator was reached. The thresholds related to the Damage Limit state too are related to a deformation-based measure (i.e., roof drift ratio). In particular, the limits are assumed according to code provisions (§7.3.7.2 NTC [2008b]) for all structural typologies but the masonry for which a pushover based criterion was considered (i.e. the onset of damage starts at RDR taken in correspondence of 70% maximum base shear on the ascending branch).

### 3.3 RESULTS

The results are presented both in terms of fragility curves and annual (nominal) rates of Collapse or of onset of Damage. The mean fragility curves are presented for each structural typology based on the results from all the configurations while the risk rates are presented singularly for each of the building case studies.

### 3.3.1 Fragility Curves

The fragility curves were obtained by fitting lognormal distributions to the RDR response values conditioned on observing fixed IM levels. The explicit estimation of the fragilities has been limited to the most common structural typologies, namely RC and Masonry structures. The parameters of the “average” curve are computed as follows:

$$\begin{aligned}\bar{\mu} &= \frac{1}{N} \cdot \sum_{i=1}^N \mu_i \\ \bar{\sigma} &= \sqrt{\text{var}(\mu_i) + \text{mean}(\sigma_i^2)}\end{aligned}\tag{3.6}$$

It should be underlined that the “average” curves are computed with slightly different assumptions for masonry and RC cases. For the former all the configurations are analyzed together, based on the hypothesis that they could be assigned to the same category: common taxonomies assume 2- to 3-story structures as low-rise buildings. Even though a distinction between regular and irregular structure is reasonable, we decided to consider all the cases together since separating them would result in sets not enough populated to be reliable. On the other hand, the RC cases are explicitly defined to model low-, mid- and high-rise buildings and, therefore, they are treated separately. Moreover, the bare-frame configurations are not included in the computation of the average curves: they are certainly interesting for research purposes representative of real structures only during the construction phase. About collapse analysis, some combinations of structure/site result in fairly low collapse probability even if conditioned at the rarest IM levels. In those cases, particularly frequent for RC structures, a fragility function cannot be defined and will not be included in the set.

The following figures from Figure 3.9 to Figure 3.12 show the fragility curves computed for RC and masonry buildings for the Onset of Damage (SLD) and Collapse (SLC) limit states. The x-axis is normalized with respect to the  $S_a(T_i)$  design value at the site, 10% and 63% in 50 years for Collapse and Damage, respectively. This expedient allows us to put all the curves in the same chart and compare them. Differently, representing them with their own, un-normalized, IM in the same chart would be meaningless because different  $T_i$  would refer to different IMs not strictly comparable. The black dotted vertical lines represent the design IM values and are useful for the evaluation of the probability of Collapse (Damage) conditioned on observing that ground motion level. Regarding SLC, both masonry and RC structures observe low probability of collapse; only the masonry structures in L’Aquila have about 3.5% probability of collapse (Figure 3.11). On the other hand, looking at the Onset of Damage limit state, the conditional probabilities, at the ground shaking level to be verified for SLD, are not negligible but lower than 20%. In particular, the Masonry structures seem to be less prone to early damage with respect to the RC ones; this behavior could be justified recalling the different design philosophies

followed for those structural typologies. Indeed, well designed RC structures typically rely on ductility and, therefore, on the capability of dissipating the energy input induced by the earthquake through a “controlled” damage pattern. On the other hand, since the use of masonry walls is less versatile, those structures rely rather on pure resistance and strength and, therefore, their seismic behavior show a later onset of damage but a lower post-elastic margin before collapse. That is the reason why the masonry structures are less “safe” towards collapse but more protected from early damage. However, it should be underlined that the previous considerations are based solely on deformation-based responses (EDPs). A more comprehensive performance analysis would also include acceleration-based EDPs, such as peak floor acceleration, and these latter EDPs might alter those arguments. Moreover, both for masonry and RC structures, the following figures clearly show the dependency of the fragilities on the site. In particular, mostly for masonry, the structures located in the most hazardous zones seem to be more vulnerable, i.e., their median capacities are nearer to the design acceleration. This is especially evident for SLD for which a proper fragility can be computed for nearly all the cases. For example, both in Figure 3.10 and Figure 3.12, the curves related to structures located at sites with lower hazard are on the rightmost part of the chart. Therefore, their probability of damage for  $S_a/S_{a,SLD}$  ratio tends to be lower than that of similar buildings designed for higher-hazard sites. Hence, we could argue that the lower the site hazard, the larger is the distance between the median capacity and the design level. This implies that buildings that are designed according to the NTC08 for lower hazard sites are “safer”. These results could be seen as first evidence, which will be later confirmed convolving hazard and fragilities, of a non-uniform risk of buildings designed for sites throughout the country.

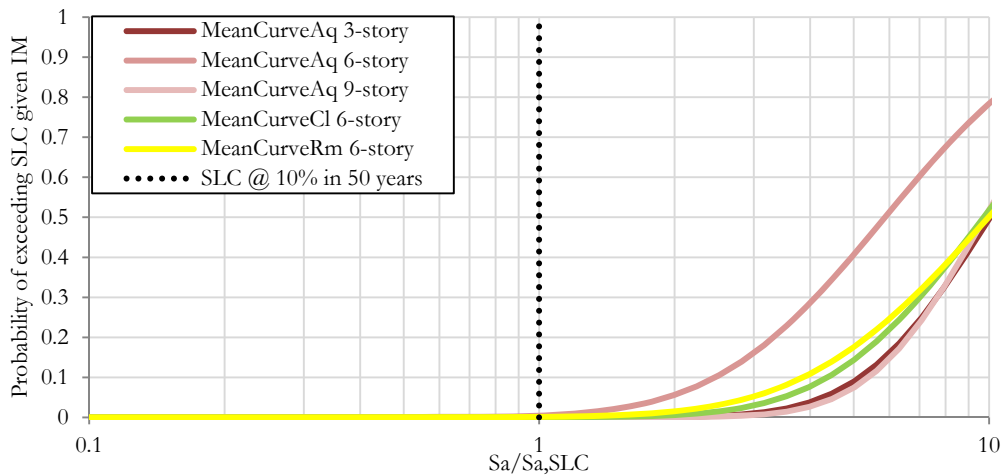


Figure 3.9 Mean Fragility curves for SLC of RC structures on soil type C. The x axis is normalized by the elastic  $S_a$  value extracted from the UHS corresponding to the 10% in 50 years hazard level

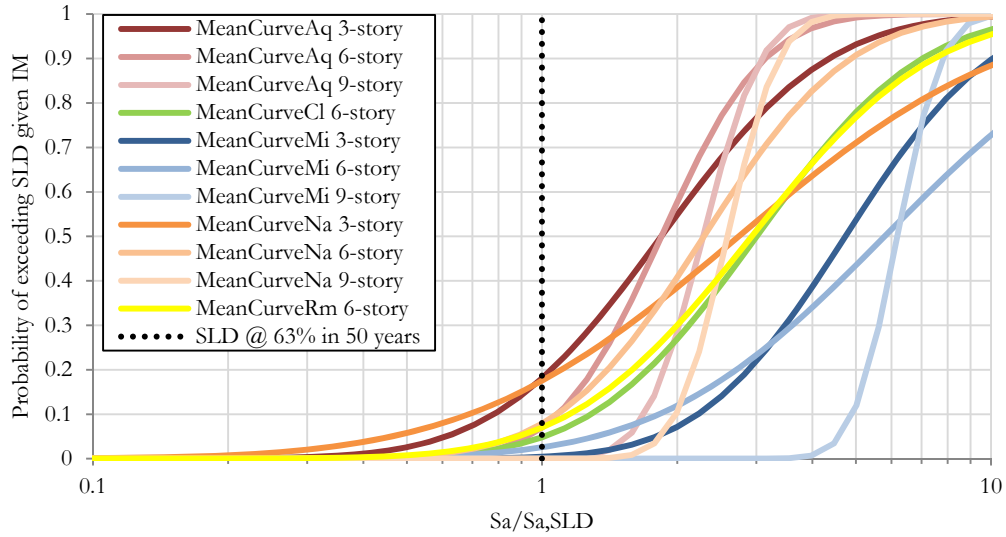


Figure 3.10 Mean Fragility curves for SLD of RC structures on soil type C. The x axis is normalized by the elastic  $S_a$  value extracted from the UHS corresponding to the 63% in 50 years hazard level.

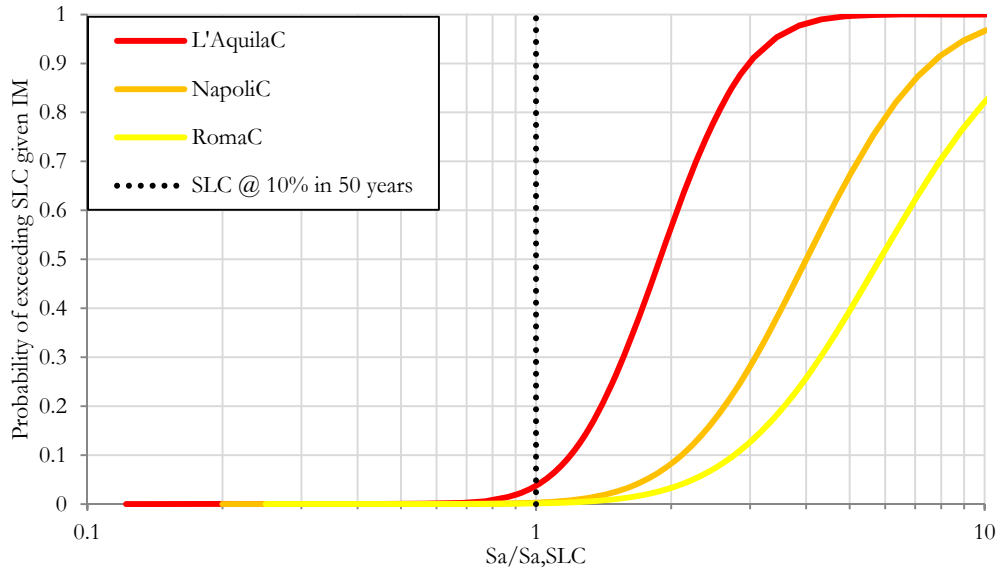


Figure 3.11 Mean Fragility curves for SLC of URM structures on soil type C. The x axis is normalized by the elastic  $S_a$  value extracted from the UHS corresponding to the 10% in 50 years hazard level.

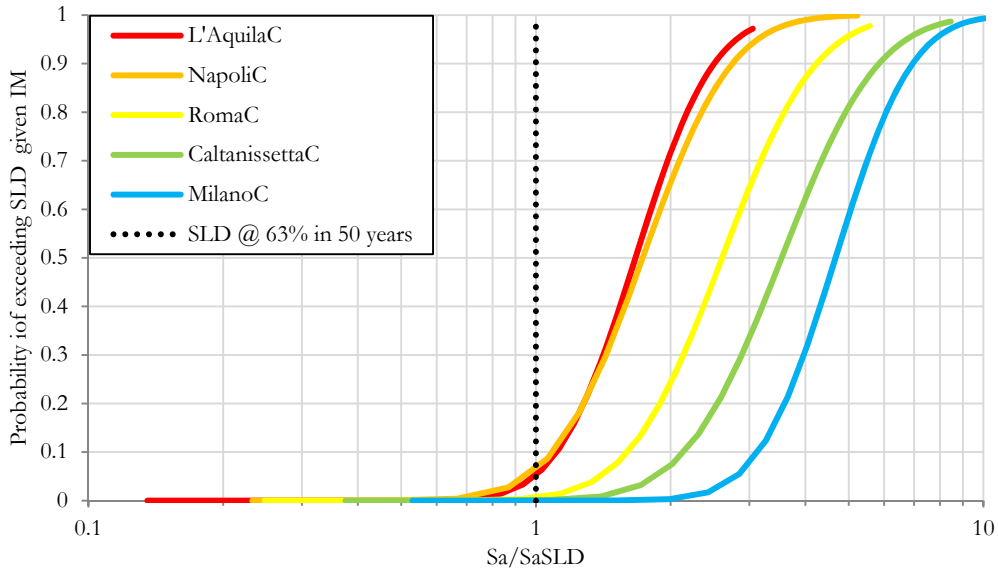


Figure 3.12 Mean Fragility curves for SLD of URM structures on soil type C. The x axis is normalized by the elastic Sa value extracted from the UHS corresponding to the 63% in 50 years hazard level.

### 3.3.2 Risk Nominal Rates

The following charts show the annual nominal collapse rates for all the case studies analyzed, subdivided per city and soil type. Different marker colors and shapes refer to different structural typologies. The numerical values of the rates are given in the 5.1 Appendix D.

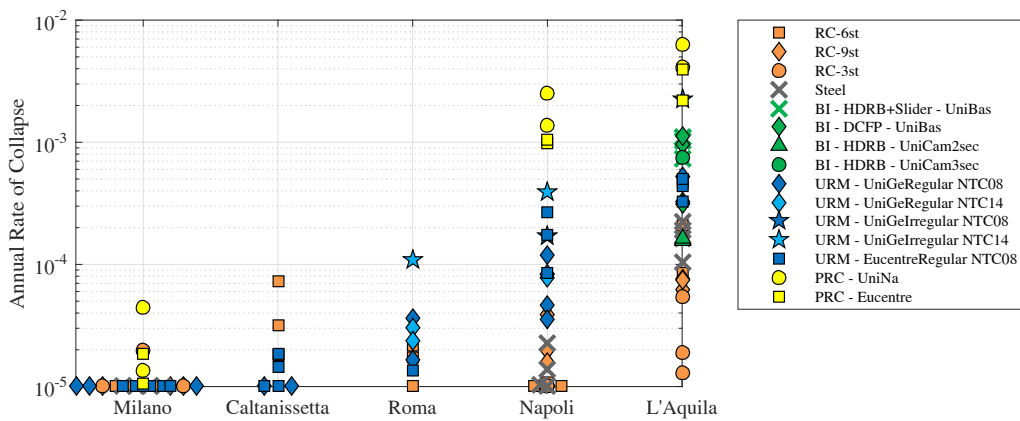
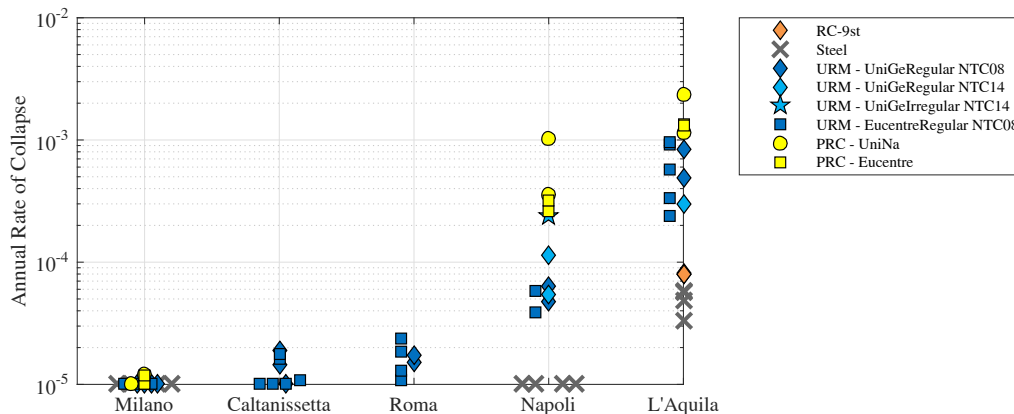


Figure 3.13 Annual collapse rates for different structural typologies located at five sites on soil type C.



**Figure 3.14.** Annual collapse rates related to different structural typologies placed in five sites on soil typology A.

Figure 3.13 and Figure 3.14 show clearly that the collapse risk of different building types at different locations is far from uniform. In particular, the rates increase with increasing values of site hazard, namely the higher is the hazard the higher is the collapse rate. For some combinations site-structure, the rates are so low that only an upper bound of  $10^{-5}$  can be assigned. Overall, the most vulnerable structures are the precast and the unreinforced masonry ones. The major weakness of the former is mainly related to the connections behaviour under seismic loading; indeed, if their failure is not accounted for, the collapse rates observe a drastic drop but the estimates would not be realistic. Recent events (e.g., the Emilia Romagna earthquakes of 2011) have dramatically brought to light this singularity which should be carefully considered by regulators since the structures analysed herein are designed according to the current code provisions. However, the connections are simply modelled as hinges and the actions induced by the earthquake ground motion are simply compared at the end of the analysis with the connection resistance. This modelling choice is not state-of-the-art. A more accurate modelling choice for the connections could bring significant improvements in the reliability and robustness of the results for this structural typology and likely decrease the quite high collapse rates shown here.

Unreinforced masonry structures are characterized by significant collapse rates, mostly in their irregular configurations and at sites with high hazard. For masonry structures, the walls' thickness and their plan configurations are among the most effective design choices that the engineer can control to improve the performance of a structure against seismic action. However, as a consequence of the increase of walls' thickness, the building mass will grow and so will the inertia forces induced by the ground motion. Therefore, it is not possible to have an unreinforced masonry building with the same performance of a RC

one in a high seismicity area. In line with this concept and aiming at achieving a more uniform risk, a possible way forward could be disallowing the design of URM buildings in the most hazardous zones altogether or, to a bare minimum, limiting the design to some more regular configurations.

Another interesting outcome is the collapse rate of base-isolated structures. Indeed, the use of a proper designed isolation system allows decoupling the seismic action from the dynamic characteristics of the structure, which, therefore, does not experience the dangerous frequency range of the ground motion. However, the analyses performed show significant collapse rates (Figure 3.13). Analysing directly the structural response, the structure behave well until the buildings experience design level ground motions (i.e., those corresponding to the 6<sup>th</sup> stripe, that has about 1000 years return period), after which a significant number of collapses are observed. In particular, the main critical issues are related to the devices: the results seem to show them to have low “residual resistance” after the attainment of their design intensity level. However, a possible influence of the selected records should be considered. Finally, it should be emphasized that the base isolators reaching their maximum displacement capacity may not necessarily mean that the superstructure will collapse too. Therefore, these buildings may still possess some additional safety margin not accounted for here.

Figure 3.15 and Figure 3.16 give the annual rates related to Damage limit state. These results are preliminary since all research units have not yet decided a consensus-based shared criterion for SLD definition. However, some reasonable assumptions are made herein for each structural typology; the thresholds and criteria that will later be agreed upon are not expected to significantly modify the following results and consequent considerations. In particular, the assumed damage thresholds are summarized in the following list:

- Masonry. Roof drift in correspondence of the 70% of the maximum base shear in the increasing branch of the pushover. This assumption roughly corresponds to the end of the linear branch of the pushover curve.
- RC-frames: code definition of LS threshold in terms of Maximum Interstory Drift. A value of 0.5% was assumed for bare frames and 0.3% for Infilled and Pilotis cases.
- PRC: also in this case a code-based criterion was adopted. In particular, a 1% MIDR was chosen in order to guarantee “the damage prevention of non-structural components fixed in a way so as not to interfere with structural deformations, or without non-structural elements.” (see §7.3.7.2 of NTC [2008b], equation 7.3.17).
- Steel: 0.5% threshold (§7.3.7.2 of NTC [2008b]) considering rigidly anchored infills that interacts with the structural deformation.

- Base isolated structure: defined in line with the RC frames since simply related to superstructure damages. Therefore, the damage threshold is estimated as the 0.3% of MIDR (in compliance with table C8.3 of the commentary document, NTC [2008a])

Interestingly, for soil type C and in line with what seen for fragility curves, the RC structures seem to be more vulnerable, in terms of onset of damage, than to the masonry buildings. This is due to the higher flexibility of the RC frames that at lower excitation levels typically observe higher displacements; that cause damage to infills and partitions. This level of damage does not occur in masonry buildings until they experience higher levels of accelerations. However, the irregular masonry buildings located in Napoli and L'Aquila show higher rates of onset of damage than the other cases. As expected, the base-isolated cases, contrarily to what seen for SLC, show a significantly lower rates than the other typologies.

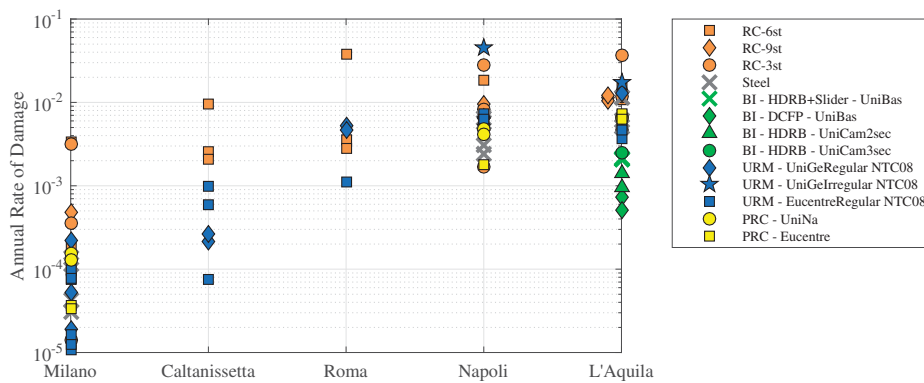


Figure 3.15 Annual rates of onset of damage for different structural typologies located at five sites on soil type C.

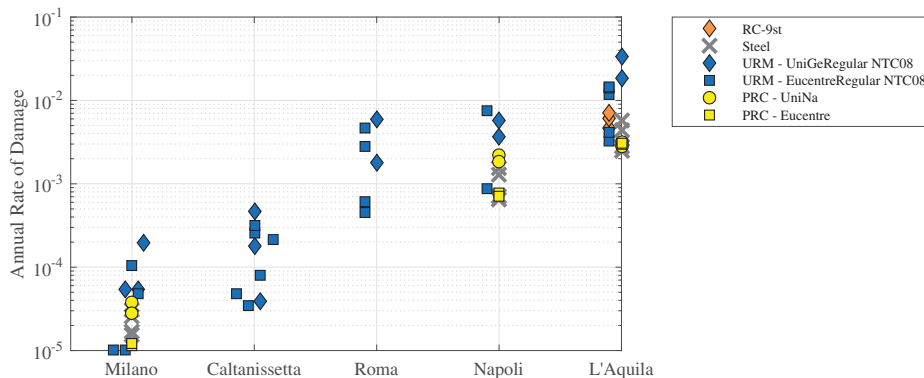


Figure 3.16 Annual rates of onset of damage for different structural typologies located at five sites on soil type A.

### 3.4 VALIDATION OF THE RESULTS

The calculations conducted until now are based on widespread assumptions and procedures, For example, we represented the ground shaking severity by means of Spectral acceleration at the natural period of the structure and selected, coherently, the records by means of the CS-based method conditioning on this IM. In this last part of the work we wanted to modify some of these assumptions in order to verify the robustness of the obtained collapse rates. In particular, the following paragraphs will investigate the influence of a) using different ways of calculating the annual rates of exceedance of a limit state and of b) adopting different selection techniques and IM types.

#### 3.4.1 Calculation of annual rate of collapse

The risk calculation has been performed combining the information about hazard and structural response (expressed in terms of probability of collapse conditioned on observing a fixed IM value).

$$\lambda_{LS} = \int_{allIML} P[LS | IM = x] \cdot dH_{IM}(x) + \lambda_{IM \geq IM10} \quad (3.7)$$

In particular, the first key point is about the discretization of the hazard curve and the second one is about the calculation of the conditional probability of collapse. The different approximation of the hazard curve impacts the importance of  $(dH_{IM}(x))$ , namely the weight given to the conditional probability  $(P[LS | IM=x])$  for each of the 10 stripes. More precisely, the rates computed previously are based on hazard curve discretized in 11 points, the first is the rate of all the earthquakes above the minimum magnitude expected in the region around the site and each one of the remaining ten is the inverse of the return period associated to the corresponding stripe (see Table 3.4). The proposed alternative is to discretize the hazard curve again in 11 points but chosen in order to define 10 intervals containing the 10 IM values representative of each stripe. Figure 3.17 shows how the discretization of the hazard curve changes the occurrence rate,  $dH_{IM}(x)$ , assigned to each IM level; for example, the red shaded rectangle represents the importance given to the probability of collapse conditioned on IML1.

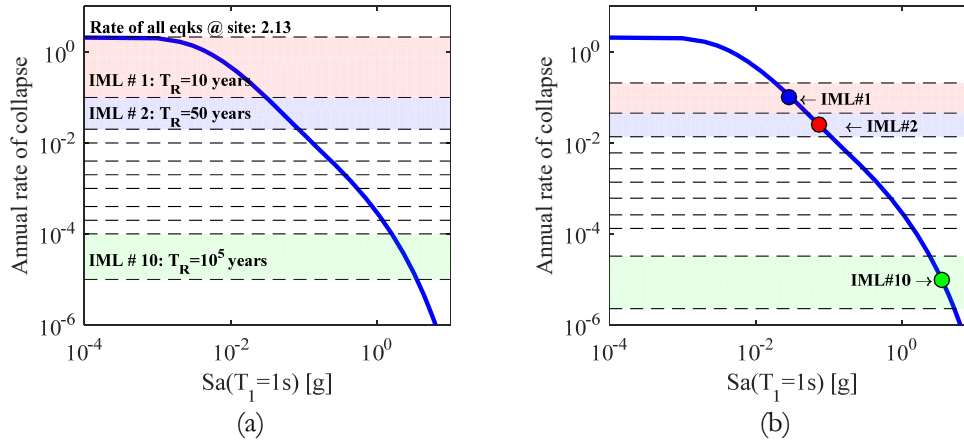


**Figure 3.17** Proposed Hazard curve discretization approaches: (a) Method 1, IML assigned to the lower bound of the interval and (b) Method 2, IML assigned to the middle point of the interval. The dashed lines defines the 11 points in which the hazard curve is discretized; in the panel (a) the first one is the rate of all the earthquakes above minimum magnitude in the region around the site and the others coincide with the rates of the 10 IMLs.

Secondly, the conditional probability could be computed in a simpler way with respect to the equation (3.3) that includes a lognormal fitting of the finite responses of the structure combined with certain collapse (i.e. numerical/dynamic instability) by means of total probability theorem. Indeed, this conditional probability could be calculated as the ratio of the number of collapses over the total (twenty) cases of each stripe, including both the instabilities and the exceeding of the collapse threshold.

According to these considerations the convolution integral could be approximated in three ways:

1. Tails+ $T_R$ . The results presented in the previous paragraphs are based on this method: hazard curve discretized in correspondence of the  $T_R$  of each stripe and of the  $T_r$  of acceleration equal to zero (namely the rate of all the earthquakes above the minimum magnitude in the region around the site, as shown in Figure 3.17(a). The conditional probability is computed according to the equation (3.3).
2. Tails+HC. The conditional probability is calculated as in the previous point while the hazard curve is discretized in order to have the 10 stripes in the middle of the 10 intervals that approximate the hazard curve, Figure 3.17(b).
3. Empirical+HC. The hazard curve discretization is the same of point 2 while the conditional probability is computed as the fraction of cases that causes collapse (irrespective of instability or threshold exceeding) out of the total of twenty.

Other approaches for convolution calculation are possible, e.g. fitting a fragility curve through the conditional probability data points and directly combining it with the hazard curve. Nevertheless, approaches like this are not considered, for the time being, because of additional considerations and possible shortcoming related to the type and quality of fitting strategy. The following Figure 3.18 and Figure 3.19 compare the rates obtained with the three described approaches for some RC and masonry buildings. It should be underlined that the rates are computed until the last IM, i.e.  $10^5$  years return period without the additional  $\lambda_{IM \geq IM10}$  factor of equation ( 3.4 ). Overall the hazard curve discretization based on  $T_R$  (Figure 3.17(a)) gives a higher estimate of the rate observed in all cases; this is due to the fact that the other method discards the first part of the hazard curve where there are low probabilities of collapse but high frequency of that level of ground shaking. However, the rates always remain in the same order of magnitude and therefore the test conducted herein confirms their robustness with respect to the method of calculation.

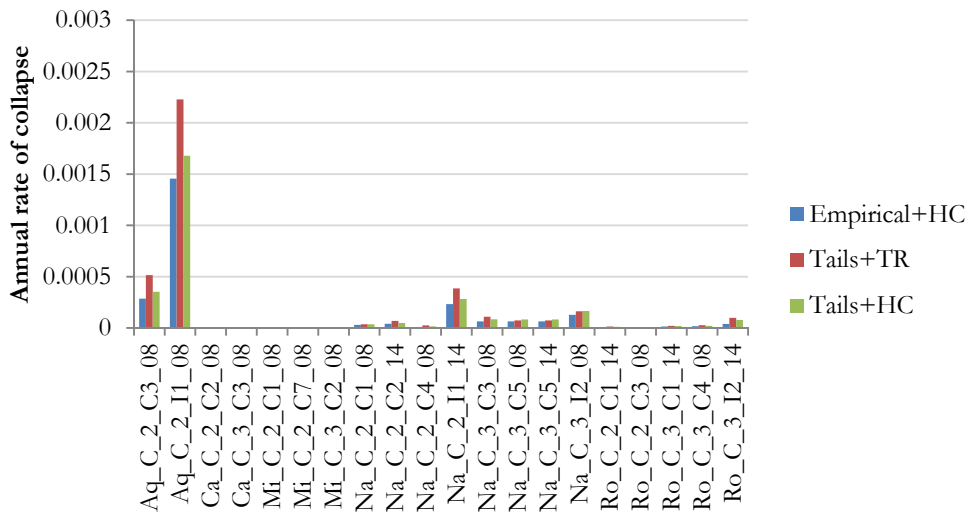


Figure 3.18. Impact of convolution integral approximation for some configurations of masonry building located at five cities on soil type C.

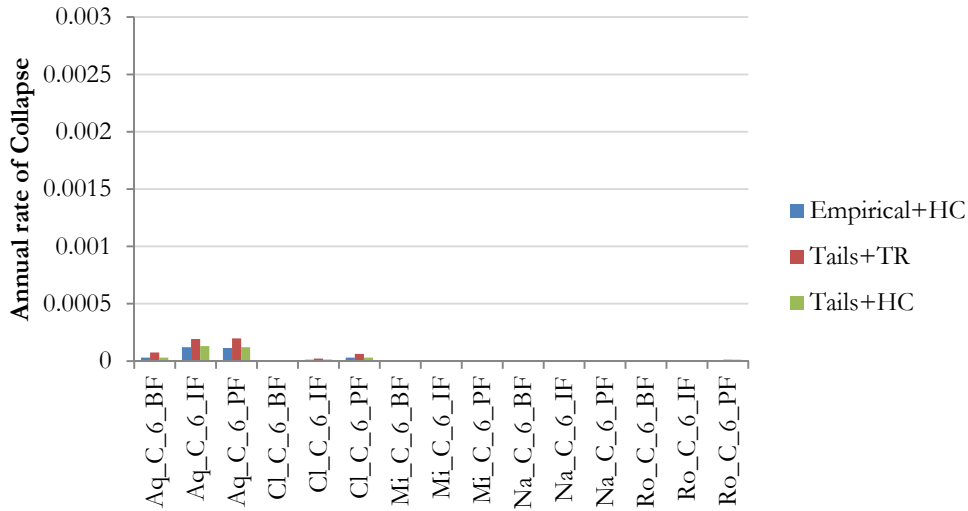


Figure 3.19. Impact of convolution integral approximation for six-story RC frame buildings (in three configurations, namely bare, BF, infilled, IF, and pilotis, PF) located at five cities on soil type C.

### 3.4.2 Influence of different record selection techniques and IM types

The additional calculation proposed herein aim at investigating three aspects: the influence of i) another, more advanced IM with respect to the classical  $Sa(T)$ , ii) a lighter record selection technique that could decrease the computational effort, and iii) the measure (EDP) adopted to represent the structural response.

First, about ground shaking measure, Lin et al. [2013c] have shown that the choice of conditioning period ( $T^*$ ) for spectral acceleration does not affect much the output if the performance of the structure is quantified by means of a “Risk based assessment”, i.e. evaluating the rate of exceeding a given level of response, that define the limit state threshold. However, a wise choice of  $T^*$  can certainly help to obtain a more precise and robust response prediction. For example, spectral accelerations at  $T_1$  or, much better,  $1.5T_1$  were proven to be good choices for collapse prediction, which is mainly influenced by deformation-related EDPs, e.g. Maximum inter-story drift ratio (MIDR). However, long period spectral accelerations are not good choices if one is interested in lower-deformation limit states and acceleration-related (peak floor acceleration, PFA) limit states that are essential for loss estimation. A dichotomy is appearing, here: a) base the analyses on long period spectral accelerations, capturing well the ultimate behavior of the structure, or b) on low period ones, focusing more on non-structural damage that usually constitute the major contribution to monetary losses? It is in this context that an intensity measure as the average spectral acceleration, AvgSA, could be very helpful. Indeed, being slightly more complex than a canonical  $Sa$  (it is defined as the geometric mean of  $Sa(T)$

over a range of periods), it has been proven to perform well both for deformation (MIDR) and acceleration (PFA) related EDPs. In addition, it does not need an ad-hoc ground motion prediction model and is, typically, more efficient than spectral acceleration (Kohrangi et al. [2015a]; Kohrangi et al. [2017a]).

Secondly, aiming at decreasing the computational burden, it is certainly interesting to investigate the possible adoption of a record selection procedure that defines a unique record set for a series of cities. If the results were to be coherent with those obtained from the site specific record selection, one would be able to decrease the number of analyses needed to obtain a robust estimation of the structural response and, therefore, of the risk.

Lastly, we consider the measure adopted for the structural response. The previous computations are based on Roof Drift Ratio as EDP, calibrated on non-linear static analyses data. If the Limit State threshold is not properly chosen, the assessment of the ultimate behavior of the structure may be affected. Therefore, the choice of RDR-based thresholds for ultimate capacity is tested against the more robust Maximum inter-story drift ratio (MIDR) based thresholds for incipient collapse.

#### 3.4.2.1 *Analysis scheme and case study*

The critical issues described previously will be addressed by testing a reference structural typology among those included in the RINTC project, i.e. a six-story RC frame with soft story (i.e., pilotis configuration) designed for three cities namely L'Aquila, Napoli and Milano. These structures will be subjected to record sets selected on the basis of three strategies:

1. Approach 1. Site specific record selection based on  $Sa(T1)$ ; one record set per site. Multiple Stripe Analysis (MSA) at 10 fixed Hazard Levels (from 10- to  $10^5$ -year return periods). This is our reference: the results presented previously are based on this approach.
2. Approach 2. Site specific record selection based on AvgSA; one record set per site. Multiple stripe analysis at 10 fixed Hazard Levels. The only difference with the previous approach is the IM used to perform the assessment.
3. Approach 3. Multi-site CS record selection based on AvgSA; just one record set selected accounting for the scenarios that most contribute to the hazard at each site. MSA performed at 10 levels characterized by the same AvgSA value (from 0.03g to 2.25g). This choice was dictated by the need of having a record set suitable for all the sites and that could allow the comparison among them.

The structural response will be evaluated to assess the risk for the collapse limit state (SLC). The attainment of the LS is evaluated on the basis of deformation based EDP (i.e., RDR and MIDR). The thresholds that define the achievement of the LSi are summarized in Table 3.5.

**Table 3.5 Assumed EDP thresholds for Collapse and Damage limit states.**

Limit State	Engineering Demand Parameter (EDP)	Threshold
Damage (SLC)	Roof Drift Ratio (RDR)	RDR @ 50% Drop on Pushover Curve
	Maximum Interstory drift ratio (MIDR)	Assumed as a function of the RDR

The collapse thresholds used so far are defined in terms of the RDR corresponding to the 50% of the maximum base shear extracted from the pushover curve. This threshold could potentially be unsuitable for defining the collapse of the structure because of the non-linear deformed shape of the building expected at severely post-elastic response levels. Hence, the “new” analyses (in terms of AvgSA) are post-processed considering also another, and more reliable, response measure, i.e. MIDR. For the considered buildings, the RDR corresponding to collapse was selected to be about 5%. To be consistent we need to estimate the MIDR threshold that is reached, on average, when the RDR is equal to 5%. It is expected the MIDR at collapse to be larger than 5%. Moehle [1992] suggested a 1.5 factor for a five story frame designed to withstand lateral loads and a 1.8 factor for a structure designed for vertical loads only. However, the results of the response analyses carried out so far can be harvested to derive an ad-hoc relationship between RDR and MIDR for these buildings. In particular, a linear regression between MIDR and RDR is conducted separately in the two directions and for buildings located at each city (Figure 3.20). The data points are only the cases for which the structural response is non-linear (after yielding) but finite, i.e. the cases corresponding to dynamic/numeric instability are obviously screened out.

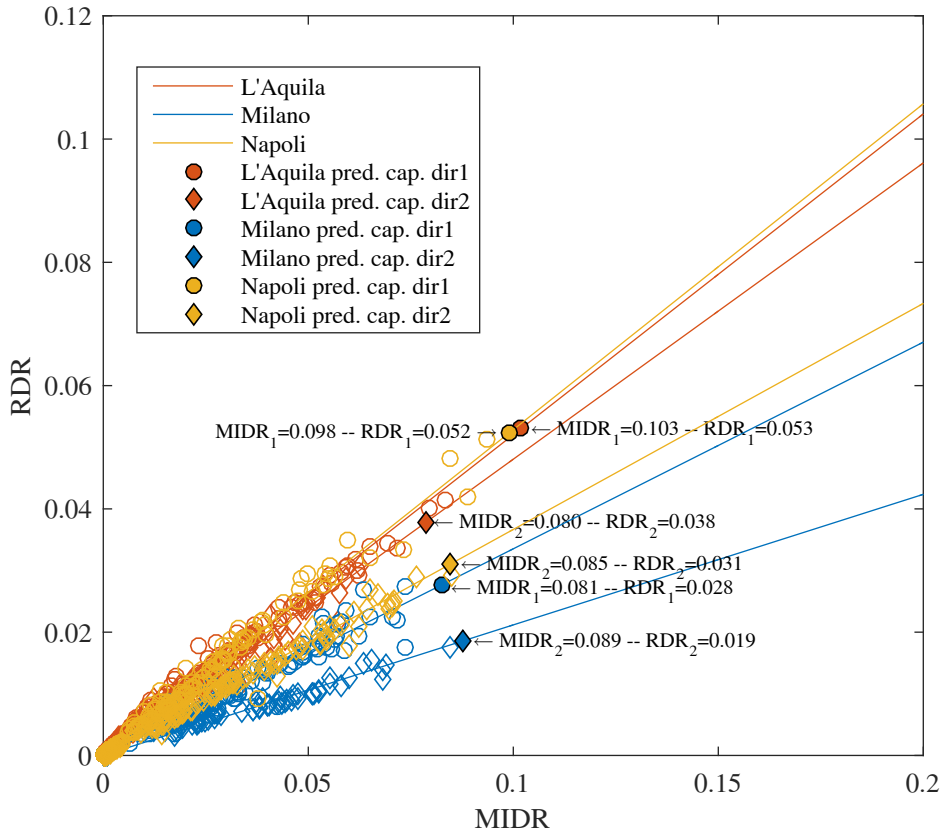


**Figure 3.20** Regression analyses on output data for each of the three structures carried out separately for each horizontal direction. The markers represent the RDR collapse threshold and the corresponding MIDR.

Analysing Figure 3.20, it is interesting to notice that the ratios are higher than those proposed by Moehle [1992]; this could be due to the pilotis (weak story) configuration of the building. However, the trend of the RDR/MIDR ratios is in line with Moehle’s suggestions, indeed the weaker structure, the one located in Milano, is characterized by a higher MIDR/RDR ratio. This is expected since, for a fixed roof displacement (drift) a weaker structure will observe higher degree of deformation with respect to a stronger one. However, deriving the structural capacity expressed in terms MIDR threshold using these factors could bring to non-realistic values. For example, comparing the Milano and L’Aquila capacity in direction 2, the RDR capacity of the latter is double the one of the former but when “translated” in terms of MIDR it becomes basically the same. This latter evidence could be questionable since L’Aquila and Milano are characterized a considerably different seismic hazard and the structures are expected to reflect this

distinction. Several studies (e.g. Miranda and Aslani [2003]) support the use of MIDR as response measure for predicting structural performance and, probably, the issue observed herein is another proof that supports its adoption in place of RDR. The structural responses coming from the analyses of Approach 2 and Approach 3 will be post-processed using collapse thresholds (Table 3.6) expressed in terms of a) RDR, b) MIDR estimated from RDR using regression data ( $MIDR_{SD}$ ) and c) MIDR thresholds chosen in order to maintain a reasonable capacity difference between the structures ( $MIDR_{SF}$ ). The outcomes will be compared between each other and to those coming from the Approach 1 both in terms of fragility curves and collapse rates.

**Table 3.6 Collapse threshold assumed for different EDPs of reference**

EDP type	Bldg. dir.	L'Aquila	Napoli	Milano
a) RDR	Dir1	0.053	0.052	0.028
	Dir 2	0.038	0.031	0.019
b) $MIDR_{SD}$	Dir1	0.103	0.098	0.081
	Dir 2	0.080	0.085	0.089
c) $MIDR_{SF}$	Dir1	0.106	0.104	0.056
	Dir 2	0.076	0.062	0.038

### 3.4.2.2 Results

The outputs will be compared both at structural response level, by means of fragility curves, and at the risk level, in terms of annual rates of reaching the LS of interest, namely collapse. Approach 1, again, refers to the  $Sa(I)$ -based assessment described in the previous chapter and represents the evidence to be tested. In particular, the following Figure 3.21 and Table 3.7 show the collapse fragility curve, its parameters and the associated collapse rate for the building at the given site. The cases of Napoli and Milano do not observe collapses and, for this reason, it was not possible to reliably define a collapse fragility curve. Therefore, in these cases, the collapse rate is conservatively estimated to be equal to its upper bound, namely  $10^{-5}$ . Since the stripes are defined at the same hazard level, those structures do not observe collapses in Approach 2 as well and, therefore, the collapse rates are assumed to be less than  $10^{-5}$ .

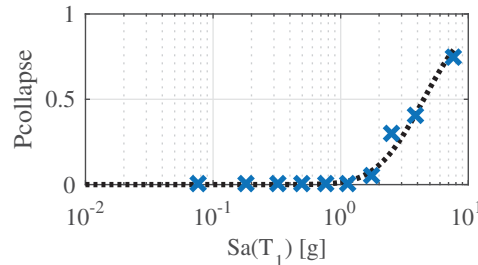


Figure 3.21 Fragility curve for a pilotis six-story frame designed for L'Aquila on soil type C.

Table 3.7 Parameters of the computed Fragility curves and corresponding collapse rate.

City	RDR as EDP for Collapse		
	Median [g]	$\sigma_{\ln Sa}$	MAF <sub>collapse</sub>
L'Aquila	4.47	0.67	1.98e-4
Napoli	---	---	<10 <sup>-5</sup>
Milano	---	---	<10 <sup>-5</sup>

The outputs, derived for different EDP choices and coming from the aforementioned Approaches 2 and 3 are summarized in the following Figure 3.22, Table 3.8 and Table 3.9 in the form of fragility curves and corresponding collapse rates. Looking at fragilities it can be observed that:

- The choice of the EDP influences only the multi-site case, i.e. Approach 3 (right column of Figure 3.22 and Table 3.9). Indeed it is the only approach that, by design, allows defining fragility curves for all the sites and, therefore, to compare them.
- The fragility curves based on AvgSA (Figure 3.22) are characterized by lower variability than those based on classical Sa (Figure 3.21). This is due to the superior properties of AvgSA already brought to light by Kohrangi et al. [2017c].
- The multi-site case (Approach 3, right column of Figure 3.22) shows that the fragility curves of Napoli and L'Aquila could be reasonably considered (despite the IM choice) as statistically equivalent. This evidence suggests that code provisions, in mid-to-high hazard zones, lead to define structures not so different from each other. The fragility related to the Milano building is far from the other

two because its design is basically dictated by the code minimum requirements and not by the seismic design loads.

- The fragilities coming from Approach3 highlight the influence of the EDP choice. Indeed, adopting RDR or its corresponding MIDR, i.e.  $MIDR_{SD}$ , could cause counterintuitive results. For example, the fragility related to the building located in L'Aquila, even though very close to the one in Napoli, is characterized by higher conditional probabilities of collapse. More specifically, since the two structures were subjected to the same records and L'Aquila is a more hazardous site, the designed building is expected to be more resistant than the one located in Napoli (i.e. having lower probability of collapse). In contrast, the use of a proper MIDR threshold seems to put the fragility curves in a more reasonable and intuitive order.

Moreover, focusing on risk estimates, the multisite case (Approach3), which makes use of just one record set for all the sites, provides a sufficiently accurate assessment of the collapse rate for L'Aquila. Indeed, the collapse rate is in the same order of magnitude of those coming from the other two, site specific, approaches. Additionally, Approach3 allows defining explicitly fragility functions for Milano and Napoli that, in the other approaches are approximated simply as step-functions that assumed collapse for all records with IM values larger than those in the last IM stripe. If Approach 1 and 2, for those cases, could give only upper bounds ( $1e-5$ ), Approach3 allows a direct convolution of hazard and fragility obtaining collapse rates consistent with the aforementioned limits. Therefore, we can argue that the collapse rates do not seem to be particularly influenced by the EDP choice; probably the convolution of the fragility with the hazard helps to smooth the differences observed at the fragility level. Notwithstanding this latter evidence, a MIDR-based collapse rate is likely to be more robust and near to the "true" but unknown value.

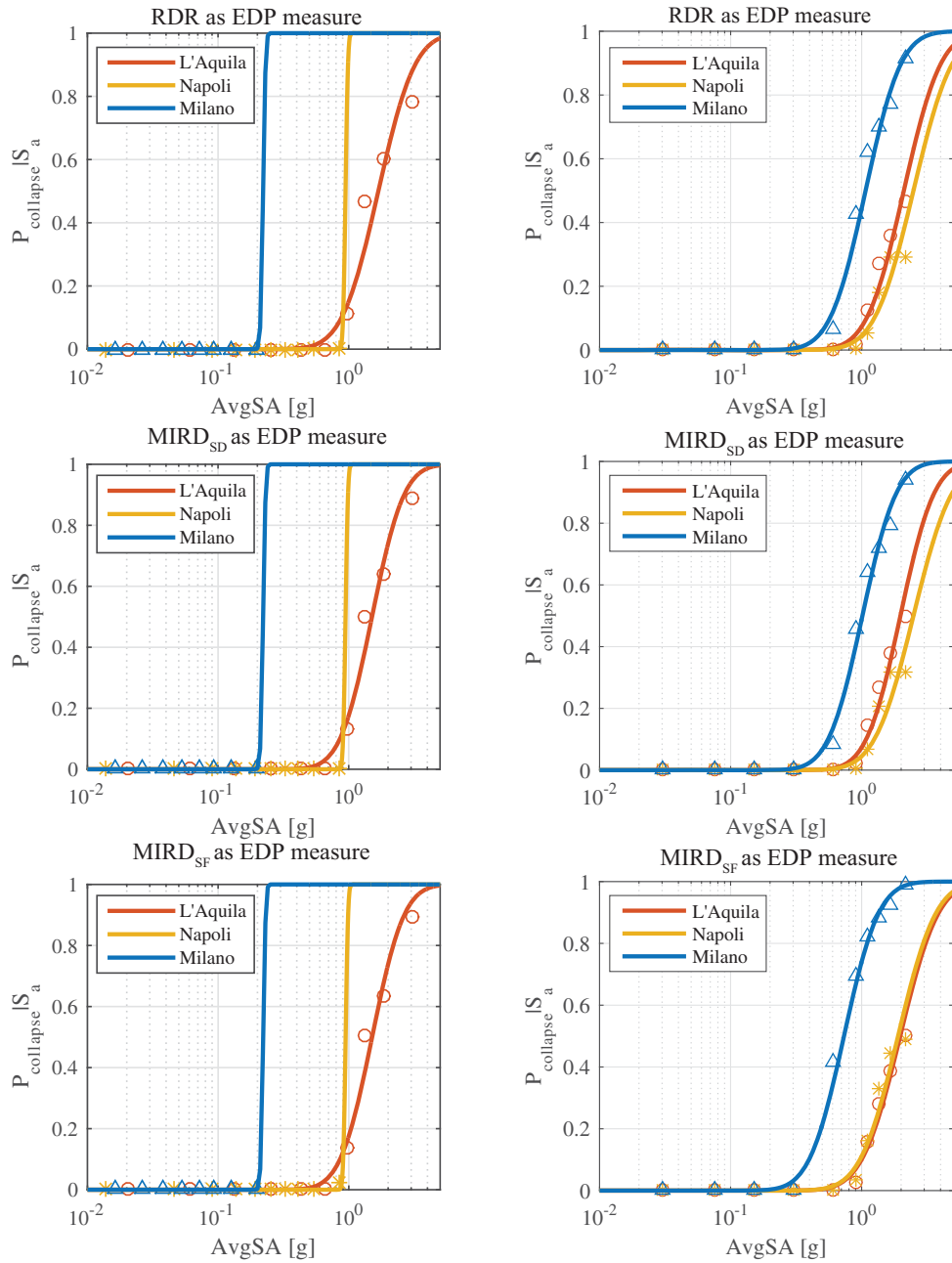


Figure 3.22 Fragility curves for a pilotis six-story frame designed for L'Aquila on soil type C. The left column is related to Approach2 (site-specific, AvgSA-based) while the right one refers to Approach3 (multi-site, AvgSA-based). Each row represents a different EDP choice namely RDR (first),  $MIDR_{SD}$  (second) and  $MIDR_{SF}$  (third).

**Table 3.8** Parameters of Fragility curves and corresponding collapse rates based on different EDPs and derived by means of Approach 2.

City	RDR as EDP for Collapse – Approach2			MIDR <sub>SD</sub> as EDP for Collapse – Approach2			MIDR <sub>SF</sub> as EDP for Collapse – Approach2		
	Median [g]	$\sigma_{InSa}$	MAF <sub>collapse</sub>	Median [g]	$\sigma_{InSa}$	MAF <sub>collapse</sub>	Median [g]	$\sigma_{InSa}$	MAF <sub>collapse</sub>
L'Aquila	1.69	0.51	1.83e-4	1.51	0.44	2.07e-4	1.51	0.44	2.07e-4
Napoli	---	---	<10 <sup>-5</sup>	---	---	<10 <sup>-5</sup>	---	---	<10 <sup>-5</sup>
Milano	---	---	<10 <sup>-5</sup>	---	---	<10 <sup>-5</sup>	---	---	<10 <sup>-5</sup>

**Table 3.9** Parameters of Fragility curves and corresponding collapse rates based on different EDPs and derived by means of Approach 3.

City	RDR as EDP for Collapse – Approach3			MIDR <sub>SD</sub> as EDP for Collapse – Approach3			MIDR <sub>SF</sub> as EDP for Collapse – Approach3		
	Median [g]	$\sigma_{InSa}$	MAF <sub>collapse</sub>	Median [g]	$\sigma_{InSa}$	MAF <sub>collapse</sub>	Median [g]	$\sigma_{InSa}$	MAF <sub>collapse</sub>
L'Aquila	2.10	0.51	1.11e-4	1.97	0.46	1.16e-4	1.97	0.53	1.37e-4
Napoli	2.48	0.53	1.27e-6	2.48	0.53	1.27e-6	1.90	0.52	3.49e-6
Milano	1.07	0.49	3.69e-8	1.01	0.47	3.86e-8	0.73	0.48	2.28e-7

### 3.5 CONCLUSIONS

The objective of this work is to estimate the annual rates of collapse of different types of buildings designed for different Italian sites according to the NC08 code provisions. The code provides ground motion design prescriptions that account for the site hazard but do not provide any indications of the expected performance of the designed buildings in terms of either an operational limit state or in terms of an ultimate limit state (i.e., collapse). Hence, the practicing engineer does only know that the buildings just designed are code-conforming. In particular, the design is carried out for a fixed level of ground motion severity (e.g. 10% in 50 years) and it is meant to ensure a limit state (Life Safety) that is defined qualitatively. Moreover, the application of amplified actions and decreased material property values (i.e. LRFD) during design is a step that goes in the direction of safety but the collapse rates achieved are really unknown.

A systematic approach has been devised in order to analyze several types of buildings designed for sites with an increasing level of seismic hazard. In particular, a discrete number of case studies were defined with structures designed specifically for each site according to the current Italian code provisions. Later, they were tested by means of non-

linear dynamic analyses (NLTHA) according to a multi-stripe approach (MSA). The input ground motions were selected in order to be hazard consistent and also coherent with the causal parameters (namely magnitude and distance) expected to mainly influence the site hazard. This procedure allows accounting for the uncertainty related to the record-to-record variability. For a fixed structure and site, the conditional probabilities that result from the NLTHA responses were coupled with the site hazard curve, obtaining this way the annual rates associated to the considered LS. Two limit states (LS) were taken as reference, the onset of damage and the collapse, with particular attempt to the latter that has been investigated more deeply. The thresholds associated to the two LS were deterministic and based on a global criterion, i.e. roof drift as response measure; this choice allows a meaningful comparison of the rates related to different structural typologies.

The results of this work clearly show that the code provisions do not guarantee any fixed level of performance across building types and sites. In other words, the risk is not uniform. In particular, the collapse risk tends to increase with the hazard, i.e. the higher is the hazard the higher is the collapse rate. In other words, the code prescriptions for low hazardous areas are much more conservative than those for high hazardous areas. In L'Aquila, the most hazardous site, unreinforced masonry with irregular configuration and pre-cast structures show rates comparable to the rate of occurrence of the design ground motion. Therefore, the design procedure and standards for URM buildings in high seismic hazard should be revised in order to make these structures safer or, more drastically, their use should be discontinued. The failure rates of base-isolated structures resulted to be higher than what could be expected; this may be due to their more controlled behavior during design and the lower margin of safety with respect to collapse beyond the maximum design displacement. Conversely, base-isolated structures show lower onset of damage failure rates if compared to the other structural typologies.

The last part of the chapter investigated the impact of adopting different measures for describing ground motion severity and of structural response, together with another record selection technique; the rates, being in the same order of magnitude, seem not to be much affected by these different working hypothesis. However, it should be kept in mind that the use of parameters that are less prone to variability could help in defining a more reliable risk estimates. In particular, using MIDR in place of RDR seems to have more impact in weaker structures (see the fragility curves for Milano in the right column of Figure 3.22) but, once we compare the collapse rates, the low frequency of more severe events smooths all the differences.

This work is part of a project funded by Civil protection that is still ongoing; the future work will be focused on deepening diverse aspects, such as uncertainty in the LS threshold and structural modelling, adoption of response parameters dependent on

acceleration rather than just on deformation (Peak floor acceleration in parallel with drift ratios) and also focusing on the even more challenging existing buildings. In the next chapter we will discuss a series of methodologies that could help in decreasing the risk variability among sites/structures and could be helpful to improve the future generation of the code.

## **4. HARMONIZING SEISMIC PERFORMANCE VIA RISK TARGETED SPECTRA: STATE OF THE ART, DEPENDENCIES AND IMPLEMENTATION PROPOSALS**

### **4.1 SUMMARY**

Eurocode-based Design Spectra are commonly defined for a constant value of hazard (typically 10% in 50 years) associated to an ultimate limit state of reference. For any given structure, this approach could result in different levels of risk even for sites characterized by the same design peak ground acceleration (PGA), mainly because of hazard curve shape variability. Luco et al. [2007] have proposed Risk Targeted design maps (currently applied in ASCE7-10) that suggest the application of suitable spectra adjustment factors or risk coefficients in order to ensure a reasonably and, more importantly, explicitly agreed upon collapse risk throughout the country. The aim of this work is to test the effectiveness of the computed adjustment factors in, at least, harmonizing the risk (defined for three limit states) among six reference sites. In this endeavor we make use of simplified single degree of freedom structures defined in several configurations in terms of period and ductility. The results of the present work provide insights for possible future adoption of Risk Targeted Spectra in the European code provisions.

### **4.2 INTRODUCTION**

Current provisions of many seismic design codes, including the last version of Eurocode 8 [ref], are based on a paradigm that imposes the design of structures on the basis of an intensity measure (IM) associated with a constant seismic hazard level or return period, e.g. PGA at 475 years. In such codes, every structural performance level, e.g., Damage Limitation or Life Safety, is checked using intensities connected to this predefined hazard level. In other words, this level of hazard specifies the seismic actions for which the design of structural elements should be seismically verified. For instance, in Eurocode 8 (CEN [2004]), a seismic event with 10% probability of exceedance in 50 years is used for design verifications of the Life Safety limit state. This design procedure, which includes partial safety factors that increase actions and decrease material resistances, is assumed to provide sufficient safety margins against earthquakes for newly designed buildings. Nevertheless, it does not specifically determine the expected seismic risk related to any performance level or limit state. This design approach, therefore, may result in non-uniform risk for buildings located at different sites within a region (e.g. a country), even for places with identical design intensity level.

The reason behind this discrepancy can be best explained by considering the approximate formula of (Cornell [1994]; Shome and Cornell [1999]), for determining the MAF  $\lambda_{LS}$  of exceeding (or violating) a limit-state LS:

$$\lambda_{LS} \approx H(IM_{c50\%}) \exp(0.5k^2\beta^2) \quad (4.1)$$

$IM_{c50\%}$  and  $\beta$  are the median and dispersion (standard deviation of the log) of the IM values of capacity that define the fragility function for LS.  $H(\cdot)$  is the site hazard function for the IM, approximated via a straight line of slope  $k$  in logarithmic coordinates,  $H(IM) \approx k_0 \cdot IM^{-k}$  (Figure 4.1a). Equation ( 4.1 ) clearly states that the slope of the hazard and the dispersion of the fragility introduce an amplification factor that increases the MAF of the LS vis-à-vis the MAF of the IM.

Arguably the most comprehensive approach to tackle this issue is to introduce risk at the output level of response, rather than at the input level of (design) spectral acceleration, essentially designing for  $\lambda_{LS}$ , rather than  $H(IM)$ . This is the premise of performance-based design, and it requires a paradigm shift with an entirely new process for designing structures (Krawinkler et al. [2006]; Vamvatsikos et al. [2016]). A more practical (and limited) approach was proposed instead by Luco et al. [2007]. Their idea was to stay within the confines of current design practice and only try to modify the input design spectral acceleration to a ‘risk-targeted’ (RT) value that indirectly accounts for the effects of hazard and fragility, in other words doing the probability calculations behind the scenes and then hiding them under the carpet. The code does not need to change beyond the design spectra itself and designers can keep working according to their usual practices.

Specifically, Luco et al. [2007] proposed modifying the seismic design maps of the US code provisions (e.g. ASCE 7-10ASCE [2010]) into ‘risk targeted maps’ by means of Spectrum Adjustment Factors (SAFs, also called risk coefficients, RCs) to target a uniform mean annual frequency (MAF) of collapse. These maps are derived for spectral acceleration ( $S_a$ ) at two periods (0.2s and 1.0s), which are the primary information needed to build the ASCE-type design spectrum ASCE [2010]. The adjustment factors result from a risk analysis involving the definition of a generic collapse fragility curve that is defined to be consistent with the definition of FEMA P695 (ATC-63 [2009]) strength reduction R-factors. These factors are determined specifically to offer a 10% probability of failure given the Maximum Considered Earthquake, MCE, which is typically defined at an  $S_a$  intensity level corresponding to a MAF of 2% in 50yrs. Keeping constant its assumed variability, the generic fragility curve is shifted, by means of adjusting the  $S_a$  at 10% collapse probability via an iterative procedure, until it produces the target MAF; the ratio between the “shifted”  $S_a$  and the original one defines the SAF for the given period.

In line with this idea, Douglas et al. [2013] proposed the adoption of risk targeted maps for Europe. The core of the procedure is the same as in Luco et al. [2007]; the difference lies in the definition of the generic fragility and in how the EN1998 spectrum is built. Indeed, since in this case the design spectrum is not computed but simply anchored to PGA, solely a PGA-based risk-targeted ground motion map (RTGM) was derived. Along the same lines, Silva et al. [2016] analyzed the impact of assuming different (in terms of anchoring point and standard deviation) fragility curves on the adjustment factors computation. All such reincarnations of RT spectra invariably accept a compromise between simplicity and accuracy. While a precise building- and site-specific performance-based design would ensure reaching the targeted performance objectives, the same is not necessarily true for RT spectra. By virtue of defining a single design spectrum at each site, one bundles together all types of structures (steel, masonry, etc.) that happen to have similar modal periods by employing a ‘structure-agnostic’ generic fragility function to describe their behavior. At the same time, one needs to choose a single performance objective (i.e. a limit state) to target. Such choices, all legitimate, may make for a wealth of options when applying RT spectra. Each choice would have, with its own advantages and disadvantages, vis-à-vis ease of application and accuracy and all would produce potentially different output spectra. To level the field, we shall discuss in detail the definition of each element of RT spectra applications and investigate its effect using simple single-degree-of-freedom (SDoF) systems to represent different buildings. Using a potential Eurocode 8 (EN1998: CEN [2004]) application as a vehicle, a number of different approaches shall be discussed that can offer different degrees of risk harmonization among a population of sites and buildings.

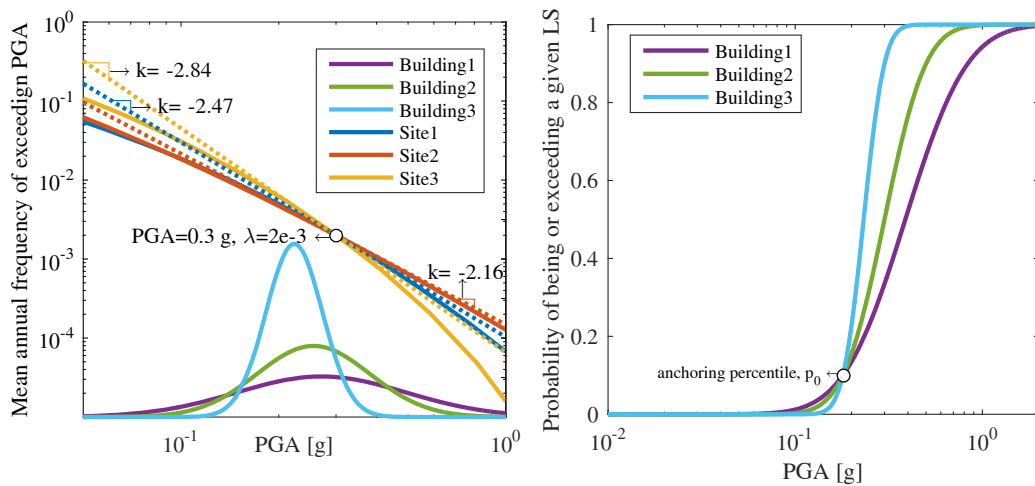


Figure 4.1 (a) Hazard curves for three sites having the same design PGA at 10% in 50 years but different slope\shape, and (b) three different fragility curves to be employed for risk harmonization, each representing a different weighting of the importance of the shape of the hazard curve.

### 4.3 ELEMENTS OF RISK-TARGETED SPECTRA

#### 4.3.1 Fragility Functions

The first element in RT spectra application is the definition of the fragility function(s) used to idealize the performance of the building stock. It is well known, however, that fragility curves are building specific, meaning that they are significantly dependent on the structural type, the ductility characteristics and natural period of the structure. In addition, they are site dependent, i.e. the building response statistics are a function of the seismological characteristics of region around the site of interest (see Kohrangi et al. [2017c]). Nevertheless, the application of site and building specific fragility curves to derive design maps would be too complex and computationally expensive, also requiring considerable prior investigations to back it up. Therefore, the currently preferred approach is to adopt a generic, structure-agnostic fragility curve definition for all building types and all sites within the region of interest that can only be modified by shifting its central value (or median IM capacity) to reflect the difference in design intensities from site to site (Douglas et al. [2013]; Luco and Bazzurro [2007]; Silva et al. [2016]).

Such generic curves are typically assumed to be lognormal and can be broadly defined by four parameters: (a) An anchor percentile  $p_0$ , (b) an IM definition, (c) an anchor MAF for the IM,  $\lambda_0$ , typically chosen to be the hazard level that is used to define the uniform hazard design spectrum, and (d) the dispersion,  $\beta$ . For instance, Luco et al. [2007] used a generic fragility function based on  $S_a$ , anchored at collapse probability of  $p_0 = 0.1$ , and an intensity MAF of 2% in 50 years assuming a dispersion of  $\beta = 0.8$ . Douglas et al. [2013], aiming at a (EN1998: CEN [2004]) application, anchored the fragility at  $p_0 = 10^{-5}$  in correspondence to PGA at 10% in 50 years, together with  $\beta = 0.5$ . More recently, Silva et al. [2016] while generating risk targeted maps for Europe, investigated the impact of different combinations of generic fragility curve parameters, showing large variations in the SAFs by even minor alteration of these parameters. They employed PGA as the IM, with  $p_0 = 10^{-2}$ – $10^{-5}$ , at  $\lambda_0$  of 10% in 50 years, with a dispersion of  $\beta = 0.5$ – $0.7$ .

As such, Douglas et al. [2013] and Silva et al. [2016] working with Eurocode 8 proposed RTGM maps for PGA; whereas Luco et al. [2007] generated maps for the anchoring points of ASCE7 at  $S_a(0.2s)$  and  $S_a(1.0s)$ . This means that the choice of the Intensity Measure (IM), in all these cases, was dictated by the characteristics of the design spectrum implemented in the code of reference. However, many studies, in recent years, have shown that PGA is not an efficient and sufficient IM for building response prediction while building specific IMs, such as spectral acceleration at the first mode of vibration of the building,  $S_a(T_1)$ , typically perform better. Therefore, investigations are required to find suitable IMs for a risk targeted approach for design.

It can be argued that, from a computational point of view, the generic fragility curve is essentially a mechanism for weighting the effect of the hazard curve shape (or its local slope) and taking it into account when estimating the risk that is targeted by the procedure. The anchor percentile and MAF determine the central point of the fragility,  $IM_{.50\%}$ , selecting what part of the hazard curve one wants to emphasize. The dispersion,  $\beta$ , selects how broad or narrow an area of the hazard curve will be accounted for in the risk calculations. Figure 1a presents an example of the PGA hazard curves from three different sites, all having the same intensity at the 10% in 50yrs level, but different shapes, here characterized by the tangent slope. According to Equation 1, each site will result in a different MAF for any of the three fragility curves shown in their probability density function form in Figure 1a or as cumulative distribution functions in Figure 1b. We can choose to harmonize the risk estimated at each site for any given fragility curve by appropriately shifting up or down the 10% in 50yrs value used for design. If  $\beta = 0$ , then the hazard shape (or slope) becomes irrelevant and no adjustment shall take place. The broader the fragility that we choose (larger  $\beta$ ), the more emphasis will be placed on the hazard curve shape (or the steepness of the slope in Figure 1a via Equation 1) necessitating larger adjustments in terms of the SAF to match a target risk.

For a given  $\beta$  and  $\lambda_0$ , the latter typically fixed to the value corresponding to the uniform hazard spectrum. The definition of the anchoring percentile,  $p_0$ , is one of the key-points of the entire procedure and, as mentioned, different researchers have made significantly different assumptions. Therefore, this number should depend on an analysis of several buildings or it could be chosen in order to ensure the adoption of SAFs that are, on average, equal to one, i.e. guaranteeing minimal changes on the current provisions. On the other hand, if one selects this percentile based on actual studies (e.g. the implicit risk project, whose results are shown in Chapter 3 of this thesis, suggests  $p_0 < 5e-3$  for collapse and between 0.1 and 0.2 for damage of reinforced-concrete frame buildings) then he/she would have a better chance to actually guarantee the risk target in real practice. The major advantage of having an average SAF of one is that, as said, minimizes the changes and one would have less complaints from the practitioners; it will be shown later how this approach allows to still guarantee and excellent risk harmonization but not real risk mitigation.

None of the abovementioned studies, however, explored the feasibility of site and building specific fragilities in this procedure. More importantly, it is necessary to investigate what would the impact be of disregarding the importance of site and building dependency of the fragility curves and using, instead, a generic fragility curve in risk targeted design approach.

### 4.3.2 Performance objectives

The second is the performance objective targeted, or, in other words, a limit state (LS), such as global collapse or life safety, coupled with a target MAF of exceedance,  $\lambda_{tgt}$ . The original proposals for RTGMs were mainly deemed to be used for design of new structures by focusing on the collapse limit state. Nevertheless, current codes include also provisions to limit damages to the structures that observe relatively low ground motion intensities. For instance, Eurocode 8, in addition to the ‘classical’ design requirements at a 475 years return period, dictates damage limitations for 95 years return period ground motion level. In line with this, Silva et al. [2016] suggested to generate RTGM maps for multiple damage limit states (namely yielding and collapse), while Douglas et al. [2013], observing the high uncertainty related to collapse limit state, proposed to target LS lower than collapse. Moreover, lower LS, such as those connected to the onset of damage, are much more influential if we are dealing with limiting monetary losses rather than only targeting an ultimate structural performance. Moreover, the choice of the LS to be targeted influences the anchoring percentile that should be picked in the fragility curve corresponding to the selected LS. As already shown by Douglas et al. [2013] and confirmed by the RINTC-Workgroup [2017] results the anchoring point related to Collapse limit state could be considerably low and, therefore, prone to criticism since very much related to the tails of the distribution. All these aspects bring to light the need for further investigations on the impact of the LS choice in the whole procedure. In other words, the question remains: Will one obtain a uniform risk for all of the LSs when only one LS is targeted? And if not, is it possible to quantify such discrepancies over the entire building population?’

### 4.3.3 Design spectrum shape and parameterization

The third is the design spectrum shape and flexibility, defining the degree to which one can alter the shape of code-spectra at different periods to achieve the risk targets set. Seismic design codes typically provide a design spectrum whose intensity is defined by anchoring it to one or two spectral ordinates coming from hazard maps (i.e. defined by seismic zonation maps or a web-based PSHA tool), while its shape is adjusted by the soil type, vicinity to the faults, etc. For instance, Eurocode 8 uses as anchoring point the PGA, while ASCE 7-10 employs two spectral ordinates at 0.2 s and 1.0 s. Obviously, the rigidity of the spectrum shape curtails the capability of an RT-spectra approach to harmonize risk across different periods for any given site.

For simplicity we shall categorize the different design spectra based on the number of spectral ordinates that are employed to parameterize its shape. A *flexible* shape is the ideal case where any spectral ordinate can be individually adjusted for a particular site. This may make for a highly discontinuous shape, thus some flexible non-parametric function, e.g. a spline, can be fitted to restore continuity. Obviously, such an approach would best

be coupled with a web-based software tool, as there would be too many parameters to put in paper. Instead, a *semi-flexible* shape, based on the ASCE 7-10, is characterized by two anchor points, typically  $S_{ds} = S_a(0.2s)$ , and  $S_{d1} = S_a(1.0s)$ . The first ordinate defines the start and height of the horizontal plateau while the second anchors the constant velocity part. Finally, the *rigid* shape of an EN1998-type spectrum is defined by a single pivot point, the PGA.

#### 4.3.4 Optimized spectral ordinates

The fourth and final element of RT spectra application is the range of periods and associated spectral ordinates that have been employed to tune the spectrum, and especially how these are weighted when considering an inflexible spectrum shape. In the flexible case, naturally all periods in the range of interest need to be employed. What happens for the other two shapes is not necessarily as straightforward. Having only a limited number of parameters for tuning the spectrum shape versus a multitude of periods to employ, makes for an interesting choice. The simplest approach is to only harmonize the risk at the same spectral ordinates as the ones that define the spectrum, letting the rigid or semi-flexible shape of the spectrum carry over this harmonization to other spectral ordinates. This has been the typical approach so far: Douglas et al. [2013] and Silva et al. [2016] optimized the EN1998 spectrum by only computing SAFs for PGA, while Luco et al. [2007] similarly estimated SAFs only the  $S_{ds}$  and  $S_{d1}$  ordinates. A more comprehensive approach would entail estimating SAFs over extended range of practical periods, say  $[0, 3\text{sec}]$  and then appropriately weighting the SAFs from each period to determine the optimal adjustment of the few knobs available due to the inflexible shape.

#### 4.4 CASE STUDY BUILDINGS AND SITES

The main goal is to investigate and quantify the effectiveness of the RT spectra approach and the effect of each of the aforementioned factors that go into their definition. In particular, two sets of sites located in three European cities characterized by the same design PGA at the 10% in 50 years return period level are taken as reference for this study. To address the impact of building specific fragility curves in the risk targeted design procedure, we generated them for three different LS's and for multiple buildings, differentiated by their ductility class and natural period. In other words, we are investigating to what extent the state-of-the-art RT approach is successful in offering uniform risk when designing new buildings. We repeat this procedure based on two main approaches: i) using building- and site-specific fragility curves; ii) using a generic fragility curve similar to the approach of Luco et al. [2007] or Silva et al. [2016]. In the following, we present a brief summary of the case study sites, buildings, assumptions made for the design of the buildings and the hazard computations.

#### 4.4.1 Selected sites and hazard computation

Two sets of three case study sites representing ‘medium’ and ‘high’ seismicity regions based on the web-based PSHA tool of EFEHR [ref] are selected. This tool basically stands on the latest hazard model developed for Europe under the EU-SHARE project [ref]. Three cities of Athens, Perugia and Focsani with coordinates of (37.976°N, 23.751°E), (43.111°N, 12.389°E) and (45.969°N, 27.179°E) represent the high seismicity sites with PGA value on bedrock equal to  $\sim 0.30g$  for a 475 years return period (i.e. corresponding to  $PGA=a_g=0.30g$  in EN1998); and three cities of Baden, Montreux and Aachen with coordinates of (47.999°N, 16.218°E), (46.433°N, 6.899°E) and (50.776°N, 6.085°E) stand for the sites with medium seismicity with PGA value on bedrock equal to  $\sim 0.15g$  for a 475 years return period (i.e.  $a_g=0.15g$ ). Figure 4.2(a) shows the location of the selected sites on the map and Figure 4.2(b) shows the hazard curves for PGA.

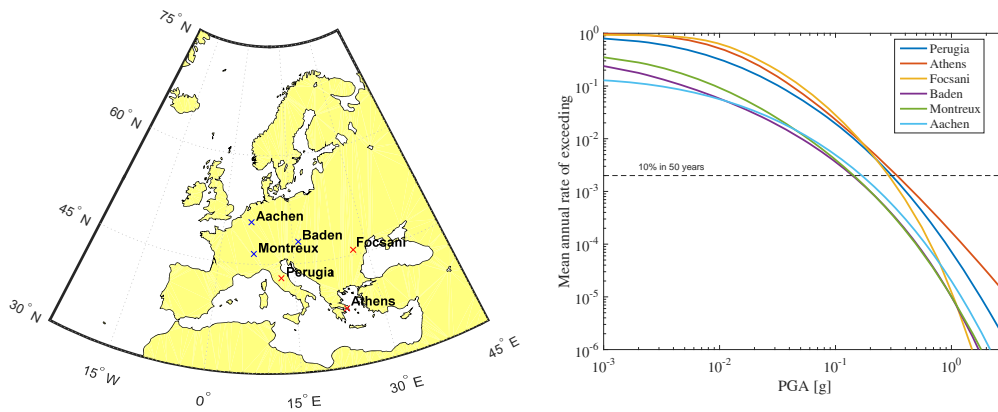


Figure 4.2 (a) Map of cities chosen as representative of high (red) and medium (blue) hazard zones, and (b) the corresponding PGA hazard curves on rock

#### 4.4.2 Structural systems, design procedure and limit state definition

Herein, SDoF systems are used as reference to model multiple buildings. This choice allows us to perform a considerable number of dynamic analyses while updating the system characteristics according to the design requirements. To cover a wide range of different structures, our generic SDoF is defined as an elasto-plastic system with 3% hardening backbone designed for two levels of ductility, namely medium (ductility class medium, DCM) and high (ductility class high, DCH), with three different fundamental periods of 0.5s, 1.0s and 2.0s. What is from now on called a “design” consists of the definition of the backbone characteristics of the SDoF. These are the ultimate displacement  $\delta_u$ , the base shear coefficient  $C_b$ , and the yield displacement  $\delta_y$ :

$$C_y = Sa_{UHS} \cdot \frac{OS}{q} \quad \delta_y = C_y \cdot \frac{9.81}{(2\pi/T_1)^2} \quad \delta_u = \mu_u \cdot \delta_y \quad (4.2)$$

$T_1$  is the fundamental period of the structure;  $\mu_u$  is the ultimate ductility before global collapse occurs;  $Sa_{UHS}$  is the spectral acceleration at  $T_1$  obtained from the uniform hazard spectrum of the site, while  $q$  and  $OS$  are, respectively, the behavior factor and the over-strength, here taken to be dependent on the ductility class of the system;  $C_y$  is the base shear coefficient, or the maximum base shear strength divided by the total weight, numerically equivalent to the yield spectral acceleration in units of  $g$ .

Having the perfect values for the above parameters is not our goal, yet keeping close to reality is clearly of benefit. Thus, the behavior factor is taken according to EN1998 provisions for reinforced concrete moment resisting frames as a function of the ductility class (Table 4.1) and the  $a_u/a_1$  ratio of ultimate base shear over the base shear at first yield. The latter is taken equal to 1.3 in line with what is suggested by the code provisions for multi-story frame structures. Note that in EN1998,  $a_u/a_1$  is not necessarily the true overstrength of the structure, as it is measured from the first-yield point along the pushover capacity curve rather than from the design base shear. This distinction is clearly made in the US guidelines (e.g., FEMA P695) and it is supported by the RINTC project results. Therefore,  $OS$  is taken to be higher than  $a_u/a_1$  in Table 4.1, ranging from 1.5 to 2.0 for DCM and DCH, respectively. Finally,  $\mu_u$  values were based on RINTC data for reinforced concrete frames (see 5.1 Appendix E), where the ultimate point was taken at a 15% strength drop from the maximum observed along the building capacity curves. Corresponding ductility values of 5 and 7 were adopted for DCM and DCH, respectively.

**Table 4.1 Behavior factor and over-strength assumptions**

Ductility class	Behavior factor $q$	Overstrength OS	Ultimate ductility $\mu_u$
DCH	$q = 4.5 \cdot a_u/a_1 = 4.5 \cdot 1.3 = 5.85$	2.0	5
DCM	$q = 3.0 \cdot a_u/a_1 = 3.0 \cdot 1.3 = 3.90$	1.5	7

Structural performance is evaluated for three LSs defined in terms of ductility thresholds. In order to include the uncertainty in LS definition, an additional dispersion of  $\beta_u = 0.2 - 0.3$  has been incorporated, larger values employed for the more uncertain LSs (Table 4.2). Figure 4.3 shows the backbone characteristics and the LS ductility thresholds adopted for DCH and DCM structures

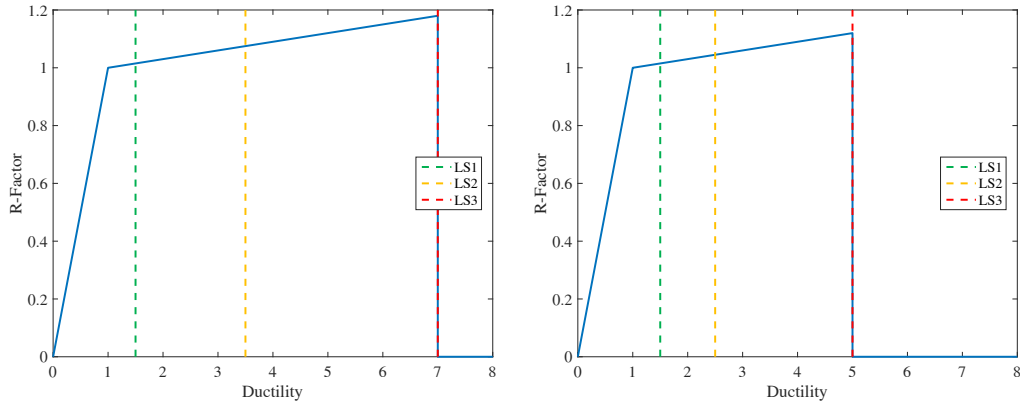


**Figure 4.3** Single degree of freedom backbone curves expressed in terms of the ductility and the strength ratio (base shear over yield base shear) and limit state definition according to building's ductility class: DCH - high ductility (left) and DCM - medium ductility (right).

**Table 4.2** Limit state definitions

Limit State	DCH		DCM	
	Median, $\hat{\mu}$	Additional Dispersion, $\beta_U$	Median, $\hat{\mu}$	Additional Dispersion, $\beta_U$
Global Collapse (LS3)	7.0	0.3	5.0	0.3
Severe Damage (LS2)	3.5	0.3	2.5	0.3
Moderate Damage (LS1)	1.5	0.2	1.5	0.2

## 4.5 FRAGILITY CURVES AND PRELIMINARY ASSESSMENT

Two conceptually different kinds of fragility curves are considered. The first is represented by building-and-site specific fragility curves obtained by means of a PSHA-based record selection applied to the generic SDoF systems representing a wide variety of structures. The second kind is defined in line with the currently preferred 'generic' fragility approach, disregarding any site and building dependence beyond the design intensity at the site of interest.

### 4.5.1 Building and site specific fragility curves

These curves are derived specifically for each site and SDoF system (building) described in detail in the previous section. To do so, for each case-study, a set of 30 records have been selected by means of the conditional spectrum (CS) approach [ref] based on the Intensity Measure (IM) chosen to describe the severity of ground shaking. The record selection has been performed on the basis of the probabilistic seismic hazard assessment (PSHA) disaggregation data of the site, estimated at the hazard level that, according to

EN1998, is associated to design, i.e. 10% in 50 years probability of exceedance of the IM of choice. Two types of IMs were employed, namely spectral acceleration at the first modal period of the structure,  $Sa(T_1)$  (Baker [2011]; Jayaram et al. [2011]; Lin et al. [2013a]), and geometric mean spectral acceleration evaluated over the period range of  $[T_1, 2 \cdot T_1]$  with a period spacing of 0.1s,  $AvgSA(T_1)$  (Kohrangi et al. [2017a]). The result is a total of 36 site and building specific record sets. Note that the same sets of records are used for DCH and DCM SDoFs of the same fundamental vibration period. Kohrangi et al. [2017c] showed the advantages of a ‘multi-site’ record selection approach which allows generating a single set of records that corresponds to multiple sites in one round. This technique helps avoiding a large number of record selection repetitions by employing only one set that combines the characteristics of multiple sites. Herein, we also selected two additional sets of records for the ‘high’ and ‘medium’ hazard sites using a generic  $AvgSA$  definition over the period range of [0.3, 3.0] s with a period spacing of 0.2s. This choice of period range is especially interesting because it could be considered as a reasonably adequate IM for all the selected SDoFs of this study with  $T_1=0.5, 1.0$  and  $2.0$  s. Figure 4.4 shows a sample of record spectra selected for Athens at  $T_1=1$ s.

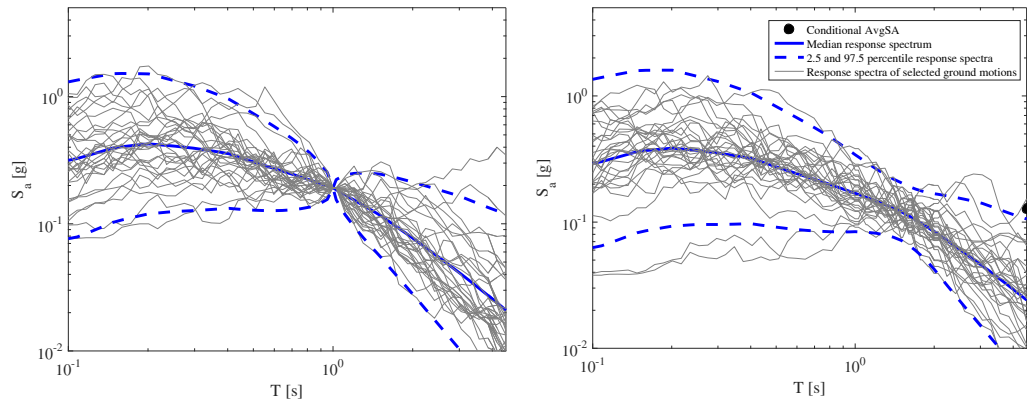


**Figure 4.4. Records selected for Athens and SDoFs with  $T_1=1$ s using  $Sa(T_1)$  (left) and  $AvgSA$  (right) as conditioning IM.**

Incremental dynamic analysis (IDA, Vamvatsikos and Cornell [2002]) is applied for all the defined cases, assuming that the same set of records is appropriate for application at all levels of intensity. This hypothesis might produce a certain level bias to our final output. Nevertheless, we accept this additional uncertainty to reduce our computation burden following the recommendations of Kohrangi et al. [2017b]. The top panels of Figure 4.5 show the IDAs and fragility curves for a DCH structure with a natural period of 1.0 s located in Athens while the bottom panels compare the impact of using different ground motion IMs. Apart from the median value of the collapse fragility it is interesting to notice the lower record-to-record variability (shown by the lognormal standard deviation

values) of the AvgSA-based curve with respect to the one expressed in terms of  $Sa(T_1)$ . It is of interest to investigate how such a reduced dispersion could improve the accuracy of RT-spectra.

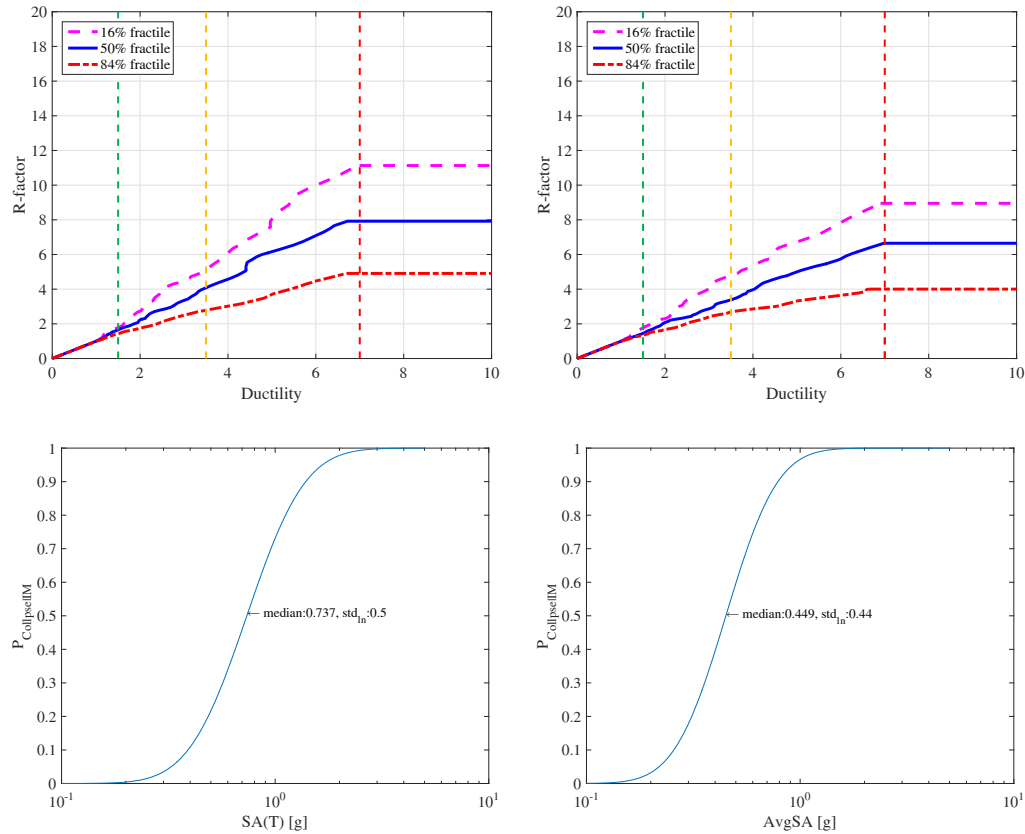


**Figure 4.5** Example of IM impact,  $Sa(T_1)$  (left panels) versus AvgSA (right panels) on Collapse fragility curves. These cases are related to a DCH structure with  $T=1.0s$  designed for Athens. The vertical lines of the upper panels represent the (median) displacement threshold used to define LS1 (green), LS2 (yellow) and LS3 or collapse (red).

After the definition of the fragility and the integration with the hazard curve we have the initial, unharmonized case of Figure 3.6, represented by the MAFs' distribution according to the different combinations of structural types, period, city, LS and coming from the risk assessment of the structures designed according to the EC8 provisions. The results are shown in a synthetic way using the well-known boxplot representation: the edges of the colored boxes represent the first and the third quartile,  $Q_1$  and  $Q_3$  (or 25%, 75% percentiles), while the mid-point depicts the median. The circles that sometimes appear are the points that were judged to be outliers, namely those away from  $Q_1$  and  $Q_3$  by

more than 1.5 times the interquartile range of  $Q_3-Q_1$ . Overall, when grouping all cities together, the median of the MAF values seems to be relatively constant with period for any given LS. Still, the MAF variability per individual structure is quite substantial, as highlighted by the size of the boxes. The obvious question is whether there is a trend, or systematic bias, to this variation. Figure 4.7 shows, solely for  $S_a(T_1)$ , the same data as in Figure 4.6 only reshaped in order to appreciate the effect of the site for each of the cities considered in this study. As expected, now there are evident differences in the achieved risk from site to site for all LSs. Note here a minor departure from what has been observed in recent literature, and especially the RINTC project RINTC-Workgroup [2017]. Due to the enforcement of code minima (see for example Žižmond and Dolšek [2016]) and associated capacity design rules, buildings designed according to high-ductility rules at moderate/low-seismicity sites will in general have higher overstrength than similar configurations designed in high-seismicity areas. Due to the site-independent overstrength values adopted in Table 4.1, this trend is not observed when comparing Figure 4.7a to Figure 4.7b. Appropriately incorporating such a disparity with a faithful definition of fragility curves can become a powerful argument in favor of building/site-specific versus generic fragility curves. Still, for the purpose of our investigation this is not considered an issue of importance.

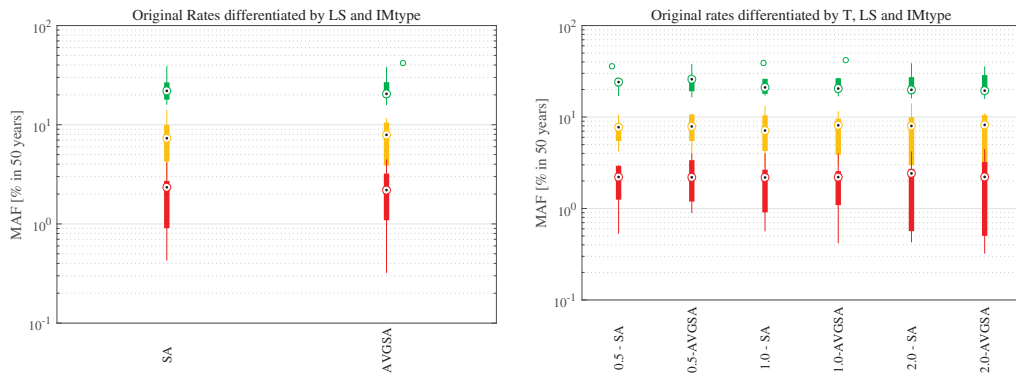
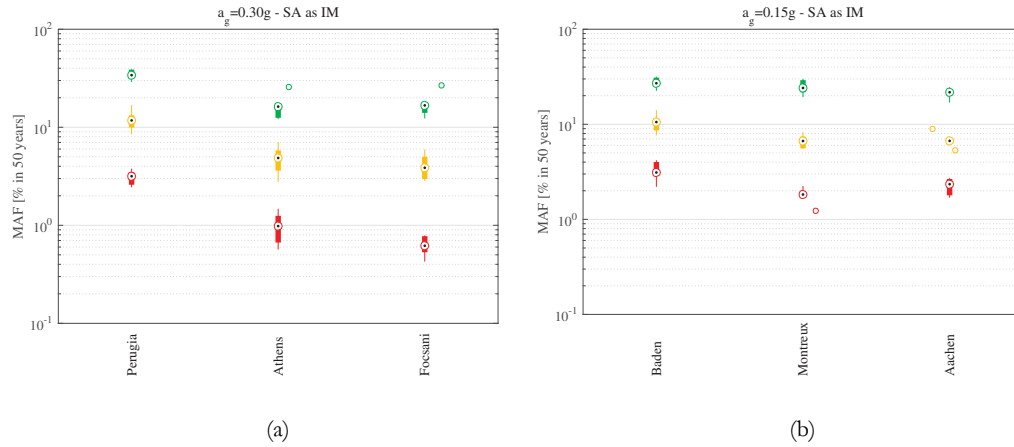


Figure 4.6 Initial MAF distribution for LS1 (green), LS2 (yellow) and LS3 (red) for different system periods and IM types.



**Figure 4.7 Initial MAF distribution for LS1 (green), LS2 (yellow) and LS3 (red) differentiated by cities belonging to (a) high and (b) moderate hazard zones.**

Since the basis for our investigation is an EN1998 application, one may rightfully ask why results based on PGA are not shown. After all, PGA is the anchor point of the EN1998 spectrum and it has been employed in two prior studies for RT-spectra application for the Eurocode (Douglas et al. [2013]; Silva et al. [2016]). PGA has been shown to be an inefficient and insufficient IM (Kohrangi et al. [2015a], [2015b]), prone to giving biased results when applied to systems of moderate or long periods are concerned. One may still argue that when PGA is coupled with a reliable record-selection approach, such as CS, such problems may be remedied. As good as CS may be, there are limits to its applicability. To prove our point, we repeated the analysis process for PGA, using CS to select appropriate sets of records at the 10% in 50 years PGA and perform an IDA. The results are compared to those coming from different sets selected on the basis of  $S_d(T_i)$  and  $AvgSA$  in Figure 4.8 for LS3 and for  $T=1s$  and  $2s$  systems. For most cities, there is a clear conservative bias in the MAFs estimated by PGA versus those based on the other two IMs that, conversely, offer quite similar results. Therefore, in this study PGA will not be employed any further.

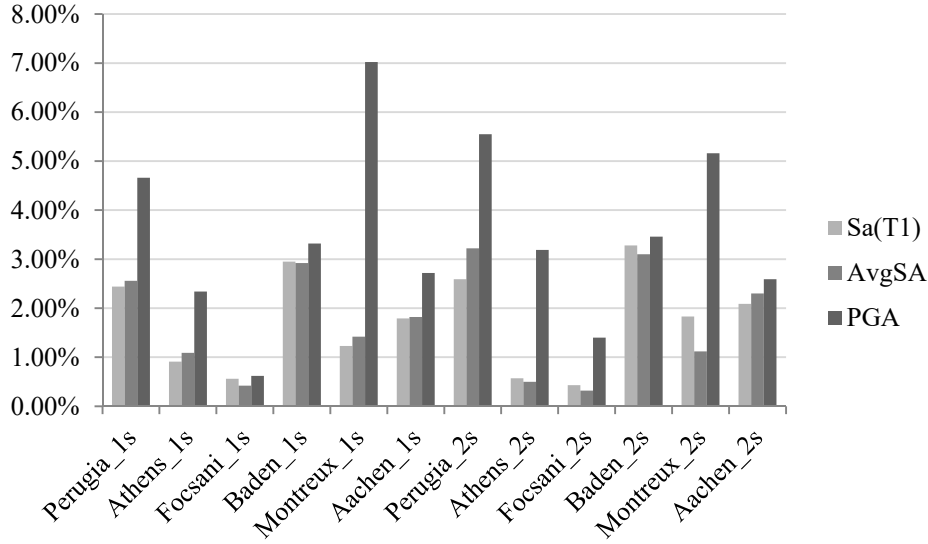


Figure 4.8 Comparison of MAFs computed using three different IMs: PGA, Sa(T1) and AvgSA.

#### 4.5.2 Generic fragility curves

Generic fragilities are not tied to any specific system or site, beyond their scaling to match the site design intensity at the anchoring percentile and MAF. They may be based on some limited analytical data and/or expert opinion to maintain some contact with reality, yet they are clearly not meant to represent any specific system. Herein, to maintain some consistency, the generic fragilities employed are based on the data coming from SDoF systems and sites mentioned previously. In particular, the analyzed cases result in 36 different combinations of period, ductility class and site; the definition of the generic fragilities follows two main paths, with different levels of “generalization”:

- Generic A: it considers the entire database defining a single generic fragility without any consideration of period, ductility or site. The  $p_0$  anchoring percentile is defined as the median among the probabilities of exceeding the limit-state of interest,  $LS_i$  ( $i = 1,2,3$ ), at the design IM level (10% in 50yrs for EN1998). The associated dispersion is the square-root of the sum of the variance of the (log) mean of IM capacity,  $\mu_{ln}(IM_{LSi})$  and the mean of the IM capacity variances of the individual SDoF fragilities,  $\sigma_{ln}^2(IM_{LSi})$ , according to the law of total variance:

$$\sigma_{ln,A} = \left( E[\sigma_{ln}^2(IM_{LSi})] + Var[\mu_{ln}(IM_{LSi})] \right)^{1/2} \quad (4.3)$$

- Generic B: it is characterized by slightly less generic definition of the fragilities: The anchoring point and the variance are computed exactly in the same way as Generic A but the structure population is differentiated by period. Therefore, for each period we will have different anchoring percentile and dispersion.

#### 4.6 RISK TARGETED SPECTRA: CALCULATION AND PRACTICAL IMPACT

##### 4.6.1 Estimation of SAFs

Given a performance objective, estimation of the SAF requires a process of adjusting the design intensity of  $S_{a,UHS}$ , estimating the new corresponding fragility curve, estimating the new limit-state MAF and repeating until convergence. For the generic fragility curves, this process is trivial, as one directly scales the central value of the fragility via the adjusted design IM level that corresponds to the anchor probability of  $p_0$ . Given the lognormal shape of the fragilities, this means that the median capacity in terms of  $S_a$  becomes:

$$S_{ae50\%} = S_{a,UHS} \cdot SAF \cdot \exp(-K_{p_0} \cdot \beta) \quad (4.4)$$

where  $K_{p_0}$  is the standard normal variate that corresponds to  $p_0$ , i.e.,  $K_{p_0} = \Phi^{-1}(p_0)$ , where  $\Phi(\cdot)$  is the standard normal cumulative distribution function. For building specific fragility functions, estimating the fragility is only slightly more complex as it actually requires “redesigning” each SDoF system; practically speaking the system’s properties need to be modified according to Equation ( 4.2 ) to match then new design intensity. Thus, the strength of the system becomes:

$$C_y = S_{a,UHS} \cdot SAF \cdot \frac{OS}{q} \quad (4.5)$$

Deriving the corresponding  $IM_{50\%}$  to define the median of the fragility in terms of the IM of choice becomes only a postprocessing issue. Thankfully, one does not need to rerun the SDoF IDAs, as the original results can be normalized into coordinates of strength ratio  $R$  (or base shear over yield base shear) versus ductility  $\mu$  and reused at will for each of the 36 ductility, period and site combinations. This trick is, after all, the basis of all  $R$ - $\mu$ - $T$  relationships in the literature and it has been heavily exploited before (e.g., Vamvatsikos and Cornell [2006])

The calculation of the proper SAF itself is performed by a rather simple procedure that involves a hunting phase and a bisection phase. Let  $MAF_{tgt}$  be the target value and  $MAF_1$  the currently estimated value at the initial step, for  $SAF = 1$ . If  $MAF_{tgt} > MAF_1$  then the target LS is observed too infrequently, the design is too conservative and, therefore, the SAF should be less than 1, i.e., the design intensity should be lowered. In line with this, a

trial value of  $SAF < 1$  is chosen and it is step-by-step decreased, e.g. by constant steps, until we reach  $MAF_{tgt} < MAF_j$  in step  $j$ . The opposite approach with  $SAF > 1$  applies if  $MAF_{tgt} < MAF_1$  was originally observed. In the end of this “hunting” phase, we shall have two trial MAF points,  $MAF_j$  and  $MAF_{j-1}$  that bracket  $MAF_{tgt}$ . Then, we employ a bisection procedure to further refine the SAF and bring the estimated MAF close enough to  $MAF_{tgt}$ ; see Figure 4.9 for a graphical explanation.

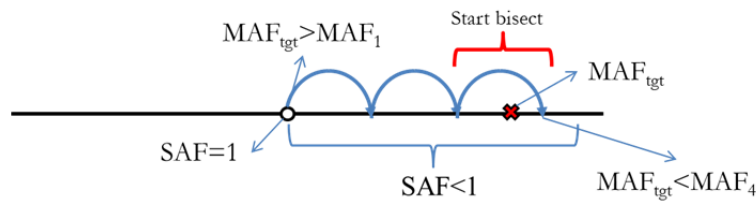


Figure 4.9 Graphical representation of the hunting and bisection procedure through which the SAFs are computed. The figure refers to the case where we start with  $MAF_{tgt} > MAF_1$

#### 4.6.2 Target MAF and harmonization strategy

The target definition is still an open question since, starting from the initial MAF rates of the “code conforming” SDOFs, the harmonization strategy could follow different paths. In particular, once the target LS is defined one could decide to opt for a *narrow* class-specific target, i.e. picking the median value as estimated for a given ductility class and period, or a *broad* one, i.e. considering the median among all the analyzed cases. The following Figure 4.10 allows us to compare the overall distribution of the MAF rates for both the narrow (left) and broad (right) approaches; this particular case was built targeting LS3 and using  $S_d$  as IM. Comparing the boxplot with the original case (Figure 4.5,  $S_a$  box plot on the left panel), the improvement for all LS is visually (the major impact is obviously on LS3, the targeted one) and also it is apparent that the broader approach offers a lower MAF dispersion among different structures.

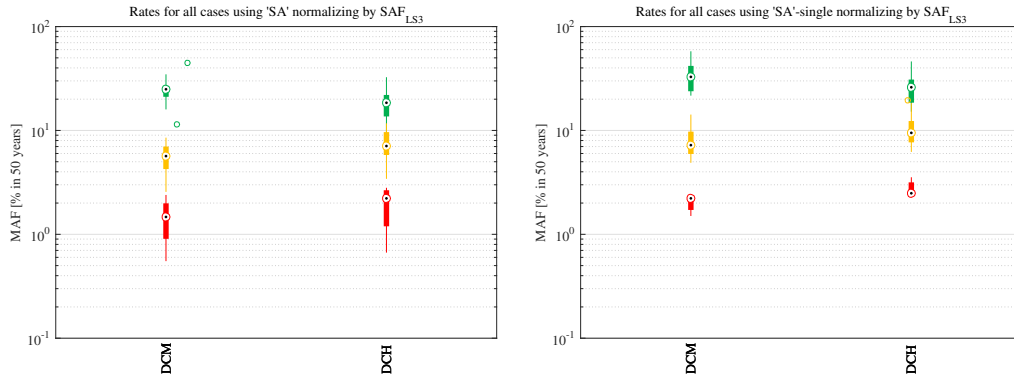


Figure 4.10 Effect of the target MAF on the resulting MAF distribution for LS3. Narrow (left) or broad (right).

As already seen, an interesting effect of modifying the structural design to target a MAF value is the reduction of its dispersion among all the considered combination of sites/periods/ductility classes, mainly for the targeted Limit State. However, one of the main concerns of this work is to stress the practicality issue, i.e. examine the actual effect of the harmonization for cases different from targeted one. This aspect will show how the concept of targeting a risk by means of the described procedure is only theoretical and limited to the specific cases considered for the computation of the SAF. What is actually obtained is risk harmonization among the examined locations. In line with this idea, following the procedure previously described, we decided to investigate the influence on the whole set of case-studies of what we defined as *broad harmonization*. This approach will be applied for three fixed MAF targets, one for each LS (Table 4.3), obtained as an integer approximation of the median values observed among the analyzed cases.

Table 4.3 Target MAF for each LS considered

Limit-State	Target Probability in 50 years
LS1	20%
LS2	6%
LS3	2%

#### 4.6.3 Practical implementation of SAFs: dependency on design spectrum characteristics

Once the SAFs are computed it is interesting to evaluate their actual impact on design, meaning how they could be applied and, on the basis of this, if their adoption can indeed provide some advantages, particularly for non-targeted cases (e.g. the structures/LS for

which the SAF are not computed). The actual implementation of the SAF factor is highly dependent on both the design spectrum shape and also on how flexible it is to capture the different SAFs required at each period.

Even for our limited case study, where three different periods have been employed, the harmonization procedure results in three SAFs, i.e. three spectral acceleration ordinates, to which the code spectrum should be fitted. In the case of a Semi-Flexible approach, we shall employ the  $T=0.5s$  SAF to directly determine the plateau, while the constant velocity  $1/T$  segment will be determined by the  $T=1s$  and  $2s$  values by minimizing the sum of squared errors. This may not necessarily produce an ASCE 7-10 compatible spectrum, especially if the corner period where the constant acceleration plateau and the constant velocity segment intersect ends up being less than  $0.5s$ . Still, this was not a problem for our investigation.

In the case of a Rigid EN1998-like spectrum, all three SAFs can be used separately to scale up the spectrum or employed together to obtain an optimal fit. In the latter case, the anchoring spectral ordinate (PGA) of the spectrum is simply estimated by minimizing the sum of squares of the errors for the three spectral coordinates.

$$e_{EC8}(x) = (Sa(0.5) - 2 \cdot x)^2 + (Sa(1) - x)^2 + (Sa(2) - x/2)^2 \quad (4.6)$$

#### 4.7 RESULTS

To quantify the effect of applying different combinations of fragility curve definitions, target limit-states and spectrum shapes, we show the variability in terms of the coefficient of variation (COV) of the MAFs and of their square root of the sum of the squares (SRSS) error with respect to the targeted MAF. The SRSS error is meant to measure accuracy, i.e., how well each approach captures the target MAF. A low error signifies a method that would rightly deserve the performance-based designation, as it could guarantee the target MAF at least for a single LS definition. On the other hand, the COV conveys the degree of harmonization, i.e., how uniform the MAF values are among the different systems, sites, periods and LS definitions, regardless of whether the target MAF is met. Three different approaches will be tested, namely the two Generic fragility approaches A and B, and the Building-specific case C. Table 4.4 summarizes the defining characteristics of our three proposals vis-à-vis current literature approaches.

**Table 4.4** Different definitions of RT-Spectra determination approaches as adopted in the literature and as proposed herein for the case of EN1998.

	Method	Anchor percentile, $p_0$	Anchor IM MAF, $\lambda_0$	Dispersion $\beta$	Target LS and MAF, $\lambda_{tgt}$	IM	Spectrum shape	Spectral ordinates optimized
Literature	Luco et al. [2007]	0.1	2% in 50yrs	0.6 – 0.8	Collapse 1% in 50 yrs	$S_a(T_i)$	Semi	$S_a(0.2)$ , $S_a(1.0)$
	Douglas et al. [2013]	$10^{-5}$	10% in 50yrs	0.5	Collapse 0.05% in 50yrs	PGA	Rigid	PGA
	Silva et al. [2016]	$10^{-2} - 10^{-5}$	10% in 50yrs	0.5 – 0.7	Collapse 0.25% in 50yrs	PGA	Rigid	PGA
Our proposals	Generic A	0.125	10% in 50yrs	1.0	Severe Damage 6% in 50yrs	$S_a(T_i)$	Any	All
	Generic B	0.12 – 0.16 <sup>i</sup>	10% in 50yrs	0.7 – 0.9	Severe Damage 6% in 50yrs	$S_a(T_i)$	Any	All
	Building-specific C	0.07 – 0.20 <sup>ii</sup>	10% in 50yrs	0.3 – 0.5	Severe Damage 6% in 50yrs	$S_a(T_i)$ , $AvgSA$	Flexible	All

<sup>i</sup> Dependent on period

<sup>ii</sup> Dependent on site, period and building type

#### 4.7.1 Application of SAF based on building-specific fragility curves

Figure 4.11 depicts the impact of employing building-specific C fragilities with a Flexible shape and targeting any of the three LSs, employing  $S_a$  as the IM and only the DCH subset for estimating SAFs. Additional results, not shown herein, have been evaluated for different spectrum shapes and using different subsets of the 36 systems to achieve normalization. It can be said that after whatever kind of harmonization we employ in terms of IM, system subset or spectrum shape, we do observe significant decrease of both the SRSS error and of the variability of the MAF (COV). Obviously, the best results, perfectly matching the target MAF, are achieved when SAFs are customized to each of the individual SDoF systems. Still, this is an impractical mode of application beyond the confines of our study, as customizing SAFs to a particular structure is actually performance-based design, to be applied by the design engineer for the case at hand, not something that could be done widely for code-level RT spectra applications. At the same time, it would be an interesting proposition to consider a web-tool that would offer some customization of RT-spectra for the salient characteristics, e.g., period, ultimate ductility, overstrength, of any system of interest. In our opinion this would be the best approach for RT-spectra, especially if actually matching the target MAF is sought.

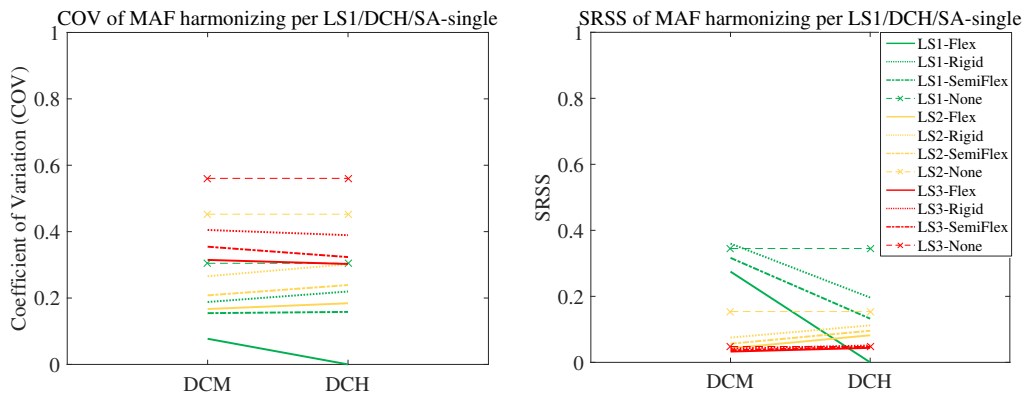
As the results in Figure 4.11 clearly show, even using one half of the building population (DCH) to derive the SAFs, the other half of the population (DCM) is quite imperfectly matching the target risk. Despite this near-perfect-information scenario, the SRSS error is at best halved for buildings that SAFs are not optimized for. In several cases, though, it remains almost the same as the initial, pre-adjustment error. The results are considerably better for the variability. While non-targeted buildings also get about a 50% reduction in COV, this reduction is consistent. In other words, we may not necessarily be getting the MAF that we are targeting, but we are certainly getting less variability among the MAFs of different designs. In other words, RT-spectra seem to harmonize the MAF across different buildings and sites, probably by taking care of the effect of the hazard curve shape/slope in terms of Equation 1, but they cannot match the MAF to any specific target, even for simple SDoF systems.

Looking across different LSs, it is clear that the single LS that is employed to derive the SAFs (for example LS1 for the top row of Figure 4.11) will get the most benefit. Still, the effect spreads to a certain degree also to the other non-targeted cases. The LS further from the target, e.g. LS1 if the harmonization is performed for LS3 (Figure 4.11, bottom panel on the right), will receive the lower benefits, thus a relatively higher SRSS error and COV, but still generally better than having no harmonization at all. Correspondingly, if harmonization is performed for LS2, then LS1 and LS3 observe similar and relatively low COV and SRSS error, which is a good compromise. Given that monetary loss, rather than collapse, is cited as the main (and more frequent) consequence of seismic events (e.g. Northridge, Kobe, Christchurch) for newly designed buildings (Mitrani-Reiser [2007]; Ramirez and Miranda [2009]), achieving harmonization across multiple limit-states can be widely beneficial in capturing the performance of the building stock where it matters the most. Therefore, LS2 can be a useful target.

Additional, perhaps more subtle, advantages can be also gained by targeting an intermediate limit-state like LS2, especially when considering EN1998 applications. The reason is the disparity between the targeted limit-state MAF,  $\lambda_{tgt}$ , and the fragility anchor intensity MAF of  $\lambda_0$ . If the two MAFs are widely different, then the anchoring percentile,  $p_0$ , will have to make up for the difference, moving further into the lower tail of the fragility. For example, for USA application,  $\lambda_0$  is 2% in 50yrs and  $\lambda_{tgt}$  is set at 1% in 50yrs (Luco et al. [2007]). The two are close enough that an anchoring percentile of  $p_0 = 0.1$  can be used (Table 4.4). For EN1998 application, Douglas et al. [2013] and Silva et al. [2016] employed a  $\lambda_0$  at 0.05 – 0.25% in 50yrs (a reasonable collapse MAF for EN1998 compatible buildings) coupled with the (essentially fixed) EN1998  $\lambda_0$  of 10% in 50yrs. This is practically a hundredfold disparity that has naturally led to  $p_0 = 10^{-2} - 10^{-5}$ . Mathematically speaking, this is not an issue, but it becomes important if we start considering the assumptions employed and the limits of our knowledge. The tails of distributions are typically their most uncertain part. Employing rare, low MAF hazard

estimates together with the lowest end of the collapse fragility, where our lognormality assumption places non-zero collapse probability even for extremely low IMs, is not a recipe for good results. Even if our data was perfect, this would not even make sense from an optimization stand point, as we would not be harmonizing for the body of our building stock, but for the few bad buildings that might fail during an extreme phenomenon. Instead, targeting an LS2-like limit-state, allows us to pull back to more reasonable  $p_0$  values in the order of 0.10 – 0.20 (Table 4.4), which can be estimated with some confidence. The results clearly show that the benefits do spread to LS3 anyway, so collapse probabilities are not left unattended. For such reasons, we shall exclusively target LS2 in the following.

Spectrum flexibility obviously has an impact as well. A Flexible shape generally offers good harmonization typically on par with the Semi-Flexible case but with some random exceptions for off-target cases. In further support of this observation, Figure 4.12 shows the results solely for the LS2 normalization case using the subset of DCH buildings, differentiating for ductility class and period of the structure. Therein, the impact of spectrum flexibility becomes clearer; indeed the Semi-Flexible case is more or less coincident with the Flexible case at a period of  $T=0.5\text{sec}$ ; this is to be expected as this spectral ordinate fully defines the constant acceleration plateau in the Semi-Flexible case, allowing it to perfectly match the optimal SAF, similarly to the Flexible case. When moving to  $T=1\text{sec}$  or  $T=2\text{sec}$  where the Semi-Flexible shape can only use one parameter (or SAF) to match two MAFs, the flexible approach is clearly better. Still, the most important conclusion remains that, regardless of the approach adopted, the improvement with respect to the initial case is evident.



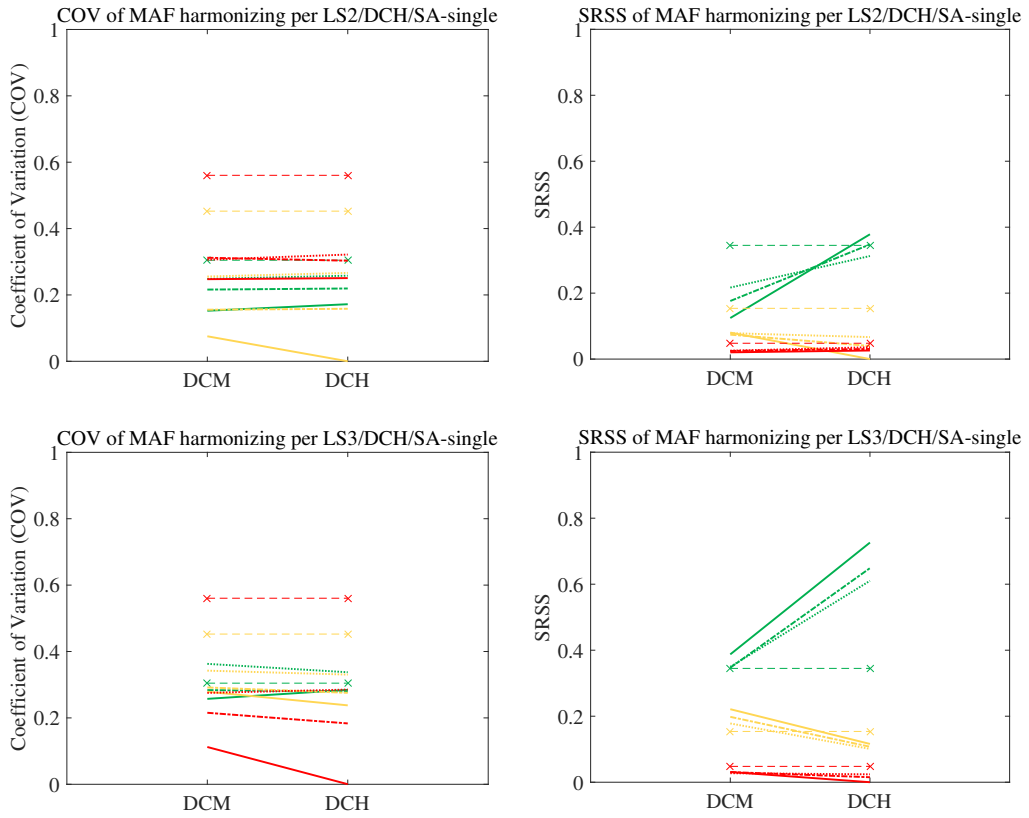


Figure 4.11 Building-specific C fragilities with Flexible spectrum. COV (left) and SRSS (right) using  $S_a$  as IM. Each row represents a different target  $LS_a$  from 1 (top row) to 3 (bottom row). SAFs are estimated only for the DCH subset at each period.

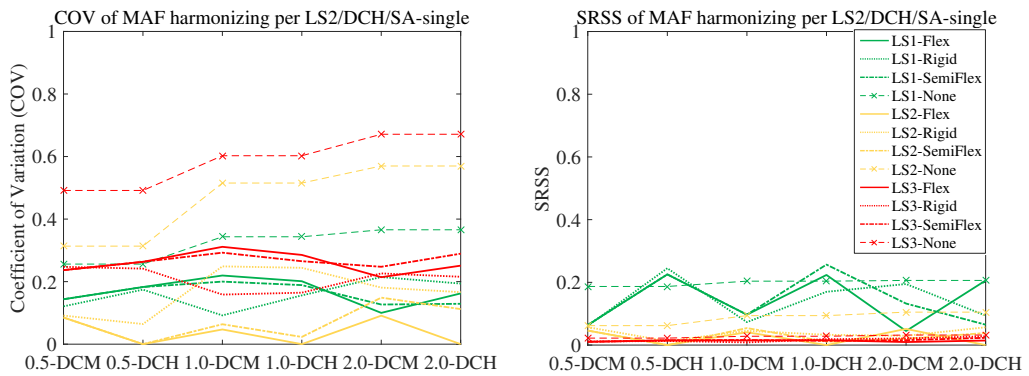
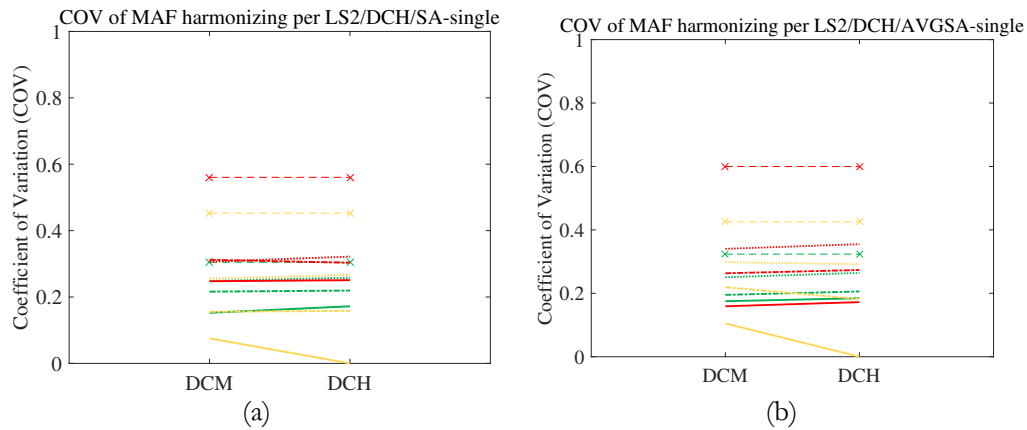


Figure 4.12 Building-specific C fragilities with Flexible spectrum. COV(left) and SRSS (right) using  $S_a$  as IM and targeting LS2. SAFs are estimated only for the DCH subset at each period.

Figure 4.13 shows the effect of using different IMs and record selection approaches. The multi-site CS record selection approach seems to help further decrease the variability of all limit states, above all for LS2 (full data not shown herein), and also among the different spectral shapes and IM types. Still, the magnitude of this improvement is not such as to discount the fact that the actual reason behind this is simply the use of a single set for the sites of similar seismicity. Therefore, one cannot recommend the use of a multi-site approach for determining building-specific fragilities for reasons other than the simple practicality of having fewer ground motion sets to contend with across different sites.

Going to single-site record selection, the differences between using  $AvgsA$  and  $S_a(T_1)$  are also not that remarkable; the lower record-to-record variability ensured by  $AvgsA$  does not seem to offer particular improvements in terms of error and COV here. Probably, CS record selection does a good job covering the possible inefficiencies of  $S_a(T_1)$  that are less prominent in  $AvgsA$ , while the use of a simple SDoF and the focus on global deformation response (rather than local deformations and acceleration of a multi-story structure) and does not permit to fully take advantage of the efficiencies offered by the adoption of  $AvgsA$ . In other words, the only reason to suggest its use for deriving building-specific fragility curves is computational efficiency and lower scaling: due to the lower record-to-record variability fewer records are needed to derive the fragility with a given fidelity and lower scaling factors are needed to match the target  $AvgsA$ -based CS.



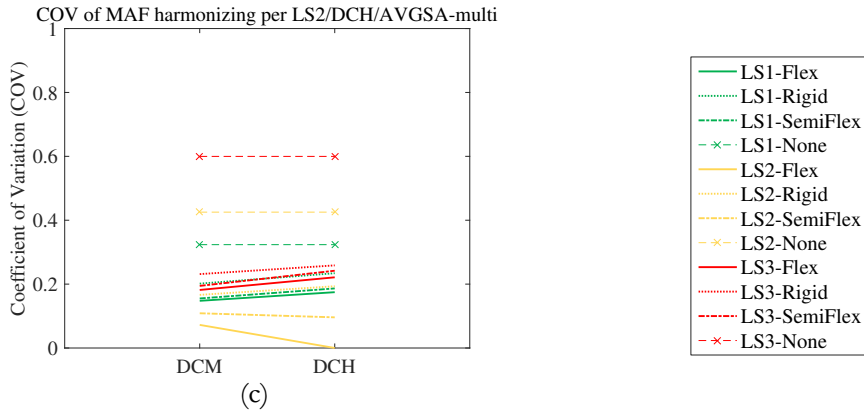
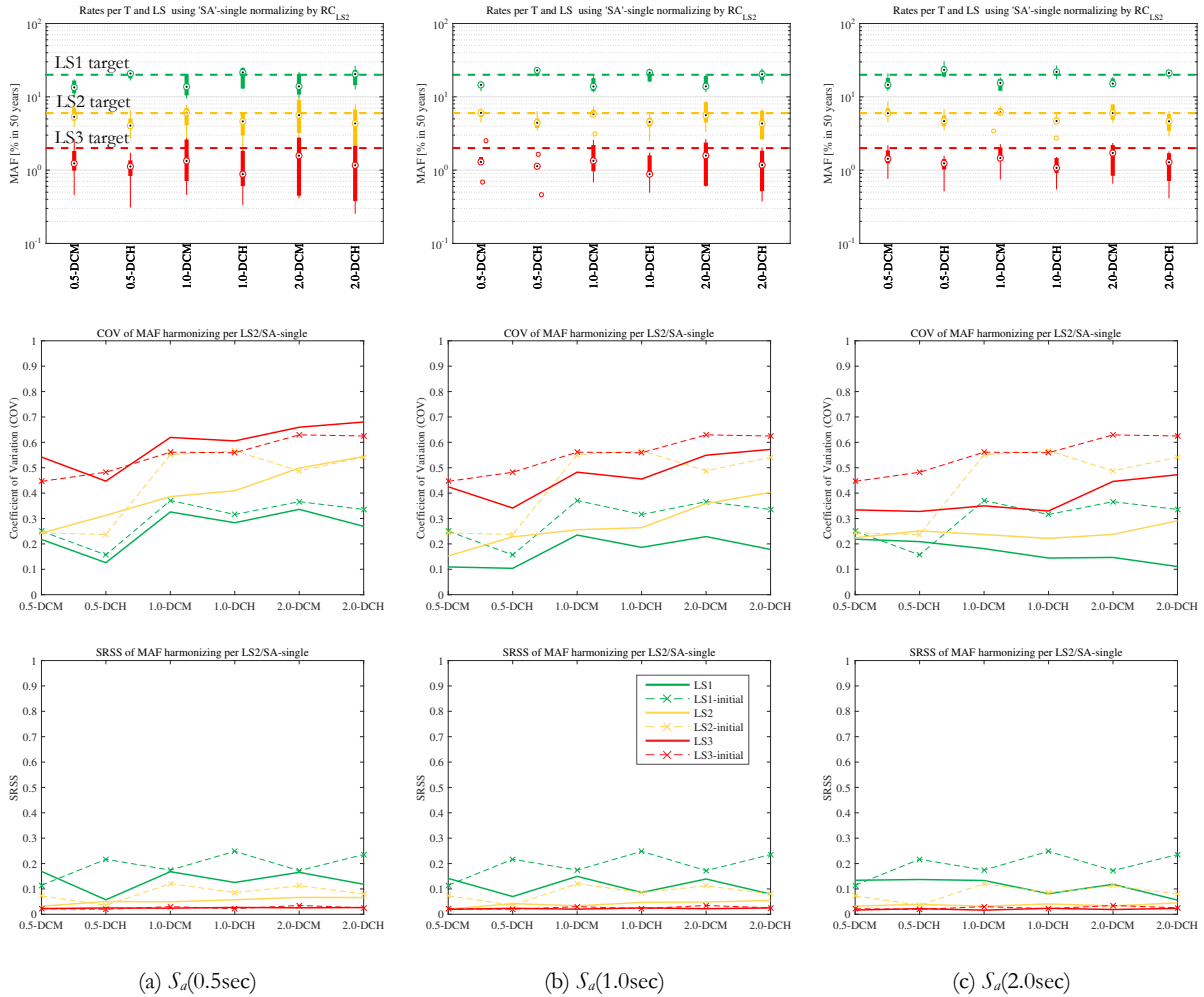


Figure 4.13 Building-specific C fragilities with Rigid/Semi-Flexible/Flexible spectra. Impact of the IM and CS record selection approach when targeting LS2 and employing only the DCH designs to achieve harmonization: There is little difference when using site-specific selection with (a)  $S_a$  or (b)  $AvgSA$ . Employing (c)  $AvgSA$  with record sets compatible with multiple sites of similar seismicity does seem to improve harmonization but to a small degree and may be an artificial effect of lower fragility variability.

#### 4.7.2 Application of SAF based on generic fragility curves

Based on the previous findings, we expect that generic fragilities would perform worse than building-specific ones. Still, they are best suited to practical applications that do not require any ancillary software. To evaluate their performance, SAFs were computed for Generic A and B fragilities, using  $S_a(T_1)$  as the IM and targeting LS2. Generic fragility types can be applied for any type of spectrum shape, yet a practical application is only compatible with less flexible shapes. In our case, Generic A fragilities will be combined with a Rigid shape, paralleling the work of Douglas et al. [2013] and Silva et al. [2016]. For the fragility and the SAF calculation, the entire set of 36 systems will be employed. As a low-cost improvement, the ‘period-dependent’ Generic B fragilities will be applied on the Rigid as well as the Flexible shape cases to quantify potential benefits. Now, a different fragility is estimated by employing all 12 systems for a given period.

Figure 4.14 shows that even applying the simplest Generic A fragility definition on a Rigid shape, the procedure goes in the right direction by decreasing both the variability and the error with respect to the target. It should be noted that, surprisingly enough, the application of SAFs estimated at  $T=1s$  induces a lower variability for structures characterized by  $T=0.5s$  when compared to what happens if the “optimal” SAF estimated for  $T=0.5s$  is applied. The reason for this apparent counterintuitive conclusion lies in the definition of the Generic A fragility that includes different periods and ductility classes having, therefore, a very high variability (around 1.0). Apparently, despite trying to normalize on the basis of  $S_a(0.5sec)$ , using such a blunt instrument only produces mediocre results for  $T=0.5s$  systems.



**Figure 4.14** Generic A fragilities with a Rigid spectrum shape. Box-plot (top), COV (middle) and SRSS (bottom) results when targeting LS2 and harmonizing with respect to (a)  $S_a(0.5\text{sec})$ , (b)  $S_a(1.0\text{sec})$  and (c)  $S_a(2.0\text{sec})$ .

This conclusion is confirmed in Figure 4.15, which shows the effect of applying period-dependent Generic B fragilities with a Rigid shape. These results show more realistically the impact of scaling an inflexible spectrum on the basis of SAFs derived at a single given period. Both the MAF variability and its SRSS error with respect to the target decrease in any case but this cutback is much more evident for the structures having the same period as the applied SAF. Now, contrary to what happened with Generic A fragilities, the  $T=0.5\text{sec}$  structures do achieve lower COV when SAFs optimized for  $T=0.5\text{s}$  are applied. Moreover, if the SAFs coming from Generic B fragilities are applied only to the periods at which they belong, i.e. implementing a Flexible shape, the improvement that we

previously saw separately in each of the columns is now obtained simultaneously (see Figure 4.16). Once again, introducing flexibility into the design spectrum clearly helps RT-spectra achieve their target. Even if a fully flexible shape is not practical, implementing a two- or three-parameter spectrum shape that is fitted by minimizing the error at multiple spectral ordinates as estimated via period-dependent generic fragilities is expected to offer considerable improvements.

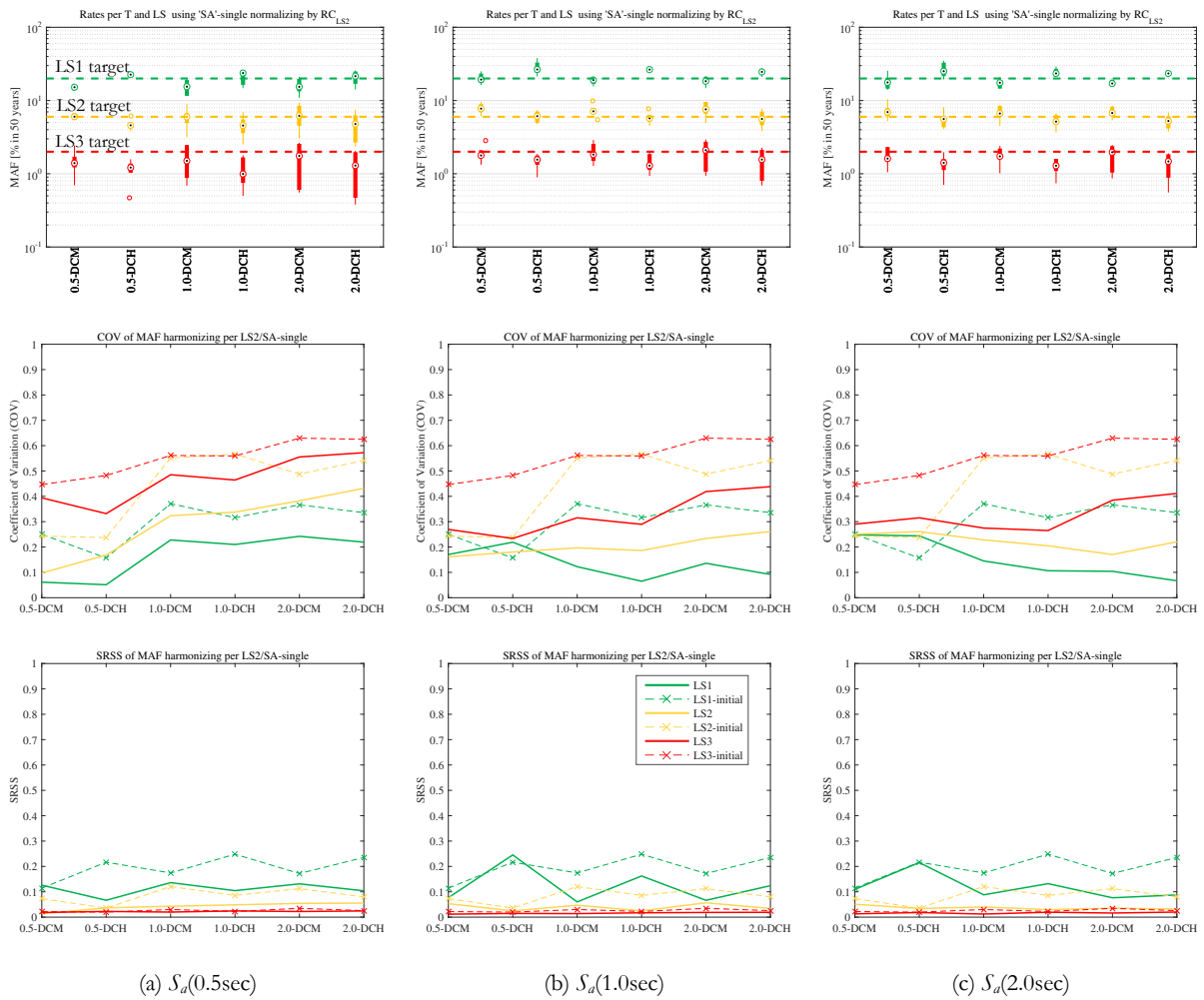


Figure 4.15 Generic B fragilities with a Rigid spectrum shape. Box-plot (top), COV (middle) and SRSS (bottom) results when targeting LS2 and harmonizing with respect to (a)  $S_a(0.5\text{sec})$ , (b)  $S_a(1.0\text{sec})$  and (c)  $S_a(2.0\text{sec})$ .

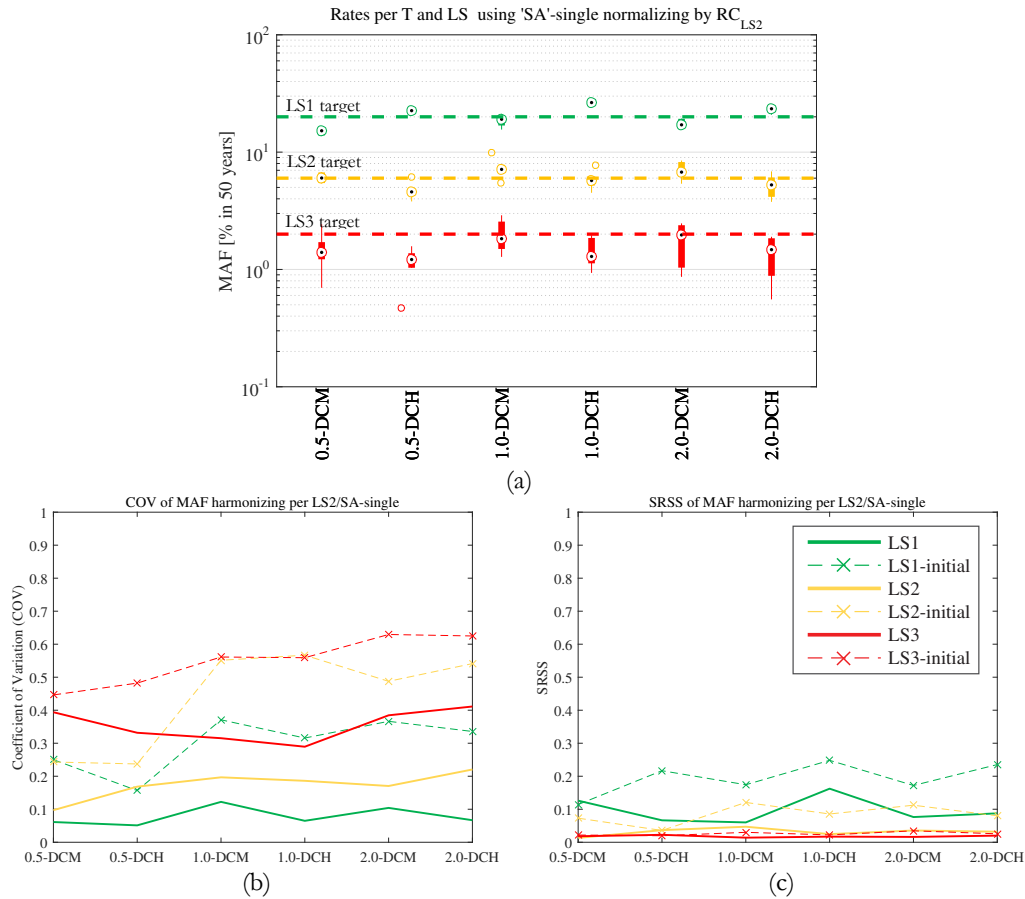


Figure 4.16 Generic B fragilities with a Flexible spectrum shape: (a) Box-plots, (b) COV, and (c) SRSS results when targeting LS2 and harmonizing each system at its corresponding oscillator period.

#### 4.8 CONCLUDING REMARKS

Risk-targeted spectra can be computed in a myriad of combinations, targeting different limit-states and corresponding MAFs, employing generic or building-specific fragilities and optimizing different period ranges to adjust design spectra shapes of different parameterization and flexibility. In all cases tested, one single theme seems to emerge: RT-spectra are not a panacea for performance-based design. They simply cannot guarantee risk *matching* for any limit-state. This would only be possible with case-specific customized fragilities that have been derived for the building and site of interest. Simply put, a single design spectrum, however adjusted, cannot simultaneously cater to the needs of multiple different structures at a given site. On the other hand, RT spectra provide a fairly good risk *harmonization*. A given risk may not be matched for any specific building,

but similar risk values are achieved among different buildings and sites. At best, some degree of risk assurance would be possible if one estimated RT spectra by using, at the very least, fragilities that depend on the salient characteristics of the structure of interest (period, ductility, overstrength), something that could be easily offered as a web application. Further improvements can be realized by also employing risk-consistent behavior (or strength-reduction) factors (Vamvatsikos et al. [2017]) to design the building, or simply by directly adopting an elaborate performance-based design approach (Krawinkler et al. [2006], Vamvatsikos and Aschheim [2016]).

Overall, RT spectra do confer considerable benefits practically regardless of the method used to determine them. Therefore, unless one goes all the way to implement building-specific fragilities, it makes little sense to overcomplicate their mode of application. Still, based on our limited investigation, there are some simple pointers to follow that generally make for better harmonization than others:

- Avoid large disparities between the target MAF and the fragility anchoring intensity MAF that the code uniform hazard depends on. This expedient would prevent harmonizing for the tails of the hazard and of the fragility curve but rather would do it for their body.
- Prefer targeting an intermediate LS, closer to life-safety than to collapse, to better harmonize for frequent structural and non-structural damage (and thus loss metrics) while also achieving some non-negligible harmonization of both lower (serviceability) and higher (collapse) limit-states.
- Avoid using PGA-based fragilities, as they can bias the results even if careful record selection is employed. Prefer  $S_a$  or  $AngSA$  as the intensity measure, focusing on the latter if building-specific fragilities are to be employed as it requires fewer ground motions to achieve good accuracy.
- More flexibility (i.e., more spectral ordinates to tune) in the design spectrum shape makes for better harmonization. Rigid shapes, such as the EN1998 shape anchored only on PGA, cannot simultaneously achieve good harmonization at multiple periods.
- Even when having few spectral ordinates to tune, it is better to estimate spectral adjustment factors at multiple periods and then optimally fit the spectrum shape, rather than directly optimizing only for the tunable spectral ordinates. The more rigid the shape, the more important this consideration seems to become.

## 5. CONCLUSIONS

This work is based on the framework and the concepts of Performance Based Earthquake Engineering (PBEE) that was originally conceived to evaluate the earthquake performance of buildings. The PBEE methodology discretizes the problem into four main parts: *hazard analysis*, *demand analysis*, *fragility analysis* and *loss analysis*. The pieces of information coming from each of these components are integrated together to allow risk quantification. The connection between each of the four steps of the framework is done via only a single parameter: ground motion Intensity Measure, IM, between hazard and demand analyses; an Engineering Demand Parameter, EDP, between demand and fragility analyses; a Damage Measure, DM, between fragility and loss analyses. Separating the risk analyses in four smaller parts is brilliant in the sense that it makes apparent to all players to which part of the large problems or risk assessment their research is contributing. However, relying on a single parameter the liaison between the four parts can generate inaccuracies unless attention is paid to details.

Here we concentrated our efforts mainly in improving the connection between hazard and demand analyses. More specifically, given the uncertainty and possible sources of bias in the response estimated by conditioning on the ground motion intensity measure (IM) as a part of the demand analysis step, there is room for additional research to better understand and reduce the source of this uncertainty and perhaps to reduce if not remove the bias. This could be done through improving the choice of the IM adopted to describe the ground motion and/or enhancing the ground motion record selection procedures. The record selection connects the *hazard analysis* and *building response* (i.e. *demand analysis*) and, if properly conducted, can reduce the deficiencies due to an approximated representation of the ground motion via a single IM. *Chapter 2* has the main objective of defining a record selection procedure that, besides the spectral shape, can implicitly account for other parameters important for the structural response. Here, as an example, particular attention is given to ground motion duration, which is gauged in terms of the so-called effective duration ( $D_{5-75}$ ) as the additional parameter (other than spectral shape) having an impact on structural response. To investigate this topic, the risk assessment of a single building (2D Reinforced Concrete frame located in Seattle) has been conducted in a Multiple Stripe Analysis (MSA) manner adopting four different record sets selected according to four different methods: the Conditional Spectrum, CS, method with magnitude,  $M$ , and source-to-site distance,  $R$ , consideration (called CS-MR, which is our proposal), the exact CS-only method, the CS-approximate method and the Generalized Conditional Intensity Measure (GCIM) method. All four methods ensure spectral shape consistency with site hazard. However, out of these four methods only the CS-MR, implicitly, and the GCIM, explicitly, select records whose duration is consistent with the seismicity in the region around the site identified via PSHA disaggregation. The resulting

annual rates of collapse have shown that the GCIM and CS-MR method predict similar rates with the estimates from the latter being around 15% higher than those from the former. Because of its capability of explicitly accounting for any parameter that could influence the structural response, the GCIM method could reasonably be preferred to the proposed CS-MR method. However, GCIM requires a certain degree of arbitrariness in selecting a priori the IMs (or giving them different weights) that matter for structural response prediction. Moreover, once the important IM/IMs are chosen during the implementation of GCIM it may happen that they do not have the proper GMPE needed to compute a truly hazard-consistent target distribution (this is indeed the case of the duration of ground motion records caused by large magnitude subduction zone events analyzed in this work). In addition, since there is no control on the M-R characteristics of the selected records, the GCIM method could potentially pick ground motions whose causal parameters do not matter for the considered site and, therefore, ground motions that the analyzed structure might never encounter during its lifetime. These possible shortcomings could theoretically render the output coming from GCIM inaccurate if compared to that of the CS-MR method. (Of course, this statement is strictly speaking true in the limit, namely when the ground motion database is very rich in any M and R bin of interest, This is not the case now for some large M and short R bins but the number of ground motions collected by the engineering seismology community increases by quantum leaps every year.) The latter procedure can bypass those problems by using Magnitude and source-to-site distance, R, as proxies so that additional information relevant to the structural response can be naturally accounted for. No need to foresee which additional non-spectral IMs are relevant to assessing the EDP of interest and no need for selecting an appropriate GMPE for those additional non-spectral ground motion parameters, whether they are duration or else.

Taking advantage from the record selection method proposed in *Chapter 2*, *Chapter 3* deals with the assessment of the risk, quantified in terms of nominal rates of reaching or exceeding two limit states (Collapse and of Onset of Damage) of structures designed according to the current Italian code provisions (i.e.NTC [2008b]). The work part of this thesis is included in a large research project funded by the Italian Department of Civil Protection and carried out in collaboration with other research units within ReLUIS, the Italian Laboratories University Network of seismic engineering. The methodology adopted to compute the risk reflects the aforementioned PBEE structure in all its parts with the exception of the *loss analysis*. Different structures located at different sites are designed according to the current Italian code procedure to withstand acceleration inputs with low probability of being exceeded (e.g. a fixed level of hazard  $H_{LS}=10\%$  in 50 years or, equivalently, having a 475 years return period) and applying safety factors to both seismic actions and values of material properties. However, the actual impact of these factors is neither known nor quantified by the code. The objective of the project was exactly to cover this lack of knowledge and to define a strong base, also from the

methodological point of view, that could be used for future code improvements. Considering the amount of possible combinations of sites, soil types and structural typology/configuration, the problem has been reduced to a manageable number of pilot building case studies that, however, represent a wide range of realistic examples. In particular, the combinations of five sites (of increasing seismic hazard levels), two soil types and five structural typologies (in several configurations), which constitute the population of buildings that were assessed, represent the large majority of buildings in the Italian inventory. Each building has been designed according to the current code provisions and modeled so that it could be tested by means of non-linear dynamic analyses. In particular, the structural performance was assessed in a MSA fashion: 10 record sets (each of them defining a stripe) were selected by means of the CS-MR method developed in *Chapter 2*. Each set is related to a different hazard level (from 10 to  $10^5$  years return period at each site) and selected to be simultaneously consistent with the spectral acceleration distribution conditioned on observing spectral acceleration at first period ( $Sa(T_1)$ ) and with the causal parameters (M-R) that mostly contribute to the site hazard. The results of the assessment were presented in terms nominal annual rates of reaching or exceeding the two limit states. These results clearly show levels of performance that differ among the various structural typologies analyzed, namely non-uniform risk rates for both the collapse and the onset of damage limit states. In particular, the risk was shown to increase with the level of site hazard and, in the most hazardous sites, some structures (i.e., irregular unreinforced masonry and precast structures) were characterized by collapse rates with the same order of magnitude of the hazard level used to design the structure itself. These collapse rates are high also considering that they were computed assuming the absence of design and construction deficiencies. Hence, given these findings we recommended that the design provisions of precast structures be revised in future releases of the code and that perhaps unreinforced masonry buildings be disallowed in in the most hazardous areas.

The evidence of a non-uniform risk among different locations (even if such locations have the same ground motion hazard) and structural typologies could persuade rethinking the design paradigm that codes such as NTC08 and, more generally, EC08 is based on. In particular, a code that could guarantee, at least theoretically, a certain uniformity of risk would be fairer and, certainly, more ethical. The best approach to improve future design paradigm is probably to introduce explicitly risk ( $\lambda_{LS}$ ) at the output level of response. In simple words, this means designing for  $\lambda_{LS}$  rather than for a fixed level of hazard,  $H_{LS}$ . However, this kind of approach would require a complete overhaul of the process for designing structures and, therefore, it is probably not implementable for a number of years. An approximated way to solve this risk heterogeneity across building types and sites could be to simply change the design spectral accelerations in such a way that they do not have anymore the same return period at all sites for all structures. In this case, the rather complex risk calculations would be hidden into the design ground motion levels

and would be invisible to the practicing engineers. The latter approach is basically what proposed by Luco et al. [2007] and currently adopted in US code (ASCE [2010]), i.e. the so-called Risk Targeted Ground Motion (RTGM) maps. These maps are based on the direct scaling of design spectral acceleration coming from PSHA by an ‘adjustment factor’ (or risk coefficient) that shifts the design capacity of a generic structure in order to “guarantee”, under some pretty heavy assumptions, a pre-specified collapse risk that has been explicitly agreed upon as an acceptable target. The same approach was later embraced by Douglas et al. [2013] and Silva et al. [2016] who proposed PGA-based RTGM maps for Europe. All these applications are different expressions of the same idea: the definition of a risk targeted spectrum (RT-spectrum) to be adopted for design. *Chapter 4* revisited the details and the definitions of each element of RT-spectra and then moved on investigating the effects caused by different legitimate choices made during the implementation of the RTGM method on the final design of different buildings represented here, for ease of computation, as single-degree-of-freedom (SDoF) systems. The different choices of fragility functions, performance objective and design spectrum parameterization are the elements playing a central role in the architecture of RT-spectra that we investigated here.

More specifically, we focused our attention on three aspects of the implementation of RTGM. The first aspect that has been questioned is related to the adoption of generic fragilities in contrast with the possible implementation of building-specific fragility curves. This latter option brings to light common issues in PBEE, such as the IM choice and record selection procedures (see Chapters 2 and 3 of this thesis), which the adoption of generic fragilities might be easily neglect. Secondly, the impact of targeting limit states different from collapse was examined; this is interesting to us because lower damage states are typically of high interest for loss estimation analyses. The third facet is related to the way the computed risk coefficients (SAF) can be applied to modify the design spectrum.

One of the main outcomes of this work unveils the false assertion about RTGM maps and RT-spectra that is intrinsic in the ‘targeted’ label. Strictly speaking, designing structures using the ground motions specified in RTGM maps does not ensure any uniform risk level. Indeed, the targeted risk could only be theoretically achieved if the assumed fragility curve were exactly representative of the structure under design (i.e., using a building specific fragility) and the risk coefficient were tailored for the structure itself. However, RTGM spectra (and maps when considered for a region) are indeed useful even if they cannot guarantee risk uniformity across building types and sites. Despite the assumptions that one could make in terms of fragility, targeted-LS and SAF application, the RT-Spectra were proven to confer considerable benefits in terms of risk harmonization, which is the next best thing after risk uniformity. In particular, we provided four main recommendations in order to guarantee a better harmonization.

- First, try to enforce harmonization for the body of the distributions that relate to the hazard IM, usually represented via the site hazard curve, and the building capacity usually represented via the fragility curve for the limit state selected during the application. This objective can be achieved by keeping similar values of the target MAF (e.g., for example, 5% frequency of observing life safety conditions in 50 years) and the hazard design level (e.g., ground motion IM level with 10% frequency of exceedance in 50 years).
- Second, targeting for design an intermediate limit state (LS) (e.g. life safety rather than collapse) will guarantee a better harmonization for both operational (serviceability) and ultimate (collapse) limit states.
- Third, the adoption of PGA-based fragilities (and, therefore, for anchoring design spectra, as done in the EN1998 code) is discouraged since this choice can bias the results even when one carries out a careful hazard-consistent record selection.  $SA$  and  $AvgSA$  are better choices of ground motion intensity measures; The latter is preferred if one employs building-specific fragilities since it requires fewer ground motions to achieve good accuracy.
- Fourth, a more flexible representation of the design spectrum (i.e. one anchored to more than one spectral ordinates or, better, not anchored at all and simply inherited by site-specific PSHA results) guarantees a better harmonization of risk for buildings with different fundamental periods of vibration. Even if the focus is on few spectral ordinates it is preferable to use all of them to define a unique adjustment factor (SAF) fitting the spectral shape, rather than use just one arbitrarily selected spectral ordinate.

In summary, the our attention went first to improving the risk assessment for specific buildings by promoting a more intuitive records selection approach that accounts explicitly for the causative parameters of the earthquakes of interest for the site. This procedure may remove, at least when the ground motion databases increase in size, some difficulties and arbitrary decisions that are necessary for the applications of other record selection methods in the literature. We then tested this methodology in a very ambitious, large-scale project whose scope is the estimation in quantitative terms of the performance of Italian buildings designed according to the current code. This project considered a finite number of pilot buildings that were selected to be representative of the entire Italian building stocks. The findings showed clearly that, as expected, the current codes whose design paradigm only requires considering levels of ground motions with a uniform probability of being exceeded in a given period (e.g., 10% in 50 years) do not ensure a uniform level of risk across building types and sites. The safety margins of structures built in more seismically hazardous areas are smaller than those in low seismicity areas and for some building configurations they may be considered dangerously small. These non-uniform building performance estimates can be considered robust,

since they were confirmed using alternative ground motion intensity measures and different ground motion record sets.

These considerations led us to the third effort of this thesis, namely a critical analysis of a new design paradigm that was proposed a few years ago in USA, the so-called risk target ground motion approach. The application of the RTGM approach for design is appealing because theoretically is meant to ensure buildings with uniform risk (e.g., 1%) of reaching the objective limit state (usually collapse) within a given lifetime of the structure (e.g. 50 years). This method, however, only ensures a harmonization of risk rather than uniformity, which is still a valuable objective to pursue. We provided recommendations that would harmonize the risk in a more efficient way. The target risk can only be achieved with a theoretical precision for single buildings located at given sites using the approaches discussed in Chapter 2 and applied in Chapter 3. For mass applications to the entire building stocks, the approaches presented in Chapter 4 can only harmonize the risk around the explicitly accepted target but not guarantee it. In our opinion, this still a worthwhile new design paradigm to pursue, vastly superior to the hazard-consistent but current risk-independent one.

## 5.1 FUTURE DIRECTIONS

- CS-MR method could be tailored to work with IM other than simple  $S_a$ , such as AvgSA in order to improve the consistency of the selected record sets with the causal parameters expected to influence the site hazard.
- The CS-MR post processing algorithm could be applied to GCIM method to but it requires higher level of precision since it should keep the consistency with i) spectral shape, ii) the conditioned distribution of the other parameter/s (e.g. duration) and iii) M-R characteristics. This may not be doable because of limited number of record database unless, maybe, very high scaling factors are allowed (with all the consequent disadvantages and criticisms).
- The use of physics-based ground motions could be investigated aiming to fill in the database used for record selection applied to CS or GCIM method.
- The method could be tested also to see whether it could naturally account for other parameters than duration that could influence structural response, but they should not be dependent on scaling.
- The CS-MR framework could be useful to define a record selection procedure that accounts for pulse like records, maybe accounting also for  $T_p$ , the period of velocity pulse, i.e. the period in correspondence of the maximum value of velocity response spectrum. This parameter, together with the source to site distance and the direction of propagation of the earthquake rupture with respect to the building, are typically used to define the chance of observing a pulse-like ground motion.

- The Implicit Risk project will continue in the next years investigating the influence of modelling uncertainty and consolidating the current results. The work will be also focused on assessing the risk of existing buildings with well-defined characteristics in terms of construction age and design code requirements.
- About RT-Spectra it would be interesting to evaluate the chance of developing a web based tool that could implement the SAF calculation on the basis of SDoF systems knowing backbone characteristics of the building. In this way it could be possible to be more close to the risk target that we want to guarantee.

## REFERENCES

- (CSLP), C. S. d. L. P. (2008). Spettri-NTC ver 1.03. from [http://www.cslp.it/cslp/index.php?option=com\\_docman&task=doc\\_details&gid=3280&Itemid=165](http://www.cslp.it/cslp/index.php?option=com_docman&task=doc_details&gid=3280&Itemid=165)
- Abrahamson, N. A., and Silva, W. J. (1996). Empirical Ground Motion Models. Upton (NY): Report to Brookhaven National Laboratory.
- Akkar, S., and Bommer, J. J. (2010). Empirical equations for the prediction of PGA, PGV and spectral accelerations in Europe, the Mediterranean region and the Middle East. *Seismological Research Letters*, 81.
- Ambraseys, N. N., Simpson, K. A., and Bommer, J. J. (1996). Prediction of horizontal response spectra in Europe. *Earthquake Engineering & Structural Dynamics*, 25(4), 371-400.
- Arias, A. (1970). A measure of earthquake intensity. *Seismic Design for Nuclear Power Plants*, R.J. Hansen, ed., The MIT Press, Cambridge, MA, 438-483.
- ASCE. (2010). Minimum Design Loads for Buildings and Other Structures (ASCE 7-02), American Society of Civil Engineers. Reston, VA.
- ATC-58. (2011). Seismic Performance Assessment of Buildings, Volume 1 – Methodology.
- ATC-63. (2009). Quantification of Building Seismic Performance Factors (FEMA p-695).
- Atkinson, G. M., and Boore, D. M. (2003). Empirical Ground-Motion Relations for Subduction-Zone Earthquakes and Their Application to Cascadia and Other Regions. *Bulletin of the Seismological Society of America*, 93(4), 1703-1929.
- Baker, J. W. (2007). Probabilistic structural response assessment using vector-valued intensity measures. *Earthquake Engineering & Structural Dynamics*, 36, 1861-1883. doi: 10.1002/eqe.700
- Baker, J. W. (2011). The conditional mean spectrum: A tool for ground motion selection. *ASCE Journal of Structural Engineering*, 137, 322–331.
- Baker, J. W., and Cornell, C. A. (2005). A Vector-Valued Ground Motion Intensity Measure Consisting of Spectral Acceleration and Epsilon. *Earthquake Engineering and Structural Dynamics*, 34(10), 1193-1217.
- Baker, J. W., and Cornell, C. A. (2006a). Spectral shape, epsilon and record selection. *Earthquake Engineering and Structural Dynamics*, 35(9), 1077–1095.
- Baker, J. W., and Cornell, C. A. (2006b). Which Spectral Acceleration Are You Using? *Earthquake Spectra*, 22(2), 293–312.

- Baker, J. W., and Jayaram, N. (2008). Correlation of spectral acceleration values from NGA ground motion models. *Earthquake Spectra*, 24(1), 299-317.
- Baker, J. W., and Lee, C. (2016). An Improved Algorithm for Selecting Ground Motions to Match a Conditional Spectrum. *Journal of Earthquake Engineering (in press)*.
- Bazzurro, P., and Cornell, C. A. (1999). On disaggregation of seismic hazard. *BSSA*, 89(2), 501-520.
- Bertoldi, S. H., Decanini, L., and Gavarini, C. (1993). *Telai tamponati soggetti ad azioni sismiche, un modello semplificato, confronto sperimentale e numerico*. Paper presented at the 6° Convegno Nazionale L'ingegneria Sismica in Italia, Perugia.
- Beyer, K., and Bommer, J. J. (2007). Selection and Scaling of Real Accelerograms for Bi-Directional Loading: A Review of Current Practice and Code Provisions. *Journal of Earthquake Engineering*.
- Bolt, B. A. (1973). *Duration of strong ground motion*. Paper presented at the 5th World Conference on Earthquake Engineering, Roma, Italy.
- Bommer, J. J., and Acevedo, A. B. (2004). The use of real earthquake accelerograms as input to dynamic analysis. *Journal of Earthquake Engineering*, 8, 43-91.
- Bommer, J. J., Magenes, G., Hancock, J., and Penazzo, P. (2004). The Influence of Strong-Motion Duration on the Seismic Response of Masonry Structures. *Bulletin of Earthquake Engineering*, 2(1), 1-26.
- Boore, D. M., and Atkinson, G. M. (2008). Ground-Motion Prediction Equations for the Average Horizontal Component of PGA, PGV, and 5%-Damped PSA at Spectral Periods between 0.01 s and 10.0 s. *Earthquake Spectra*, 24(1), 99-138.
- Bradley, B. A. (2010). A generalized conditional intensity measure approach and holistic ground-motion selection. *Earthquake Engineering and Structural Dynamics*, 39(12), 1321-1342.
- Bradley, B. A. (2011). Correlation of Significant Duration with Amplitude and Cumulative Intensity Measures and Its Use in Ground Motion Selection. *Journal of Earthquake Engineering*, 15, 809-832.
- Bradley, B. A. (2012). A ground motion selection algorithm based on the generalized conditional intensity measure approach. *Soil Dynamics and Earthquake Engineering*, 40, 48-61.
- Camata, G., Celano, F., De Risi, M. T., Franchin, P., Magliulo, G., Manfredi, V., . . . Verderame, G. (2017, 15-17 June 2017). *RINTC project: Nonlinear Dynamic Analyses of Italian code-conforming Reinforced Concrete Buildings for Risk of Collapse Assessment*. Paper presented at the COMPDYN 2017 - 6th ECCOMAS Thematic Conference on Computational Methods in Structural Dynamics and Earth-quake Engineering, Rhodes Island, Greece.
- Camilletti, D., Cattari, S., Lagomarsino, S., Bonaldo, D., Guidi, G., Bracchi, S., . . . Rota, M. (2017). *RINTC project: Nonlinear dynamic analyses of Italian code-conforming URM buildings for collapse risk assessment*. Paper presented at the COMPDYN 2017 - 6th

- ECCOMAS Thematic Conference on Computational Methods in Structural Dynamics and Earthquake Engineering, Rhodes Island, Greece.
- Campbell, K. W., and Bozorgnia, Y. (2008). NGA Ground Motion Model for the Geometric Mean Horizontal Component of PGA, PGV, PGD and 5 % Damped Linear Elastic Response Spectra for Periods Ranging from 0.01 to 10s. *Earthquake Spectra*, 24(1), 139-171.
- Cardone, D., Conte, N., Dall'Asta, A., Di Cesare, A., Flora, A., Leccese, A., . . . Ragni, A. (2017, 15–17 June 2017). *RINTC project: Nonlinear analyses of Italian code-conforming base-isolated buildings for risk of collapse assessment*. Paper presented at the COMPDYN 2017 - 6th ECCOMAS Thematic Conference on Computational Methods in Structural Dynamics and Earthquake Engineering, Rhodes Island, Greece.
- Cattari, S., and Lagomarsino, S. (2013). Masonry structures. In T. Sullivan and G. M. Calvi (Eds.), *Developments in the field of displacement based seismic assessment*. Pavia: IUSS press - Eucentre.
- CEN. (2004). Design of Structures for Earthquake Resistance - Part 1: General rules, seismic actions and rules for buildings. Brussels, Belgium.
- CESMD. (2012). Strong Motion Virtual Data Center from <http://www.strongmotioncenter.org/vdc/scripts/default.plx>
- Chandramohan, R., Baker, J. W., and Deierlein, G. G. (2016a). Impact of hazard-consistent ground motion duration in structural collapse risk assessment. *Earthquake Engineering & Structural Dynamics*, 45(8), 1357-1379.
- Chandramohan, R., Baker, J. W., and Deierlein, G. G. (2016b). Quantifying the influence of ground motion duration on structural collapse capacity using spectrally equivalent records. *Earthquake Spectra*, 32(2), 927-950. doi: 10.1193/122813EQS298MR2
- Chiou, B. S.-J., and Youngs, R. R. (2008). An NGA Model for the Average Horizontal Component of Peak Ground Motion and Response Spectra. *Earthquake Spectra*, 24(1), 173-215.
- Cornell, C. A. (1968). Engineering seismic risk analysis. . *Bulletin of Seismological Society of America*, 58, 1583-1606.
- Cornell, C. A. (1994). *Risk Based Structural Design*. Paper presented at the Symposium on Risk Analysis, Ann Arbor (MI).
- Cornell, C. A., and Krawinkler, H. (2000). Progress and Challenges in Seismic Performance Assessment. *PEER Center News*, 3(2).
- Decanini, L. (2001). *Approcci innovativi in termini di energia e di spostamento per la valutazione della risposta sismica di strutture a più gradi di libertà*. “Sapienza” University, Roma, Italy.
- Decanini, L., and Fantin, G. E. (1986). Modelos simplificados de la mamposteria incluida en porticos. Características de rigidez y resistencia lateral en estado limite. *Jornadas Argentinas de Ingeniería Estructural*, 2, 817-836.

- Decanini, L., Liberatore, L., and Mollaioli, F. (2014). Strength and stiffness reduction factors for infilled frames with openings. *earthquake Engineering and Engineering Vibration*, 13(3), 437-454.
- Decanini, L., Mollaioli, F., Mura, A., and Saragoni, R. (2004, August, 1st-6th). *Seismic performance of masonry infilled R/C frames*. Paper presented at the 13th WCEE, Vancouver, B.C. Canada.
- Douglas, J., Ulrich, T., and Negulescu, C. (2013). Risk-targeted seismic design maps for mainland France. *Natural Hazards*, 65(3), 1999-2013.
- Electrical Power Research Institute, E. (1988). A Criterion for Determining Exceedance of the Operating Basis Earthquake, *EPRI NP-5930*. Palo Alto, CA.
- Ercolino, M., Cimmino, M., Magliulo, G., Bellotti, D., and Nascimbene, R. (2017, 15-17 June 2017). *Nonlinear analyses of Italian code conforming precast R/C industrial buildings for risk of collapse assessment*. Paper presented at the COMPDYN 2017 - 6th ECCOMAS Thematic Conference on Computational Methods in Structural Dynamics and Earthquake Engineering, Rhodes Island, Greece.
- Fischinger, M., Kramar, M., and Isakovic, T. (2008). Cyclic response of slender RC columns typical of precast industrial buildings. *Bulletin of Earthquake Engineering*, 6(3), 519-534.
- Goda, K., and Atkinson, G. M. (2011). Seismic performance of wood-frame houses in south-western British Columbia. *Earthquake Engineering & Structural Dynamics*, 40(8), 903-924.
- Grant, D. N., Fenves, G., and Whittaker, A. (2004). Bidirectional modelling of high-damping rubber bearings. *Journal of Earthquake Engineering*, 8(1), 161-185.
- Hancock, J., and Bommer, J. J. (2006). A State-of-Knowledge Review of the Influence of Strong-Motion Duration on Structural Damage. *Earthquake Spectra*, 22(3), 827-845.
- Hancock, J., and Bommer, J. J. (2007). Using spectral matched records to explore the influence of strong-motion duration on inelastic structural response. *Soil Dynamics and Earthquake Engineering*, 27(4), 291-299.
- Haselton, C., Liel, A., and Deierlein, G. G. (2009). *Simulating structural collapse due to earthquakes: model idealization, model calibration, and numerical solution algorithms*. Paper presented at the Computational Methods in Structural Dynamics and Earthquake Engineering (COMPDYN).
- Haselton, C., Liel, A., Deierlein, G. G., Dean, B. S., and Chou, J. H. (2010). Seismic collapse safety of reinforced concrete buildings. I: Assessment of ductile moment frames. *Journal of Earthquake Engineering*, 137(4), 481-491.
- Hsiao, P. C., Lehman, D. E., and Roeder, C. W. (2012). Improved analytical model for special concentrically braced frames. *Journal of Constructional Steel Research*, 73, 80-94.

- Hsiao, P. C., Lehman, D. E., and Roeder, C. W. (2013). Evaluation of the response modification coefficient and collapse potential of special concentrically braced frames. *Earthquake Engineering & Structural Dynamics*, 42(10), 1547-1564.
- Husid, L. R. (1969). Características de Terremotos, Análisis General. *Revista del IDIEM*, 8, 21-42.
- Ibarra, L. F., Medina, R. A., and Krawinkler, H. (2005). Hysteretic models that incorporate strength and stiffness deterioration. *Earthquake Engineering & Structural Dynamics*, 34(12), 1489-1511. doi: 10.1002/eqe.495
- Iervolino, I., Manfredi, G., and Cosenza, E. (2006). Ground motion duration effects on nonlinear seismic response. *Earthquake Engineering & Structural Dynamics*, 35(1), 21-38.
- INGV-DPC, C. (2004 – 2006). Progetto S1 Proseguimento della assistenza al DPC per il completamento e la gestione della mappa di pericolosità sismica prevista dall'Ordinanza PCM 3274 e progettazione di ulteriori sviluppi.
- Jalayer, F. (2003). *Direct Probabilistic Seismic Analysis: Implementing Non-linear Dynamic Assessment*. (Ph.D.), Stanford University, Stanford, CA.
- Jalayer, F., and Cornell, C. A. (2009). Alternative Nonlinear Demand Estimation Methods for Probability-Based Seismic Assessments. *Earthquake Engineering & Structural Dynamics*, 38(8), 951-972. doi: Alternative Nonlinear Demand Estimation Methods for Probability-Based Seismic Assessments
- Jayaram, N., and Baker, J. W. (2008). Statistical tests of the joint distribution of spectral acceleration values. *Bulletin of the Seismological Society of America*, 98(5), 2231-2243.
- Jayaram, N., and Baker, J. W. (2010). *Ground-motion selection for PEER Transportation Systems Research Program*. Paper presented at the 7th CUEE and 5th ICEE Joint Conference, Tokyo.
- Jayaram, N., Lin, T., and Baker, J. W. (2011). A Computationally Efficient Ground-Motion Selection Algorithm for Matching a Target Response Spectrum Mean and Variance. *Earthquake Spectra*, 27(3), 797–815.
- Kaklamanos, J., Baise, L. G., and Boore, D. M. (2011). Estimating Unknown Input Parameters when Implementing the NGA Ground-Motion Prediction Equations in Engineering Practice. *Earthquake Spectra*, 27(4), 1219–1235.
- Kazantzi, A. K., and Vamvatsikos, D. (2015). Intensity measure selection for vulnerability studies of building classes. *Earthquake Engineering and Structural Dynamics*, DOI: 10.1002/eqe.2603.
- Kohrangi, M., Bazzurro, P., and Vamvatsikos, D. (2015a). Vector and Scalar IMs in Structural Response Estimation, Part I: Hazard Analysis. *Earthquake Spectra*, 32(3), 1507-1524. doi: <http://dx.doi.org/10.1193/053115EQS080M>
- Kohrangi, M., Bazzurro, P., and Vamvatsikos, D. (2015b). Vector and Scalar IMs in Structural Response Estimation, Part II: Building Demand Assessment. *Earthquake Spectra*, 32(3), 1525-1543. doi: <http://dx.doi.org/10.1193/053115EQS081M>

- Kohrangi, M., Bazzurro, P., Vamvatsikos, D., and Spillatura, A. (2017a). Conditional spectrum-based ground motion record selection using average spectral acceleration. *Earthquake Engineering & Structural Dynamics*, 46(10), 1667-1685.
- Kohrangi, M., Vamvatsikos, D., and Bazzurro, P. (2017b). Multi-level conditional spectrum based record selection for IDA. (*Under review*).
- Kohrangi, M., Vamvatsikos, D., and Bazzurro, P. (2017c). Site dependence and record selection schemes for building fragility and regional loss assessment. . *Earthquake Engineering and Structural Dynamics*. doi: 10.1002/eqe.2873
- Kottke, A. R., and Rathje, E. M. (2008). A semi-automated procedure for selecting and scaling recorded earthquake motions for dynamic analysis. *Earthquake Spectra*, 24, 911–932.
- Krawinkler, H., Zareian, F., Medina, R. A., and Ibarra, L. F. (2006). Decision support for conceptual performance-based design. *Earthquake Engineering & Structural Dynamics*, 35(1), 115-133.
- Kumar, M., Whittaker, A., and Constantinou, M. (2015). Experimental investigation of cavitation in elastomeric seismic isolation bearings. *Engineering Structures*, 101, 290-305.
- Kutner, M. H., Nachtsheim, C. J., and Neter, J. (2004). *Applied linear regression models* (4th ed.): McGraw-Hill. .
- Liel, A., Haselton, C., and Deierlein, G. G. (2010). Seismic collapse safety of reinforced concrete buildings. II: Comparative assessment of nonductile and ductile moment frames. *Journal of Structural Engineering*, 137(4), 492-502.
- Lignos, D. G., and Krawinkler, H. (2012). Sidesway collapse of deteriorating structural systems under seismic excitations (Vol. 177). Stanford University, Stanford, CA.: The John A. Blume Earthquake Engineering Research Center,.
- Lin, T., Harmsen, S. C., Baker, J. W., and Luco, N. (2013a). Conditional spectrum computation incorporating multiple causal earthquakes and ground motion prediction models. *BSSA*, 103(2A), 1103–1116.
- Lin, T., Haselton, C., and Baker, J. W. (2013b). Conditional-Spectrum-based ground motion selection. Part II: Intensity-based assessments and evaluation of alternative target spectra. *Earthquake Engineering & Structural Dynamics*, 42(12), 1867-1884. doi: 10.1002/eqe
- Lin, T., Haselton, C. B., and Baker, J. W. (2013c). Conditional spectrum-based ground motion selection. Part I: Hazard consistency for risk-based assessments. *Earthquake Engineering & Structural Dynamics*. doi: 10.1002/eqe
- Luco, N., and Bazzurro, P. (2007). Does amplitude scaling of ground motion records result in biased nonlinear structural drift responses? *Earthquake Engineering and Structural Dynamics*, 36(13), 1813-1835. doi: 10.1002/eqe.695
- Luco, N., Ellingwood, B. R., Hamburger, R. O., Hooper, J. D., Kimballm, J. K., and Kirchner, C. A. (2007). *Risk-targeted versus current seismic design maps for the conterminous United States*. Paper presented at the SEAOC convention proceedings.

- Magenes, G., Morandi, P., and Penna, A. (2008). *Experimental in-plane cyclic response of masonry walls with clay units*. Paper presented at the 14th WCEE, Beijing, China.
- Magliulo, G., Ercolino, M., and Manfredi, G. (2015). Influence Of Cladding Panels On The First Period Of One-Story Precast Buildings. *Bulletin of Earthquake Engineering*, 13(1531-1555).
- McGuire, R. K. (1995). Probabilistic seismic hazard analysis and design earthquakes: closing the loop. . *Bulletin of Seismological Society of America*, 85(5), 1275-1284.
- McKenna, F., Fenves, G., Jeremic, B., and Scott, M. (2000). Open system for earthquake engineering simulation. <<http://opensees.berkeley.edu>> (Jan 2014).
- Meletti, C., and Montaldo, V. (2007). Stime di pericolosità sismica per diverse probabilità di superamento in 50 anni: valori di ag. Progetto DPC-INGV S1 *Deliverable D2*.
- Miranda, E., and Aslani, H. (2003). Probabilistic Response Assessment for Building-Specific Loss Estimation. In U. o. C. Berkeley (Ed.): Pacific Earthquake Engineering Research Center (PEER).
- Mitrani-Reiser, J. P. D. t. (2007). *An ounce of prediction: probabilistic loss estimation for performance-based earthquake engineering*. Pasadena, California.
- Moehle, J. P. (1992). Displacement-Based Design of RC Structures Subjected to Earthquakes. *Earthquake Spectra*, 8(3).
- Monelli, D., Pagani, M., Weatherill, G., Silva, V., and Crowley, H. (2012). *The hazard component of OpenQuake: The calculation engine of the Global Earthquake Model*. Paper presented at the 15th World Conference on Earthquake Engineering, Lisbon, Portugal.
- Montaldo, V., and Meletti, C. (2007). Valutazione del valore della ordinata spettrale a 1sec e ad altri periodi di interesse ingegneristico. Progetto DPC-INGV S1 *Deliverable D3*.
- Naeim, F., Alimoradi, A., and Pezeshk, S. (2004). Selection and scaling of ground motion time histories for structural design using genetic algorithms. *Earthquake Spectra*, 20, 413-426.
- NTC. (2008a). Circolare 2 febbraio 2009, n. 617 - Istruzioni per l'applicazione delle "Nuove norme tecniche per le costruzioni" di cui al D.M. 14 gennaio 2008.
- NTC. (2008b). Norme Tecniche per le Costruzioni, Decreto Ministeriale del 14/1/2008, Suppl. ord. n. 30 alla G.U. n. 29 del 4/2/2008.
- Panagiotakos, T. B., and Fardis, M. N. (2001). Deformations of reinforced concrete members at yielding and ultimate. *ACI Structural Journal* 98(2), 135-148.
- Penna, A., Lagomarsino, S., and Galasco, A. (2014). A nonlinear macroelement model for the seismic analysis of masonry buildings. *Earthquake Engineering & Structural Dynamics*, 43(2), 159-179.
- Raghunandan, M., and Liel, A. B. (2013). Effect of ground motion duration on earthquake-induced structural collapse. *Structural Safety*, 41, 119-133.
- Ramirez, C. M., and Miranda, E. (2009). *Building specific loss estimation methods and tools for simplified performance-based earthquake engineering*. Stanford University.

- Reed, J. W., and Kassawara, R. P. (1990). A criterion for determining exceedance of the Operating Basis Earthquake. . *Nuclear Engineering and Design*, 123, 387-396.
- RINTC-Workgroup. (2017). Results of the 2015-2016 RINTC project. Napoli, Italy: ReLUIS.
- Scozzese, F., Terracciano, G., Zona, A., Della Corte, G., Dall'Asta, A., and Landolfo, R. (2017, 15-17 June 2017). *RINTC project: Nonlinear dynamic analyses of Italian code-conforming steel single-story buildings for collapse risk assessment*. Paper presented at the COMPDYN 2017 - 6th ECCOMAS Thematic Conference on Computational Methods in Structural Dynamics and Earth-quake Engineering, Rhodes Island, Greece.
- Shantz, T. J. (2006). *Selection and scaling of earthquake records for nonlinear dynamic analysis of first model dominated bridge structures*. Paper presented at the 8th U.S. National Conference on Earthquake Engineering, San Francisco, CA.
- Shome, N., and Cornell, C. A. (1999). *Probabilistic seismic demand analysis of nonlinear structures*. (PhD), Stanford, California. (RMS-35)
- Silva, V., Crowley, H., and Bazzurro, P. (2016). Exploring Risk-Targeted Hazard Maps for Europe. *Earthquake Spectra*, 32(2), 1165-1186.
- Spacone, E., Filipou, F. C., and Taucer, F. F. (1996a). Fibre beam-column model for non-linear analysis of RC frames: Part I. Formulation. . *Earthquake Engineering and Structural Dynamics*, 25, 711-725.
- Spacone, E., Filipou, F. C., and Taucer, F. F. (1996b). Fibre beam-column model for non-linear analysis of RC frames: Part II. Applications. *Earthquake Engineering and Structural Dynamics*, 25, 727-742.
- Spallarossa, D., and Barani, S. (2007). Disaggregazione della pericolosità sismica in termini di M-R-e. Progetto DPC-INGV S1 *Deliverable D14*.
- Stewart, J. P., Chiou, S. J., Bray, J. D., Graves, R. W., Somerville, P. G., and Abrahamson, N. A. (2001). Ground motion evaluation procedures for performance-based design. In P. E. E. R. Centre (Ed.): University of California, Berkeley.
- Stucchi, M., Meletti, C., Montaldo, V., Crowley, H., Calvi, G. M., and Boschi, E. (2011). Seismic hazard assessment (2003–2009) for the Italian building code. . *Bulletin of Seismological Society of America*, 101, 1885-1911.
- Tarbali, K., and Bradley, B. A. (2016). The effect of causal parameter bounds in PSHA-based ground motion selection. *Earthquake Engineering and Structural Dynamics*, 45(9), 1515-1535
- Trifunac, M. D., and Brady, A. G. (1975). A study on the duration of strong earthquake ground motion. . *Bulletin of the Seismological Society of America*, 65(3), 581-626.
- USGS. (2008). US geological Survey, interactive disaggregation web tool. from <http://geohazards.usgs.gov/deaggint/2008/>
- USGS. (2012). US Geological Survey, Hazard web tool. from <http://geohazards.usgs.gov/hazardtool/application.php>

- Vamvatsikos, D., and Aschheim, M. A. (2016). Performance-based seismic design via Yield Frequency Spectra. *Earthquake Engineering and Structural Dynamics*, 45(11), 1759-1778.
- Vamvatsikos, D., Castiglioni, C., Bakalis, K., Calado, L., D' Aniello, M., Degee, H., . . . Vayas, I. (2017). *A risk-consistent approach to determine behavior factors for innovative steel lateral load resisting systems*. Paper presented at the EUROSTEEL 2017, Copenhagen, Denmark.
- Vamvatsikos, D., and Cornell, C. A. (2002). Incremental dynamic analysis. *Earthquake Engng. Struct. Dyn.*, 31(3), 491–514.
- Vamvatsikos, D., and Cornell, C. A. (2006). Direct estimation of the seismic demand and capacity of oscillators with multi-linear static pushovers through Incremental Dynamic Analysis. *Earthquake Engineering & Structural Dynamics*, 35(9), 1097-1117.
- Vamvatsikos, D., Kazantzi, A. K., and Aschheim, M. A. (2016). Performance-based seismic design: Avant-garde and code-compatible approaches. *ASCE-ASME Journal of Risk and Uncertainty in Engineering Systems, Part A: Civil Engineering*, 2(2).
- Wang, G. (2011). A ground motion selection and modification method capturing response spectrum characteristics and variability of scenario earthquakes. *Soil Dynamics and Earthquake Engineering*, 31(4), 611-625.
- Watson-Lamprey, J. A., and Abrahamson, N. A. (2006). Selection of ground motion time series and limits on scaling. *Soil Dynamics and Earthquake Engineering*, 26, 477-482.
- Youngs, R. R., Chiou, B. S. J., Silva, W. J., and Humphrey, J. R. (1997). Strong Ground Motion Attenuation Relationships for Subduction Zone Earthquakes. *Seismological Research Letters*, 68(1), 58-73.
- Youngs, R. R., Power, M. S., Wang, G., Makdisi, F. I., and Chin, C. C. (2007). *Design ground motion library (DGML) - Tool for selecting time history records for specific engineering applications*. Paper presented at the SMIP Seminar on Utilization of Strong-Motion Data.
- Zhao, J. X., Jian Zhang, Akihiro Asano, Yuki Ohno, Taishi Oouchi, Toshimasa Takahashi, . . . Fukushima, Y. (2006). Attenuation Relations of Strong Ground Motion in Japan Using Site Classification Based on Predominant Period. *Bulletin of the Seismological Society of America*, 96(3), 898-913.
- Žižmond, J., and Dolšek, M. (2016). Evaluation of factors influencing the earthquake-resistant design of reinforced concrete frames according to Eurocode 8. *Structure and Infrastructure Engineering*, 12(10), 1323-1341.



# Appendix A. Additional details on CS-MR method

## A.1 Added Subduction Records

The following table summarizes the main characteristics of the subduction records added to the NGAw2 database including location, date, Magnitude and number of records per event. The records were downloaded from Strong motion Virtual Data Center (VDC, <http://strongmotioncenter.org/vdc/scripts/default.plx>) and from the National Research Institute for Earth Science and Disaster Resilience (NIED) strong motion seismograph network (<http://www.kyoshin.bosai.go.jp/>).

**Table A.1** Ground motion recordings from subduction events added to the NGA-w2 crustal database

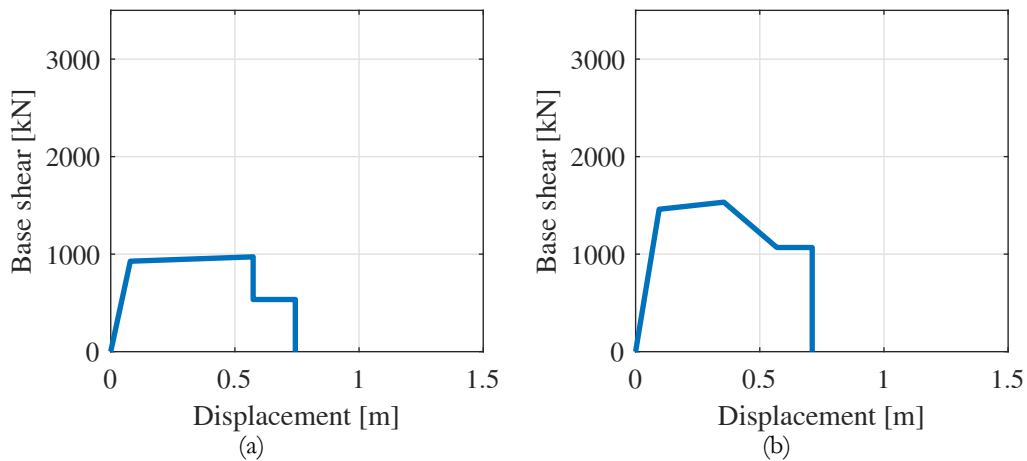
Event ID	Event Name	# Records per Event	Magnitude	Date
21540	Indonesia	1	7.8	12 September 2007
21541	Sumatra	1	8.4	12 September 2007
From 21542 to 21550	Illapel-Chile	8	8.3	16 September 2015
21551	Nepal	1	7.8	25 April 2015
21552	Samoa	1	8.1	29 September 2009
From 21553 to 21554	Iquique Chile	2	8.2	1 April 2014
From 21555 to 22356	Tohoku Mainshock	801	9	11 March 2011
From 21357 to 22732	Tohoku Off Coast	1357	7.5	11 March 2011
From 21733 to 23099	Tohoku Near Coast	1366	7.7	11 March 2011
From 23100 to 23381	Tokachi	281	8.3	26 September 2003
From 23382 to 23470	Kuril Island	88	8.2	13 January 2007
From 23471 to 23491	Okhotsk Sea	20	8.4	24 May 2013
From 23492 to 23671	Chi Chi Shima	179	8.1	30 May 2015

## A.2 Sdof tests to check CS-MR dependencies

This section shows the results of a series of analyses conducted on Single degree of Freedom (SDoF) systems with the aim of defining the main characteristics of the lumped plasticity model to be implemented in the MDoF system (analyzed in the core of the thesis). In particular, SDoF systems are thought to represent modern reinforced concrete (RC) frames with fundamental periods of 0.5, 1.6 and 2.5 seconds. These systems are modelled with a zero-length element in two different configurations:

- Modelling approach 1: Elasto-Plastic with hardening (*EPH*) without strength and stiffness degradation
- Modelling approach 2: Strength and Stiffness degradation including Pinching (*Pinch*) according to the model of Ibarra et al. [2005].

The backbones that characterize the SDoFs are obtained from the approximation of a series of MDoF systems (<https://www.csuchico.edu/structural/index.shtml>). The choice of performing this testing phase with simplified SDoF models is mainly due to the easiness of implementation and to the lower computational weight required. The following Figure A.1 and Table A.2 show the assumed backbone curves and some details of the structures.



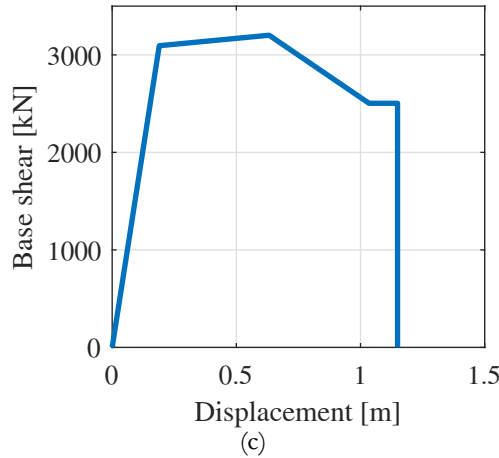


Figure A.1 Pushover approximation for 0.5 (a), 1.6(b), 2.5(c) seconds structures

Table A.2 Details about MDoF systems taken as reference

Structure ID	1001a	1011	1020
# of stories	2	8	20
Period [s]	0.56	1.71	2.63

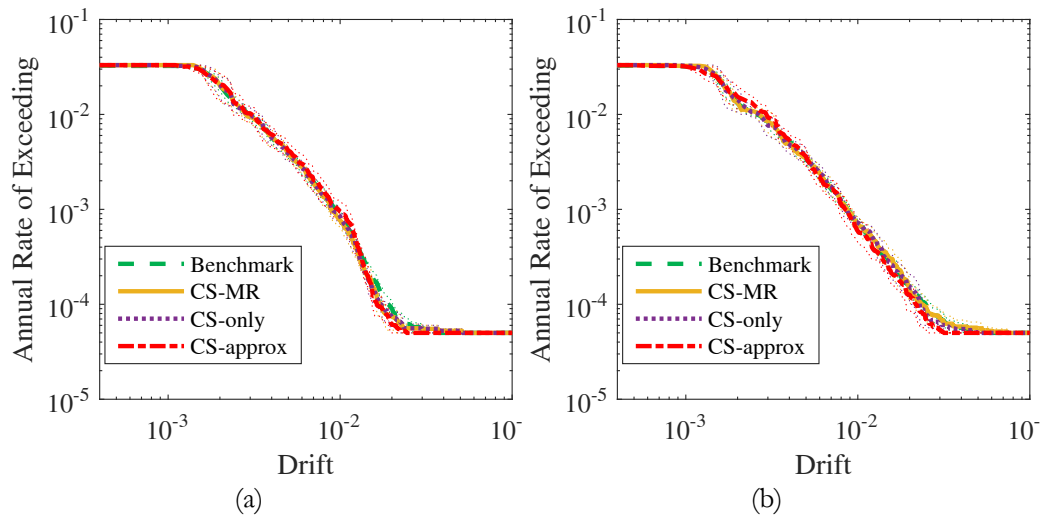
The SDoF systems were tested against four record sets selected according to different methods. Since

- CS approx: the target distribution is computed considering the median scenario of disaggregation and the most contributing GMPE; the selection is performed among the entire record database without restrictions.
- CS exact (CS only): the target distribution is computed considering the whole Magnitude-Distance disaggregation of the seismic hazard and all GMPEs with their relative weights. The selection is performed as in the previous approach.
- CS with causal parameters (CS-MR): the target distribution is defined as in CS exact but in the second stage the selection is performed forcing the records to be loyal to M-R disaggregation.
- Benchmark: a set of 20 records is selected for each of the most contributing scenarios of the disaggregation of the hazard at the IM level of interest. For each of the M-R bin, a CS record selection is performed defining a higher order problem with respect to the other cases. Indeed, the structure will be subjected to a higher amount of records increasing the reliability and robustness of the response prediction.

**Table A.3** Number of records selected according to the considered selection criteria

Selection Criteria	(#records per IML)
Classical Conditional Spectrum (CS-exact) / (CS-only)	☑ (20)
Classical Conditional Spectrum (CS-approx)	☑ (20)
Conditional Spectrum including Causal Parameters(CS-MR);	☑ (20)
Benchmark (CS-based)	☑ (20 per each bin)

The idea, here, is to test the effectiveness of the proposed procedure (CS-MR) with respect to with the Benchmark case, assumed to be the nearest approach to the “truth” but not suitable to be used in current practice (mainly because of the computational effort needed to perform it). Figure A.2 and Figure A.3 show the drift hazard curves related to different combinations of SDoFs models and periods subjected to the four record sets described earlier. The collapse rate is defined in correspondence of the horizontal plateau on the right of the figure. Since the analyses were carried out in a Multiple Stripe Analysis (MSA) fashion, it has been hypothesized certain collapse for ground motion intensities higher than the last IM level considered. In line with this, after the last IML the collapse rate is coincident with the hazard and, therefore, a factor of  $5e-5$  has been added to the collapse rate coming from the MSA. Table A.4 and Figure A.4 give the differences in percentage of the analyzed cases with respect to the Benchmark one.



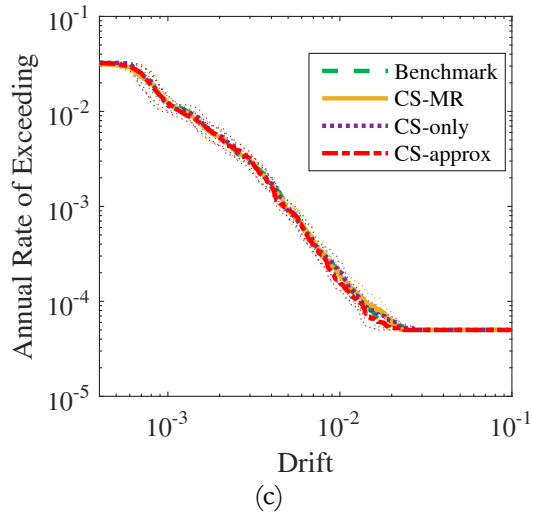
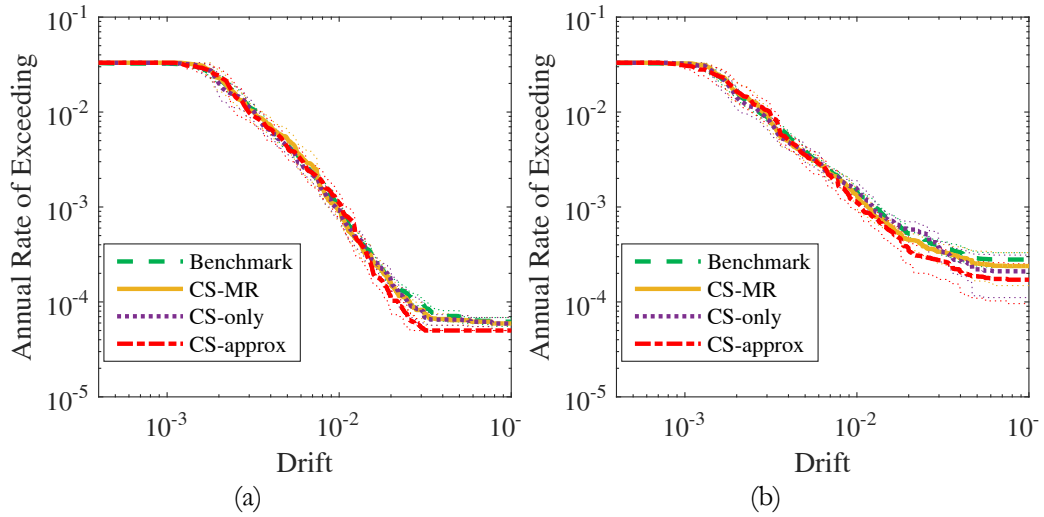


Figure A.2 Drift Hazard curves for SDoF characterized by  $T=0.5$  s (a),  $T=1.6$  s (c),  $T=2.5$  s (e) for modelling approach 1 (EPH).



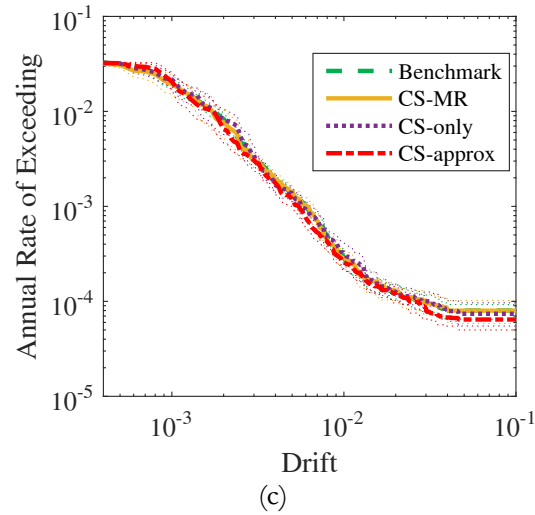


Figure A.3 Drift Hazard curves for SDoF characterized by  $T=0.5$  s (a),  $T=1.0$  s (b),  $T=1.6$  s (c),  $T=2.0$  s (d),  $T=2.5$  s (e) for modelling approach 2 (Stiffness and Strength degradation with Pinching).

Table A.4 Collapse rates differentiated by Period, Structural type and Record Selection procedure

T=0.5 s	EPH		Pinch	
	<i>Collapse rate</i>	<i> %  diff respect to BM</i>	<i>Collapse rate</i>	<i> %  diff respect to BM</i>
Benchmark	5.00E-05	0.00%	6.19E-05	0.00%
CS M-R dependent	5.00E-05	0.01%	5.93E-05	4.13%
CS exact	5.00E-05	0.01%	5.92E-05	4.38%
CS Approx	5.00E-05	0.01%	5.00E-05	19.18%
T=1.6 s	EPH		Pinch	
	<i>Collapse rate</i>	<i> %  diff respect to BM</i>	<i>Collapse rate</i>	<i> %  diff respect to BM</i>
Benchmark	5.00E-05	0.00%	2.78E-04	0.00%
CS M-R dependent	5.00E-05	0.02%	2.38E-04	14.62%
CS exact	5.00E-05	0.03%	2.09E-04	25.03%
CS Approx	5.00E-05	0.03%	1.70E-04	38.66%
T=2.5 s	EPH		Pinch	
	<i>Collapse rate</i>	<i> %  diff respect to BM</i>	<i>Collapse rate</i>	<i> %  diff respect to BM</i>
Benchmark	5.00E-05	0.00%	7.98E-05	0.00%
CS M-R dependent	5.00E-05	0.00%	7.96E-05	0.23%
CS exact	5.00E-05	0.00%	7.39E-05	7.50%
CS Approx	5.00E-05	0.00%	6.43E-05	19.44%

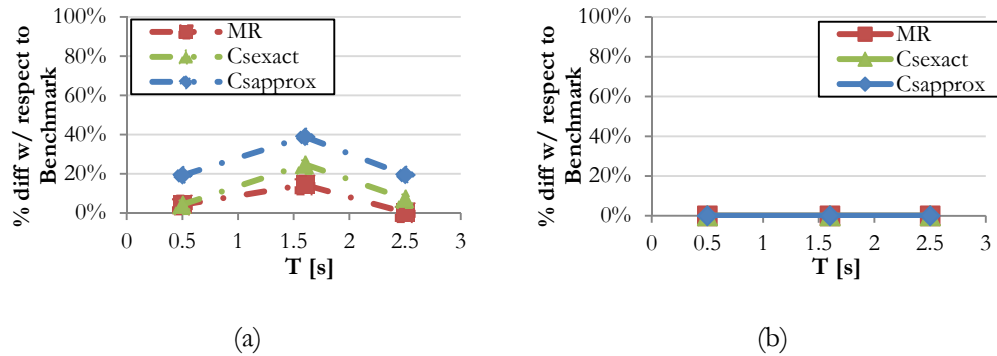


Figure A.4 Charts representing collapse rates varying periods and selection approach for the two SDoF model analyzed, namely Pinch (a), EPH (b).

Analyzing this first set of outputs, the following considerations can be raised:

- A simple EPH modelling is not able to properly capture the influence of record selection approaches; indeed varying the period the collapse rate is the same for all the four record sets.
- The highest differences can be found for the cases with intermediate periods, while for the upper and lower ones the influence of selection approach seems to be less important.
- Among the cases that show higher differences the proposed selection approach is always the one that best approximate the Benchmark case with percentages always around 10%.
- The low differences for higher period cases can be due to the not suitable SDoF approximation for this kind of structures that are known to be influenced by higher-modes.

These first series of analyses were very fruitful to choose the characteristics of a reference MDoF system to be tested; in particular we focused on a 1.6 s period structure characterized by lumped plasticity model which includes strength and stiffness in cycle degradation. About the record selection procedure, the CS-MR method was shown to be satisfactory near to the Benchmark case, ensuring a significantly lower degree of computational effort. Therefore, it is worth testing our CS-MR approach against the more advanced GCIM method that explicitly accounts for both spectral shape and duration.

### **A.3 DURATION DISTRIBUTIONS, SPECTRA AND M-R CHARACTERISTICS OF SELECTED RECORD SETS**

This section summarizes the characteristics of the record sets used to analyze the MDoF system (i.e. CS-MR, GCIM, CS-only and CS-approx thoroughly described in the core of the thesis) in terms of:

1. Duration distribution
2. Spectral shape
3. M-R characteristics

The CS-approx set is shown to have, as expected, not negligible differences in terms of both spectral shape and duration distribution with respect to the other cases; these discrepancies are the cause of the 30% difference in collapse rate predicted by means the GCIM set. Spectral shape is confirmed to be the most influencing parameter for collapse prediction: the GCIM, CS-only and CS-MR sets have fairly similar spectral acceleration distributions and the collapse rate differences are not that remarkable if GCIM is taken as reference. The CS-MR method selects longer records (more demanding if the spectral shape is similar) that cause, consequently, more frequent collapse rates. Since the GMPE adopted in the GCIM method is not exact because not tailored for high magnitude events, the CS-MR approach can be considered, at least in these conditions, as the most reliable since it captures the most important parameters that affect the structural response through M-R, without the need of an attenuation relationship.

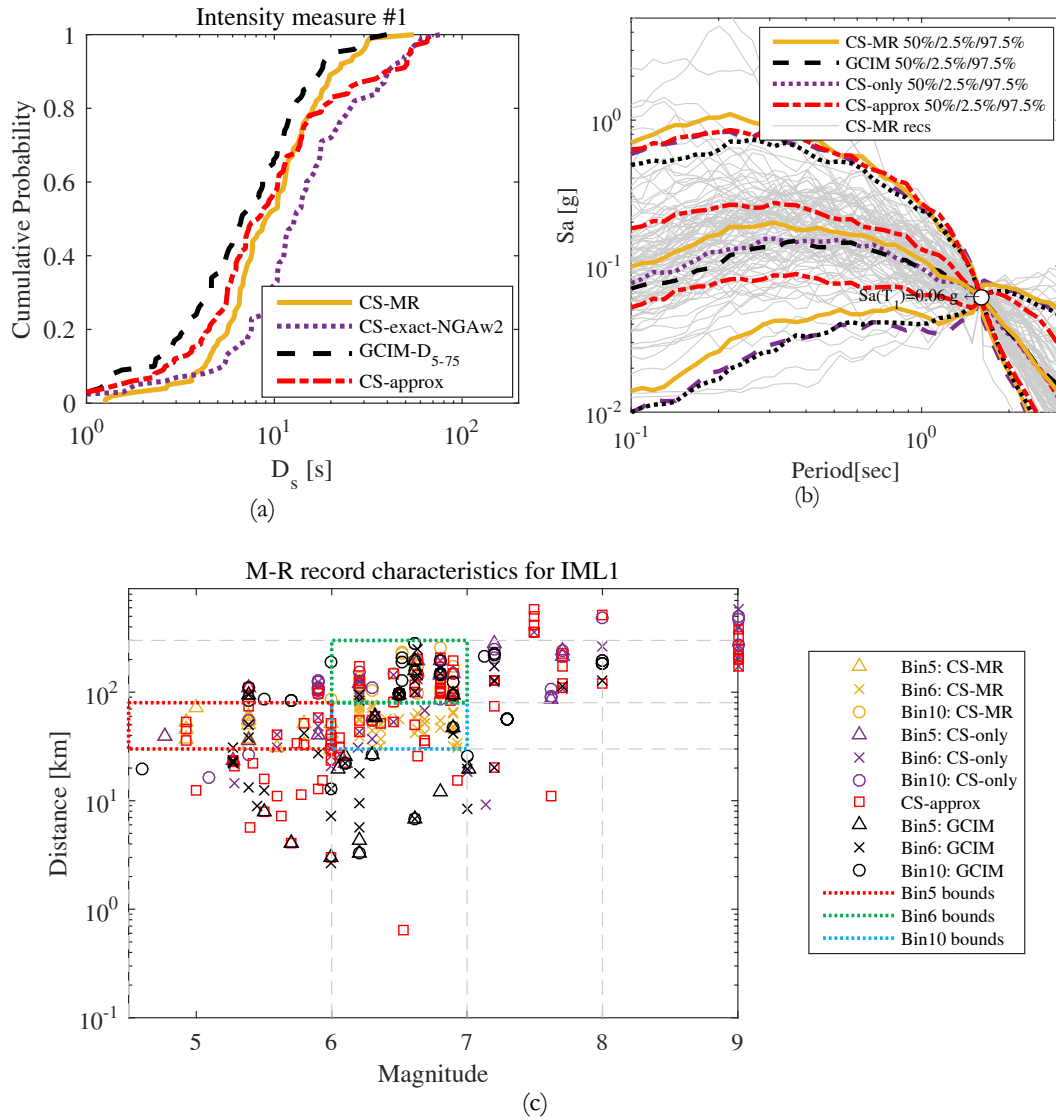


Figure A.5 Comparison of the  $D_{S_{5-75}}$  and  $S_a$  conditional distributions for all the 100 records selected by the GCIM, CS only, CS approx., and CS-MR approaches for the 56% in 50 years IM level for a site in Seattle. (a)  $D_{S_{5-75}}$  distribution of the selected records and the target obtained from GCIM; (b) 2.5/50/97.5-th percentiles of the empirically-derived conditional distribution of spectral acceleration of the records selected by the four approaches; (c) Scatter plot of the magnitude and distance pairs of the records selected by the four approaches.

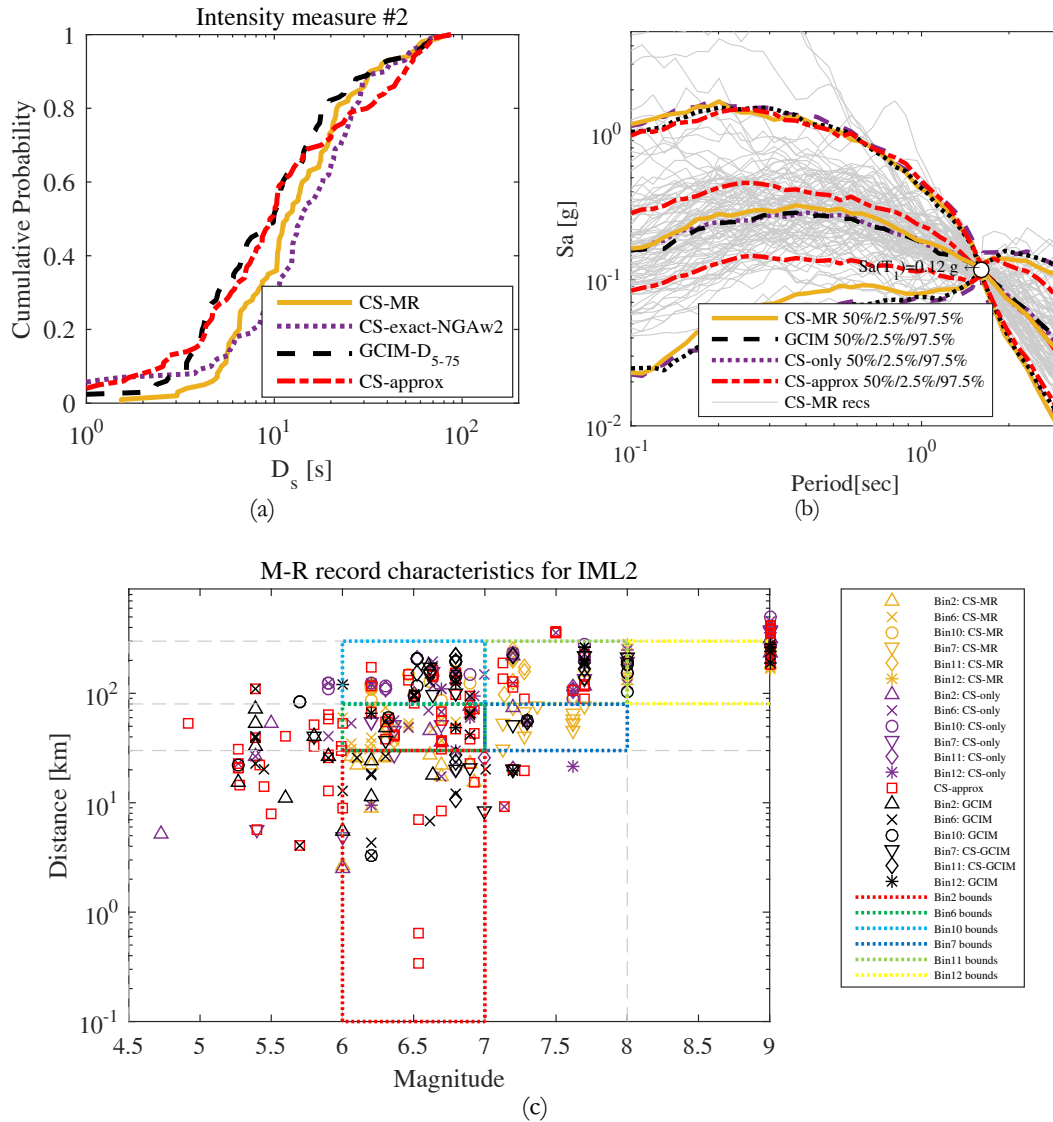


Figure A.6 Comparison of the  $D_{5-75}$  and  $S_a$  conditional distributions for all the 100 records selected by the GCIM, CS only, CS approx, and CS-MR approaches for the 29% in 50 years IM level for a site in Seattle. (a)  $D_{5-75}$  distribution of the selected records and the target obtained from GCIM; (b) 2.5/50/97.5-th percentiles of the empirically-derived conditional distribution of spectral acceleration of the records selected by the four approaches; (c) Scatter plot of the magnitude and distance pairs of the records selected by the four approaches.

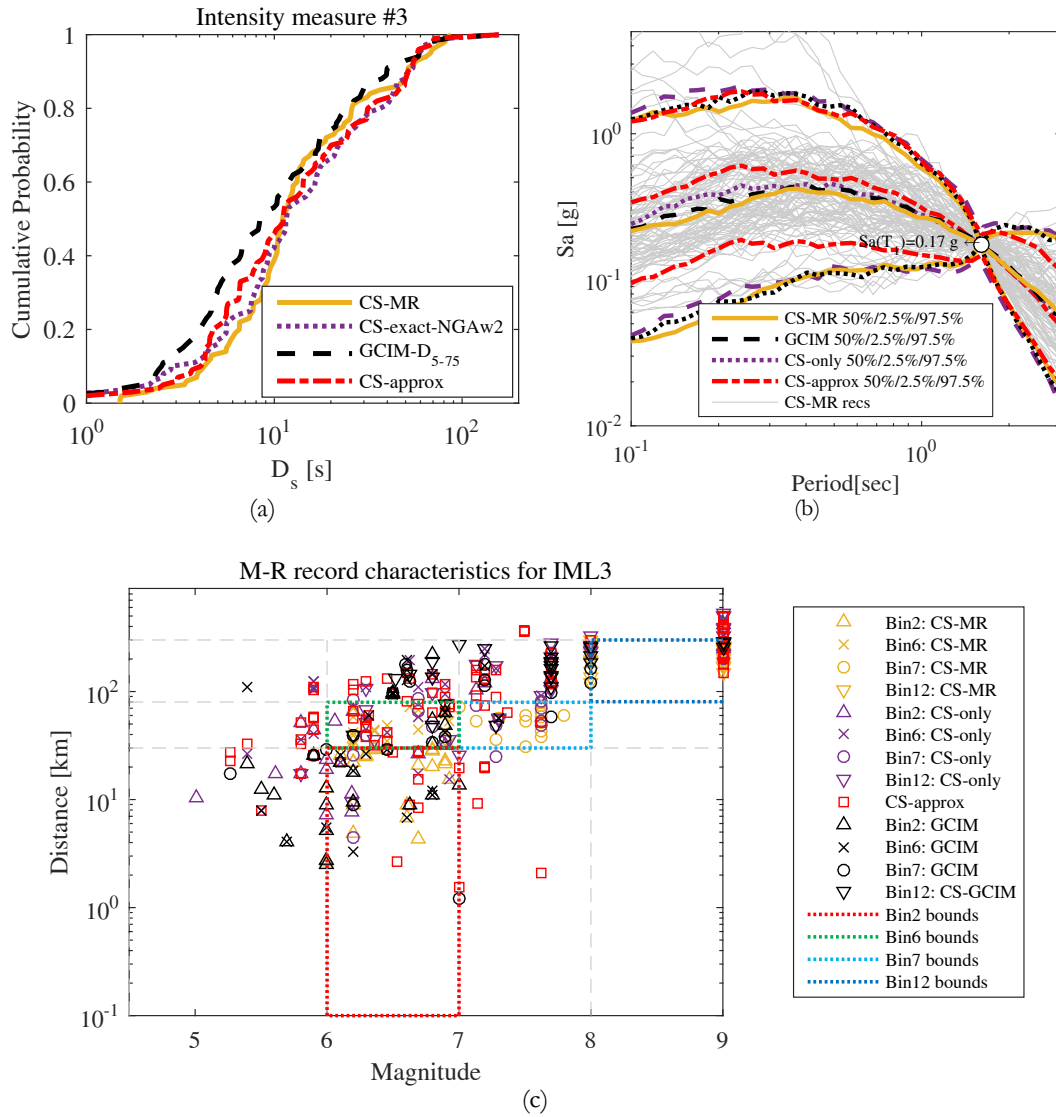


Figure A.7 Comparison of the  $D_{s-75}$  and  $S_a$  conditional distributions for all the 100 records selected by the GCIM, CS only, CS approx, and CS-MR approaches for the 17% in 50 years IM level for a site in Seattle. (a)  $D_{s-75}$  distribution of the selected records and the target obtained from GCIM; (b) 2.5/50/97.5-th percentiles of the empirically-derived conditional distribution of spectral acceleration of the records selected by the four approaches; (c) Scatter plot of the magnitude and distance pairs of the records selected by the four approaches.

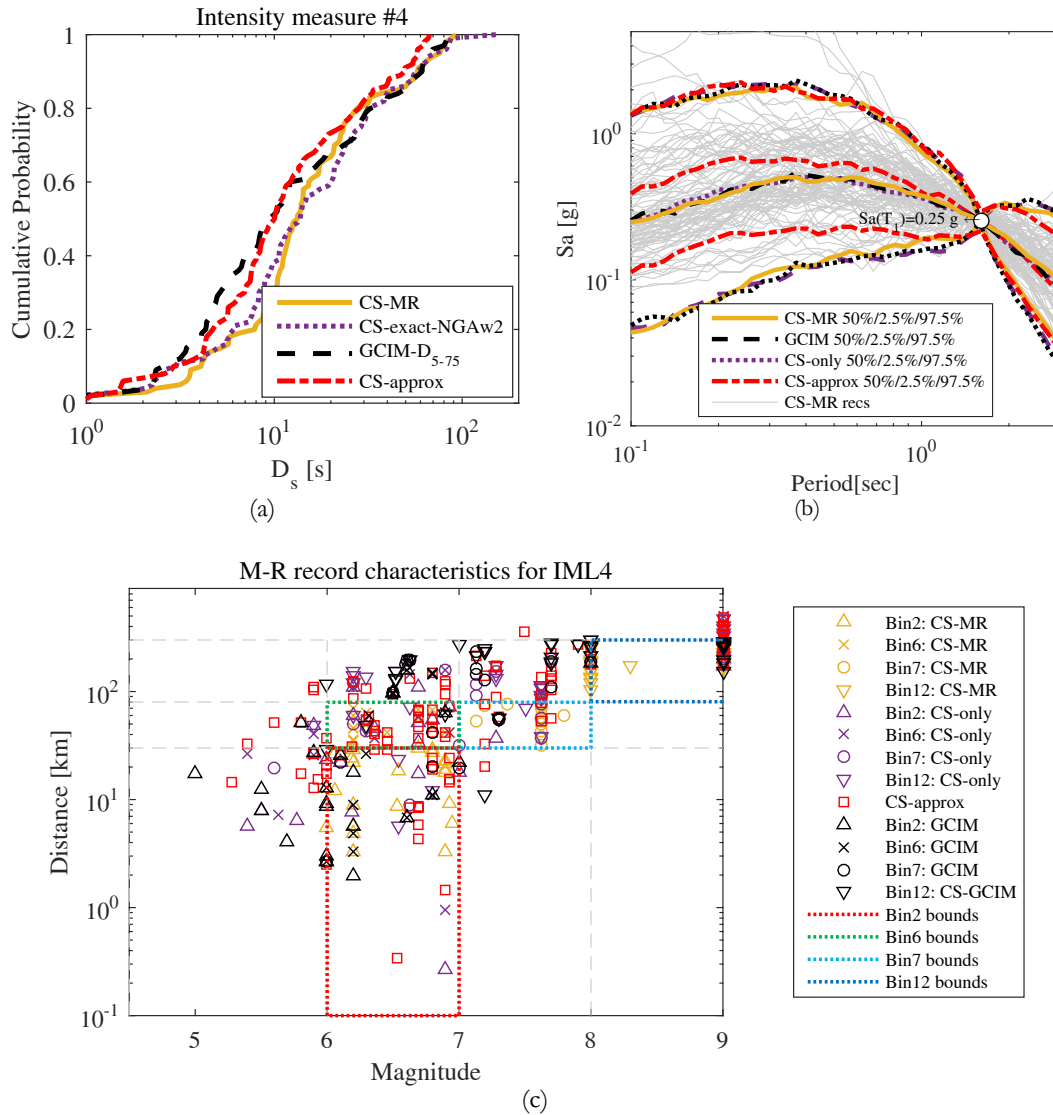


Figure A.8 Comparison of the  $D_{5-75}$  and  $S_a$  conditional distributions for all the 100 records selected by the GCIM, CS only, CS approx., and CS-MR approaches for the 9% in 50 years IM level for a site in Seattle. (a)  $D_{5-75}$  distribution of the selected records and the target obtained from GCIM; (b) 2.5/50/97.5-th percentiles of the empirically-derived conditional distribution of spectral acceleration of the records selected by the four approaches; (c) Scatter plot of the magnitude and distance pairs of the records selected by the four approaches.

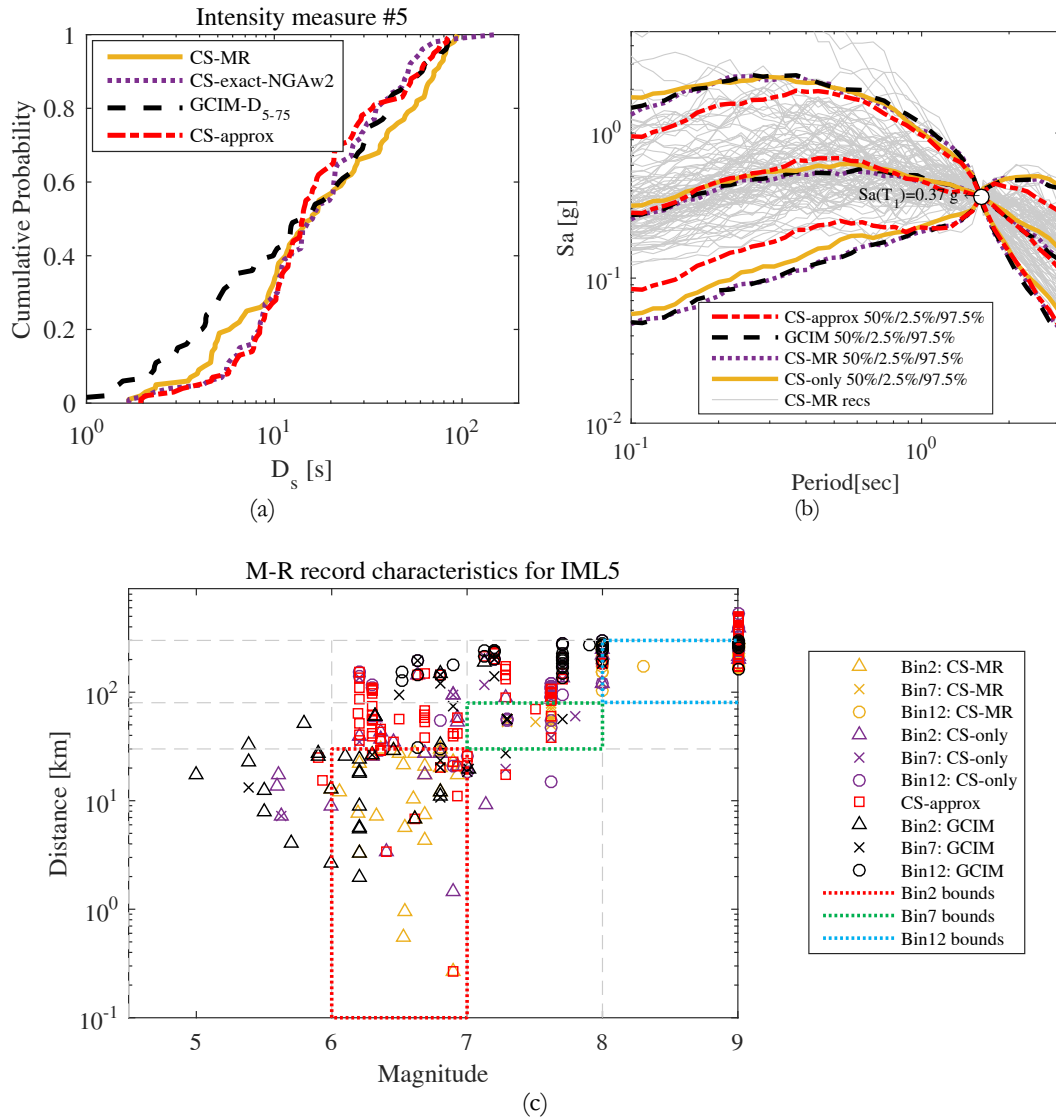


Figure A.9 Comparison of the  $D_{S_{5-75}}$  and  $S_a$  conditional distributions for all the 100 records selected by the GCIM, CS only, CS approx. and CS-MR approaches for the 5% in 50 years IM level for a site in Seattle. (a)  $D_{S_{5-75}}$  distribution of the selected records and the target obtained from GCIM; (b) 2.5/50/97.5-th percentiles of the empirically-derived conditional distribution of spectral acceleration of the records selected by the four approaches; (c) Scatter plot of the magnitude and distance pairs of the records selected by the four approaches.

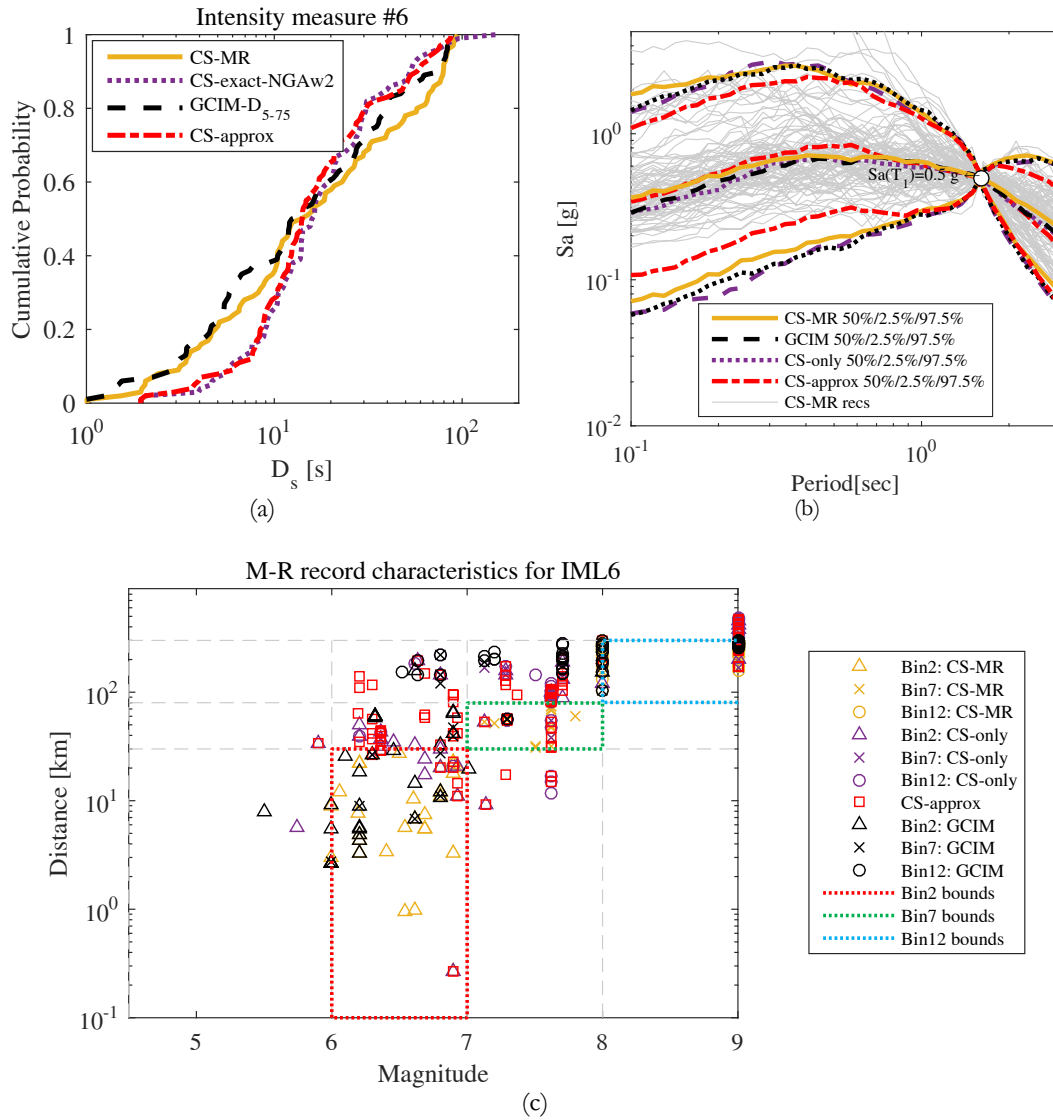


Figure A.10 Comparison of the  $D_{S_{5-75}}$  and  $S_a$  conditional distributions for all the 100 records selected by the GCIM, CS only, CS approx. and CS-MR approaches for the 2% in 50 years IM level for a site in Seattle. (a)  $D_{S_{5-75}}$  distribution of the selected records and the target obtained from GCIM; (b) 2.5/50/97.5-th percentiles of the empirically-derived conditional distribution of spectral acceleration of the records selected by the four approaches; (c) Scatter plot of the magnitude and distance pairs of the records selected by the four approaches.

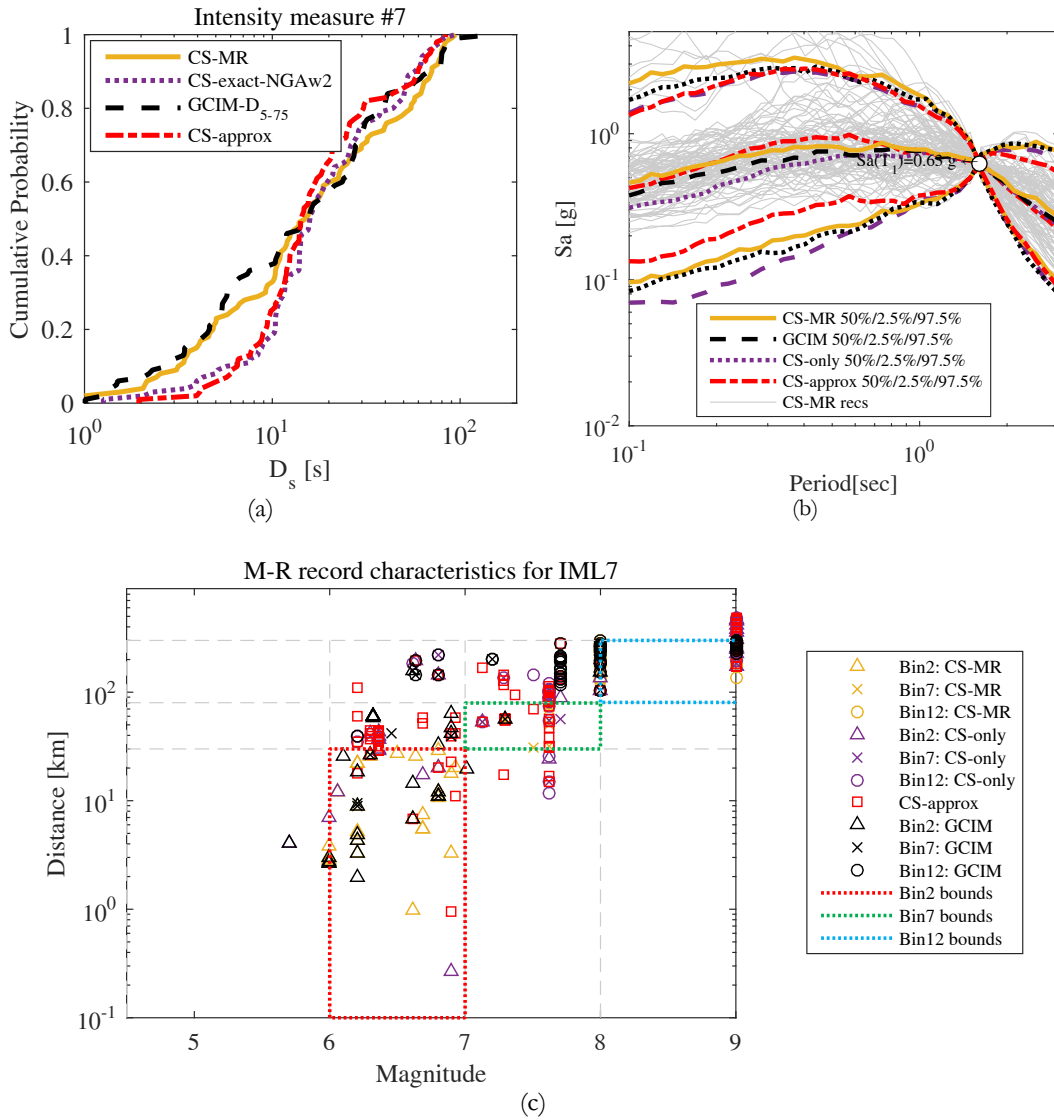


Figure A.11 Comparison of the  $D_{S_{5-75}}$  and  $S_a$  conditional distributions for all the 100 records selected by the GCIM, CS only, CS approx. and CS-MR approaches for the 1% in 50 years IM level for a site in Seattle. (a)  $D_{S_{5-75}}$  distribution of the selected records and the target obtained from GCIM; (b) 2.5/50/97.5-th percentiles of the empirically-derived conditional distribution of spectral acceleration of the records selected by the four approaches; (c) Scatter plot of the magnitude and distance pairs of the records selected by the four approaches.

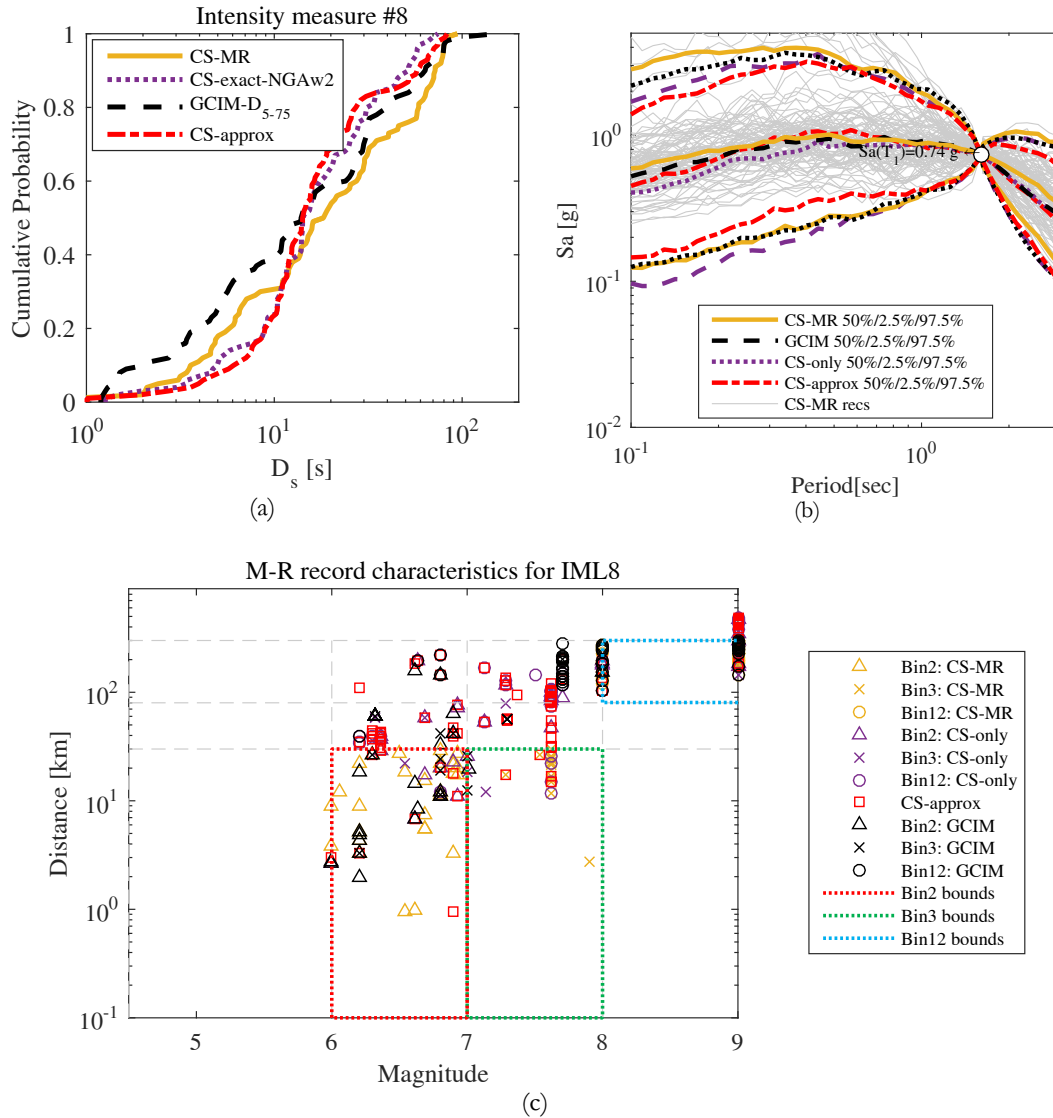


Figure A.12 Comparison of the  $D_{s-75}$  and  $S_a$  conditional distributions for all the 100 records selected by the GCIM, CS only, CS approx. and CS-MR approaches for the 0.8% in 50 years IM level for a site in Seattle. (a)  $D_{s-75}$  distribution of the selected records and the target obtained from GCIM; (b) 2.5/50/97.5-th percentiles of the empirically-derived conditional distribution of spectral acceleration of the records selected by the four approaches; (c) Scatter plot of the magnitude and distance pairs of the records selected by the four approaches.

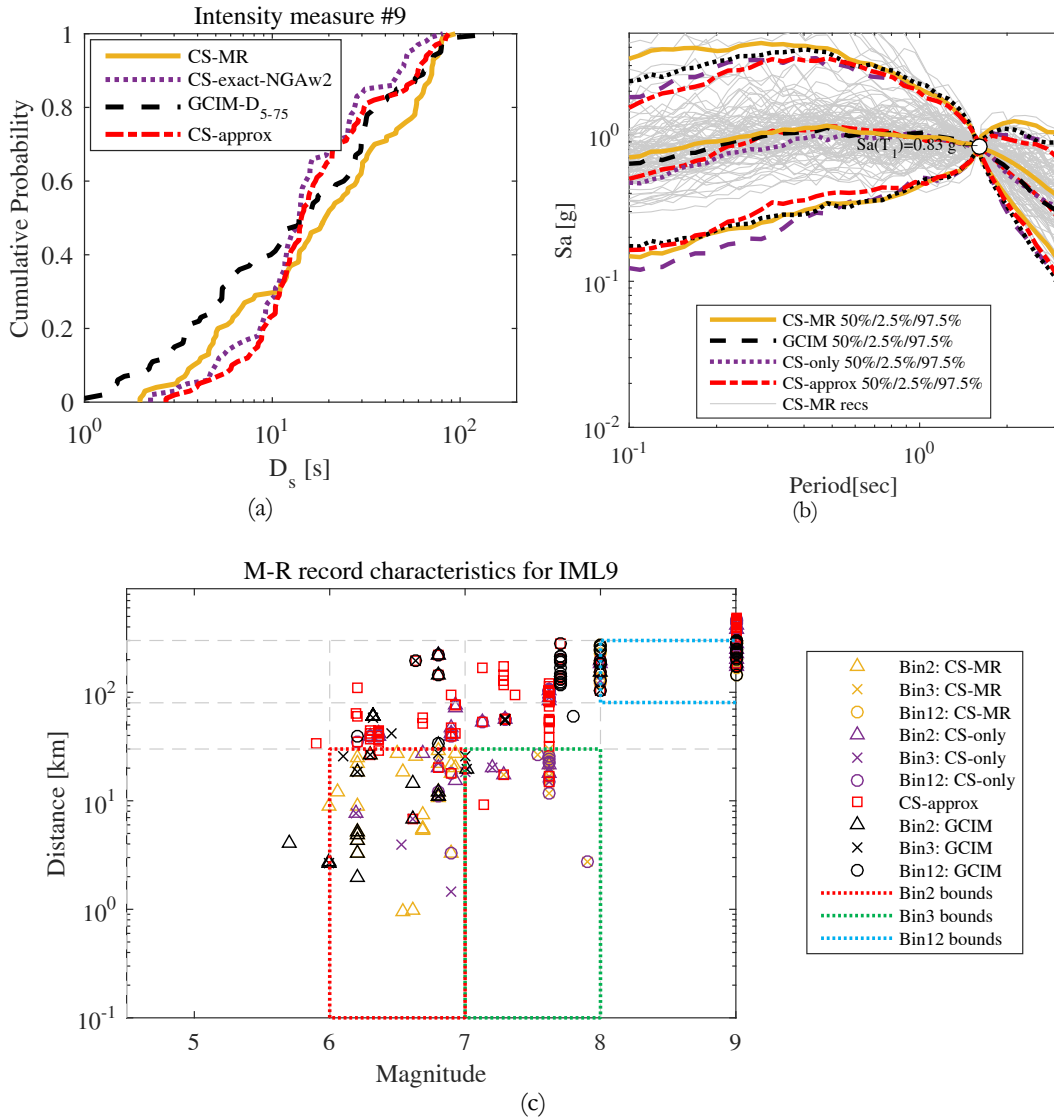


Figure A.13 Comparison of the  $D_{s_{5-75}}$  and  $S_a$  conditional distributions for all the 100 records selected by the GCIM, CS only, CS approx, and CS-MR approaches for the 0.6% in 50 years IM level for a site in Seattle. (a)  $D_{s_{5-75}}$  distribution of the selected records and the target obtained from GCIM; (b) 2.5/50/97.5-th percentiles of the empirically-derived conditional distribution of spectral acceleration of the records selected by the four approaches; (c) Scatter plot of the magnitude and distance pairs of the records selected by the four approaches.

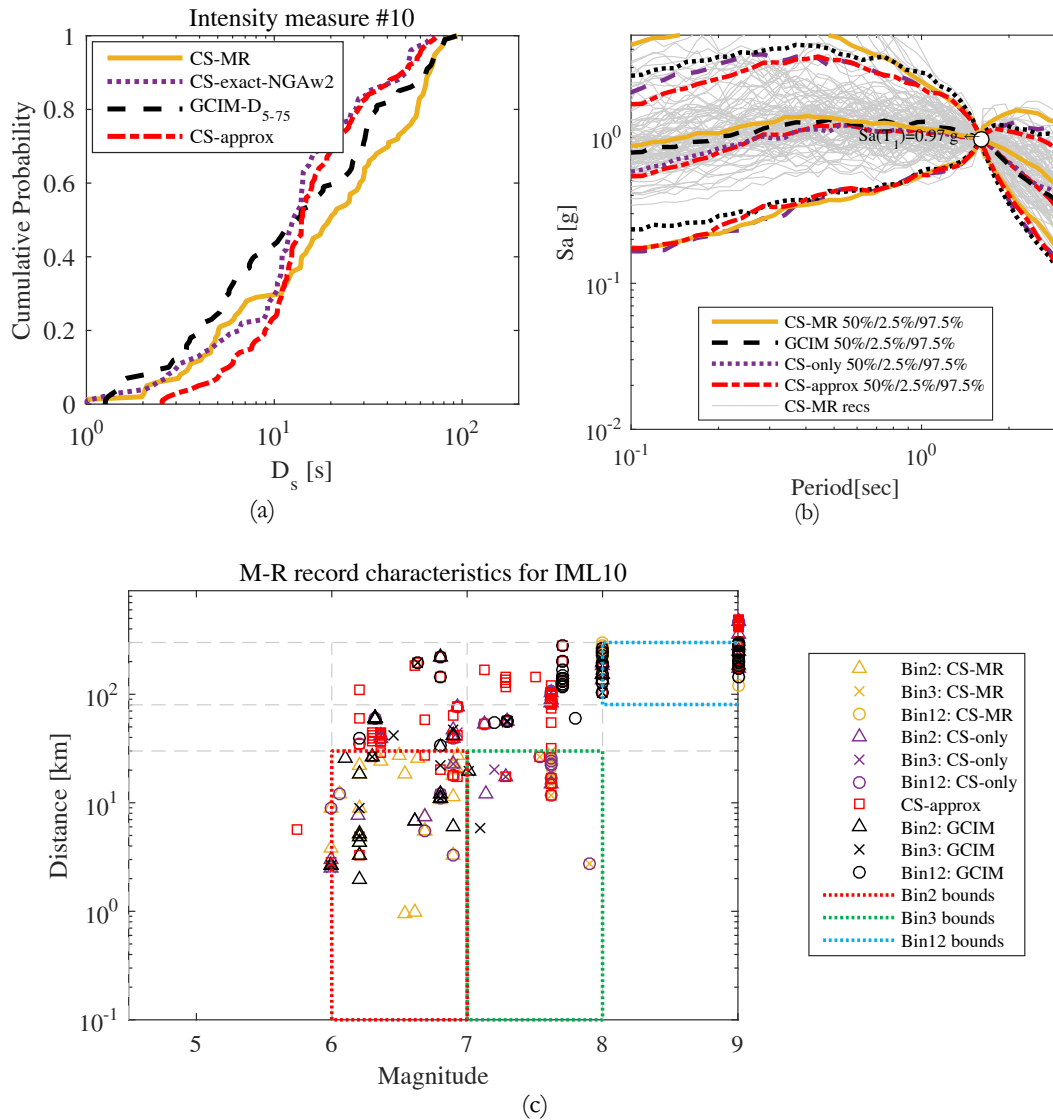
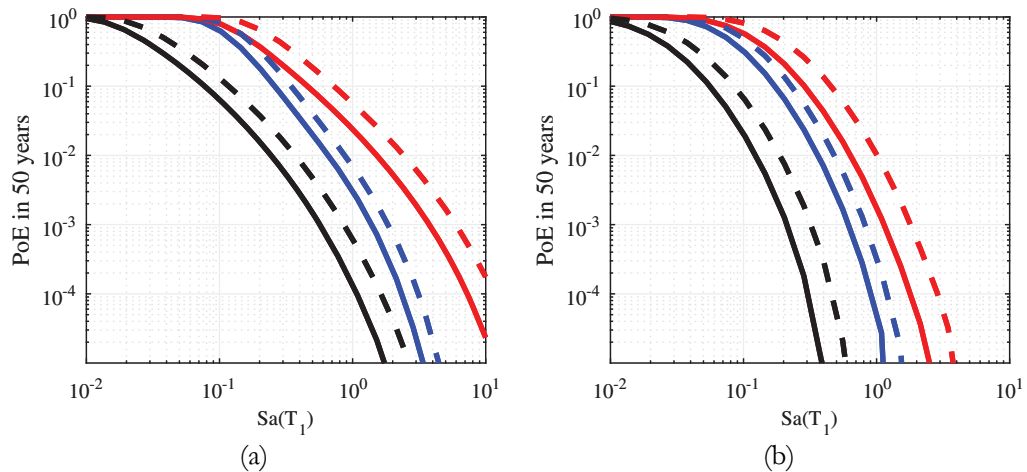


Figure A.14 Comparison of the  $D_{s_{5-75}}$  and  $S_a$  conditional distributions for all the 100 records selected by the GCIM, CS only, CS approx. and CS-MR approaches for the 0.4% in 50 years IM level for a site in Seattle. (a)  $D_{s_{5-75}}$  distribution of the selected records and the target obtained from GCIM; (b) 2.5/50/97.5-th percentiles of the empirically-derived conditional distribution of spectral acceleration of the records selected by the four approaches; (c) Scatter plot of the magnitude and distance pairs of the records selected by the four approaches.

## Appendix B. Hazard Analysis and Record Selection details for Implicit Risk Project

### B.1 Hazard Curves

The following charts of Figure B.1 are related to the hazard curves computed for PGA and spectral accelerations at  $T=0.5$  and 2 seconds, two soil categories (A and C) and five sites with increasing level of hazard, namely Milano, Caltanissetta, Roma, Napoli and L'Aquila. The calculations are based on PSHA evaluated by means of Openquake (Monelli et al. [2012]) platform implementing the INGV source model INGV-DPC [2004 – 2006].



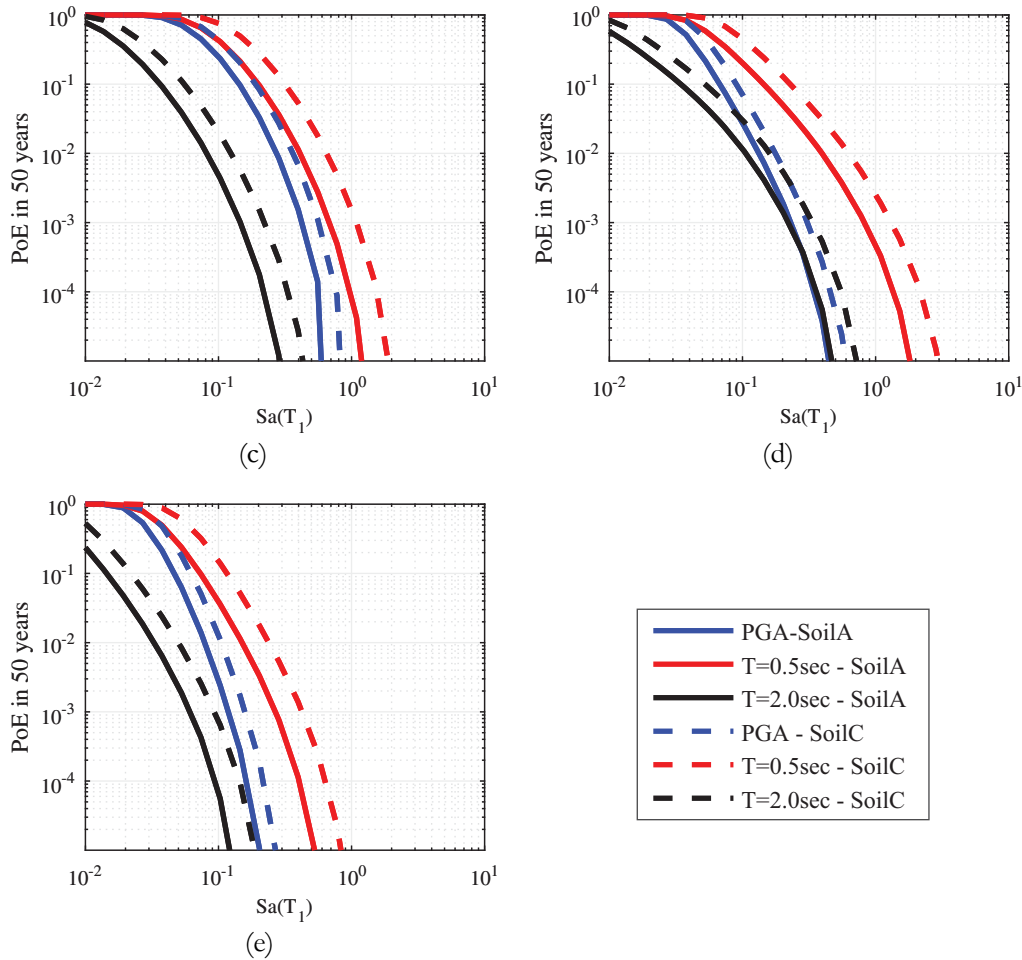


Figure B.1 Hazard curves for PGA, and  $Sa$ 's at  $T=0.5s$  and  $T=2$  computed for Soil Type A conditions for L'Aquila (a), Napoli (b), Roma (c), Caltanissetta (d) e Milano (e).

## B.2 Record Selection Sets

This paragraph contains the spectra of the selected record sets for some specific cases among those considered in this work. In particular, out of the total ten IMLs, two soil types and five conditioning periods the following figures will show the spectra on soil C of the records selected at the 5<sup>th</sup> IML that is close to the typical design level hazard (i.e. 10% in 50 years). The spectra are related to both horizontal directions and the charts include also the percentiles curves of the selected set. It should be highlighted that, as the

charts are showing, the records are selected on the basis of the maximum component among the horizontals; this is in line with the GMPE of Ambraseys et al. [1996] that is the reference of the hazard model and, therefore, of the record selection procedure.

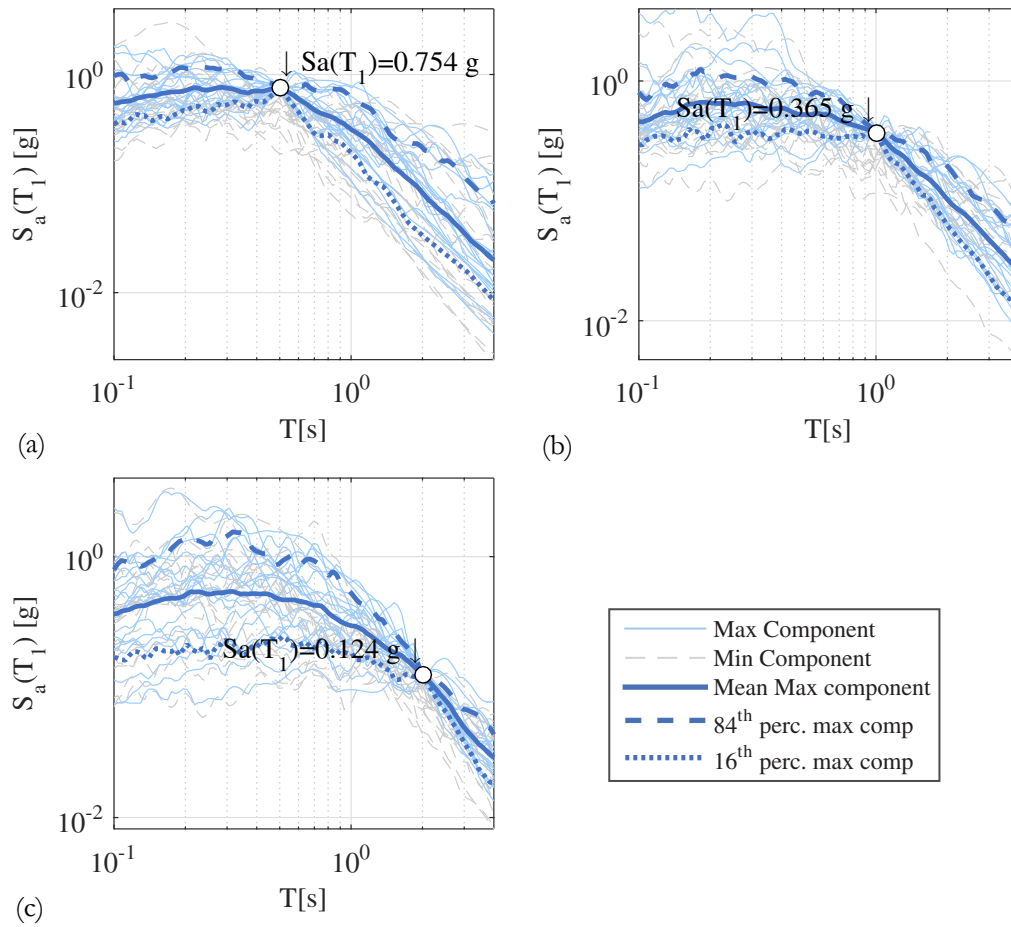


Figure B.2. Spectra of selected records with percentiles curves for the case of L'Aquila, soil C, and conditioned on Spectral acceleration at 0.5s (a), 1.0s (b), 2.0 s (c).

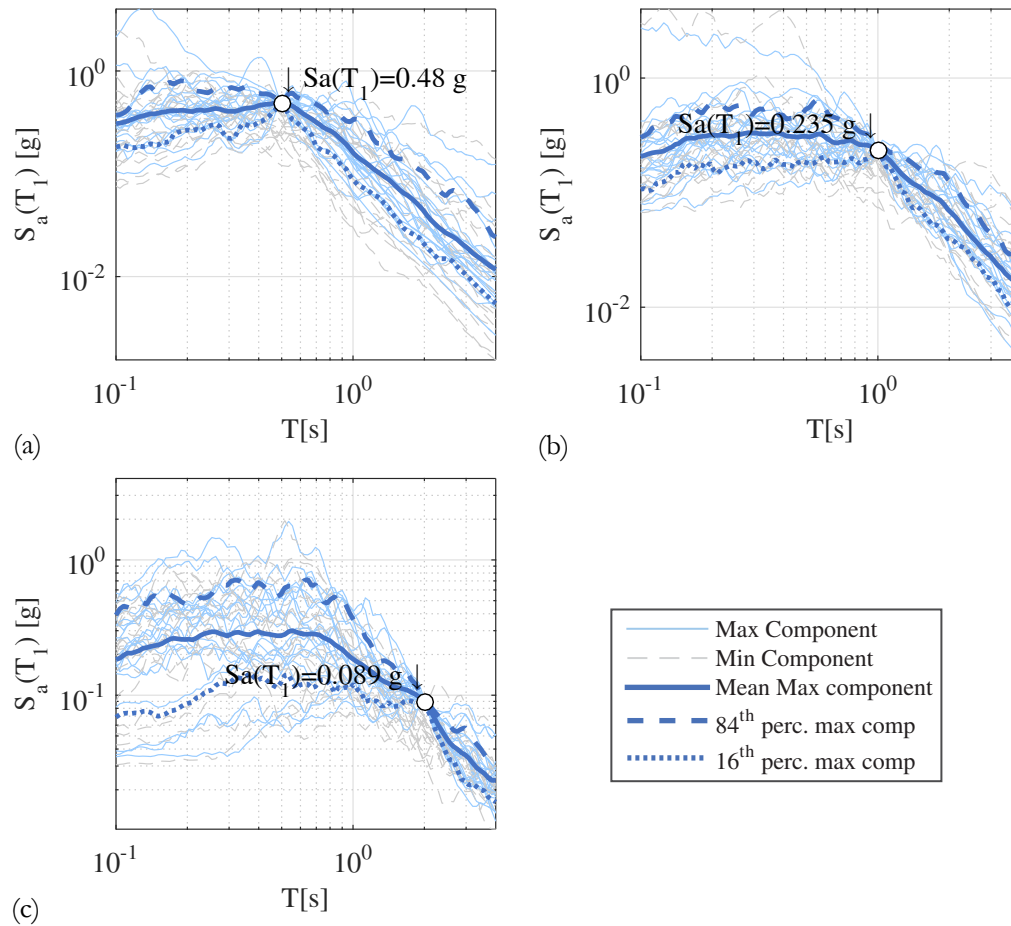


Figure B.3 Spectra of selected records with percentiles curves for the case of Napoli, soil C, and conditioned on Spectral acceleration at 0.5s (a), 1.0s (b), 2.0 s (c).

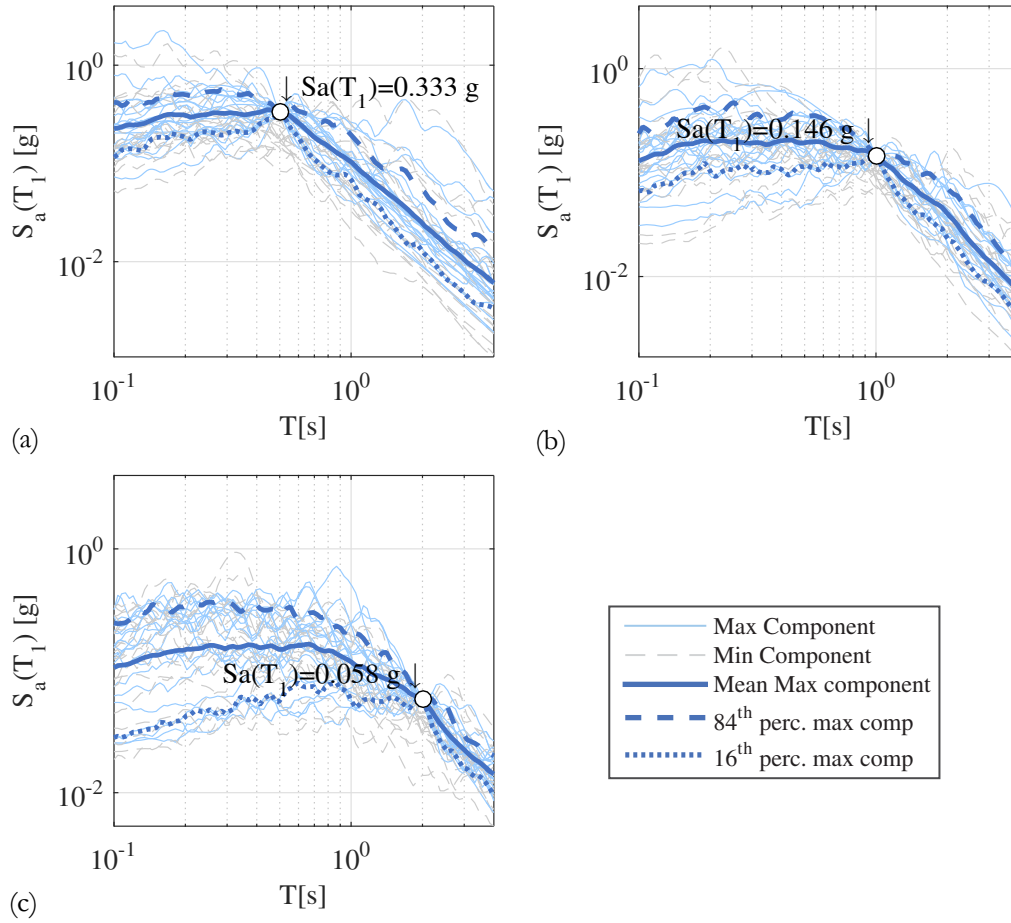


Figure B.4 Spectra of selected records with percentiles curves for the case of Roma, soil C, and conditioned on Spectral acceleration at 0.5s (a), 1.0s (b), 2.0 s (c).

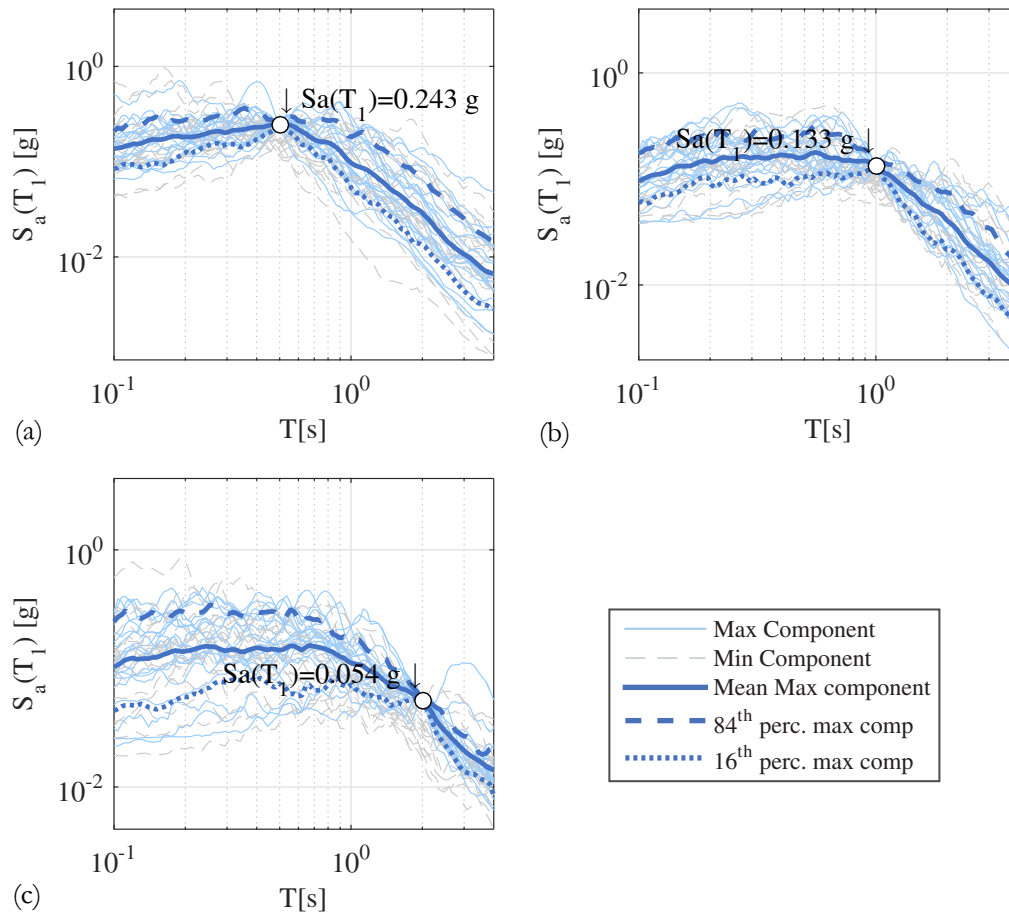


Figure B.5 Spectra of selected records with percentiles curves for the case of Caltanissetta, soil C, and conditioned on Spectral acceleration at 0.5s (a), 1.0s (b), 2.0 s (c).

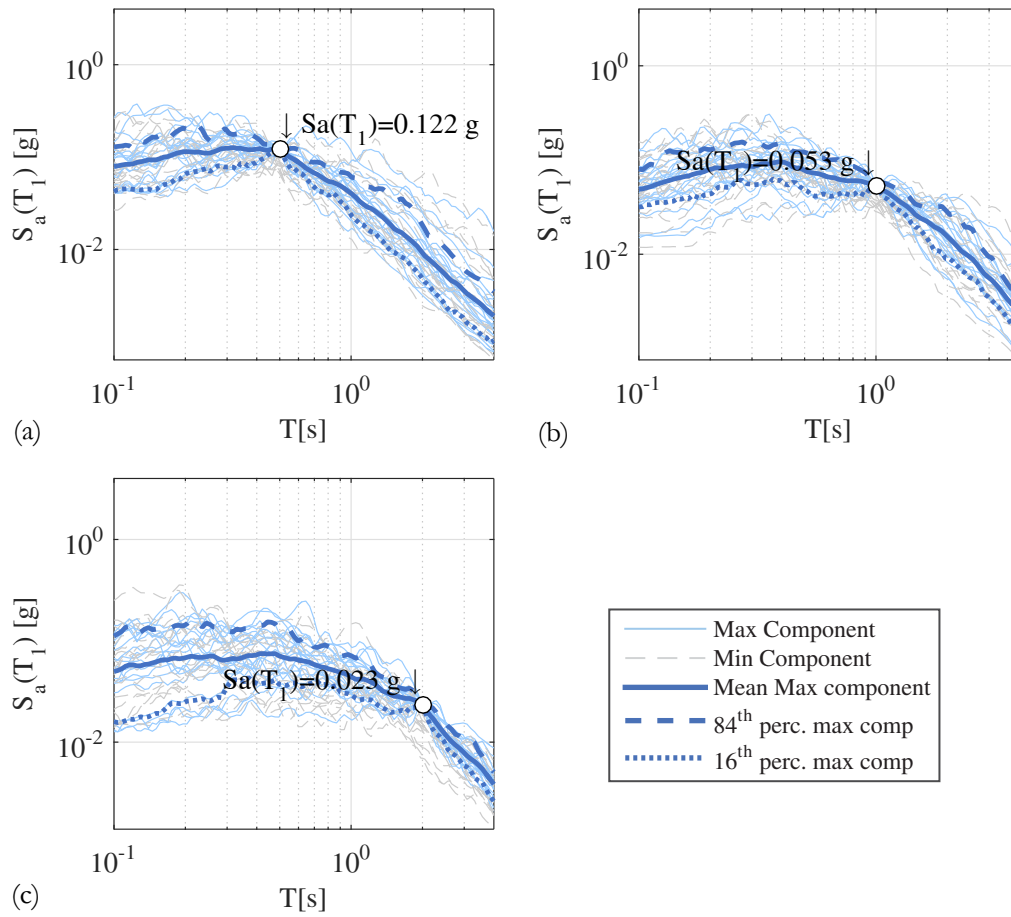


Figure B.6 Spectra of selected records with percentiles curves for the case of Milano, soil C, and conditioned on Spectral acceleration at 0.5s (a), 1.0s (b), 2.0 s (c).

## Appendix C. Notes on structural Modelling about Implicit Risk Project

This appendix wants to give a general overview of modelling of the structures analyzed in the Implicit Risk Project. Each section is just a summary of the works of Camata et al. [2017]; Camilletti et al. [2017]; Cardone et al. [2017]; Ercolino et al. [2017]; RINTC-Workgroup [2017]; Scozzese et al. [2017] and is intended to be of guidance for the reader, giving a general idea of the strategies and methodologies adopted to properly represent the behavior under severe seismic loading. For additional details, the reader is redirected to the proper reference.

The buildings belonging to the five considered typologies refer, as much as possible, to standard modern construction and design provisions. In particular, the following list summarizes their main properties:

- Cast-in-place reinforced concrete (RC): regular 3-, 6-, and 9-storey moment-resisting-frame structures designed via modal analysis (i.e. linear with response spectrum);
- Unreinforced Masonry (URM): 2- and 3-storey regular and irregular buildings designed with the simple building and/or non-linear static analysis approaches;
- Precast reinforced concrete (PRC): 1-storey industrial buildings with four different plan geometries and heights;
- Steel: 1-storey industrial buildings with two different plan geometries and heights;
- Base-isolated (BI): 6-storey reinforced concrete building with base isolation system made of rubber bearings, friction pendulums and hybrid.

### C.1 MODELLING DETAILS

*RC – buildings (Camata et al. [2017])*

RC structures are usually modelled by means of two different modeling approaches:

- The physical one, usually labelled as “fiber-model” (Spacone et al. [1996a]; Spacone et al. [1996b]), according to which the section is discretized and associated to a distributed or concentrated plasticity frame element formulation. Usually, this approach requires a simple uniaxial formulation at fiber level

(according to the material of the fiber itself) and relies on the hypothesis that the plane sections remain plane.

- The phenomenological one, i.e. the “plastic hinge model”, according to which the behavior at the section level is represented by a piece-wise moment curvature law integrated with a lumped plasticity frame element formulation. Here, several models exist with diverse level of detail in describing the moment curvature relationship.

The first option allows to properly, and better, describing the flexural behavior by accounting biaxial moment and axial force interaction. However, at larger response level the plane section constraint does not hold anymore and, consequently, the fiber model fails to describe the negative stiffness branch of the response. For this reason, and because of computational and storage burden, the second approach is preferred. The chosen model is the well-tested model by Ibarra et al. [2005], in the most recent OpenSees (McKenna et al. [2000]) implementation (modIMKmodel) that is able to account for strength and stiffness degradation. The model has already been used in a similar setting, i.e. for the probabilistic seismic performance assessment of both existing and code-conforming (plane) frame structures (Haselton et al. [2010]; Liel et al. [2010]). Another advantage of this model is the availability of predictive equations for the IMK model parameters. These equations are obtained by statistical regression on actual test results for several hundreds of RC specimens (predictive equations by Haselton et al. [2009]) and steel specimens (Lignos and Krawinkler [2012]). Those equations allow estimating easily the parameters of the model starting from the geometric and mechanical characteristics of the members giving, as output, the median and the associated dispersion of each parameter. This latter capability will be particularly useful to account for model error and uncertainty.

Two configurations of the RC buildings (Pilotis and Infilled) include infills panels that are included in the non-linear numerical model too. In particular, the infills are modelled as an equivalent strut working only in compression. The model adopted to define the monotonic and cyclic behavior of the strut is the one developed by Decanini et al. (Bertoldi et al. [1993]; Decanini [2001]; Decanini and Fantin [1986]; Decanini et al. [2014]; Decanini et al. [2004]) and is based on the mechanical and geometric characteristics of the infills.

#### *PRC – Buildings (Ercolino et al. [2017])*

Also for this structural typology, the phenomenological approach has been adopted in its lumped plasticity formulation. In particular, the plastic hinges are included only at the column base and their parameters evaluated by means of the relationships proposed by Fischinger et al. [2008]. Moreover, beams and girders are represented as elastic elements

and rigid blocks are adopted to model the geometrical eccentricities of the elements. The column-beam and the column-girder connection are modelled by means of perfect hinge constraints. The possible collapse of the connections, which recent real events have brought to light as the failure mode most likely to happen for this structural typology, is accounted for simply by post-processing the actions in correspondence of the connections themselves and verifying their resistance.

The interaction of the cladding panels with the structure is accounted for by means of the model proposed by Magliulo et al. [2015]; each panel consists of an elastic 2D frame and it is connected at the top to the structure (beam) by means of fixed constraints that avoid the panel-to-structure relative displacement. During the analyses, the forces acting on the panel are monitored until the achievement of the maximum strength in the connection system. Once the failure (evaluated only in terms of shear) is achieved, the panel is removed from the model and the analysis keeps going with a “new” structural configuration.

#### *URM – Buildings (Camilletti et al. [2017])*

The modelling of masonry structures has been carried out in order to properly simulate i) the stiffness and strength degradation of masonry panels made by hollow clay blocks and cement mortar and, ii) a cyclic hysteretic behavior able to capture the different failure modes (i.e. rocking, diagonal cracking, sliding and mixed, when possible) expected to happen in piers and spandrels. In particular, two modelling approaches are adopted:

- *Nonlinear beam with piecewise-linear force-deformation relationship* (Cattari and Lagomarsino [2013]), according to which the masonry panels are modelled as nonlinear beam elements with lumped inelasticity idealization and a piecewise-linear behavior. The adopted law is able to model progressing strength decays at fixed drift values and a hysteretic response (by means of a phenomenological approach) that allows capturing different failure modes that might happen. The parameters that define the constitutive law can be subdivided in two groups: i) those related to the backbone shape and ii) those that contribute to define the hysteretic loop. Those parameters are estimated based on experimental data and on literature/code relationships.
- *Macroelement mechanical model*. It is able to represent “the cyclic nonlinear behavior associated with the two main in-plane masonry failure modes, namely bending-rocking and shear mechanisms Penna et al. [2014]. [...] The macroelement formulation can represent both the cyclic shear and flexural response of masonry panels. [...]” In particular, “the nonlinear description of the coupled relation between the flexural and axial degrees of freedom allows the explicit evaluation of how cracking affects the rocking motion. The macroelement model includes

also a nonlinear degrading model for rocking damage, which accounts for the effect of limited compressive (i.e., toe-crushing) strength. [...] The parameters of the masonry type used in the numerical models for dynamic analyses were calibrated to be representative of a typical unreinforced masonry with perforated clay blocks. The parameters were compared with some literature experimental data, many of which derived from tests on masonry piers carried out at the Eucentre laboratory Magenes et al. [2008]”

*Steel – Buildings (Scopcese et al. [2017])*

For this structural typology, the research unit in charge has tackled the modelling adopting what previously has been defined as “physical model” by means of distributed plasticity elements. This approach was thought to represent more realistically the yielding processes occurring along the elements. In particular, Opensees is again the reference software and the structures are modelled by means of Force-Based *nonlinearBeamColumn* elements discretized in a conveniently chosen number of fibers characterized by the uniaxial material Steel02 constitutive law (Giuffre-Menegotto-Pinto steel material object with isotropic strain hardening). The corotational approach is adopted in order to take into account the nonlinear geometric effects due to both the large displacements and the local imperfections of the lateral bracing systems.

The lateral braces are modelled by means of the method of (Hsiao et al. [2012], [2013]) that implementing a rotational nonlinear spring located at the physical end of the brace is able to account for two main aspects:

- The buckling in compression
- The gusset plate connections that, in reality, are neither pinned nor fixed joints.

“In order to simulate the buckling of the lateral braces during the compression phases, each brace has been discretized into a proper number of nonlinear (with distributed plasticity) sub-elements and a sinusoidal curvature is assigned by modifying parametrically the coordinates of the nodes of the intermediate sub-elements.”

*BI – Buildings (Cardone et al. [2017])*

The design of the superstructure has been carried out neglecting the capacity design and considering structural details related to low ductility class. On the other hand the modelling strategy is reflecting entirely the approach proposed for reinforced concrete structures.

### HDRB devices

The cyclic behavior of these devices is described by means of the model recently developed by Kumar et al. [2015] and implemented in Opensees as HDR Bearing Element. In particular, the model consists in as a two-node, twelve degrees-of-freedom discrete element. In the axial direction the material is modelled in line with what proposed by Kumar et al. [2015] capturing “the cavitation and post-cavitation behavior in tension, the variation of the critical buckling load and the vertical axial stiffness with horizontal displacement in compression”. Moreover, the behavior under the two shear directions is described by the model of Grant et al. [2004], accounting for “degradation of bearing stiffness and damping due to scragging effects in shear, which is of particular importance for high dissipative rubbers”. Finally, torsion and the other two rotational directions are represented through elastic models. The parameters needed to set up the models are based on experimental tests or can be obtained from rubber bearings with similar properties.

### Steel-PTFE sliders

In order to reduce the computational and modeling effort, a simple truss element characterized by suitable axial stiffness values (depending on the coupled HDRB device) has been used to model the Steel/PTFE sliders.

### FPS devices

“In SAP2000 the nonlinear behavior of the FPSs has been modelled by using one joint link element type biaxial Friction-Pendulum Isolator. The friction and pendulum forces are directly proportional to the compressive axial force in the element which cannot carry axial tension.” The parameters of the element are based on manufacturer data and on experimental tests performed on similar bearings.

## Appendix D. Fragility Curves and Nominal annual Rates from Implicit Risk Project

### D.1 FRAGILITY CURVES

In this section the computed fragility curves for the various combination of Structural type/city/soil/limit state will be reported. However, not all the combinations (particularly for Collapse) allow the definition of a reliable function and, for this reason, they are omitted here. Moreover, for risk computation purposes, if the curve is not available is assumed as a step function equal to zero until the last analyzed IM level and equal to one afterwards (meaning certain attainment of the LS for IM more severe than the 10<sup>th</sup>). The following tables summarize the parameters of the fragility curves that will be shown separately in the next paragraphs, both for Collapse and Damage Limit States.

**Table D.1** Damage- and Collapse- fragility curves parameters for Masonry structures on soil C.

L'Aquila	SLC			SLD		
	Str.ID	$\mu_{\ln S_a}$	$\sigma_{\ln S_a}$	median <sub>S<sub>a</sub></sub>	$\mu_{\ln S_a}$	$\sigma_{\ln S_a}$
RC-AqC3IF	2.11	0.62	8.22	-0.33	0.46	0.72
RC-AqC3PF	1.98	0.38	7.26	-1.48	0.34	0.23
Mean Curve	2.04	0.52	7.73	-0.90	0.91	0.41
RC-AqC6IF	1.48	0.69	4.38	-1.09	0.40	0.34
RC-AqC6PF	1.50	0.67	4.47	-1.10	0.44	0.33
Mean Curve	1.49	0.68	4.43	-1.10	0.42	0.33
RC-AqC9IF	1.24	0.45	3.47	-1.66	0.19	0.19
RC-AqC9PF	1.30	0.48	3.68	-1.92	0.09	0.15
Mean Curve	1.27	0.46	3.57	-1.79	0.24	0.17

Caltanissetta	SLC			SLD		
	Str.ID	$\mu_{\ln S_a}$	$\sigma_{\ln S_a}$	median <sub>S<sub>a</sub></sub>	$\mu_{\ln S_a}$	$\sigma_{\ln S_a}$
RC-CIC6IF	0.80	0.48	2.22	-1.18	0.34	0.31
RC-CIC6PF	0.92	0.73	2.52	-1.93	0.45	0.14

Mean Curve	0.86	0.62	2.36	-1.56	0.66	0.21
------------	------	------	------	-------	------	------

<b>Milano</b>	SLC			SLD		
Str.ID	$\mu_{\ln S_a}$	$\sigma_{\ln S_a}$	median <sub>S<sub>a</sub></sub>	$\mu_{\ln S_a}$	$\sigma_{\ln S_a}$	median <sub>S<sub>a</sub></sub>
RC-MiC3IF	---	---	---	-0.75	0.04	0.47
RC-MiC3PF	---	---	---	-1.88	0.49	0.15
Mean Curve	---	---	---	-1.31	0.87	0.27
RC-MiC6IF	---	---	---	-0.80	0.44	0.45
RC-MiC6PF	---	---	---	-1.89	0.50	0.15
Mean Curve	---	---	---	-1.34	0.90	0.26
RC-MiC9IF	---	---	---	-1.75	0.04	0.17
RC-MiC9PF	---	---	---	-2.18	0.20	0.11
Mean Curve	---	---	---	-1.97	0.34	0.14

<b>Napoli</b>	SLC			SLD		
Str.ID	$\mu_{\ln S_a}$	$\sigma_{\ln S_a}$	median <sub>S<sub>a</sub></sub>	$\mu_{\ln S_a}$	$\sigma_{\ln S_a}$	median <sub>S<sub>a</sub></sub>
RC-NaC3IF	---	---	---	-0.19	0.62	0.82
RC-NaC3PF	---	---	---	-1.76	0.46	0.17
Mean Curve	---	---	---	-0.98	1.23	0.38
RC-NaC6IF	---	---	---	-1.08	0.49	0.34
RC-NaC6PF	---	---	---	-1.51	0.55	0.22
Mean Curve	---	---	---	-1.30	0.60	0.27
RC-NaC9IF	---	---	---	-1.93	0.19	0.15
RC-NaC9PF	---	---	---	-2.04	0.19	0.13
Mean Curve	---	---	---	-1.98	0.21	0.14

<b>Roma</b>	SLC			SLD		
-------------	-----	--	--	-----	--	--

Str.ID	$\mu_{\ln S_a}$	$\sigma_{\ln S_a}$	median <sub>S<sub>a</sub></sub>	$\mu_{\ln S_a}$	$\sigma_{\ln S_a}$	median <sub>S<sub>a</sub></sub>
RC-RoC6IF	1.42	0.76	4.14	-0.93	0.64	0.39
RC-RoC6PF	0.98	0.57	2.66	-1.42	0.68	0.24
Mean Curve	1.20	0.74	3.32	-1.17	0.75	0.31

**Table D.2** Damage- and Collapse- fragility curves parameters for Masonry structures on soil C.

<b>L'Aquila</b>	SLC			SLD		
Str.ID	$\mu_{\ln S_a}$	$\sigma_{\ln S_a}$	median <sub>S<sub>a</sub></sub>	$\mu_{\ln S_a}$	$\sigma_{\ln S_a}$	median <sub>S<sub>a</sub></sub>
URM-AqC2C3	0.48	0.27	1.62	-0.61	0.28	0.54
URM-AqC2I1	-0.01	0.31	0.99	-0.78	0.35	0.46
URM-AqC2e2	0.61	0.27	1.84	-0.29	0.21	0.75
URM-AqC2e5	0.53	0.32	1.71	-0.53	0.23	0.59
URM-AqC2e8	0.53	0.25	1.71	-0.41	0.22	0.66
URM-AqC2e9	0.47	0.25	1.59	-0.43	0.26	0.65
Mean Curve	0.44	0.36	1.55	-0.51	0.32	0.60

<b>Caltanissetta</b>	SLC			SLD		
Str.ID	$\mu_{\ln S_a}$	$\sigma_{\ln S_a}$	median <sub>S<sub>a</sub></sub>	$\mu_{\ln S_a}$	$\sigma_{\ln S_a}$	median <sub>S<sub>a</sub></sub>
URM-CIC2C2	-0.17	0.05	0.84	-0.79	0.29	0.45
URM-CIC3C3	---	---	---	-0.80	0.24	0.45
URM-CIC2e8	---	---	---	-0.37	0.21	0.69
URM-CIC2e9	---	---	---	-0.41	0.15	0.66
URM-CIC3e5	-0.18	0.05	0.84	-1.19	0.17	0.31
URM-CIC3e8	-0.21	0.05	0.81	-1.09	0.12	0.34
Mean Curve	---	---	---	-0.78	0.39	0.46

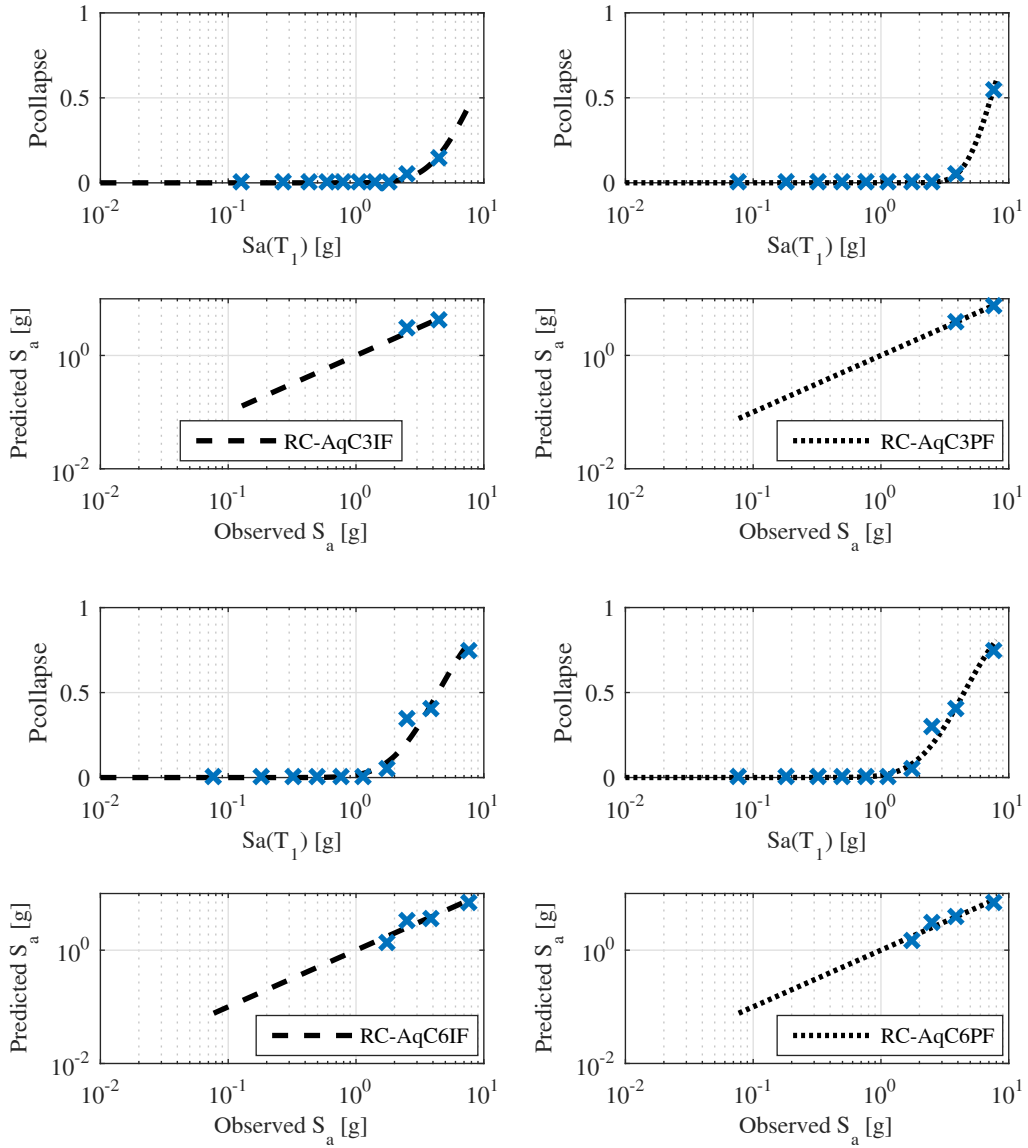
<b>Milano</b>	SLC			SLD		
Str.ID	$\mu_{\ln S_a}$	$\sigma_{\ln S_a}$	median <sub>S<sub>a</sub></sub>	$\mu_{\ln S_a}$	$\sigma_{\ln S_a}$	median <sub>S<sub>a</sub></sub>
URM-MiC2C1	---	---	---	-0.56	0.51	0.57
URM-MiC3C2	---	---	---	-1.09	0.29	0.34

URM-MiC2e8	0.89	0.50	2.44	-0.74	0.04	0.48
URM-MiC2e9	0.84	0.28	2.32	-0.74	0.04	0.48
URM-MiC3e2	0.88	0.45	2.41	-0.89	0.16	0.41
URM-MiC3e8	---	---	---	-0.98	0.16	0.38
URM-MiC3e9	---	---	---	-0.92	0.23	0.40
Mean Curve	0.87	0.22	2.39	-0.84	0.31	0.43

Napoli	SLC			SLD		
	Str.ID	$\mu_{\ln S_a}$	$\sigma_{\ln S_a}$	median <sub>S<sub>a</sub></sub>	$\mu_{\ln S_a}$	$\sigma_{\ln S_a}$
URM-NaC2C1	0.88	0.45	2.41	-0.92	0.26	0.40
URM-NaC2C4	0.84	0.28	2.32	-0.82	0.27	0.44
URM-NaC3C3	0.57	0.37	1.76	-0.91	0.19	0.40
URM-NaC3C5	0.62	0.39	1.85	-0.96	0.17	0.38
URM-NaC3I2	0.51	0.51	1.66	-1.72	0.29	0.18
URM-NaC3e2	0.91	0.56	2.48	-0.85	0.16	0.43
URM-NaC3e8	0.77	0.62	2.16	-0.99	0.17	0.37
URM-NaC3e9	0.47	0.47	1.59	-0.93	0.16	0.40
Mean Curve	0.69	0.50	2.00	-1.01	0.36	0.36

Roma	SLC			SLD		
	Str.ID	$\mu_{\ln S_a}$	$\sigma_{\ln S_a}$	median <sub>S<sub>a</sub></sub>	$\mu_{\ln S_a}$	$\sigma_{\ln S_a}$
URM-RoC2C3	0.76	0.36	2.15	-0.68	0.41	0.51
URM-RoC3C4	0.50	0.28	1.65	-0.90	0.23	0.41
URM-RoC2e8	1.28	0.58	3.60	-0.43	0.20	0.65
Mean Curve	0.85	0.58	2.34	-0.67	0.38	0.51

D.1.1 Reinforced Concrete - Collapse Limit State



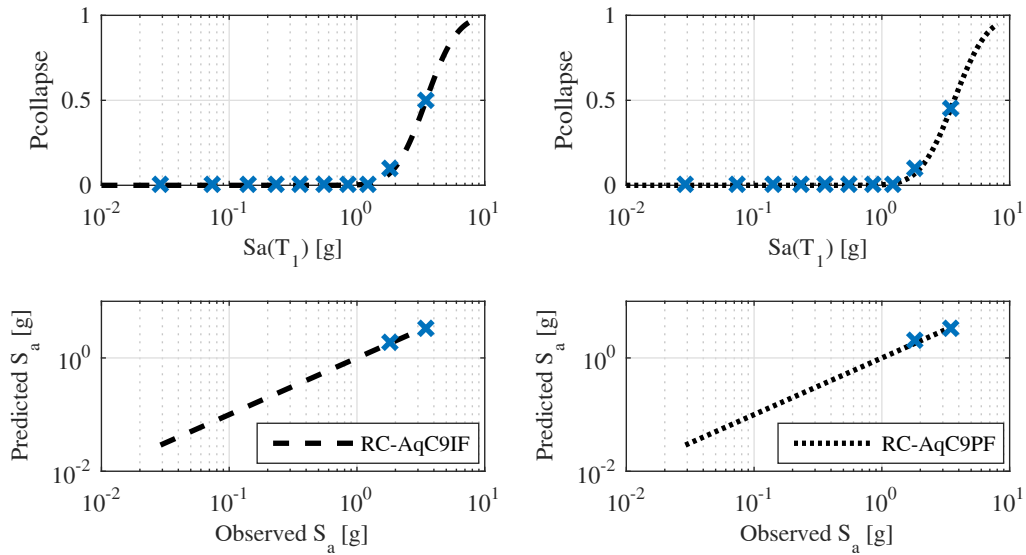


Figure D.1 Fragility curves and quantile-quantile plots for RC buildings designed for L'Aquila on soil C. The curves on the left column are related to Infilled Frame buildings while on the right refer to Pilotis (soft story) buildings. The rows distinguish the number of stories, in particular 3-, 6- and 9-story structures respectively.

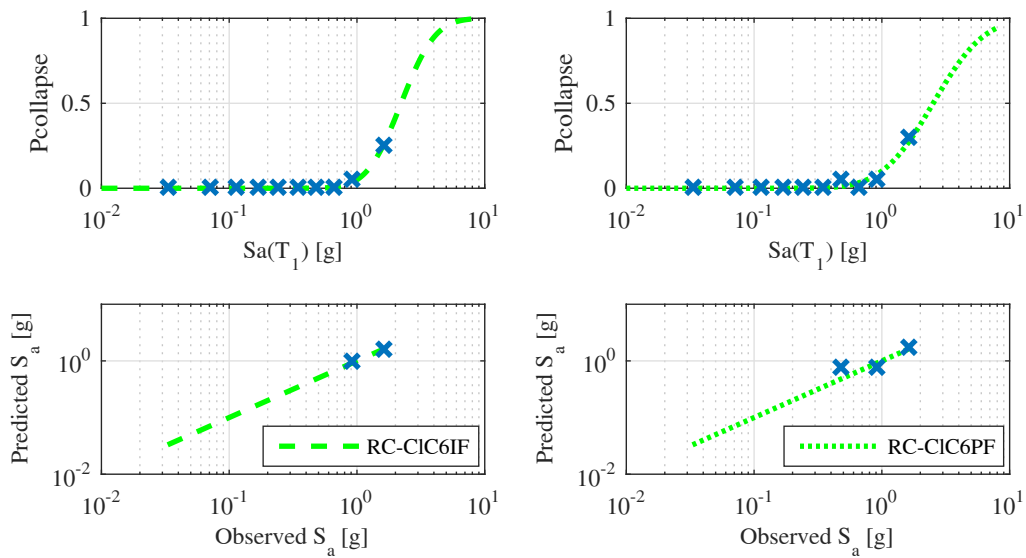


Figure D.2 Fragility curves and quantile-quantile plots for RC 6-story frame buildings designed for Caltanissetta on soil C. The curve on the left column is related to an Infilled Frame Building while on the right refers to a Pilotis (soft story) building.

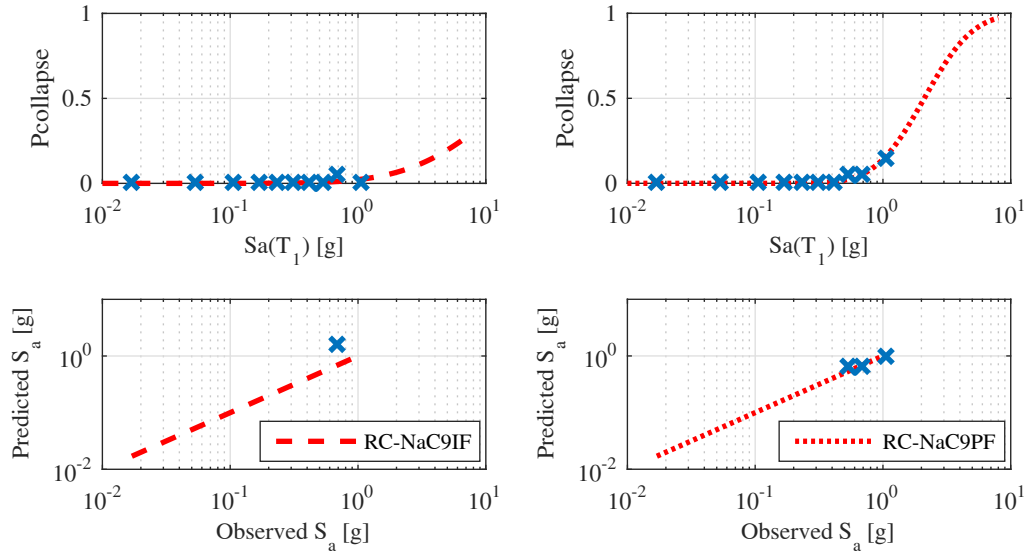


Figure D.3 Fragility curves and quantile-quantile plots for RC 9-story frame buildings designed for Napoli on soil C. The curve on the left column is related to an Infilled Frame Building while on the right refers to a Pilotis (soft story) building.

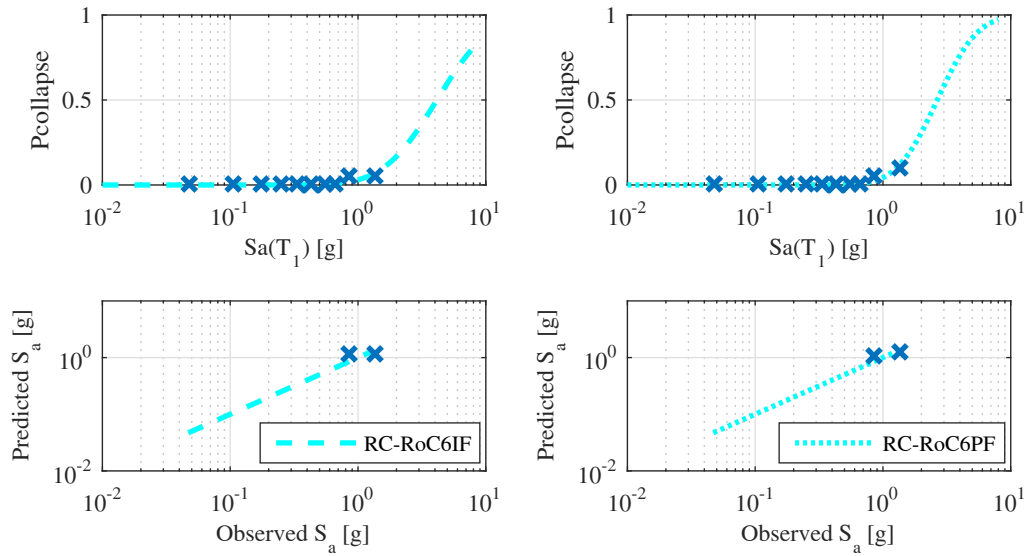
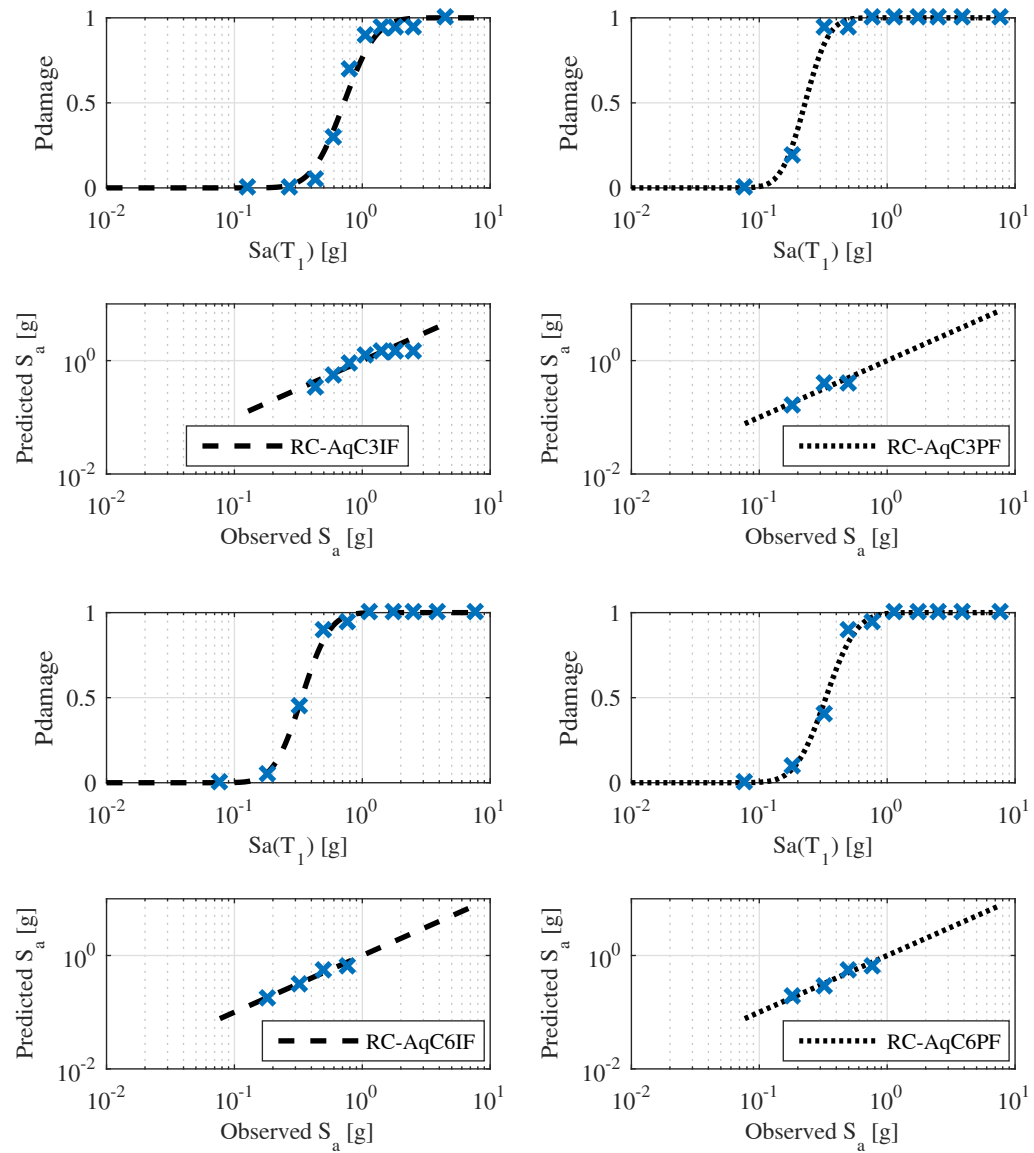


Figure D.4 Fragility curves and quantile-quantile plots for RC 6-story frame buildings designed for Roma on soil C. The curve on the left column is related to an Infilled Frame Building while on the right refers to a Pilotis (soft story) building.

D.1.2 Reinforced Concrete - Damage Limit State



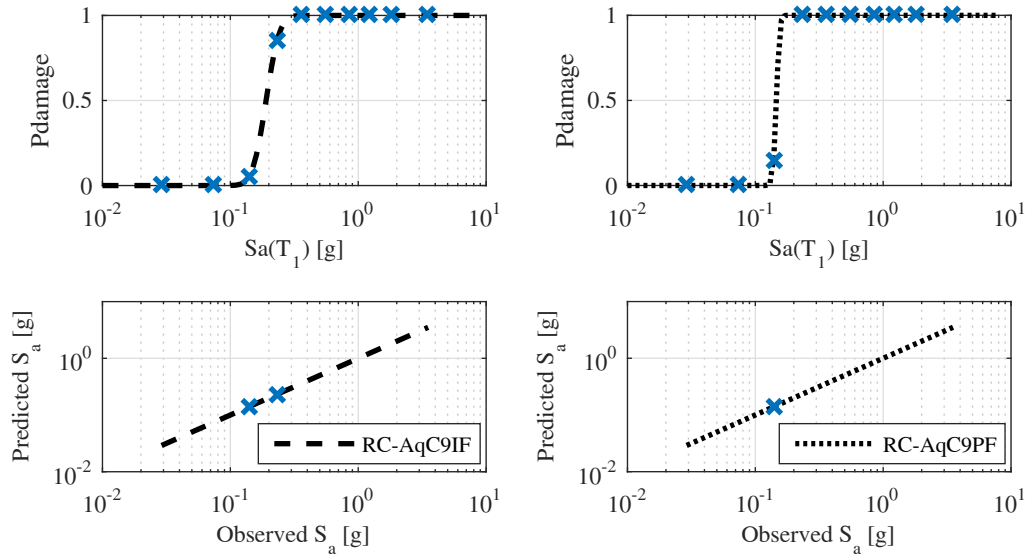


Figure D.5 Fragility curves and quantile-quantile plots for RC buildings designed for L'Aquila on soil C. The curves on the left column are related to Infilled Frame buildings while on the right refer to Pilotis (soft story) buildings. The rows distinguish the number of stories, in particular 3-, 6- and 9-story structures respectively.

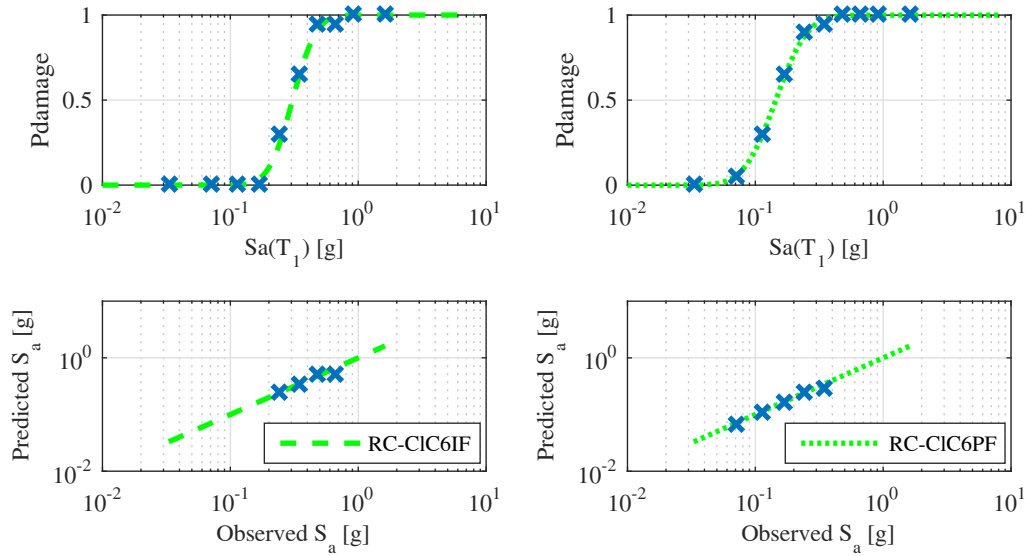
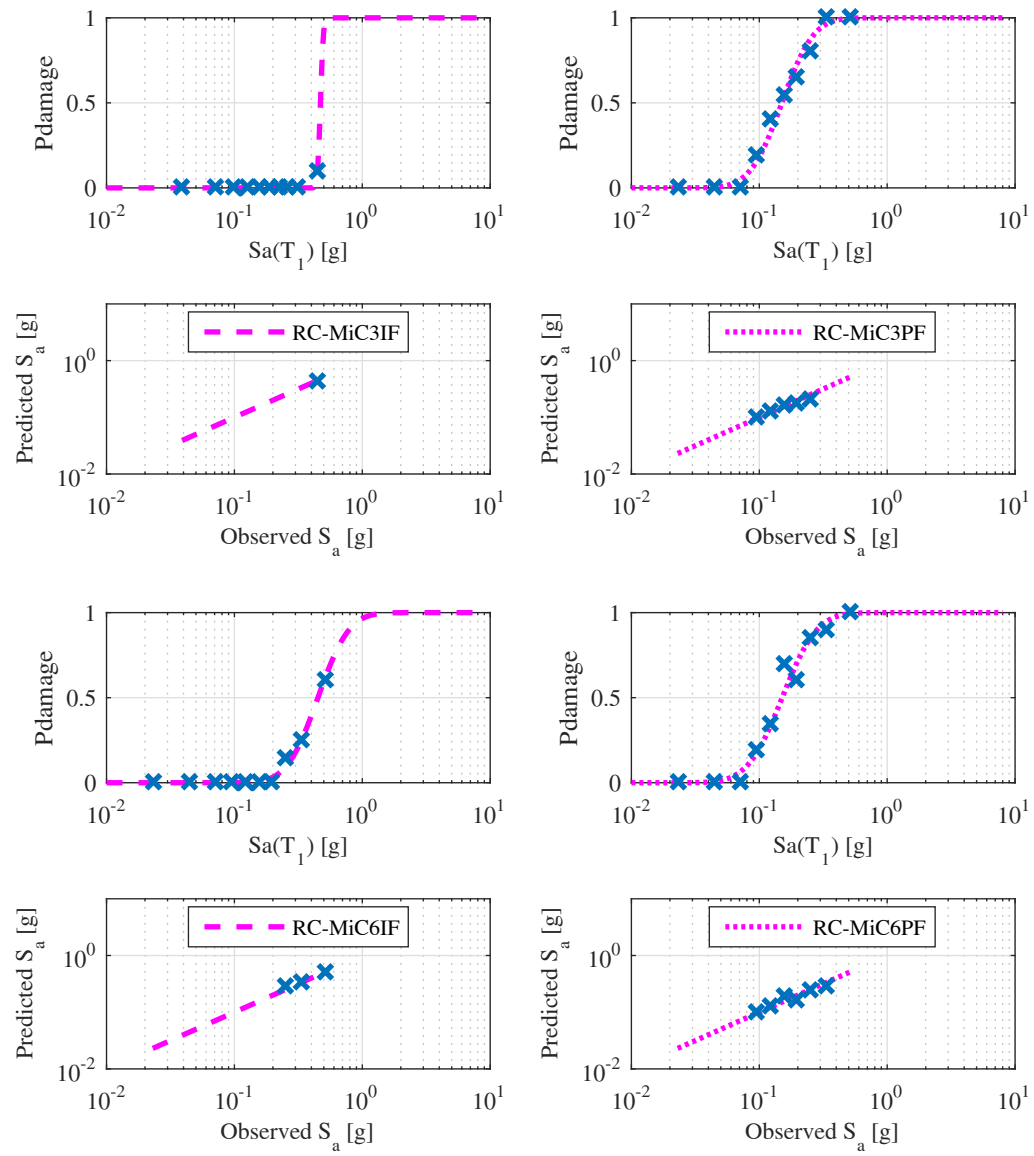


Figure D.6 Fragility curves and quantile-quantile plots for RC 6-story frame buildings designed for Caltanissetta on soil C. The curve on the left column is related to an Infilled Frame Building while on the right refers to a Pilotis (soft story) building.



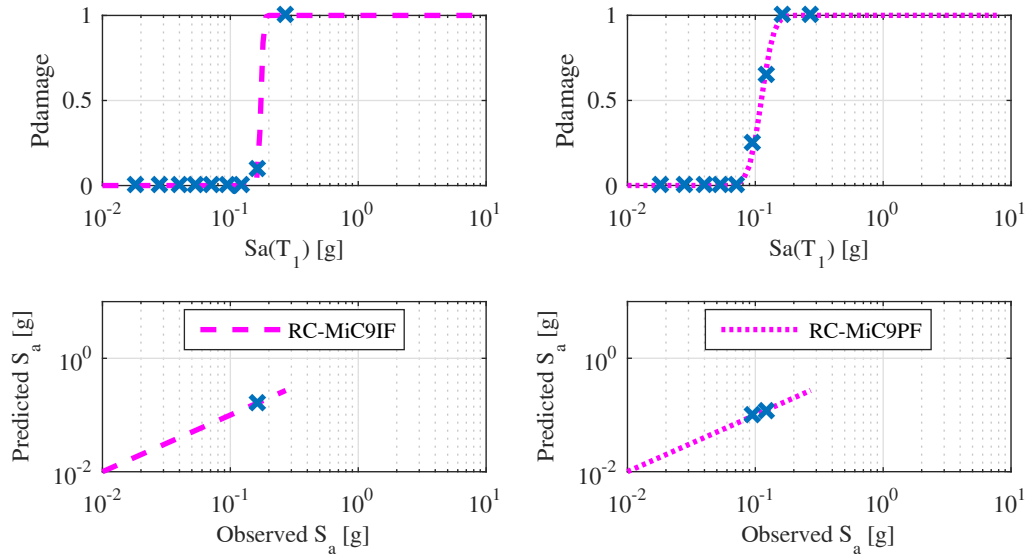
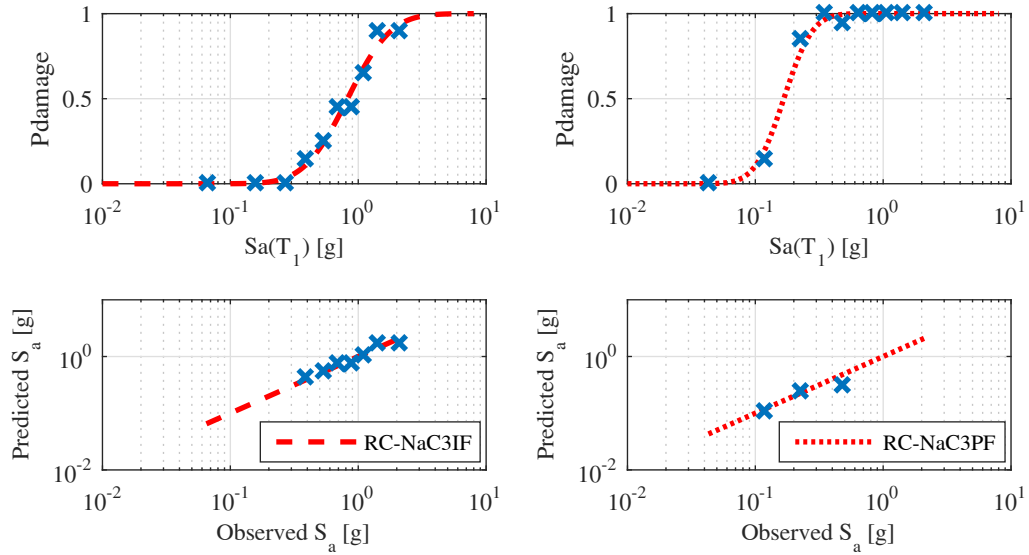
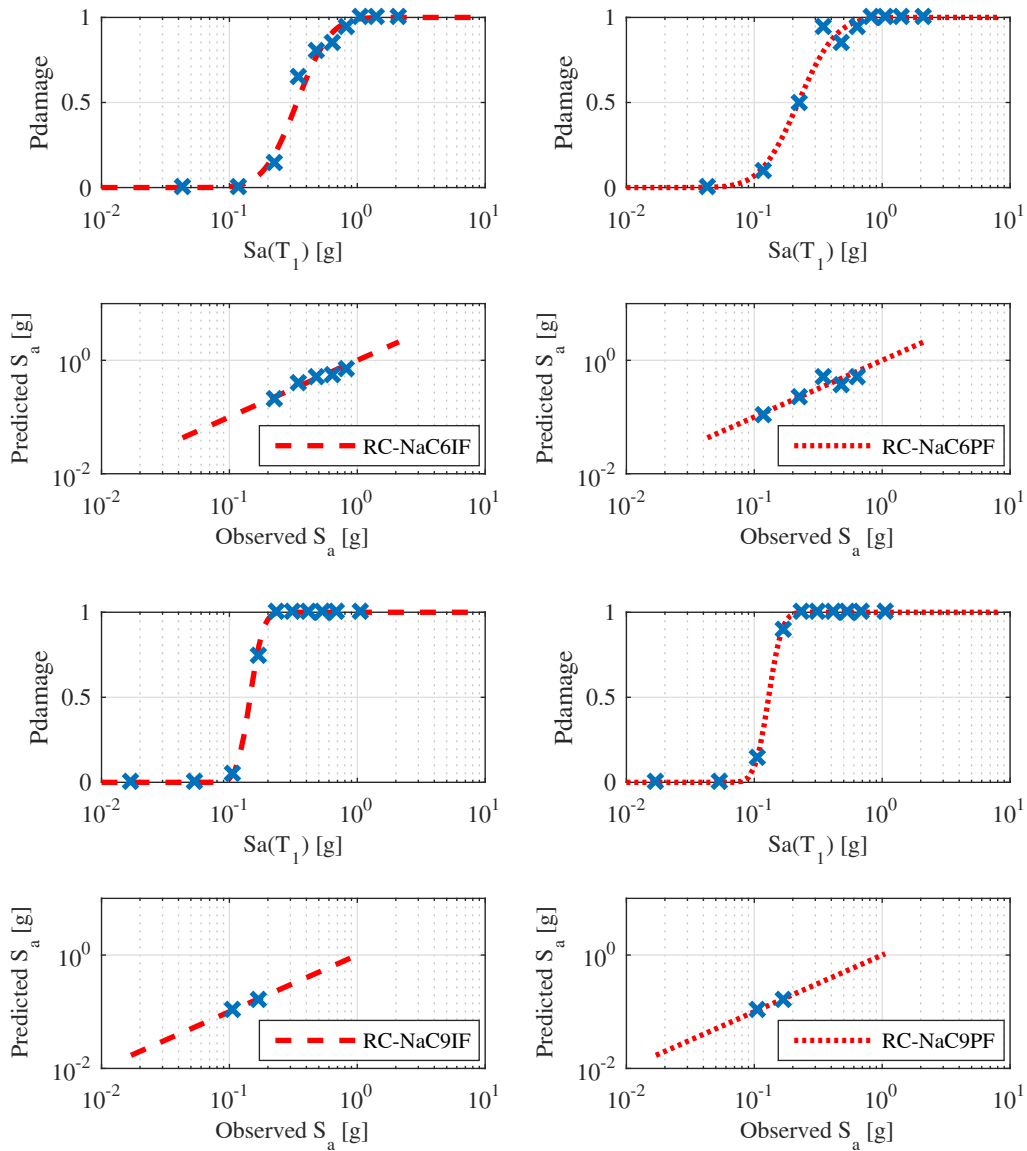


Figure D.7. Fragility curves and quantile-quantile plots for RC buildings designed for Milano on soil C. The curves on the left column are related to Infilled Frame buildings while on the right refer to Pilotis (soft story) buildings. The rows distinguish the number of stories, in particular 3-, 6- and 9-story structures respectively.





**Figure D.8** Fragility curves and quantile-quantile plots for RC buildings designed for Napoli on soil C. The curves on the left column are related to Infilled Frame buildings while on the right refer to Pilotis (soft story) buildings. The rows distinguish the number of stories, in particular 3-, 6- and 9-story structures respectively.

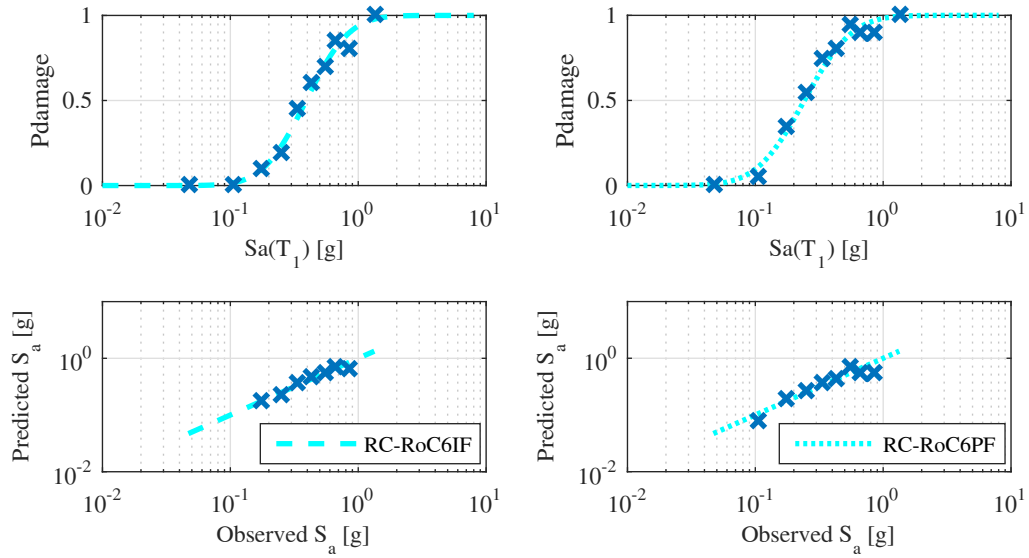
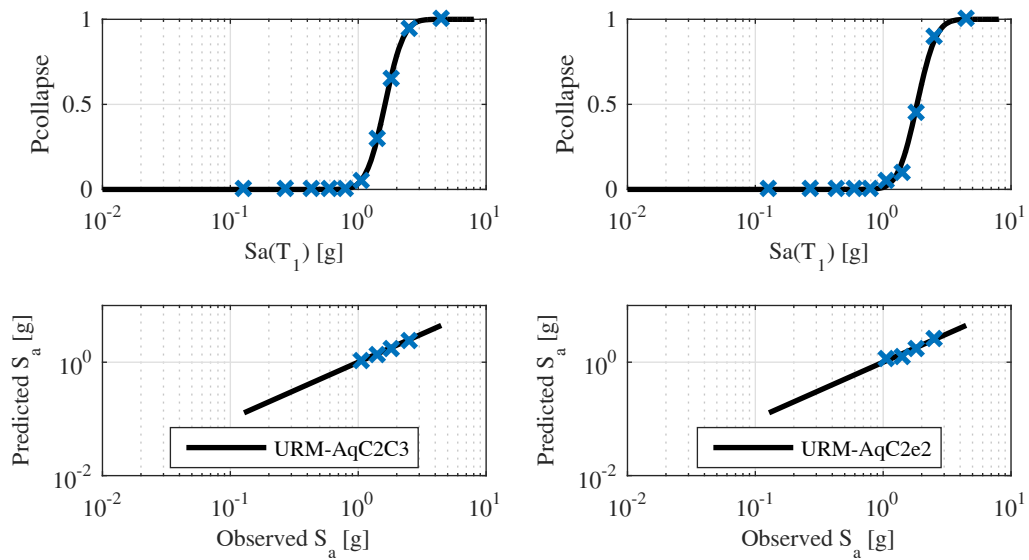
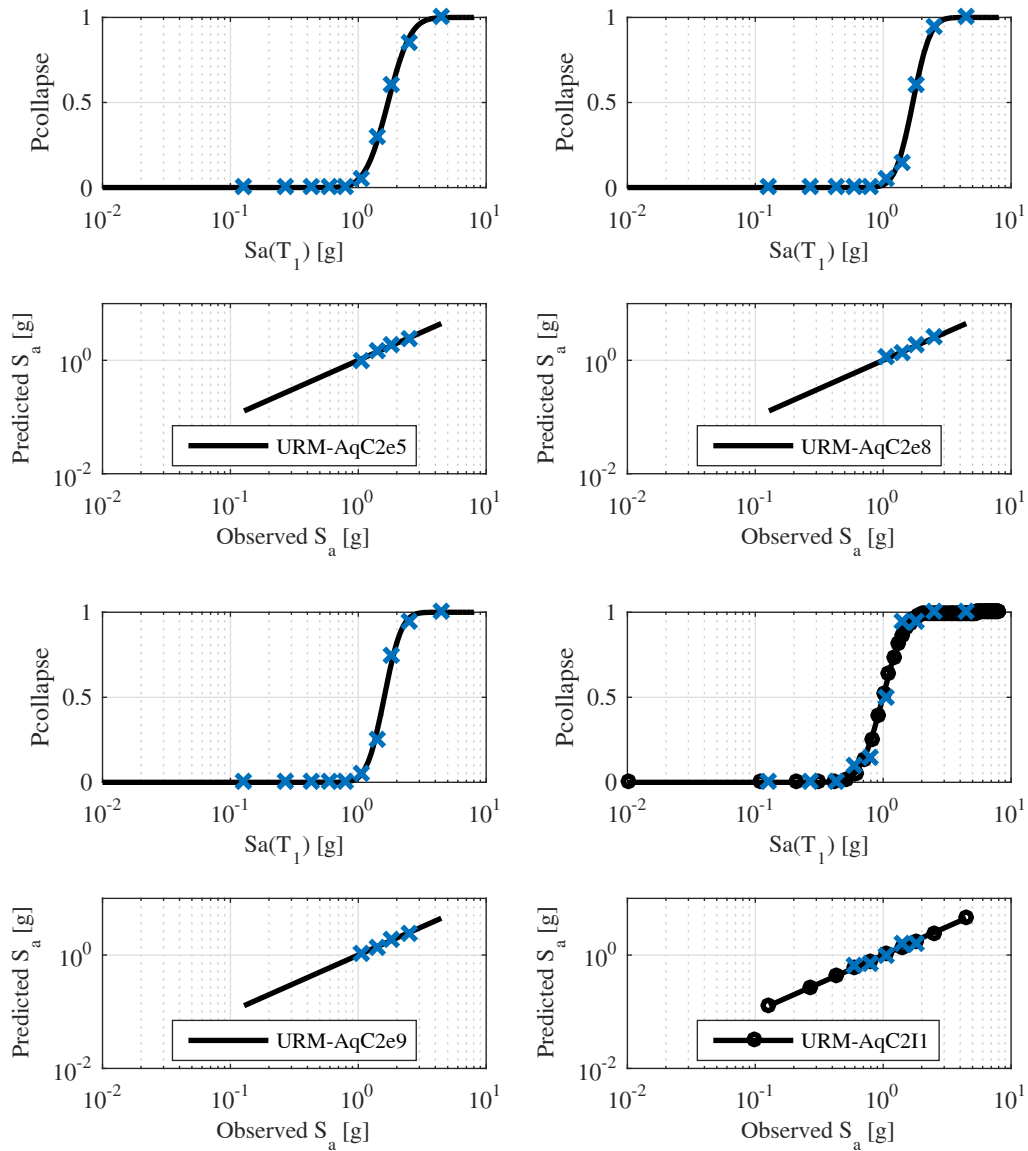


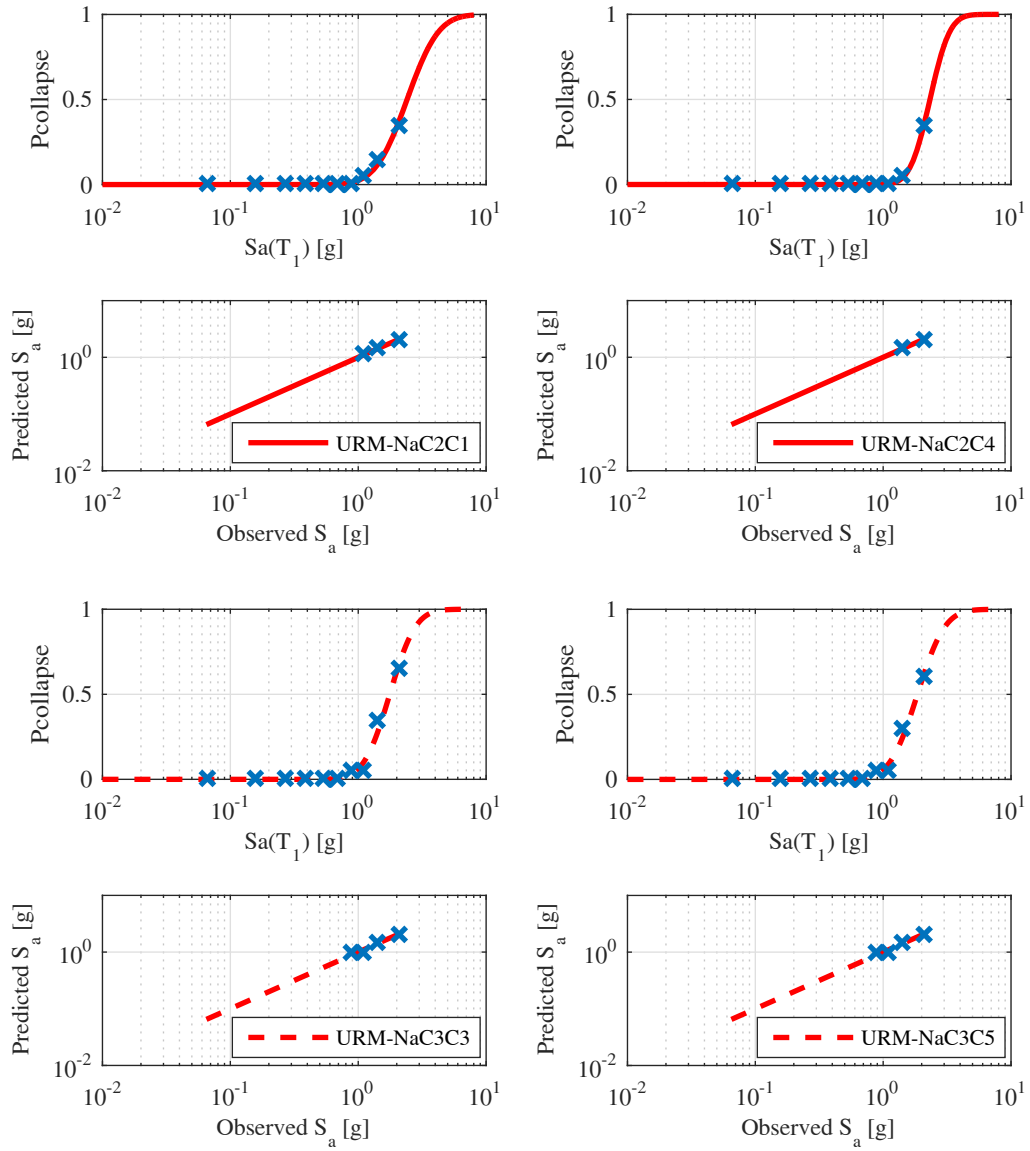
Figure D.9 Fragility curves and quantile-quantile plots for RC 6-story frame buildings designed for Roma on soil C. The curve on the left column is related to an Infilled Frame Building while on the right refers to a Pilotis (soft story) building.

### D.1.3 Unreinforced Masonry - Collapse Limit State





**Figure D.10** Fragility curves and quantile-quantile plots for URM buildings designed for L'Aquila on soil C. The line-style helps to distinguish among different structural characteristics. Solid and dashed lines represent, respectively, 2- and 3-story structures while the use of circle markers depicts an irregular configuration. Each panel represents a different configuration whose code is given in the legend name.



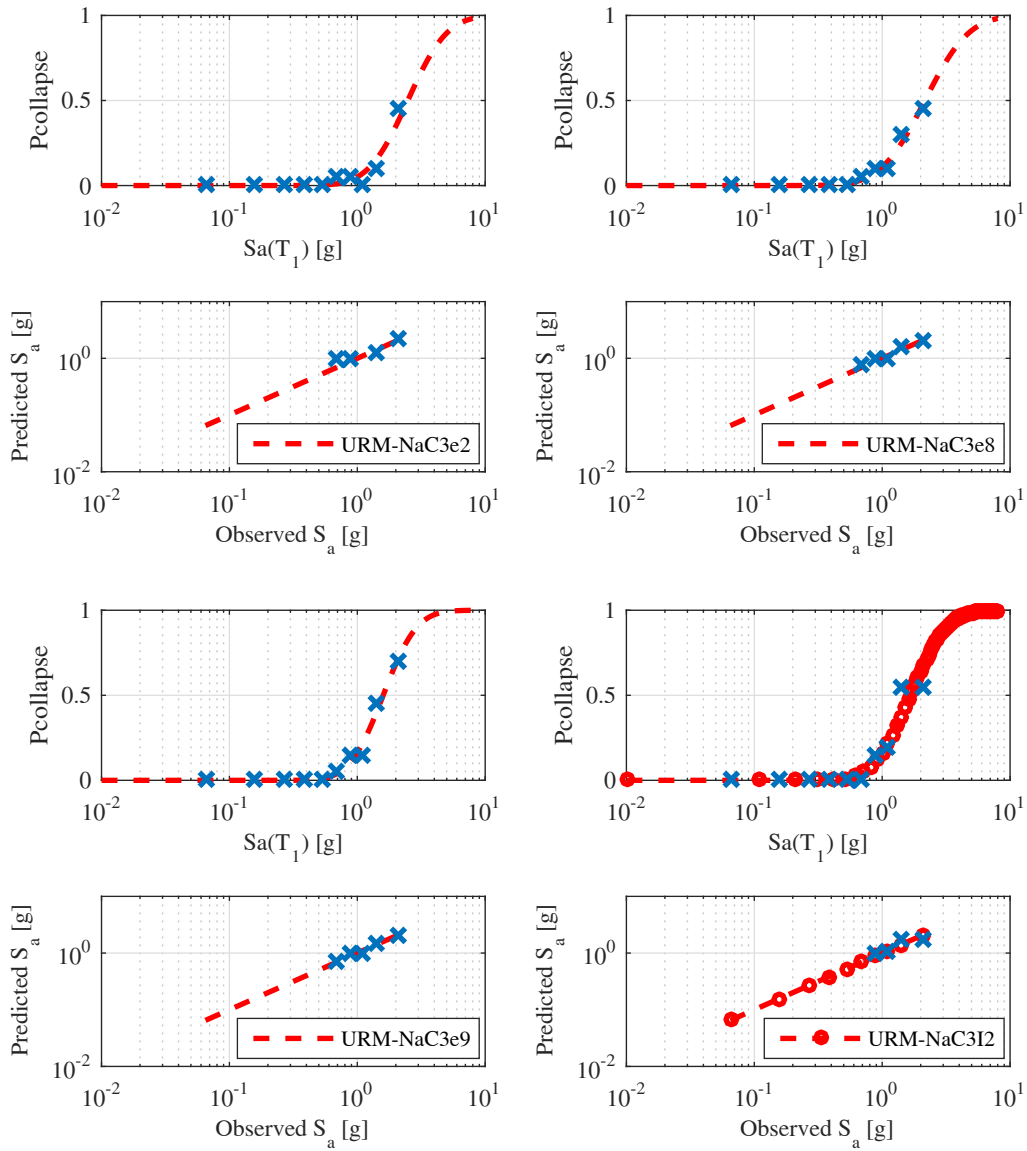


**Figure D.11** Fragility curves and quantile-quantile plots for URM buildings designed for Napoli on soil C. The line-style helps to distinguish among different structural characteristics. Solid and dashed lines represent, respectively, 2- and 3-story structures while the use of circle markers depicts an irregular configuration. Each panel represents a different configuration whose code is given in the legend name.

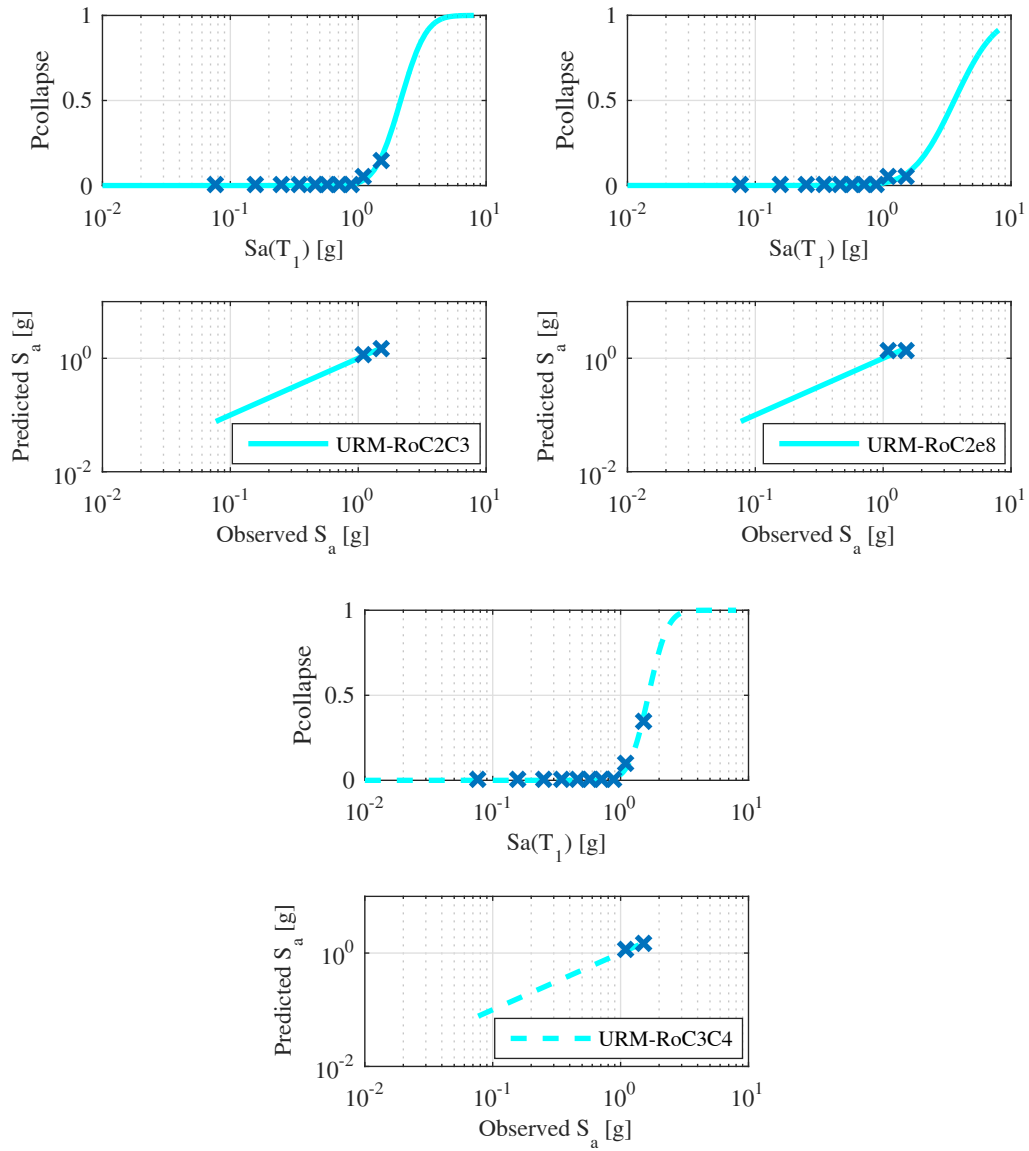
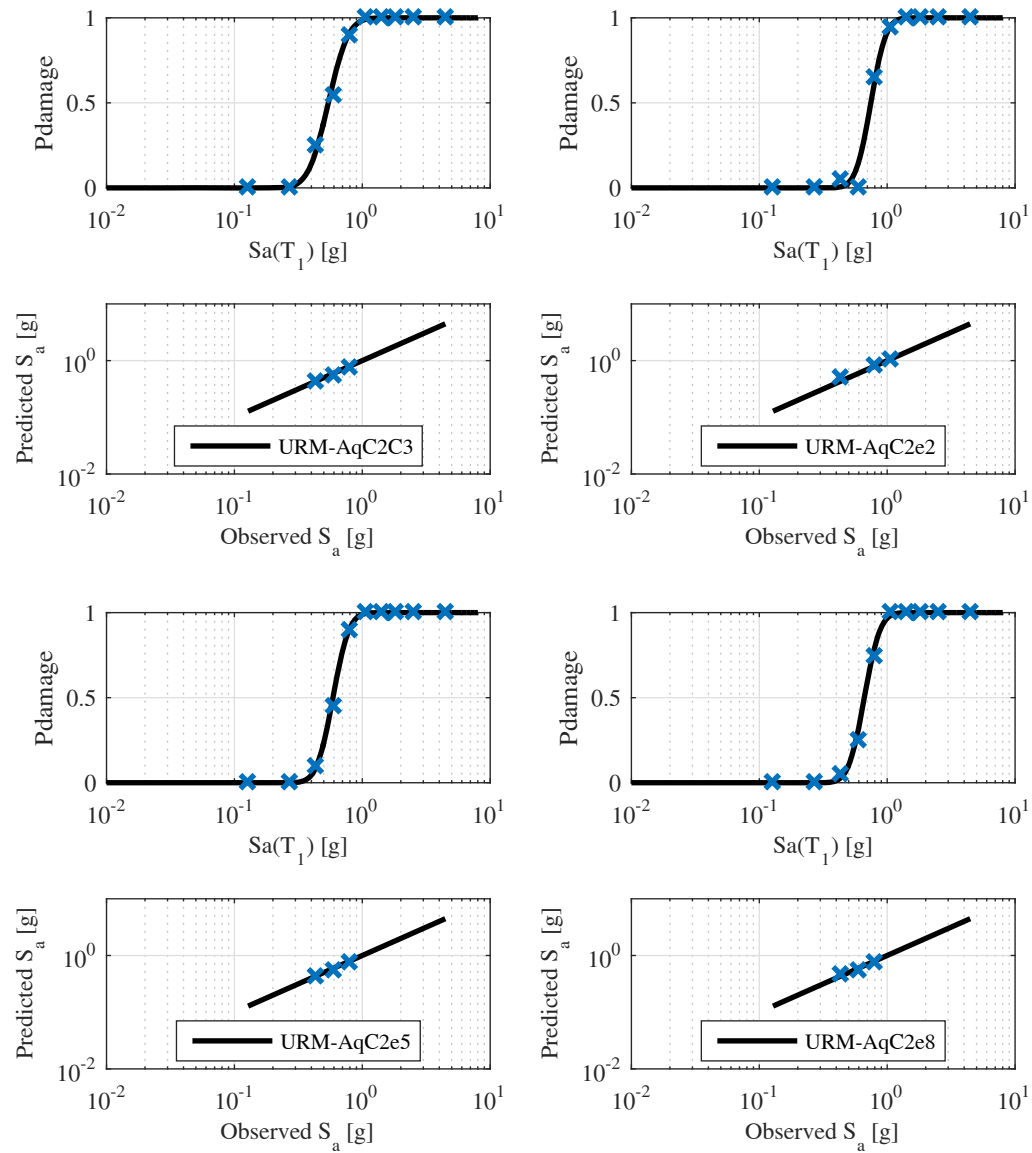


Figure D.12 Fragility curves and quantile-quantile plots for URM buildings designed for Roma on soil C. The line-style helps to distinguish among different structural characteristics. Solid and dashed lines represent, respectively, 2- and 3- story structures while the use of circle markers depicts an irregular configuration. Each panel represents a different configuration whose code is given in the legend name.

## D.1.4 Unreinforced Masonry - Damage Limit State



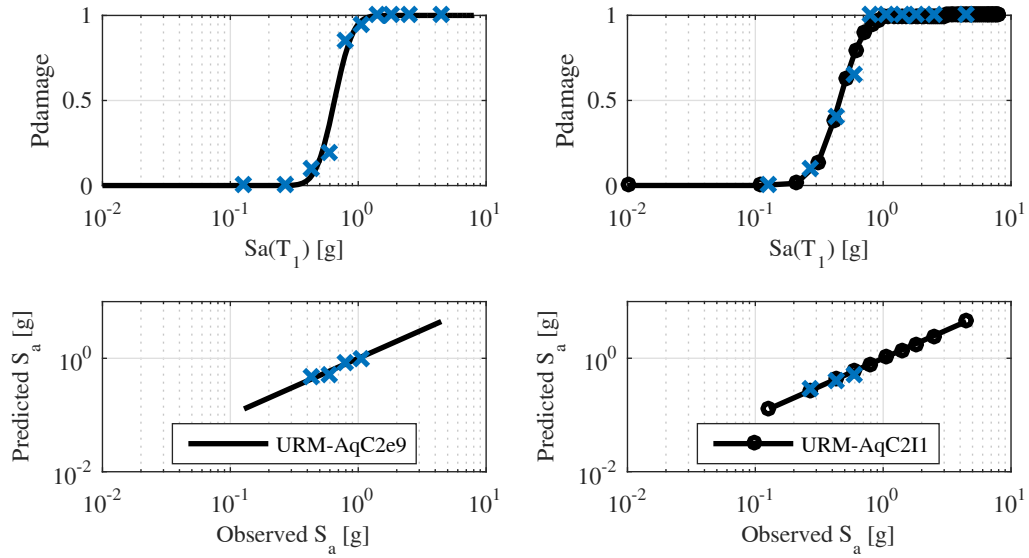
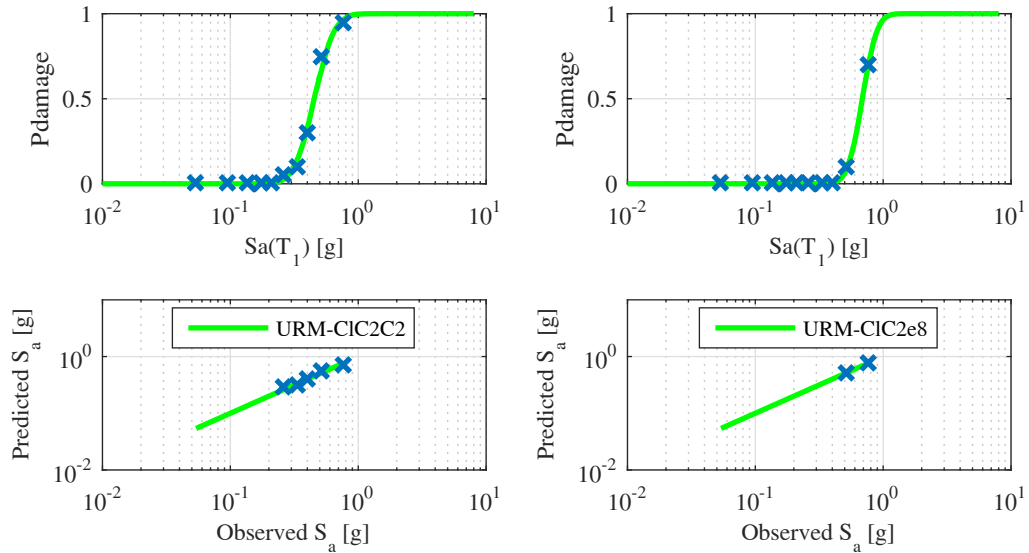


Figure D.13 Fragility curves and quantile-quantile plots for URM buildings designed for L'Aquila on soil C. The line-style helps to distinguish among different structural characteristics. Solid and dashed lines represent, respectively, 2- and 3- story structures while the use of circle markers depicts an irregular configuration. Each panel represents a different configuration whose code is given in the legend name.



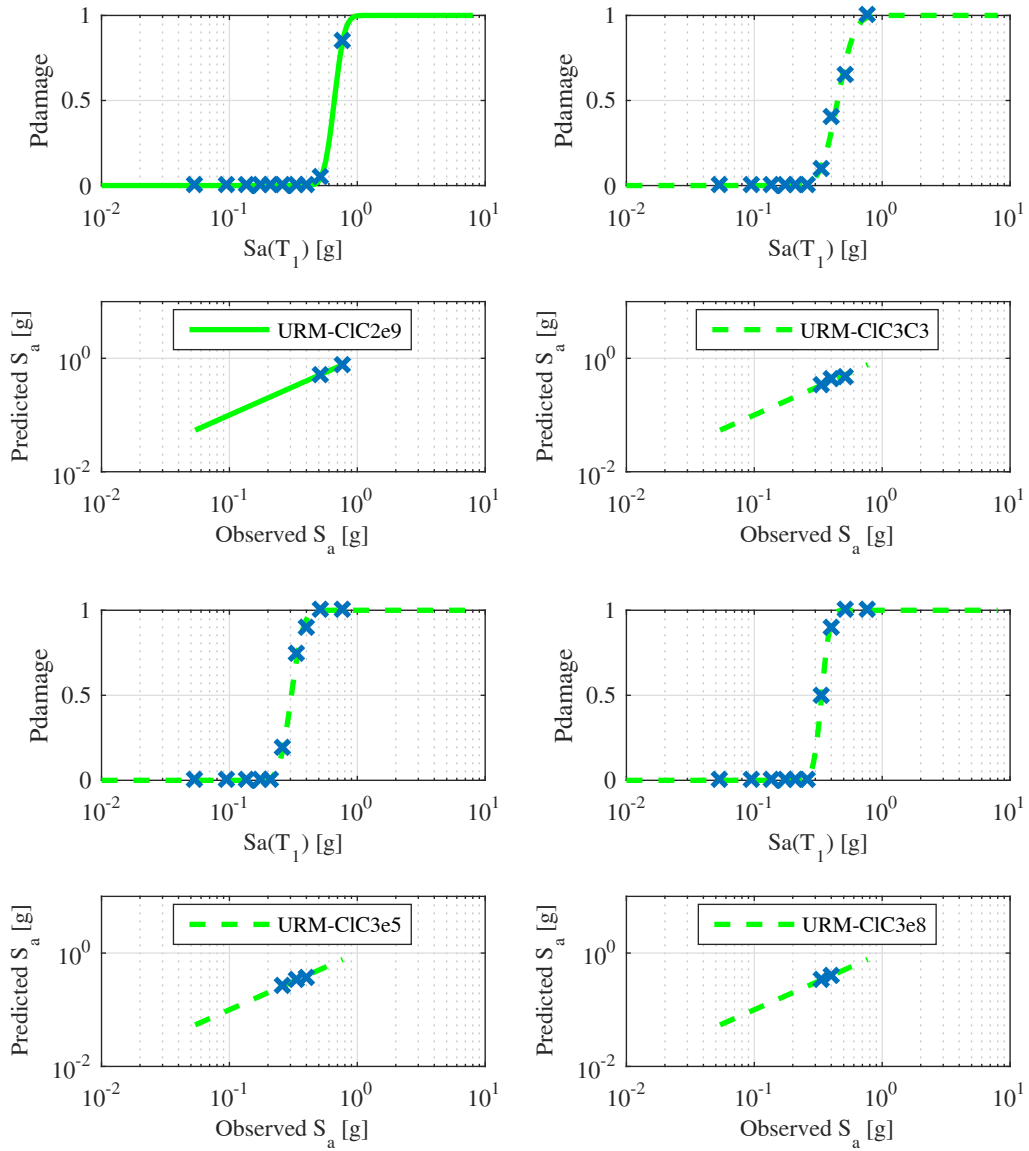
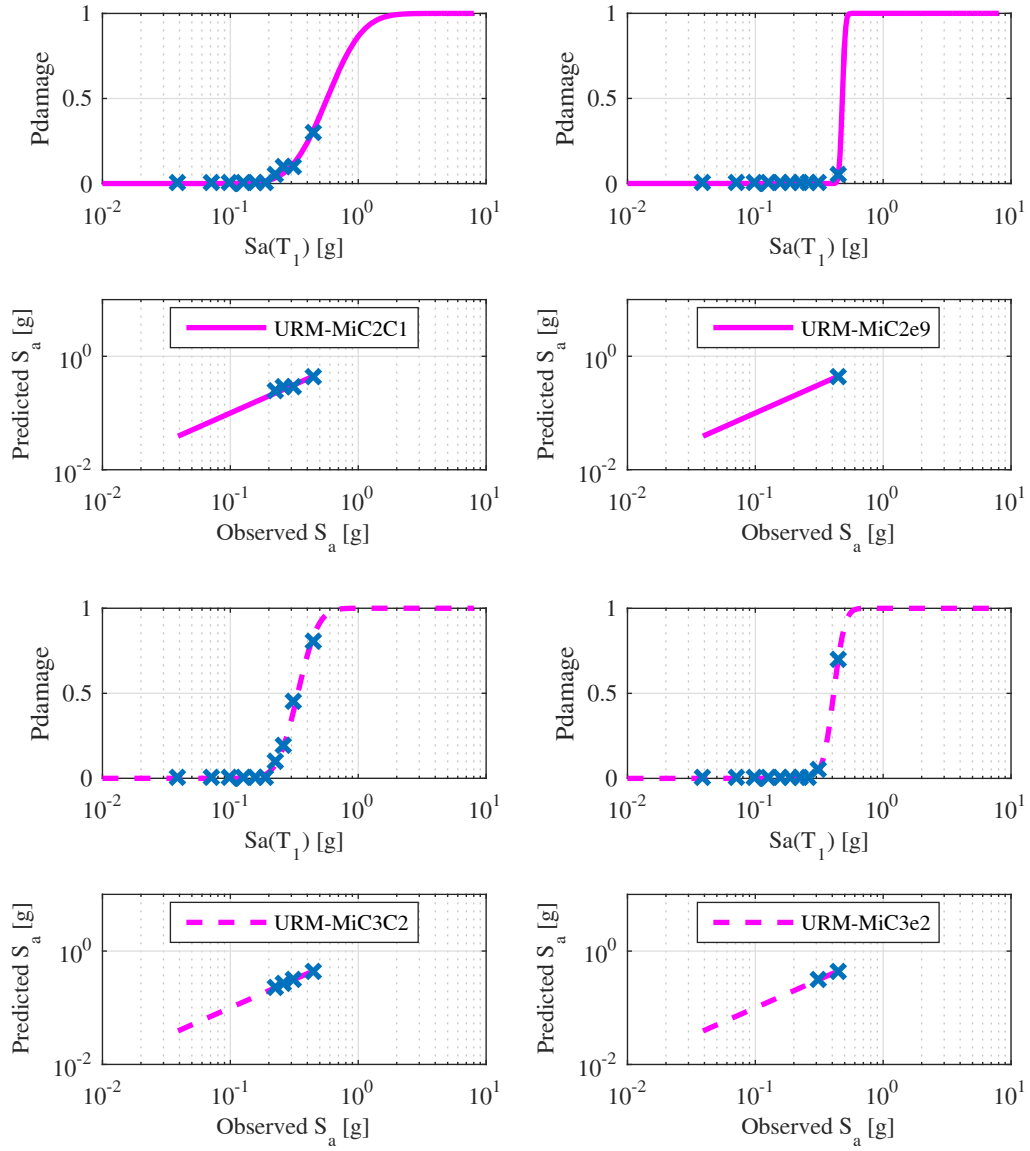


Figure D.14 Fragility curves and quantile-quantile plots for URM buildings designed for Caltanissetta on soil C. The line-style helps to distinguish among different structural characteristics. Solid and dashed lines represent, respectively, 2- and 3- story structures while the use of circle markers depicts an irregular configuration. Each panel represents a different configuration whose code is given in the legend name.



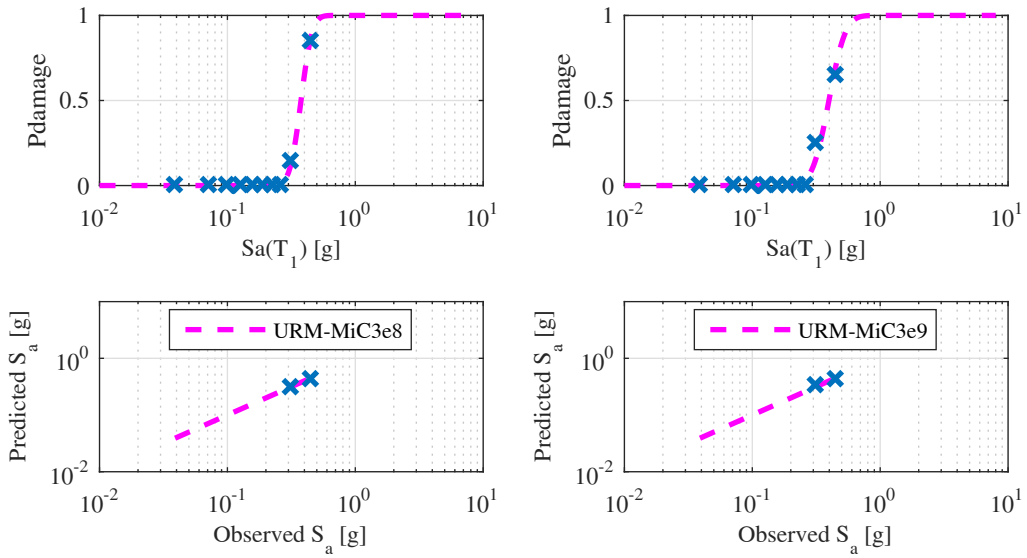
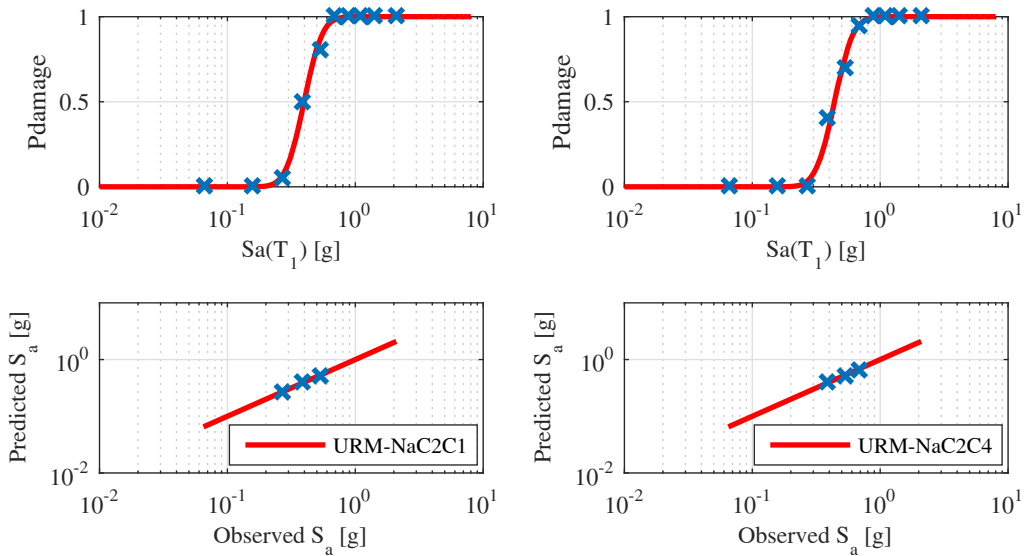
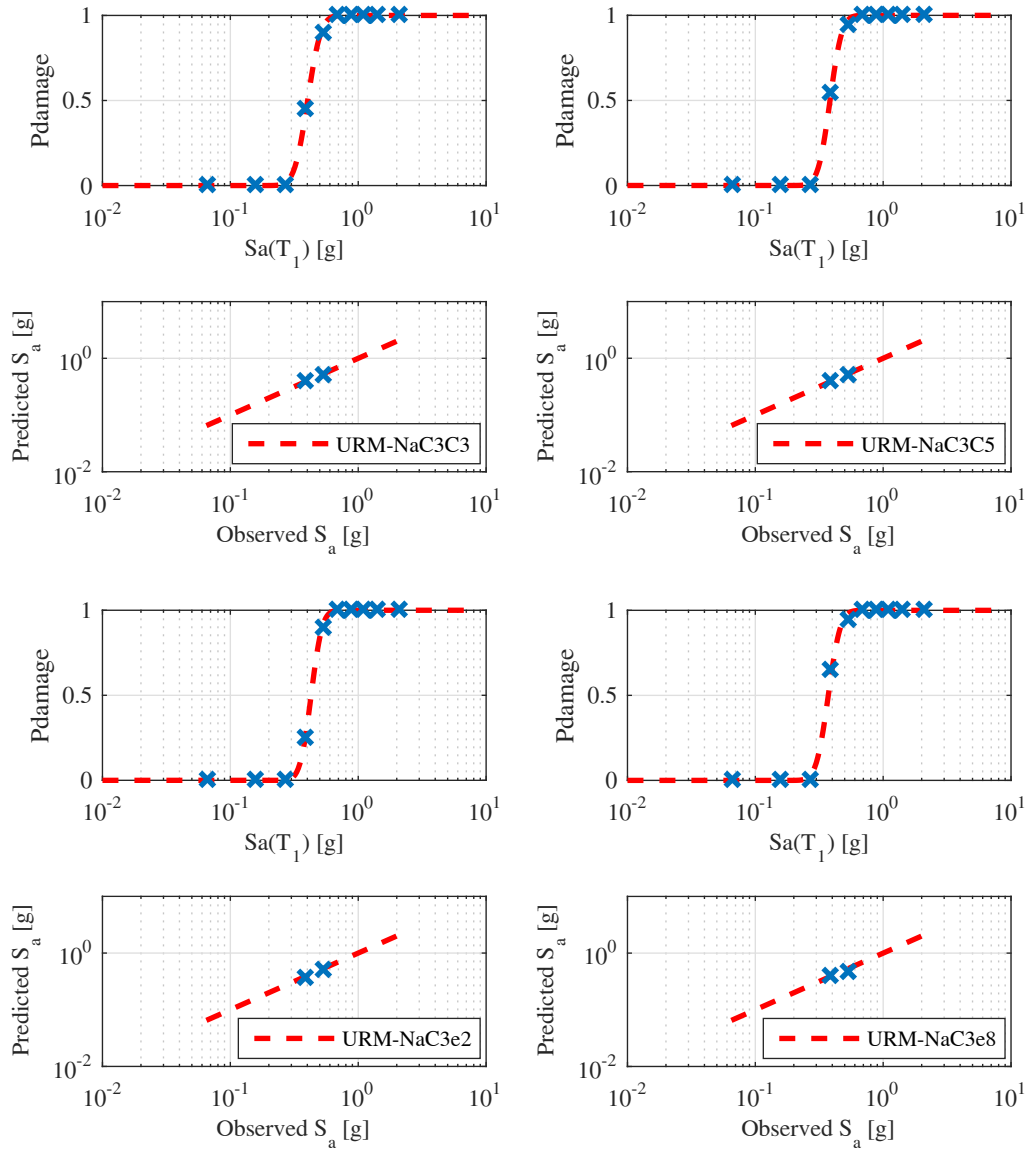


Figure D.15 Fragility curves and quantile-quantile plots for URM buildings designed for Milano on soil C. The line-style helps to distinguish among different structural characteristics. Solid and dashed lines represent, respectively, 2- and 3- story structures while the use of circle markers depicts an irregular configuration. Each panel represents a different configuration whose code is given in the legend name.





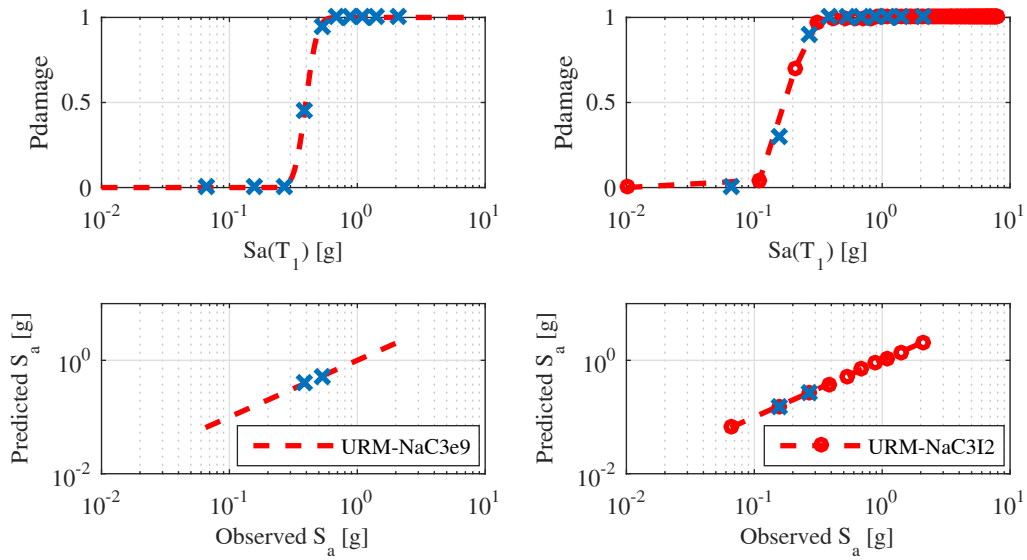
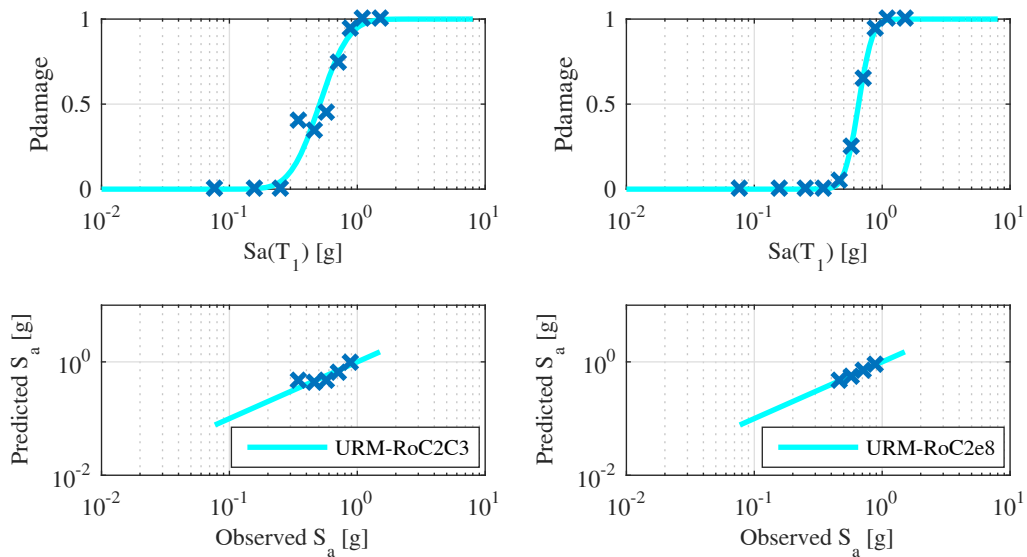


Figure D.16 Fragility curves and quantile-quantile plots for URM buildings designed for Napoli on soil C. The line-style helps to distinguish among different structural characteristics. Solid and dashed lines represent, respectively, 2- and 3- story structures while the use of circle markers depicts an irregular configuration. Each panel represents a different configuration whose code is given in the legend name.



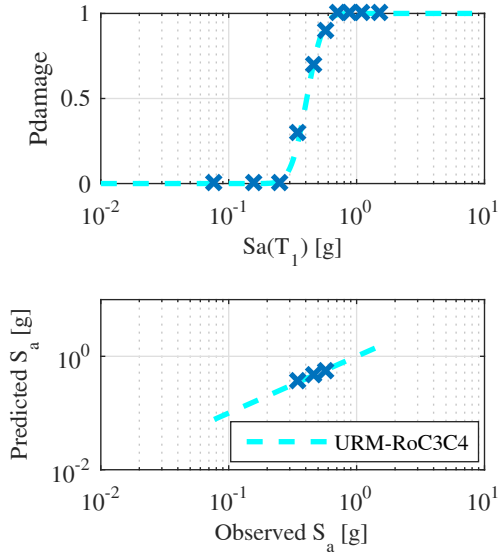


Figure D.17 Fragility curves and quantile-quantile plots for URM buildings designed for Roma on soil C. The line-style helps to distinguish among different structural characteristics. Solid and dashed lines represent, respectively, 2- and 3- story structures while the use of circle markers depicts an irregular configuration. Each panel represents a different configuration whose code is given in the legend name.

## D.2 NOMINAL ANNUAL RATES FOR COLLAPSE AND DAMAGE LIMIT STATES

### D.2.1 Unreinforced Masonry buildings

The following tables summarize the computed rates for the analyzed URM buildings; each table is related to a City/soil Class including both Damage and Collapse rates for the buildings designed in that case. The IDs (CC\_SC\_NS\_SN) are built in order to give information about the structures, in particular:

- CC indicates the site
- SC indicates the soil class
- NS indicates the number of stories
- SN indicates the structure name. Those labelled with C and E are regular structures while the I indicates an irregular structure

**Table D.3 Collapse and Damage rates Masonry Structures in L'Aquila when local site condition is C according to Eurocode 8 classification**

Soil Class C			
Regular 2-story structures			
UR	Structure ID	Collapse Rate	Damage Rate
<i>UniGe</i>	<i>Aq_C_2_C3</i>	5.24E-04	1.30E-02
<i>Eucentre</i>	<i>Aq_C_2_E2</i>	3.25E-04	3.70E-03
<i>Eucentre</i>	<i>Aq_C_2_E5</i>	4.66E-04	7.01E-03
<i>Eucentre</i>	<i>Aq_C_2_E8</i>	4.36E-04	5.30E-03
<i>Eucentre</i>	<i>Aq_C_2_E9</i>	5.04E-04	4.64E-03
Irregular 2-story structures			
<i>UniGe</i>	<i>Aq_C_2_I1</i>	2.24E-03	1.73E-02

**Table D.4 Collapse and Damage rates Masonry Structures in L'Aquila when local site condition is A according to Eurocode 8 classification**

Soil Class A			
Regular 2-story structures			
UR	Structure ID	Collapse Rate	Damage Rate
<i>UniGe</i>	<i>Aq_A_2_C1</i>	4.87E-04	1.84E-02
<i>UniGe</i>	<i>Aq_A_2_C3_NTC14</i>	2.99E-04	---
<i>Eucentre</i>	<i>Aq_A_2_E2</i>	2.41E-04	3.21E-03
<i>Eucentre</i>	<i>Aq_A_2_E9</i>	3.35E-04	4.13E-03
Regular 3-story structures			
<i>UniGe</i>	<i>Aq_A_3_C1</i>	8.41E-04	3.33E-02
<i>Eucentre</i>	<i>Aq_A_3_E2</i>	5.78E-04	1.16E-02
<i>Eucentre</i>	<i>Aq_A_3_E8</i>	9.19E-04	1.42E-02
<i>Eucentre</i>	<i>Aq_A_3_E9</i>	9.54E-04	1.45E-02

**Table D.5 Collapse and Damage rates Masonry Structures in Napoli when local site condition is C according to Eurocode 8 classification**

Soil Class C			
Regular 2-story structures			
UR	Structure ID	Collapse Rate	Damage Rate
<i>UniGe</i>	<i>Na_C_2_C1</i>	4.61E-05	6.69E-03
<i>UniGe</i>	<i>Na_C_2_C4</i>	3.56E-05	5.39E-03
<i>UniGe</i>	<i>Na_C_2_C2_NTC14</i>	7.85E-05	---
Irregular 2-story structures			

<i>UniGe</i>	<i>Na_C_2_I1_NTC14</i>	3.95E-04	---
<b>Regular 3-story structures</b>			
<i>UniGe</i>	<i>Na_C_3_C3</i>	1.19E-04	6.47E-03
<i>UniGe</i>	<i>Na_C_3_C5</i>	8.36E-05	6.57E-03
<i>Eucentre</i>	<i>Na_C_3_E2</i>	8.46E-05	5.33E-03
<i>Eucentre</i>	<i>Na_C_3_E8</i>	1.74E-04	7.23E-03
<i>Eucentre</i>	<i>Na_C_3_E9</i>	2.67E-04	6.33E-03
<b>Irregular 3-story structures</b>			
<i>UniGe</i>	<i>Na_C_3_I2</i>	1.72E-04	4.50E-02

Table D.6 Collapse and Damage rates Masonry Structures in Napoli when local site condition is A according to Eurocode 8 classification

Soil Class A			
<b>Regular 2-story structures</b>			
UR	Structure ID	Collapse Rate	Damage Rate
<i>UniGe</i>	<i>Na_A_2_C3</i>	4.80E-05	3.66E-03
<i>UniGe</i>	<i>Na_A_2_C1_NTC14</i>	5.49E-05	---
<i>Eucentre</i>	<i>Na_A_2_E8</i>	3.91E-05	8.78E-04
<b>Regular 3-story structures</b>			
<i>UniGe</i>	<i>Na_A_3_C4</i>	6.41E-05	5.81E-03
<i>UniGe</i>	<i>Na_A_3_C1_NTC14</i>	1.13E-04	---
<i>Eucentre</i>	<i>Na_A_3_E5</i>	5.84E-05	7.57E-03
<b>Irregular 3-story structures</b>			
<i>UniGe</i>	<i>Na_A_3_I2_NTC14</i>	2.38E-04	---

Table D.7 Collapse and Damage rates Masonry Structures in Roma when local site condition is C according to Eurocode 8 classification

Soil Class C			
<b>Regular 2-story structures</b>			
UR	Structure ID	Collapse Rate	Damage Rate
<i>UniGe</i>	<i>Ro_C_2_C3</i>	1.65E-05	5.24E-03
<i>UniGe</i>	<i>Ro_C_2_C1_NTC14</i>	2.39E-05	---
<i>Eucentre</i>	<i>Ro_C_2_E8</i>	1.36E-05	1.10E-03
<b>Regular 3-story structures</b>			
<i>UniGe</i>	<i>Ro_C_3_C4</i>	3.67E-05	4.60E-03
<i>UniGe</i>	<i>Ro_C_3_C1_NTC14</i>	3.03E-05	---

Table D.8 Collapse and Damage rates Masonry Structures in Roma when local site condition is A according to Eurocode 8 classification

Soil Class A			
Regular 2-story structures			
UR	Structure ID	Collapse Rate	Damage Rate
<i>UniGe</i>	<i>Ro_A_2_C2</i>	1.51E-05	5.95E-03
<i>Eucentre</i>	<i>Ro_A_2_E8</i>	1.07E-05	4.50E-04
<i>Eucentre</i>	<i>Ro_A_2_E9</i>	1.84E-05	6.18E-04
Regular 3-story structures			
<i>UniGe</i>	<i>Ro_A_3_C3</i>	1.72E-05	1.79E-03
<i>Eucentre</i>	<i>Ro_A_3_E5</i>	1.31E-05	4.71E-03
<i>Eucentre</i>	<i>Ro_A_3_E8</i>	2.39E-05	2.84E-03

Table D.9 Collapse and Damage rates Masonry Structures in Caltanissetta when local site condition is C according to Eurocode 8 classification

Soil Class C			
Regular 2-story structures			
UR	Structure ID	Collapse Rate	Damage Rate
<i>UniGe</i>	<i>Ca_C_2_C2</i>	1.00E-05	2.13E-04
<i>Eucentre</i>	<i>Ca_C_2_E8</i>	1.00E-05	7.49E-05
Regular 3-story structures			
<i>UniGe</i>	<i>Ca_C_3_C3</i>	1.01E-05	2.61E-04
<i>Eucentre</i>	<i>Ca_C_3_E5</i>	1.45E-05	1.00E-03
<i>Eucentre</i>	<i>Ca_C_3_E8</i>	1.84E-05	5.94E-04

Table D.10 Collapse and Damage rates Masonry Structures in Caltanissetta when local site condition is A according to Eurocode 8 classification

Soil Class A			
Regular 2-story structures			
UR	Structure ID	Collapse Rate	Damage Rate
<i>UniGe</i>	<i>Ca_A_2_C1</i>	1.45E-05	1.77E-04
<i>UniGe</i>	<i>Ca_A_2_C7</i>	1.00E-05	3.93E-05
<i>Eucentre</i>	<i>Ca_A_2_E2</i>	1.00E-05	3.41E-05
<i>Eucentre</i>	<i>Ca_A_2_E5</i>	1.01E-05	7.94E-05
<i>Eucentre</i>	<i>Ca_A_2_E8</i>	1.01E-05	4.79E-05
Regular 3-story structures			
<i>UniGe</i>	<i>Ca_A_3_C2</i>	1.90E-05	4.73E-04

<i>Eucentre</i>	<i>Ca_A_3_E2</i>	1.08E-05	2.15E-04
<i>Eucentre</i>	<i>Ca_A_3_E8</i>	1.63E-05	2.53E-04
<i>Eucentre</i>	<i>Ca_A_3_E9</i>	1.76E-05	3.16E-04

Table D.11 Collapse and Damage rates Masonry Structures in Milano when local site condition is C according to Eurocode 8 classification

Soil Class C			
Regular 2-story structures			
UR	Structure ID	Collapse Rate	Damage Rate
<i>UniGe</i>	<i>Mi_C_2_C1</i>	1.00E-05	5.28E-05
<i>UniGe</i>	<i>Mi_C_2_C7</i>	1.00E-05	1.92E-05
<i>Eucentre</i>	<i>Mi_C_2_E2</i>	1.00E-05	1.06E-05
<i>Eucentre</i>	<i>Mi_C_2_E8</i>	1.00E-05	1.26E-05
<i>Eucentre</i>	<i>Mi_C_2_E9</i>	1.00E-05	1.65E-05
Regular 3-story structures			
<i>UniGe</i>	<i>Mi_C_3_C2</i>	1.00E-05	2.24E-04
<i>Eucentre</i>	<i>Mi_C_3_E2</i>	1.00E-05	7.51E-05
<i>Eucentre</i>	<i>Mi_C_3_E8</i>	1.00E-05	9.88E-05
<i>Eucentre</i>	<i>Mi_C_3_E9</i>	1.00E-05	7.74E-05

Table D.12 Collapse and Damage rates Masonry Structures in Milano when local site condition is A according to Eurocode 8 classification

Soil Class A			
Regular 2-story structures			
UR	Structure ID	Collapse Rate	Damage Rate
<i>UniGe</i>	<i>Mi_A_2_C1</i>	1.00E-05	5.36E-05
<i>UniGe</i>	<i>Mi_A_2_C4</i>	1.00E-05	5.49E-05
<i>Eucentre</i>	<i>Mi_A_2_E2</i>	1.00E-05	1.00E-05
<i>Eucentre</i>	<i>Mi_A_2_E5</i>	1.00E-05	1.01E-05
Regular 3-story structures			
<i>UniGe</i>	<i>Mi_A_3_C2</i>	1.00E-05	1.97E-04
<i>UniGe</i>	<i>Mi_A_3_C6</i>	1.00E-05	2.95E-05
<i>Eucentre</i>	<i>Mi_A_3_E2</i>	1.00E-05	4.88E-05
<i>Eucentre</i>	<i>Mi_A_3_E5</i>	1.00E-05	1.03E-04

## D.2.2 Reinforced Concrete Precast buildings

The following tables summarize the computed rates for the analyzed precast buildings; each table is related to a City/soil Class including both Damage and Collapse rates for the buildings designed in that case. The IDs (CC\_SC\_GG\_TT) are built in order to give information about the structures, in particular:

- CC indicates the site
- SC indicates the soil class
- GG indicates the geometric configuration
- TT indicates the first period of the structure

**Table D.13 Collapse and Damage rates for Precast Structures in L'Aquila when local site condition is C according to Eurocode 8 classification**

Soil Class C			
UR	Structure Name	Collapse Rate	Damage Rate
UniNaM	<i>Aq_SoilC_Geom3_2sec</i>	4.14E-03	6.73E-03
UniNaM	<i>Aq_SoilC_Geom4_2sec</i>	6.35E-03	6.52E-03
Eucentre	<i>Aq_SoilC_Geom1_2sec</i>	3.97E-03	7.25E-03
Eucentre	<i>Aq_SoilC_Geom2_2sec</i>	2.21E-03	6.35E-03

**Table D.14 Collapse and Damage rates for Precast Structures in L'Aquila when local site condition is A according to Eurocode 8 classification**

Soil Class A			
UR	Structure Name	Collapse Rate	Damage Rate
UniNaM	<i>Aq_SoilA_Geom3_2sec</i>	1.14E-03	3.15E-03
UniNaM	<i>Aq_SoilA_Geom4_2sec</i>	2.37E-03	2.78E-03
Eucentre	<i>Aq_soilA_Geom1_2sec</i>	1.35E-03	3.02E-03
Eucentre	<i>Aq_SoilA_Geom2_2sec</i>	1.33E-03	3.07E-03

**Table D.15 Collapse and Damage rates for Precast Structures in Napoli when local site condition is C according to Eurocode 8 classification**

Soil Class C			
UR	Structure Name	Collapse Rate	Damage Rate
UniNaM	<i>Na_SoilC_Geom3_2sec</i>	1.36E-03	4.87E-03
UniNaM	<i>Na_SoilC_Geom4_2sec</i>	2.50E-03	4.09E-03

Eucentre	<i>Na_SoilC_Geom1_2sec</i>	9.71E-04	2.32E-03
Eucentre	<i>Na_SoilC_Geom2_2sec</i>	1.04E-03	1.78E-03

Table D.16 Collapse and Damage rates for Precast Structures in Napoli when local site condition is A according to Eurocode 8 classification

Soil Class A			
UR	Structure Name	Collapse Rate	Damage Rate
UniNaM	<i>Na_SoilA_Geom3_2sec</i>	3.60E-04	2.20E-03
UniNaM	<i>Na_SoilA_Geom4_2sec</i>	1.03E-03	1.87E-03
Eucentre	<i>Na_SoilA_Geom1_2sec</i>	2.60E-04	7.83E-04
Eucentre	<i>Na_SoilA_Geom2_2sec</i>	3.21E-04	7.04E-04

Table D.17 Collapse and Damage rates for Precast Structures in Milano when local site condition is C according to Eurocode 8 classification

Soil Class C			
UR	Structure Name	Collapse Rate	Damage Rate
UniNaM	<i>Mi_SoilC_Geom3_2sec</i>	1.34E-05	1.54E-04
UniNaM	<i>Mi_SoilC_Geom4_2sec</i>	4.40E-05	1.27E-04
Eucentre	<i>Mi_SoilC_Geom1_2sec</i>	1.06E-05	3.63E-05
Eucentre	<i>Mi_SoilC_Geom2_2sec</i>	1.83E-05	3.34E-05

Table D.18 Collapse and Damage rates for Precast Structures in Milano when local site condition is A according to Eurocode 8 classification

Soil Class A			
UR	Structure Name	Collapse Rate	Damage Rate
UniNaM	<i>Mi_SoilA_Geom3_2sec</i>	1.01E-05	3.74E-05
UniNaM	<i>Mi_SoilA_Geom4_2sec</i>	1.22E-05	2.81E-05
Eucentre	<i>Mi_SoilA_Geom1_2sec</i>	1.00E-05	1.14E-05
Eucentre	<i>Mi_SoilA_Geom2_2sec</i>	1.18E-05	1.21E-05

### D.2.3 Reinforced Concrete cast-in-place buildings

The following tables summarize the computed rates for the analyzed RC buildings; each table is related to a City/soil Class including both Damage and Collapse rates for the buildings designed in that case. The IDs (CC\_SC\_NS\_SN) are built in order to give information about the structures, in particular:

- CC indicates the site
- SC indicates the soil class
- NS indicates the number of stories
- SN indicates the structural configuration, i.e. BF (Bare Frame), PF (Pilotis Frame) and IF (Infilled Frame).

**Table D.19** Collapse and Damage rates for Reinforced Concrete Structures in L'Aquila when local site condition is C according to Eurocode 8 classification

Soil Class C			
UR	Structure Name	Collapse Rate	Damage Rate
<b>6-story frames</b>			
UniBas	<i>Aq_C_6_BF</i>	8.47E-05	1.08E-02
UniBas	<i>Aq_C_6_IF</i>	2.02E-04	1.22E-02
UniBas	<i>Aq_C_6_PF</i>	2.08E-04	1.50E-02
<b>9-story frames</b>			
UniCh	<i>Aq_C_9_BF</i>	6.21E-05	1.16E-02
UniCh	<i>Aq_C_9_IF</i>	7.64E-05	1.06E-02
UniCh	<i>Aq_C_9_PF</i>	7.40E-05	1.21E-02
<b>3-story frames</b>			
UniNaM	<i>Aq_C_3_BF</i>	1.30E-05	1.17E-02
UniNaM	<i>Aq_C_3_IF</i>	1.91E-05	4.61E-03
UniNaM	<i>Aq_C_3_PF</i>	5.44E-05	3.70E-02

**Table D.20** Collapse and Damage rates for Reinforced Concrete 9-storey frames in L'Aquila when local site condition is A according to Eurocode 8 classification

Soil Class A			
UR	Structure Name	Collapse Rate	Damage Rate
UniBas	<i>Aq_A_9_BF</i>	7.91E-05	4.63E-03
UniBas	<i>Aq_A_9_IF</i>	8.19E-05	6.08E-03
UniBas	<i>Aq_A_9_PF</i>	7.98E-05	7.12E-03

**Table D.21 Collapse and Damage rates for Reinforced Concrete Structures in Napoli when local site condition is C according to Eurocode 8 classification**

Soil Class C			
UR	Structure Name	Collapse Rate	Damage Rate
<b>6-story frames</b>			
UniCh	<i>Na_C_6_BF</i>	1.00E-05	5.97E-03
UniCh	<i>Na_C_6_IF</i>	1.07E-05	8.12E-03
UniCh	<i>Na_C_6_PF</i>	1.02E-05	1.83E-02
<b>9-story frames</b>			
UniNaV	<i>Na_C_9_BF</i>	2.00E-05	4.68E-03
UniNaV	<i>Na_C_9_IF</i>	1.58E-05	7.37E-03
UniNaV	<i>Na_C_9_PF</i>	3.85E-05	9.61E-03
<b>3-story frames</b>			
UniNaM	<i>Na_C_3_BF</i>	1.00E-05	8.28E-03
UniNaM	<i>Na_C_3_IF</i>	1.00E-05	1.67E-03
UniNaM	<i>Na_C_3_PF</i>	1.01E-05	2.83E-02

**Table D.22 Collapse and Damage rates for Reinforced Concrete Structures in Roma when local site condition is C according to Eurocode 8 classification**

Soil Class C			
UR	Structure Name	Collapse Rate	Damage Rate
UniNaM	<i>Ro_C_6_BF</i>	1.00E-05	3.61E-03
UniNaM	<i>Ro_C_6_IF</i>	1.74E-05	2.83E-03
UniNaM	<i>Ro_C_6_PF</i>	2.16E-05	3.79E-02

**Table D.23 Collapse and Damage rates for Reinforced Concrete Structures in Caltanissetta when local site condition is C according to Eurocode 8 classification**

Soil Class C			
UR	Structure Name	Collapse Rate	Damage Rate
UniNaV	<i>Ca_C_6_BF</i>	1.83E-05	2.59E-03
UniNaV	<i>Ca_C_6_IF</i>	3.21E-05	2.11E-03
UniNaV	<i>Ca_C_6_PF</i>	7.23E-05	9.55E-03

**Table D.24 Collapse and Damage rates for Reinforced Concrete Structures in Milano when local site condition is C according to Eurocode 8 classification**

Soil Class C			
UR	Structure Name	Collapse Rate	Damage Rate
<b>6-story frames</b>			
UniRm	<i>Mi_C_6_BF</i>	1.00E-05	1.86E-04
UniRm	<i>Mi_C_6_IF</i>	1.00E-05	9.61E-05
UniRm	<i>Mi_C_6_PF</i>	1.00E-05	3.40E-03
<b>9-story frames</b>			
UniRm	<i>Mi_C_9_BF</i>	1.00E-05	1.28E-04
UniRm	<i>Mi_C_9_IF</i>	1.00E-05	9.85E-05
UniRm	<i>Mi_C_9_PF</i>	1.00E-05	4.84E-04
<b>3-story frames</b>			
UniNaM	<i>Mi_C_3_BF</i>	2.00E-05	3.58E-04
UniNaM	<i>Mi_C_3_IF</i>	1.00E-05	1.40E-05
UniNaM	<i>Mi_C_3_PF</i>	1.00E-05	3.19E-03

#### D.2.4 Steel buildings

The following tables summarize the computed rates for the analyzed steel buildings; each table is related to a City/soil Class including both Damage and Collapse rates for the buildings designed in that case. The IDs (CC\_SC\_NS\_SN) are built in order to give information about the structures, in particular:

- CC indicates the site
- SC indicates the soil class
- NS indicates the number of stories
- SN indicates the structural configuration

**Table D.25 Collapse and Damage rates for Steel Structures in L'Aquila when local site condition is C according to Eurocode 8 classification**

Soil Class C			
UR	Structure Name	Collapse Rate	Damage Rate
UniNaDc+UniCamZ	<i>AQ_C_1_Lx20Lj6</i>	2.23E-04	1.15E-02
UniNaDc+UniCamZ	<i>AQ_C_1_Lx20Lj8</i>	1.05E-04	1.16E-02
UniNaDc+UniCamZ	<i>AQ_C_1_Lx30Lj6</i>	1.65E-04	5.07E-03
UniNaDc+UniCamZ	<i>AQ_C_1_Lx30Lj8</i>	1.92E-04	6.11E-03

**Table D.26 Collapse and Damage rates for Steel Structures in L'Aquila when local site condition is A according to Eurocode 8 classification**

Soil Class C			
UR	Structure Name	Collapse Rate	Damage Rate
UniNaDc+UniCamZ	<i>AQ_A_1_Lx20Ly6</i>	4.82E-05	4.43E-03
UniNaDc+UniCamZ	<i>AQ_A_1_Lx20Ly8</i>	3.32E-05	5.80E-03
UniNaDc+UniCamZ	<i>AQ_A_1_Lx30Ly6</i>	5.87E-05	2.47E-03
UniNaDc+UniCamZ	<i>AQ_A_1_Lx30Ly8</i>	5.74E-05	2.83E-03

**Table D.27 Collapse and Damage rates for Steel Structures in Napoli when local site condition is C according to Eurocode 8 classification**

Soil Class C			
UR	Structure Name	Collapse Rate	Damage Rate
UniNaDc+UniCamZ	<i>NA_C_1_Lx20Ly6</i>	1.38E-05	6.52E-03
UniNaDc+UniCamZ	<i>NA_C_1_Lx20Ly8</i>	1.01E-05	5.76E-03
UniNaDc+UniCamZ	<i>NA_C_1_Lx30Ly6</i>	1.03E-05	2.38E-03
UniNaDc+UniCamZ	<i>NA_C_1_Lx30Ly8</i>	2.27E-05	3.08E-03

**Table D.28 Collapse and Damage rates for Steel Structures in Napoli when local site condition is A according to Eurocode 8 classification**

Soil Class C			
UR	Structure Name	Collapse Rate	Damage Rate
UniNaDc+UniCamZ	<i>NA_A_1_Lx20Ly6</i>	1.00E-05	1.56E-03
UniNaDc+UniCamZ	<i>NA_A_1_Lx20Ly8</i>	1.00E-05	1.29E-03
UniNaDc+UniCamZ	<i>NA_A_1_Lx30Ly6</i>	1.00E-05	6.41E-04
UniNaDc+UniCamZ	<i>NA_A_1_Lx30Ly8</i>	1.00E-05	7.02E-04

**Table D.29 Collapse and Damage rates for Steel Structures in Milano when local site condition is C according to Eurocode 8 classification**

Soil Class C			
UR	Structure Name	Collapse Rate	Damage Rate
UniNaDc+UniCamZ	<i>MI_C_1_Lx20Ly6</i>	1.00E-05	1.36E-04

UniNaDc+UniCamZ	<i>MI_C_1_Lx20Lj8</i>	1.00E-05	1.15E-04
UniNaDc+UniCamZ	<i>MI_C_1_Lx30Lj6</i>	1.00E-05	3.09E-05
UniNaDc+UniCamZ	<i>MI_C_1_Lx30Lj8</i>	1.00E-05	4.27E-05

**Table D.30** Collapse and Damage rates for Steel Structures in Milano when local site condition is A according to Eurocode 8 classification

Soil Class C			
UR	Structure Name	Collapse Rate	Damage Rate
UniNaDc+UniCamZ	<i>MI_A_1_Lx20Lj6</i>	1.00E-05	3.06E-05
UniNaDc+UniCamZ	<i>MI_A_1_Lx20Lj8</i>	1.00E-05	2.58E-05
UniNaDc+UniCamZ	<i>MI_A_1_Lx30Lj6</i>	1.00E-05	1.54E-05
UniNaDc+UniCamZ	<i>MI_A_1_Lx30Lj8</i>	1.00E-05	1.71E-05

### D.2.5 Base isolated structures

The following table summarizes the computed rates for the analyzed RC buildings; each table is related to a City/soil Class including both Damage and Collapse rates for the buildings designed in that case. The IDs (IT\_SC\_NS\_SN) are built in order to give information about the structures, in particular:

- IT indicates the device adopted (HDRB, HDRB+sliders and DCFP)
- CC indicates the site
- SC indicates the soil class
- SN indicates the structural configuration

**Table D.31** Collapse and Damage rates for Steel Structures in L'Aquila when local site condition is C according to Eurocode 8 classification

Soil Class C			
UR	Structure Name	Collapse Rate	Damage Rate
<b>Isolation system: Rubber + Slider devices</b>			
UniBasC	<i>BI_HDRB+Slider_Aq_C_c1</i>	1.09E-03	2.10E-03
UniBasC	<i>BI_HDRB+Slider_Aq_C_c2</i>	1.03E-03	2.10E-03
UniBasC	<i>BI_HDRB+Slider_Aq_C_c3</i>	1.10E-03	2.10E-03
UniBasC	<i>BI_HDRB+Slider_Aq_C_c4</i>	7.40E-04	2.15E-03
<b>Isolation system: DCFP devices</b>			

UniBasP	<i>BI_DCFP_Aq_C_SLC_250mm</i>	9.70E-04	7.30E-04
UniBasP	<i>BI_DCFP_Aq_C_SLV_250mm</i>	3.30E-04	---
UniBasP	<i>BI_DCFP_Aq_C_SLC_300mm</i>	1.12E-03	5.10E-04
UniBasP	<i>BI_DCFP_Aq_C_SLV_300mm</i>	3.15E-04	---
<b>Isolation system: Rubber devices</b>			
UniCamD	<i>BI_HDRB_Aq_C_c1_2sec</i>	1.55E-04	1.41E-03
UniCamD	<i>BI_HDRB_Aq_C_c2_2sec</i>	1.65E-04	9.50E-04
UniCamD	<i>BI_HDRB_Aq_C_c2b_3sec</i>	7.50E-04	2.47E-03

## Appendix E. SDoFs compliance with RINTC MDoFs

The Single degree of Freedom (SDoF) systems adopted for RT-Spectra calculation (Chapter 4) have been compared to more complex and realistic Multi degree of freedom systems (MDoFs) in order to verify the representativeness of the assumptions that were made. In particular, the check was done on the basis of pushover curves and their main characteristics, i.e. ductility and over-strength. The references are the pushovers of the RC frame buildings designed and adopted in RINTC project (see Chapter 3). Those curves are related to building designed for three cities, namely L'Aquila, Napoli and Roma, that can be associated at high-to-medium hazard level. Those pushovers were computed for different patterns and direction of loading and, to be compared with the assumed elastic-plastic backbone, are bi-linearized in line with what suggested by NTC08 (§ C7.3.4.1 and Figure E.1).

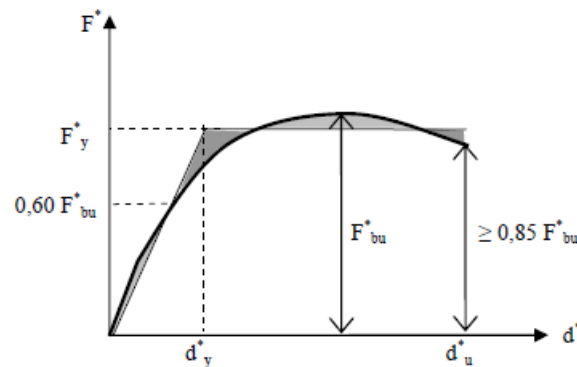


Figure E.1 Pushover bi-linearization according to NTC08 provisions

In Figure E.1  $F_y^*$  is computed in order to have the same area under the 'original' curve and the 'bi-linear' one,  $F_{bu}^*$  is the maximum base shear and  $d_u^*$  is the displacement in correspondence of a 15% drop of the base shear. After the bi-linearization, the ultimate ductility is computed as  $d_u/d_y$  and compared with the one assumed for LS3. The RINTC bi-linearized curves of reference are given in Figure E.2 while Table E.1 gives a range of ductility according to different shapes (modal/uniform) and directions (x/y and +/-) of the incremental load pattern.

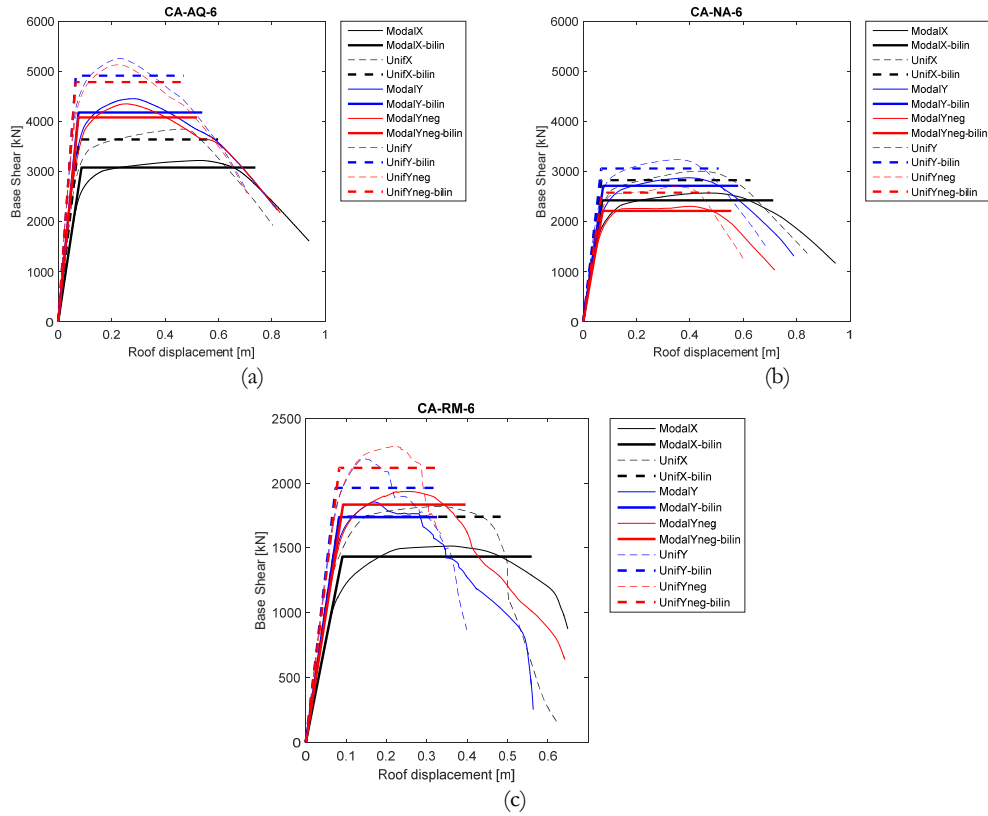


Figure E.2 Pushover curves and their bi-linearization for L'Aquila (a), Napoli(b) and Roma(c)

Table E.1 Ultimate ductilities computed from bi-linearized pushover curves

	L'Aquila	Napoli	Roma
<b>Modal X</b>	8.44	9.98	6.16
<b>Uniform X</b>	7.70	9.18	5.80
<b>Modal Y</b>	7.11	7.74	3.93
<b>Modal Y-neg</b>	6.88	7.56	4.28
<b>Uniform Y</b>	7.12	7.52	4.40
<b>Uniform Y-neg</b>	7.26	6.78	3.94

L'Aquila and Napoli are more hazardous sites than Roma and, probably, the code provisions produce, for structures located in those sites, a higher level of ductility. Therefore, it sounds reasonable to associate the structures located in Napoli and L'Aquila to a High Ductility Class (DCH) and the one in Roma to a Medium ductility class (DCM). Indeed, the ductilities given in Table E.1 are in good agreement with what we assumed for our SDoF: LS3 is associated with a ductility of 7 for DCH and 5 for DCM structures.

The other parameter to be checked is the over-strength that is computed as the ratio between the design and the maximum base shear observed in the pushover curve. The design base shear is estimated as the product of the building mass and the design spectral acceleration, i.e. the elastic one divided by the behaviour factor ( $q$ ). The results are given, for all load patterns, in the following Table 2; the results appear to be in line with what we assumed, i.e. 2 for DCH and 1.5 for DCM.

**Table E.2 Over-strength computed from bi-linearized pushover curves**

	<b>L'Aquila</b>	<b>Napoli</b>	<b>Roma</b>
<b>Modal X</b>	1.64	1.54	1.53
<b>Uniform X</b>	1.95	1.80	1.84
<b>Modal Y</b>	2.26	1.72	1.87
<b>Modal Y-neg</b>	2.21	1.38	1.96
<b>Uniform Y</b>	2.67	1.94	2.21
<b>Uniform Y-neg</b>	2.61	1.62	2.31